University of Alberta

The Role of the Na^+/H^+ Exchanger Isoform I in Cardiac Disease

by

Fatima Mraiche

A thesis submitted to the Faculty of Graduate Studies and Research
in partial fulfillment of the requirements for the degree of

Doctor of Philosophy

Medical Sciences - Pediatrics

Fall 2010
Edmonton, Alberta

Examining Committee

Dr. Larry Fliegel, Department of Biochemistry & Pediatrics

Dr. Jason Dyck, Department of Pediatrics

Dr. Peter Light, Department of Pharmacology

Dr. Gary Lopaschuk, Department of Pediatrics

Dr. Jonathan Lytton, Department of Biochemistry and Molecular Biology, University of Calgary

Dedication

In the name of Allah, the Most Gracious, the Most Merciful. All praise is due to Allah with whose grace all good work comes to completion.

To my family:

My father haj Khalil Mraiche
My mother hajji Jehan Mraiche
My brother Hassin Mraiche
My sisters Mouminat, Nouhal and Deebe
for your endless support and love

Abstract

The mammalian Na^+/H^+ exchanger isoform 1 (NHE1) is a ubiquitously expressed membrane protein that regulates intracellular pH. In the myocardium, NHE1 has been implicated in ischemia/reperfusion (I/R) and cardiac hypertrophy (CH). Hormonal, autocrine and paracrine stimuli, acidosis, cardiotoxic metabolites released during I/R and CH increases NHE1 protein expression and activity. The involvement of NHE1 in CH and I/R has been further supported with the use of NHE1 inhibitors, which have been beneficial in the prevention/regression of several models of CH and I/R injury. Despite the fact that elevation of NHE1 expression and activity have been demonstrated in several models of heart disease, it was unclear whether elevation of NHE1 protein expression was sufficient to induce a specific cardiac pathology, or whether activation of the protein was required. To understand the direct role of NHE1 in CH and I/R, an *in vivo* and *in vitro* gain-of-function model, expressing varying levels and activities of NHE1 were examined. *In vivo*, our N-line mice expressed wild type NHE1 and our K-line mice expressed constitutively active NHE1. *In vitro*, neonatal rat ventricular cardiomyocytes were infected with the IRM adenovirus containing wild type NHE1 or the K-IRM adenovirus containing active NHE1. We demonstrated that expression of constituitively active NHE1 promotes CH to a much greater degree than expression of wild type NHE1 alone, both *in vivo* and *in vitro*. This NHE1-dependent hypertrophic response occurred independent of signaling pathways involved in CH including, mitogen activated protein kinases, p^{90} ribosomal S6 kinase, calcineurin and glycogen synthase kinase. The NHE1-dependent hypertrophic effect also occurred independent of gender. In addition, the expression of active NHE1 increased the susceptibility of intact mice to neurohormonal

stimulation and progressed the hypertrophic response. When these hearts expressing active NHE1 were subjected to I/R using the *ex vivo* working heart perfusion model, fatty acid (FA) oxidation and glycolysis rates increased, thus generating greater ATP production rates. This was associated with cardioprotective effects in the myocardium, as well as a more energetically efficient myocardium. Expression of the endoplasmic reticulum (ER) stress response proteins, calreticulin and PDI were also shown to be increased relative to controls, and may contribute to the cardioprotection observed. We demonstrate that active NHE1 induces cardioprotection and alters cardiac metabolism in working hearts subjected to I/R. Overall, our results suggest that expression of active NHE1 has a double edged sword effect, on one side it induces CH while on the other side, it protects the heart against I/R injury.

Acknowledgements

I would like to thank my supervisor, Dr. Larry Fliegel for allowing me to pursue my doctoral studies in his laboratory. Thank you for all your support and mentorship. I really appreciate the opportunity.

Thank you to Dr. Jason Dyck and Dr. Peter Light who have been on my graduate committee. Your mentorship and support have been invaluable. I would also like to thank all my graduate coordinators, Dr. Gary Lopaschuk, Dr. Rick Schulz and Dr. Po Yin Cheung, who have provided great mentorship and endless support.

Thank you to my family – my parents, my brother, my sisters and their families for believing in me and providing me with endless love and support. To the new addition in my life, you are the one.

Thank you to all the past and present members of Larry's lab. A special thank you goes out to Bonnie Bullis, Heather Vandertol-Vanier and Yong Li for all their technical support. Thank you to Pratap Kirki for his friendship. I would also like to take the time to thank all our collaborators and their lab members.

And lastly, I am grateful to CIHR and AHFMR for funding my graduate studies and allowing me to pursue my love of science.

Table of Contents

Chapter 1 Introduction 1

1.1 Regulation of Intracellular pH in Mammalian Cells……2
1.1.1 Cellular Ionic Homeostasis in the Myocardium…….2
1.1.1.1 Protons……..2
1.1.1.2 Sodium and Calcium Ions..…….....4

1.2 NHE Family 8

1.2.1 NHE Subtypes and Distribution.....8
1.2.1.1 Plasma Membrane NHE Subtypes.....8
1.2.1.2 Intracellular NHE Subtypes.....9
1.2.1.3 Orphan NHE Subtypes 9

1.3 The Mammalian Cardiac-Specific NHE1 10

1.3.1 The Mammalian NHE1 Structure 10

1.4 NHE1 Inhibitors 13

1.5 NHE1 Regulation in the Myocardium.....14

1.5.1 Receptor Dependent Regulation of NHE1 15
1.5.1.1 G Protein Coupled Receptors 15
1.5.1.2 Other Receptors 18
1.5.2 Receptor Independent Regulation of NHE1 19
1.5.2.1 NHE1 Regulation Mediated by Direct Cofactor and Protein-Protein Interactions with the C-terminal Tail of NHE1 19
1.5.2.2 NHE1 Regulation Mediated by Indirect Cofactor and Protein-Protein Interactions with the C-terminal Tail of NHE1 21
1.5.3 NHE1 Regulation by Phosphorylation.....21
1.5.3.1 Direct Phosphorylation of NHE1.....21
1.5.3.2 Indirect Phosphorylation of NHE1 23
1.5.3.3 Dephosphorylation of NHE1 23
1.5.4 Developmental Regulation of NHE1 Expression 24

1.6 Physiological Roles of NHE1 24

1.6.1 Intracellular pH and Volume Regulation 24
1.6.2 Cell Growth, Progression, Differentiation and Apoptosis 25
1.6.3 Maintenance of Cytoskeletal Structure, Focal Adhesion and Cell Migration 26

1.7 NHE1 in the Myocardium 27

1.7.1 NHE1 and I/R Injury.....27
1.7.1.1 NHE1 Inhibitor Clinical Trials…… 29
1.7.2 NHE1 and Hypertension 32

1.7.3 NHE1 and Neurohormonal Activation 33
1.7.4 Cardiac Hypertrophy 33
1.7.4.1 NHE1 and Cardiac Hypertrophy 36
1.7.4.1.1 Direct Inhibition of Cardiac Hypertrophy by NHE1 Inhibitors 36
1.7.4.1.2 Inhibition of Autocrine, Paracrine and Hormonal Induced Cardiac Hypertrophy by NHE1 Inhibitors 37
1.7.4.1.3 Inhibition of Genetically Induced Cardiac Hypertrophy by NHE1 Inhibitors 38
1.7.4.1.4 NHE1 and Diabetes-Induced Cardiac Hypertrophy 38
1.7.4.2 NHE1 and Apoptosis 39
1.7.4.3 NHE1 and Congestive Heart Failure 40
1.7.5 NHE1 and Stem Cells 40

1.8 Other Pathophysiological Roles of NHE1 41

1.8.1 NHE1 and Cancer 41
1.8.2 NHE1 and Central Nervous System 42
1.8.3 NHE1 and Chronic Kidney Disease 42
1.8.4 NHE1 and Musculoskeletal 42

1.9 Thesis Objectives 43

Chapter 2 Materials and Methods 45

2.1 Transgenic Mice Expressing Cardiac-Specific NHE1 46

2.1.1 Construction of Wild Type Human NHE1-HA Tagged Plasmid 46
2.1.2 Construction of Active Human NHE1-HA Tagged Plasmid 46
2.1.3 Characterization of NHE1 Plasmid with the 1K3R4E Mutation 48
2.1.3.1 Cell Culture and Transient Transfection of AP-1 Cells 48
2.1.3.2 Western Blot Analysis of NHE1 in AP-1 Cells 49
2.1.3.3 Measurement of NHE1 Activity in Mammalian Cells 50
2.1.4 Construction of NHE1 Transgenic Mice 51
2.1.4.1 Identification of NHE1 Transgenic Mice 51

2.2 *In Vivo* Studies of NHE1 Transgenic Mice 52

2.2.1 Isolation of Adult Ventricular Cardiomyocytes from NHE1 Transgenic Hearts 53
2.2.1.1 Intracellular pH Measurements of Isolated Adult Ventricular Cardiomyocytes 54
2.2.1.2 Cell Area of Isolated Adult Ventricular Cardiomyocytes 54
2.2.2 Western Blot Analyses of Tissue from NHE1 Transgenic Mice 55
2.2.2.1 Immunoblot Analysis of Various Transgenic Tissues for Total and Exogenous NHE1 Protein Expression 55
2.2.2.2 Immunoblot Analysis of Transgenic Heart Lysates for Ion Regulatory Membrane Proteins 57
2.2.2.3 Immunoblot Analysis of Transgenic Heart Lysates for MAPK and RSK 57
2.2.2.4 Immunoblot Analysis of Transgenic Heart Lysates for Markers of Apoptosis 60
2.2.2.5 Immunoblot Analysis of Transgenic Heart Lysates for GSK-3β 63
2.2.2.6 Immunoblot Analysis of Transgenic Heart Lysates for ER Stress Response Proteins 65
2.2.3 Collection of NHE1 Transgenic Heart Specimens 65

2.2.3.1 HW/BW of NHE1 Transgenic Mice....65
2.2.3.2 Expression of ANP mRNA in Hearts from NHE1 Transgenic Mice....66
2.2.3.3 Histology of Hearts from NHE1 Transgenic Mice....69
2.2.3.4 Calcineurin Phosphatase Activity of Hearts from NHE1 Transgenic Mice....70
2.2.3.5 Electron Microscopy of Hearts from NHE1 Transgenic Mice....70
2.2.3.6 Measurement of Terminal Deoxynucleotidyl Transferase Mediated dUTP Nick End Labeling Staining in Hearts from NHE1 Transgenic Mice....71
2.2.3.7 Caspase-3 Activity of Hearts from NHE1 Transgenic Mice....72
2.2.4 Echocardiography of NHE1 Transgenic Mice....72
2.2.5 *In Vivo* Stimulation of NHE1 Transgenic Mice Using Alzet Osmotic Mini Pumps....73
2.2.5.1 Preparation of Alzet Osmotic Mini Pumps....73
2.2.5.2 Surgical Implantation of Alzet Osmotic Mini Pumps....74

2.3 *Ex Vivo* Working Heart Experiments of NHE1 Transgenic Mice....75

2.3.1 *Ex Vivo* Working Mouse Heart Perfusions....75
2.3.1.1 Measurement of Cardiac Function in Working Perfused Mouse Hearts....76
2.3.1.2 Measurement of Glycolysis, Glucose Oxidation and Fatty Acid Oxidation Rates in Working Perfused Mouse Hearts....77
2.3.1.3 Measurement of ATP Production Rates and TCA Cycle Acetyl CoA Production Rates in Working Perfused Mouse Hearts....78
2.3.1.4 Measurement of Proton Production in Working Perfused Mouse Hearts....78
2.3.2 Western Blot Analyses of Hearts Subjected to *Ex Vivo* Perfusions....79

2.4 *In Vitro* Experimentation using Isolated Neonatal Rat Ventricular Cardiomyocytes....79

2.4.1 Isolation of Neonatal Rat Ventricular Cardiomyocytes....79
2.4.2 Construction of Adenoviruses Expressing NHE1....81
2.4.2.1 Construction of NHE1 Inhibitor Resistant Plasmid....81
2.4.2.2 Construction of Active NHE1 Inhibitor Resistant Plasmid....83
2.4.2.3 Subcloning (Transferring) the cDNA of IRM and K-IRM Plasmids into the pAdTrack-CMV Plasmid....84
2.4.2.3.1 Characterization of pAdTrack-CMV Containing IRM or K-IRM in AP-1 cells....85
2.4.2.4 Generation of the Recombinant Adenoviral Plasmids Containing NHE1....85
2.4.2.5 Expansion, Precipitation, Purification, and Titration of Adenoviruses Containing NHE1....86
2.4.2.6 Determination of the Adenoviral Titer....88
2.4.3 Characterization of Neonatal Rat Ventricular Cardiomyocytes Infected with IRM or K-IRM Adenoviruses....89
2.4.3.1 Adenoviral Infection of Neonatal Rat Ventricular Cardiomyocytes....89
2.4.3.1.1 Determination of Adenoviral MOI for Neonatal Rat Ventricular Cardiomyocytes....90

2.4.3.2 Infection of Neonatal Rat Ventricular Cardiomyocytes with Adenoviruses....90
2.4.3.2.1 NHE1 Protein Expression of Infected Neonatal Rat Ventricular Cardiomyocytes....91
2.4.3.2.2. Measurement of Cell Surface Area of Infected Neonatal Rat Ventricular Cardiomyocytes....91
2.4.3.2.3 Protein Synthesis Rate Measurements of Infected Neonatal Rat Ventricular Cardiomyocytes....91

2.5 Statistical Analysis....92

Chapter 3 Activated NHE1 Induces Cardiac Hypertrophy in Female NHE1 Transgenic Mice Independent of Calcineurin and Mitogen Activated Protein Kinases 93

3.1 Introduction 94

3.2 Results 96

3.2.1 NHE1 Transgene Expression in N-line and K-line Hearts 96
3.2.2 Characterization of Constitutively Active NHE1 in AP-1 Cells 98
3.2.3 Characterization of N-line and K-line NHE1 Transgenic Mice 102
3.2.4 Developmental Expression of NHE1 in Mouse Hearts 104
3.2.5 NHE1 Activity of Adult Ventricular Cardiomyocytes Isolated from NHE1 Transgenic Hearts 106
3.2.6 Total Endogenous and Exogenous NHE1 Protein Expression of Hearts from NHE1 Transgenic Mice 108
3.2.7 Exogenous NHE1 Protein Expression in Hearts from NHE1 Transgenic Mice 110
3.2.8 *In Vivo* Characterization of Intact N-line and K-line Mouse Hearts for Cardiac Hypertrophy 112
3.2.9 Cardiac Function and Myocardial Remodeling of Control, N-line and K-line Mice 120
3.2.10 NHE1 expression in IRM and K-IRM Adenoviruses 125
3.2.11 Characterization of the pAdTrack CMV Plasmids in AP-1 Cells 125
3.2.12 Determination of the IRM and K-IRM Adenoviruses MOI 129
3.2.13 *In Vitro* Characterization of the IRM and K-IRM Adenoviruses for Myocyte Hypertrophy 131
3.2.14 Signaling Pathways Contributing to NHE1 Induced Cardiac Hypertrophy 139
3.2.15 Measurement of Indices of Apoptosis in Hearts from NHE1 TG Mice 148
3.2.16 Characterization of NHE1 Transgenic Mice Following Neuroendocrine Stimulation 157
3.2.17 Characterization of Cardiac Hypertrophy Following Neuroendocrine Stimulation in Neonatal Rat Ventricular Cardiomyocytes Infected with IRM or K-IRM Adenoviruses 168

3.3 Discussion 174

Chapter 4 Elevated Levels of Activated NHE1 Protect the Heart and Improve Myocardial Metabolism Following Ischemia/Reperfusion Injury 182

4.1 Introduction 183

4.2 Results 184

4.2.1 Preischemic and Postischemic Cardiac Function in *Ex Vivo* Working Mouse Hearts 184
4.2.2 Preischemic and Postischemic Rates of Glycolysis, Palmitate Oxidation and Glucose Oxidation in *Ex Vivo* Working Mouse Hearts 188
4.2.3 Preischemic and Postischemic ATP Production Rates in *Ex Vivo* Working Mouse Hearts 192
4.2.4 Preischemic and Postischemic Proton Production in *Ex Vivo* Working Mouse Hearts 195

4.2.5 Signaling Pathways Contributing to the NHE1 Induced I/R Effects in NHE1 Transgenic Mouse Hearts 195

4.3 Discussion 204

Chapter 5 Characterization of Male Transgenic Mice with Elevated NHE1 Expression 210

5.1 Introduction 211

5.2 Results 213

5.2.1 NHE1 Protein Expression of Male vs. Female NHE1 Transgenic Mice 213
5.2.2 Characterization of Cardiac Hypertrophy in Male vs. Female NHE1 Transgenic Mice 220
5.2.3 Effects of Neuroendocrine Stimulation on Cardiac Hypertrophy in Male NHE1 Transgenic Mice 232

5.3 Discussion 236

Chapter 6 Conclusions and Future Directions 240

6.1 Conclusions 241

6.2 Future Directions 250

6.2.1 NHE1 Loss of Function Model 250
6.2.2 Characterization of the Aging NHE1 Transgenic Mice 252
6.2.3 Modulation of Mediators Involved in NHE1 Regulation 255
6.2.5 Summary 256

Chapter 7 References 257

Appendix 1 Characterization of NHE1 Transgenic Mice Treated with NHE1 Inhibitors 291

A.1 Introduction 293

A.2 Results 294

A.2.1 Effects of EMD 87580, an NHE1 Inhibitor Administered Using Alzet Osmotic Mini Pumps, on the Cardiac Hypertrophic Phenotype in NHE1 Transgenic Mice 294

A.2.2 Effects of Administration of 700ppm EMD 87580 Mouse Chow on the Cardiac Hypertrophic Phenotype in NHE1 Transgenic Mice…….…….....297
A.2.3. Characterization of Control Mice Subjected to PE Stimulation in the Presence of EMD 87580 Chow 299

A.3 Discussion 301

A.4 References 304

List of Tables

Table I: Primary and secondary antibodies for the analysis of protein kinases..58

Table II: Antibodies used to detect markers of apoptosis. 62

Table III: Antibodies used for the detection of pGSK-3β and GSK-3β. 64

Table IV: Synthetic oligonucleotide primer sequences for real-time PCR analysis of ANP and 18S rRNA. 67

Table V: Real-time PCR conditions for ANP and 18S rRNA. 68

Table VI: Cardiac morphology and contractile function of controls, N-line and K-line mice.. 122

Table VII: Parameters of cardiac function in *ex vivo* working mouse hearts during aerobic perfusion (preischemia) and reperfusion (postischemia)..... 187

Table VIII: Echocardiographic analysis of male control, N-line and K-line mice.229

Table IX: Echocardiographic analysis of control, N-line and K-line mice, males vs. females.. 231

List of Figures

Figure 1.1. Schematic representation of a simplified ventricular cardiomyocyte and transporters/channels maintaining ionic homeostasis..... 7

Figure 1.2. Topology model of NHE1 displaying the N-terminal and C-terminal domains..... 12

Figure 1.3. G protein coupled receptor regulation of NHE1 in the myocardium. .. 17

Figure 1.4. Schematic representation of physiological and pathological cardiac hypertrophy..... 35

Figure 3.1. Gene construct used for the expression of the NHE1 protein in the mouse myocardium. 97

Figure 3.2. NHE1 protein expression of HA tagged-NHE1 in AP-1 cells. 99

Figure 3.3. Resting pH^i of AP-1 cells transfected with wild type NHE1 or constitutively active NHE1 (1K3R4E). 101

Figure 3.4. Tissue-specific protein expression of NHE1 in N-line and K-line mice. 103

Figure 3.5. Developmental expression of the NHE1 transgene in the intact myocardium of N-line and K-line hearts. 105

Figure 3.6. NHE1 activity of single isolated adult ventricular cardiomyocytes from control, N-line and K-line hearts. 107

Figure 3.7. Immunoblot analysis of total (endogenous and exogenous) NHE1 protein expression in control, N-line and K-line hearts. 109

Figure 3.8. Immunoblot analysis of exogenous HA tagged-NHE1 protein expression in control, N-line and K-line hearts. 111

Figure 3.9. Qualitative comparison of whole hearts and transverse heart cross sections stained with H&E from control, N-line and K-line mice. 113

Figure 3.10. Analysis of the HW/BW ratio in control, N-line and K-line mice. 115

Figure 3.11. Analysis of ANP mRNA expression in hearts from control, N-line and K-line mice. 117

Figure 3.12. Cross sectional area and interstitial fibrosis of control, N-line and K-line hearts..... 119

Figure 3.13. Adenovirus constructs used for the expression of NHE1 in neonatal rat ventricular cardiomyocytes..... 124

Figure 3.14. Western blot analysis of AP-1 cells transfected with pAdTrack CMV-IRM or pAdTrack CMV-K-IRM plasmids..... 126

Figure 3.15. NHE1 activity of AP-1 cells transfected with pAdTrack CMV-IRM or pAdTrack CMV-K-IRM in the presence (+) or absence (-) of EMD 87580. 128

Figure 3.16. MOI and time course of NHE1 protein expression in neonatal rat ventricular cardiomyocytes infected with the K-IRM adenovirus. 130

Figure 3.17. Western blot analysis of NHE1 protein expression in neonatal rat ventricular cardiomyocytes infected with IRM, K-IRM or GFP (control) adenoviruses. 132

Figure 3.18. Immunoblot analysis of exogenous HA tagged-NHE1 protein expression in lysates of neonatal rat ventricular cardiomyocytes infected with GFP, IRM or K-IRM adenoviruses. 134

Figure 3.19. Cell area of neonatal rat ventricular cardiomyocytes infected with IRM, K-IRM or GFP adenoviruses in the presence (+) or absence (-) of 10 μM EMD 87580. 136

Figure 3.20. Analysis of the rate of protein synthesis in neonatal rat ventricular cardiomyocytes infected with IRM, K-IRM or GFP adenoviruses in the presence (+) or absence (-) of 10 μM EMD 87580. 138

Figure 3.21. Western blot analysis of protein expression of ion transport and pH regulatory proteins in hearts from control, N-line and K-line mice.. 140

Figure 3.22. Western blot analysis of protein expression of MAPKs and RSK in hearts from control, N-line and K-line mice. 142

Figure 3.23. Western blot analysis of protein expression of GSK-3β in the cytosolic and mitochondrial fractions of hearts from control, N-line and K-line mice. 144

Figure 3.24. Calcineurin phosphatase activity in control, N-line and K-line mouse hearts. 146

Figure 3.25. Examination of TUNEL and electron microscopy in the left ventricles of control, N-line and K-line hearts..... 148

Figure 3.26. Analysis of caspase-3 activity of hearts from control, N-line and K-line mice 150

Figure 3.27. Analysis of Cyt c protein expression in the mitochondrial and cytosolic fractions of hearts from control, N-line and K-line mice. 152

Figure 3.28. Analysis of cleaved PARP protein expression in the cytosolic fraction of hearts from control, N-line and K-line mice. 154

Figure 3.29. Analysis of AIF protein expression in hearts from control, N-line and K-line mice. 156

Figure 3.30. Cell area of isolated adult ventricular cardiomyocytes from hearts isolated from control male mice treated with PBS (control) or PE.... 158

Figure 3.31. HW/BW ratio of control, N-line and K-line mice treated with PE or PBS control..... 160

Figure 3.32. Dry tissue weight to wet tissue weight ratio of hearts from control or K-line mice stimulated with PE or PBS. 162

Figure 3.33. Analysis of ANP mRNA expression in hearts from control, N-line and K-line mice treated with PE or PBS. 165

Figure 3.34. Analysis of CSA and IF in hearts from control, N-line and K-line mice stimulated with PE or PBS 167

Figure 3.35. Analysis of cell area in neonatal rat ventricular cardiomyocytes infected with IRM, K-IRM or GFP (control) adenoviruses in the presence (+) or absence (-) of 10 μM EMD 87580 and 10 μM PE. 170

Figure 3.36. Protein synthesis of neonatal rat ventricular cardiomyocytes infected with IRM, K-IRM or GFP (control) adenoviruses in the presence (+) or absence (-) of 10 μM EMD 87580 and 10 μM PE. 172

Figure 3.37. Schematic diagram of the role of active NHE1 expression in the myocardium. 176

Figure 4.1. Effects of wild type or active NHE1 expression on cardiac function in the *ex vivo* aerobically perfused and reperfused working mouse heart. 186

Figure 4.2. Rates of glucose oxidation, palmitate oxidation, and glycolysis in control, N-line and K-line hearts during preischemic and postischemic periods of the *ex vivo* working perfused hearts.. 191

Figure 4.3. Total ATP production rates and TCA cycle acetyl CoA production rates in control, N-line and K-line hearts during preischemic and postischemic periods of the *ex vivo* working perfused hearts. 194

Figure 4.4. Immunoblot analysis of total and phosphorylated AMPKα protein expression in control, N-line and K-line mouse hearts subjected to I/R.. 197

Figure 4.5. Western blot analysis of MAPKs and RSK in control, N-line and K-line mouse hearts subjected to I/R. 199

Figure 4.6. Western blot analysis of total and phosphorylated GSK-3β in control, N-line and K-line mouse hearts subjected to I/R..... 201

Figure 4.7. Immunoblot analysis of calreticulin and PDI in control, N-line and K-line mouse hearts. 203

Figure 4.8. Schematic representation of the role of active NHE1 expression during I/R. 209

Figure 5.1. Immunoblot analysis of total exogenous and endogenous NHE1 protein expression in hearts from male control, N-line and K-line mice..... 214

Figure 5.2. Immunoblot analysis of exogenous HA tagged-NHE1 protein expression in hearts from male control, N-line and K-line mice..... 215

Figure 5.3. Immunoblot analysis of total exogenous and endogenous NHE1 expression in hearts from control male and female mice. 217

Figure 5.4. Immunoblot analysis of total exogenous and endogenous NHE1 expression in hearts from K-line male and female mice. 219

Figure 5.5. HW/BW ratio of male and female control, N-line and K-line mice... 221

Figure 5.6. ANP mRNA expression of male and female hearts from control, N-line and K-line mice. 223

Figure 5.7. Cross sectional area of male and female heart cross sections from control, N-line and K-line mice. 225

Figure 5.8. Interstitial fibrosis of male and female heart cross sections from control, N-line and K-line mice. 227

Figure 5.9. HW/BW ratio of male and female control, N-line and K-line mice stimulated with PE or PBS 233

Figure 5.10. ANP mRNA expression of hearts from male and female control, N-line and K-line mice stimulated with PE or PBS 235

Figure A.1. HW/BW ratio and cross sectional area of male control and K-line mice treated with 10mg/kg/day EMD 87580. 295

Figure A.2. HW/BW ratio and cross sectional area of female control and K-line mice treated with 10mg/kg/day EMD 87580**.** 296

Figure A.3. HW/BW ratio of female control and K-line mice treated with control or EMD 87580 chow..... 298

Figure A.4. HW/BW ratio and cell area of adult ventricular cardiomyocytes in male control mice stimulated with PE, while being treated with control or EMD 87580 chow..... 300

Abbreviations

1K3R4E	Constitutively Active human Na^+/H^+ exchanger isoform 1-hemagglutinin tagged plasmid DNA
18S rRNA	18S ribosomal RNA
aa	Amino acid
α-MEM	Modified Eagle's medium, α-modification
A_1-receptor	Adenosine receptors
Ac-DEVD-pNA	Acetyl-Aspartic-Glutamic-Valine-Aspartic p-nitroanilide
AE	Na-independent Cl^--HCO_3^- exchanger, Anion exchanger
AIF	Apoptosis-inducing factor
Amp	Ampicillin
AMPK	Adenosine monophosphate (AMP)-activated protein kinase
Ang II	Angiotensin II
ANP	Atrial natriuretic peptide
AP-1	Chinese hamster ovary cell line deficient of NHE1
ARs	adrenoreceptors
ARVM	Adult rat ventricular cardiomyocytes
ATP	Adenosine 5'-triphosphate
BCECF-(*AM*)	2'-7'-bis(2-carboxyethyl)-5(6)-carboxyfluorescein *acetoxymethyl ester*
bp	base pair
BSA	Bovine serum albumin
$[Ca^{2+}]_i$	Intracellular Ca^{2+} concentration

CAII	Carbonic anhydrase II
CaM	Calmodulin
CaM Kinase II	Ca^{2+}/Calmodulin-dependent protein kinase II
cDNA	Complementary deoxyribonucleic acid
CH	Cardiac hypertrophy
CHE	Cl^--OH^- exchanger
CHF	Chronic end stage heart failure
CHP (#)	Calcineurin B homologous protein (*Isoform 1,2,3*)
CSA	Cross sectional area
CsCl	Cesium chloride
Cyt c	Cytochrome c
DAPI	4'-6-Diamidino-2-phenylindole
DMEM	Dulbecco's Modified Eagle's Medium
DNA	Deoxyribonucleic acid
dNTP	Deoxyribonucleoside triphosphate
DTT	Dithiothreitol
EDTA	Ethylenediaminetetraacetic acid
EGTA	Ethylene glycol tetraacetic acid
EMD/ EMD 87580	(N-[2-methyl-4,5-bis(methylsulfonyl)-benzoyl]-guanidine hydrochloride)
ER	Endoplasmic reticulum
ERK	Extracellular signal-related kinase
ERM	Ezrin, radixin and moesin

ET-1	Endothelin-1
FA	Fatty acid
FBS	Fetal bovine serum
GAPDH	Glyceraldehyde 3-phosphate dehydrogenase
GFP	Green fluorescent protein
GPCR	G protein coupled receptors
GSK-3β	Glycogen synthase kinase-3β
H&E	Hematoxylin and eosin
HA	Hemagglutinin
HBSS	Hanks buffered salt solution
HEK 293A	Human embryonic kidney 293A cell line
HEPES	N-2-hydroxyethylpiperazine-N'-2-ethanesulfonic acid
HW/BW	Heart weight to body weight ratio
I_{Na}	Na^+ current
IF	Interstitial fibrosis
IRM	Adenovirus containing inhibitor resistant wild type human Na^+/H^+ exchanger isoform 1-hemagglutinin tagged
I/R	Ischemia/reperfusion
JNK	c-Jun N-terminal kinase
Kan	Kanamycin
kb	kilobase
kDa	kilodalton
KHB	Krebs-henseleit bicarbonate solution

K-IRM	Adenovirus containing inhibitor resistant constitutively active human Na^+/H^+ exchanger isoform 1-hemagglutinin tagged
LB	Luria-Bertani
LF 2000	Lipofectamine™ 2000 reagent
LPA	Lysophosphatidic acid
MAPK	Mitogen activated protein kinase
MCT	Monocarboxylate transporters
α-MHC	α-myosin heavy chain
MI	Myocardial infarction
MnSOD	Mitochondrial superoxide dismutase
MOI	Multiplicity of infection
mRNA	Messenger ribonucleic acid
$[Na^+]_o$	Extracellular Na^+ concentration
$[Na^+]_i$	Intracellular Na^+ concentration
N-line	Transgenic mice expressing wild type human Na^+/H^+ exchanger isoform 1-hemagglutinin tagged
NBC	Na^+-HCO_3^- exchanger
NCX	Na^+/Ca^{2+} exchanger
NHE (#)	Na^+/H^+ exchanger (*isoform #)*
NKA	Na^+/K^+-ATPase
NRVM	Neonatal rat ventricular cardiomyocyte
PA	Polyadenylation
PARP	Poly-(ADP-ribose) polymerase

PBS	Phosphate buffered saline
PCR	Polymerase chain reaction
PCI	Phenol:chloroform: isoamyl alcohol
PDI	Protein disulfide isomerase
PE	Phenylephrine
pERK	Phosphorylated extracellular signal-regulated kinase
PFU	Plaque formation units
pH_i	Intracellular pH
PIP_2	Phosphatidylinositol 4,5-bisphosphate
pJNK	Phosphorylated-c-Jun N-terminal kinase
PKB	Protein Kinase B (AKT protein family)
PP 1	Protein phosphatase 1
PP2A	Protein phosphatase 2A
PP2B	Protein phosphatase 2B (Calcineurin)
p38	p38 mitogen activated protein kinase
pGSK-3β	Phosphorylated-glycogen synthase kinase-3β
pp38	Phosphorylated-p38 mitogen activated protein kinase
pRSK	Phosphorylated p^{90} ribosomal S6 kinase
PSR	Picrosirius red
RSK	p^{90} ribosomal S6 kinase
SDS-PAGE	Sodium dodecyl polyacrylamide gel electrophoresis
SEM	Standard error of the mean
SERCA	Sarcoendoplasmic reticulum Ca^{2+}-ATPase

Tdt	Terminal deoxynucleotidyl transferase
TM	Transmembrane
TG	Transgenic
TCA	Tricarboxylic acid
TUNEL	Terminal deoxynucleotidyl transferase mediated dUTP nick end labeling
UPR	Unfolded protein response
VGSC	Voltage-gated Na^+ channels
VSMCs	Vascular smooth muscle cells

Chapter 1

Introduction

1.1 Regulation of Intracellular pH in Mammalian Cells

Maintaining pH in mammalian cells is essential for a number of physiological processes such as cell growth, differentiation, and migration. If pH is not maintained, intracellular acidosis inhibits the activity of a variety of enzymes, and therefore various aspects of cell metabolism. Thus, numerous mechanisms exist to regulate proton flux at the plasma membrane. The Na^+/H^+ exchanger (NHE) is a major pH-regulating system in mammalian cells[13,154]. The family of NHE proteins are membrane proteins that exchange one intracellular proton (H^+) for one extracellular sodium ion (Na^+). Since the NHE removes one intracellular H^+ in exchange for one extracellular Na^+, it is also involved in volume regulation in mammalian cells. When cell shrinkage occurs, extracellular Na^+ and Cl^- are brought into the cell[154]. Thus, NHE plays a central role in important housekeeping functions in mammalian cells.

1.1.1 Cellular Ionic Homeostasis in the Myocardium

In the myocardium, regulation of the concentration of $[H^+]$, $[Na^+]$, and calcium $[Ca^{2+}]$ ions within the physiological range is of vital importance to maintaining excitability, contractility, and cell volume in cardiac myocytes, which are essential for the functioning of the heart.

1.1.1.1 Protons

The fundamental energy transduction machinery of cells is fueled by both aerobic and anaerobic metabolism, both of which generate H^+. The approximate molar concentration of dissolved H^+, the pH, determines the charge state of weak acids and

bases. This in turn affects many physical and physiological properties of biological molecules, activity of a variety of enzymes, and therefore, various aspects of cell metabolism[1]. With constant H^+ production and changes as small as 0.1 pH units in intracellular pH (pH_i) inducing physiological consequences, maintenance of pH is essential.

In the heart, it has been known since the late 1800s that enhanced intracellular H^+ accumulation decreases the heart's strength of contraction. Since then it has become clear that changes in pH_i in the heart exert a major influence on electrical excitation, ion homeostasis, intracellular signaling and myofilament sliding[2-5]. Therefore, it is no surprise that cardiomyocytes possess a sophisticated pH_i regulatory system. Five generic types of H^+ transport proteins have been identified in the mammalian ventricular cardiomyocyte, two of which are involved in H^+ efflux and three of which are involved in H^+ influx, and used to protect the cell from severe acid or alkali over-load (reviewed in[6,7]). A similar arrangement has also been identified in purkinje fibers[8-12]. Figure 1.1 is a schematic diagram demonstrating H^+ transporters, amongst other transporters, in a ventricular cardiomyocyte. H^+ efflux, activated by a fall in pH_i, is mediated by the NHE[13] and the Na^+-HCO_3^- cotransporter (NBC)[14]. H^+ influx, activated by a rise in pH_i, is mediated by the Na-independent Cl^--HCO_3^- exchanger (Anion exchanger, AE)[15] and Cl^--OH^- exchanger (CHE)[16]. NHE is Na^+ selective and uses the inwardly directed electrochemical Na^+ gradient generated by the Na^+-K^+ ATPase (NKA) to export H^+ in an electroneutral manner[17]. Another well-characterized H^+ transporter is the NBC, which translocates Na^+ and HCO_3^- into the cell independent of the transmembrane potential and dependent on the combined chemical gradient[17]. The HCO_3^- moved into the cell through

NBC combines with intracellular H^+, generating CO_2 that diffuses out of the cell. As for H^+ loading transporters, the AE facilitates transport of HCO_3^- out of the cell in exchange for Cl^-, with normal Cl^- concentrations gradient (high outside, low inside) providing the driving force for the net HCO_3^- efflux[17]. CHE transports Cl^- into the cell in exchange for OH^-. Its activity is Cl^- dependent, Na^+-independent, and is activated by low extracellular pH (pH_o) and high pH_i[18]. Lastly, the monocarboxylate transporters (MCT), which are not widespread and limited to some skeletal muscle and solid tumors, mediate the co-transport of monocarboxylic acids (predominantly lactate) and H^+. MCT operates in either efflux or influx mode[10,17,19]. In muscle, the MCT operates in efflux mode and accounts for up to 40% of the recovery of pH_i following ischemic acidosis.

Of all the H^+ transporters discussed, NHE1 plays the most essential role in the maintenance of pH_i homeostasis in the perfused heart and is responsible for 50-60% of H^+ efflux[20]. The remaining percentage of total H^+ efflux is mostly mediated by the HCO_3^- based transporters[20-22]. This was determined by perfusing hearts in the presence and absence of HCO_3^-.

1.1.1.2 Sodium and Calcium Ions

Mammalian cells maintain a large electrochemical gradient of Na^+ across the plasma membrane. Intracellular Na^+ concentrations ($[Na^+]_i$) are kept low (4-14 mM), while extracellular Na^+ concentrations ($[Na^+]_o$) are approximately 140 mM[23]. $[Na^+]_i$ is very important in modulating intracellular Ca^{2+} concentrations ($[Ca^{2+}]_i$). In many cells the electrochemical Na^+ gradient is used as a secondary active transporter, by coupling energetically unfavorable transmembrane solutes to Na^+ transport (Na^+/neurotransmitter, Na^+/glucose and Na^+/amino acids cotransporters)[23].

In the heart, an increase in $[Na^+]_i$ has been suggested to contribute to I/R injury[24-26] and heart failure[27-29]. Na^+ influx into cardiomyocytes occurs mainly through voltage-gated Na^+ channels (VGSC), which mediate the Na^+ current (I_{Na}), NCX and NHE activity. Na^+ efflux occurs through NKA. Figure 1.1 is a schematic representation of a cardiomyocyte expressing I_{Na}, NCX, NHE and NKA. Other transporters including NBC**,** $Na^+/K^+/2Cl^-$ cotransporter and Na^+/Mg^{2+} exchanger have also been shown to bring in smaller amounts of Na^+[30]. VGSC mediates the I_{Na} during the upstroke of the cellular action potential. NHE brings in approximately 2 μmol/L of Na^+ at physiological pH_i and approximately 16 μmol/L during intracellular acidosis[30]. NCX couples $[Na^+]_i$ and $[Ca^{2+}]_i$. The NCX can operate in both the forward-mode (Ca^{2+} extrusion/Na^+ entry) and reverse-mode (Ca^{2+} entry/Na^+ extrusion) depending on the internal and external concentrations of both Na^+ and Ca^{2+}, and the membrane potential. NKA, the main Na^+ extruder, pumps Na^+ out of the cell against a concentration gradient using the energy released by ATP hydrolysis. Na^+ is pumped out of the cell in exchange for K^+ in an electrogenic process ($3Na^+:2K^+$), thus keeping $[Na^+]_i$ constant. Proper regulation of Na^+ is essential, since it is capable of influencing the transfer rates and distribution of Ca^{2+} among the intracellular compartments of cardiomyocytes. Ca^{2+} enters the cell via the L-type Ca^{2+} channel and is linked to Na^+ regulation via NCX, which is the primary mechanism for Ca^{2+} efflux in cardiomyocytes[23]. Ca^{2+} is used as a signaling molecule in many cell types, from prokaryotes to eukaryotes, controlling virtually every cell function, from motility to cell death. In the myocardium, Ca^{2+} is a well known central player in cardiac cell physiology, mediating Ca^{2+} activation of myosin ATPase and contraction, stimulating Ca^{2+} activated signaling pathways and modulating mitochondrial energy production[31]. An increase in

$[Ca^{2+}]_i$ can alter excitation-contraction coupling, contribute to the generation of arrhythmias, activate proteases, and alter bioenergetics or apoptotic pathways in the mitochondria[30].

The interplay of Na^+, Ca^{2+} and H^+ in the heart is clearly demonstrated at the onset of cardiac ischemia, which activates anaerobic metabolism, contributing to intracellular acidification and a decrease in NKA activity[32]. This decrease in pH_i contributes to enhanced Na^+ influx into cardiomyocytes through NHE1, the cardiac specific NHE isoform. This rise in $[Na^+]_i$ induces the operation of NCX in reverse-mode or reduces the activity of NCX in forward-mode, with Ca^{2+} entering the cell and causing the cytoplasmic and mitochondrial compartments to load with Ca^{2+}[33]. Cellular Ca^{2+} overload contributes to postischemic electrical and contractile dysfunction and cell death[31]. Thus, targeting NHE1, the source of increased $[Na^+]_i$ induced by an increase in H^+ accumulation, and understanding its role in cardiac disease is essential for the prevention of cardiac dysfunction, and is the focus of our study.

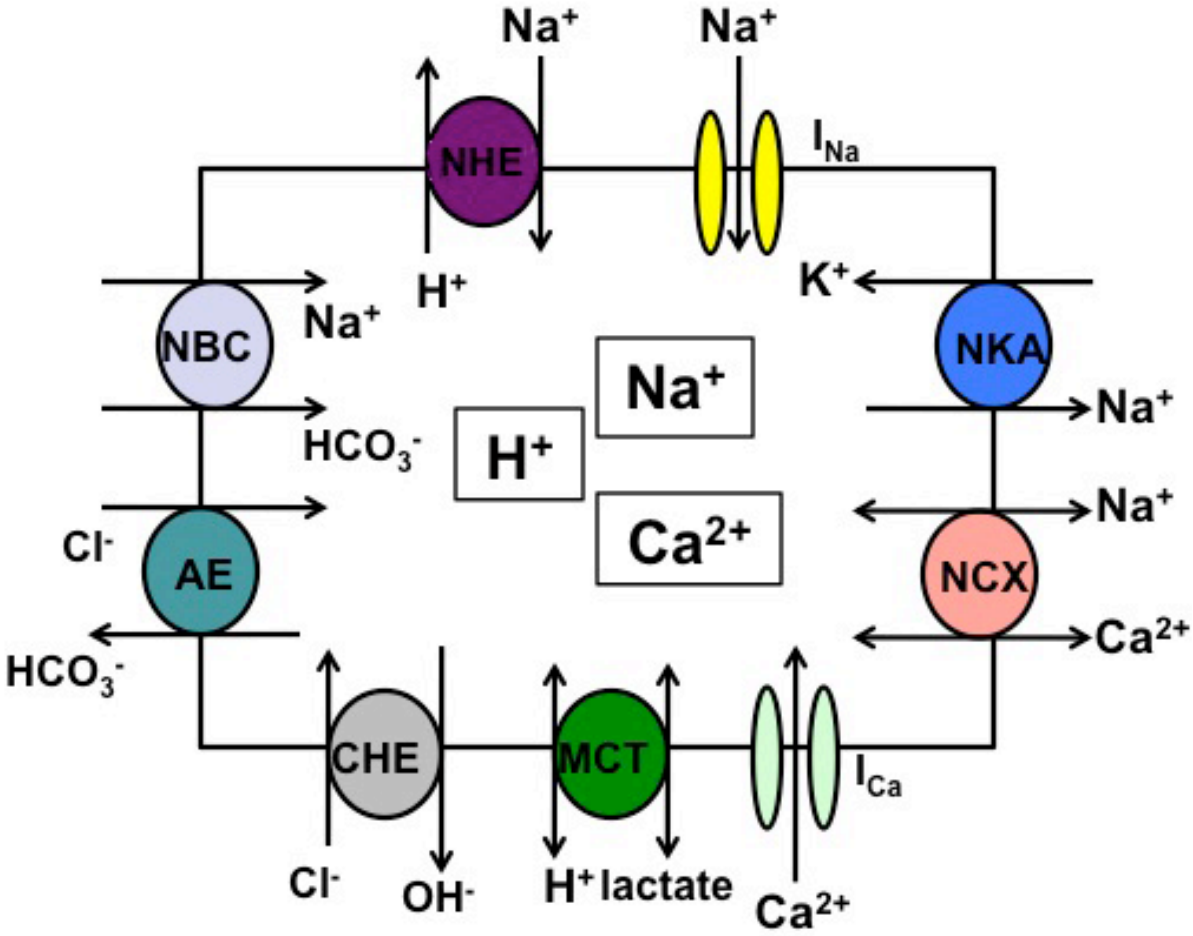

Figure 1.1. Schematic representation of a simplified ventricular cardiomyocyte and transporters/channels maintaining ionic homeostasis. Na^+ influx is mediated by NHE, NCX (forward-mode) and VGSCs (which mediate the I_{Na}); Na^+ efflux is mediated by NKA and NCX (reverse-mode). H^+ efflux is mediated by NBC, NHE and MCT (efflux mode). H^+ influx occurs through AE, CHE and MCT (influx mode); Ca^{2+} influx occurs through Ca^{2+} channels (which mediate the Ca^{2+} current (I_{Ca})) and NCX (reverse-mode); Ca^{2+} efflux occurs through NCX (forward-mode).

1.2 NHE Family

NHE was originally cloned in 1989 by Dr. J. Pouyssegur[34] and has been suggested to be one of the most primative transport systems[35]. Ten isoforms of NHE (NHE1-10) have been identified, which share 20-60% amino acid identity and a calculated molecular weight ranging from ~74kDa to 93kDa (reviewed in[36,37]). NHE isoforms are composed of 12 helical hydrophobic membrane spanning segments, a N-terminal and C-terminal segment. Despite the shared identity between isoforms, each isoform represents a distinct gene product with its own specific pattern of tissue expression, membrane localization, kinetic properties, physiological roles, and sensitivities to pharmacological inhibitors.

1.2.1 NHE Subtypes and Distribution

1.2.1.1 Plasma Membrane NHE Subtypes

NHE1, first described by Sardet et al., is ubiquitously expressed in the plasma membrane and is the primary isoform found in the heart[34,38-41]. NHE2-NHE5 isoforms are also localized to the plasma membrane, but have more restricted tissue distribution. NHE2, which is thought to mainly function in secretory processes, has been shown to be localized in the stomach, colon and small intestine[42-45]. Lower levels of NHE2 have also been detected in skeletal muscle and selected nephron segments. NHE2 was also very faintly detected in the rat myocardium[46]. NHE3, essential for absorptive processes that influence systemic electrolyte, acid-base, and blood pressure homeostasis, is mainly expressed in the colon, small intestine, kidney, stomach and in recycling endosomes[47-49].

NHE4 has a similar role to NHE1. It is highly abundant in the stomach and also present in the small intestine, the colon and basolateral membrane of collecting tubule[46]. NHE5, which has been speculated to modulate the acidity of synaptic vesicles, is expressed predominantly in nonepithelial tissue such as the brain[50-52]. A lower level of NHE5 expression has also been found in the spleen, testis and skeletal muscle.

1.2.1.2 Intracellular NHE Subtypes

NHE6-9 are ubiquitously expressed and are distributed to intracellular compartments[53]. These organellar membrane NHEs are presumed to regulate luminal pH and cation concentrations of the intracellular compartments[53]. NHE6 is localized to recycling endosomes and mitochondria rich tissue including the heart, brain, and skeletal muscle[53,54]. NHE7, which is located in the trans-Golgi network, differs from other NHE isoforms in that it mediates the influx of either Na^+ or K^+ in exchange for H^+[55]. NHE8 is mainly localized to the mid- to trans-Golgi compartments, but has also been found in skeletal muscle and kidney[53]. NHE9 isoform is localized to late recycling endosomes[53].

1.2.1.3 Orphan NHE Subtypes

The most recent NHE isoform, NHE isoform 10, is highly expressed in osteoclasts and is required for osteoclast differentiation and survival[37]. Another NHE has also been identified in the sperm and appears to be essential for sperm motility and male fertility[56,57].

1.3 The Mammalian Cardiac-Specific NHE1

NHE1, the focus of our study, is the most well characterized and only plasma membrane isoform present in the myocardium[34,38,39,41]. It resides exclusively on the plasma membrane, but also accumulates in discrete microdomains of the plasma membrane. NHE1 is localized primarily at the intercalated disk regions of atrial and ventricular myocytes in close proximity to connexin 43, and to a lesser extent at the transverse tubule systems[40]. It has also been found to concentrate along the borders of lamellipodia in fibroblasts[58] and the basolateral membrane of epithelia[59].

NHE1 removes one intracellular H^+ in exchange for one extracellular Na^+ and is acutely regulated by pH_i[60]. Under physiological conditions, NHE1 basal activity is low. As the $[H^+]$ of the cytosol increases, the activity of the transporter increases sharply and achieves near maximal velocity at approximately one pH unit below the physiological pH of 7.4[17]. This activation exhibits a Hill coefficient of around three, indicating that more than one H^+ binds to NHE1 to regulate activity[61]. The inward directed Na^+ gradient, which is maintained by the activity of NKA and NCX, provides a constant driving force for H^+ extrusion[35]. NHE1 exhibits simple Michaelis-Menten dependence on extracellular Na^+, with a reported apparent K_m of 5-50 mM[42]. Such activation of NHE1 ensures minimal exposure of the cytoplasm to excess acidification[62, 63].

1.3.1 The Mammalian NHE1 Structure

Relatively little is known about the tertiary structure of NHE1, however, some understanding of the general structure has been gained using hydropathy analysis, cysteine accessibility analysis, phylogenetic and empirical data. The human NHE1

cDNA is predicted to be an 815 amino acid protein, with the first 500 residues consisting of an N-terminal membrane domain and the remaining 315 residues consisting of a C-terminal cytoplasmic regulatory domain[38]. In 2000, Wakabayashi et al. suggested that NHE1 has 12 transmembrane (TM I-XII) segments with both the N- and C-terminius located in the cytosol[64]. The NHE1 transmembrane segments of the N-terminal have a crucial role in the function of the transport protein (ion binding and transport and inhibitor sensitivity). The C-terminal cytosolic domain is also important, as it regulates the membrane domains ion exchange activity and is the site of phosphorylation, cofactor and protein interactions.

The presence of a H^+ modifier site, which induces NHE1 activation upon binding to a H^+, has been suggested by Wakabayashi et al.[65]. The H^+ modifier site is not yet fully identified, though mutation of several amino acids could affect its function[66].

NHE1 has also been shown to be post-translationally modified with *N*- and *O*-linked glycosylations[67,68]. Thus, resulting in two forms of NHE1 when separated by sodium dodecyl polyacrylamide gel electrophoresis (SDS-PAGE), a 110 kDa and a 85 kDa band, representing the fully glycosylated mature protein and an immature partially or non-glycosylated protein, respectively. However, *N*-linked glycosylation can be removed without affecting NHE1 function[67].

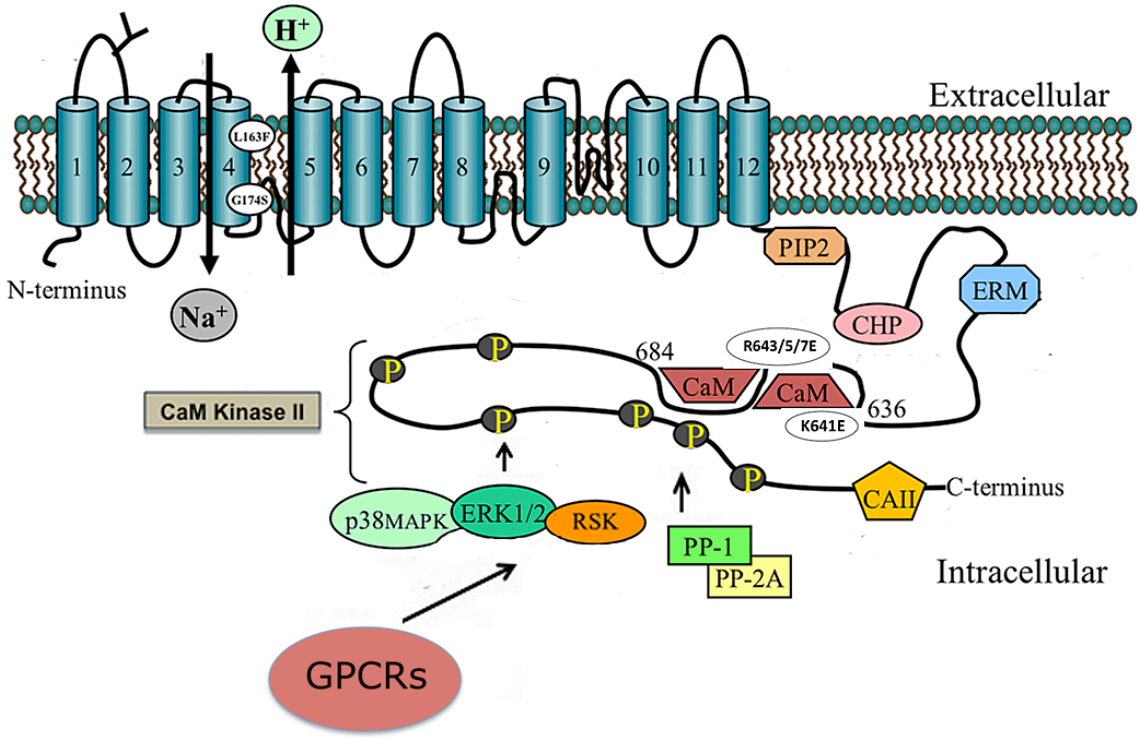

Figure 1.2. Topology model of NHE1 displaying the N-terminal and C-terminal domains. Transmembrane segment 4 of the N-terminal domain contains the sites of mutation used to create an inhibitor resistant NHE1 (IRM); leucine (L) 163 mutated to phenylalanine (F) (L163F) and glycine (G) 174 mutated to serine (S) (G174S). The C-terminal domain displays the major sites of phosphorylation, cofactor and protein interactions. PIP2, phosphatidylinositol 4,5-bisphosphate; CHP, calcineurin homologous protein; ERM, ezrin, radixin, moesin; CaM, calmodulin; CAII, carbonic anhydrase II; ERK 1/2, extracellular signal regulated kinase 1/2; RSK, p^{90} ribosomal S6 kinase; p38 MAPK, p38 mitogen activated protein kinase; CaM Kinase II, Ca^{2+}/Calmodulin-dependent protein kinase; PP1, protein phosphatase 1; PP2A, protein phosphatase 2A and GPCRs, G-protein coupled receptors. The C-terminal tail also displays the sites of mutations used to generate an active NHE1 (1K3R4E); lysine (K) 641 and arginine (R) 643/645/647 all mutated to glutamic acid (E).

1.4 NHE1 Inhibitors

Numerous NHE inhibitors have been developed since the discovery of NHE, with particular focus on NHE1 selectivity and potency. Amiloride (3,5 diamino-6-chloro-N (diaminomethylene)pyrazine-carboxamide), a K^+ sparing diuretic, was the first drug identified as an NHE1 inhibitor. In addition to its ability to inhibit NHE1, it also inhibits conductive Na^+ channels, NCX and other isoforms of NHE, including NHE2 and 5, but does not inhibit NHE3, 4 and 7 very well[69]. The first generation of amiloride analogues, the pyrazine derivatives, which includes DMA (dimethylamiloride), EIPA (5-(N-ethyl-N-isopropyl) amiloride), MIBA (5-(N-methyl-N-isobutyl) amiloride) and HMA (5-(N, N-hexamethylene) amiloride), were developed at a later stage in effort to increase the potency and selectivity of NHE1 inhibitors[70]. These pyrazine derivatives are more potent and specific than amiloride, and are not potent inhibitors of conductive Na^+ channels and NCX. Their potency for the various NHE isoforms are as follows: NHE1>NHE2>NHE5>NHE3[70]. The lack of specificity within this class lead to the development of another class of NHE1 inhibitors, the benzoylguanidine derivatives, another form of modified analogs of amiloride. Inhibitors that fall into this category include EMD 87580 (N-[2-methyl-4,5-bis(methylsulfonyl)-benzoyl]-guanidine hydrochloride)[71], HOE-694 ((3-methylsulphonyl-4-piperidinobenzoyl]-guanidine hydrochloride)[72], cariporide (HOE-692)[73], eniporide (EMD 85131)[74] and BIIB 513[75], all of which are more selective towards NHE1[70]. They still exhibit a slight efficacy for NHE2 inhibition, but little inhibition of NHE3 or 5. It has also been suggested that HOE-694 inhibits conductance Na^+ channels[76]. Cariporide and eniporide were used in clinical trials. Despite their improved selectivity and potency, they resulted in only minimal

beneficial effects in specific subgroups of the study[77,78]. This lead to another generation of NHE1 inhibitors which include KR-32511 ([5-(4-Fluorophenyl) furan-2-yl carbonyl]guanidine), KR-33028 (4-cyano (benzo[b]thiophene-2-carbonyl)guanidine) and KR-32570 ([5-(2-methoxy-5-chlorophenyl) furan-2-yl carbonyl]guanidine)[79-81]. These inhibitors show no inhibitory effects on NHE3 or conductance Na^+ channels, but a very slight inhibitory effect on NHE2[82]. The order of potency of these inhibitors relative to the benzoylguanidine derivatives were KR-32570≥KR-33028>cariporide>KR-32511[82]. Quite recently, a novel series of substituted (quinolinecarbonyl) guanidine derivatives were designed and synthesized as NHE1 inhibitors, including compound 7f. Compound 7f was shown to be 23 times more potent than cariporide. *In vivo*, rat hearts subjected to I/R in the presence of compound 7f showed superior cardioprotective outcomes when compared to groups treated with cariporide[83]. Further studies are required to determine the sensitivity of these inhibitors to other NHE isoforms, channels and exchangers.

Although the NHE inhibitors discussed lack complete selectivity and potency, all of the inhibitors do show selectivity to NHE1. The benzoylguanidine derivatives are commonly used as tools to understanding the role of NHE1. However, pharmacological inhibitors quite often lack absolute selectivity and potency. Therefore, when attempting to understand the mechanisms of a disease, a need for a gain of function or loss of function model is essential to confirm data obtained via pharmacological tools.

1.5 NHE1 Regulation in the Myocardium

Regulation of NHE1 has been investigated in a number of *in vivo* and *in vitro* models, in a number of systems. Understanding how NHE1 is regulated is of particular

importance, as it aids in the elucidation of mechanisms that induce NHE1 activation or inhibition and means to prevent/stimulate these regulators. The major regulatory stimulus for NHE1 is intracellular acidosis[60]. The relationship between pH_i and sarcolemmal NHE1 activity is steep in cardiomyocytes[84]. In adult rat ventricular cardiomyocytes (ARVMs), a 2.5-fold increase in intracellular $[H^+]$ concentration, indicative of a reduction in pH from 6.90 to 6.50, has been shown to produce an approximate 7 fold increase in sarcolemmal NHE1 activity[84]. Extension of the duration of intracellular acidosis (to ≥3 min) also produces a marked increase in sarcolemmal NHE1 activity in both neonatal rat ventricular cardiomyocytes (NRVMs) and ARVMs[85,86]. Additional regulation of NHE1 activity occurs in response to various hormonal, autocrine and paracrine stimuli, which act through receptor dependent pathways (reviewed in[87]). This interaction may involve phosphorylation/dephosphorylation of NHE1 upon receptor binding. NHE1 is also regulated by receptor independent pathways, which are mediated by cofactors or protein-protein interactions, that act either directly or indirectly with NHE1. Development and transcriptional regulation of NHE1 have also been identified.

1.5.1 Receptor Dependent Regulation of NHE1

1.5.1.1 G Protein Coupled Receptors

NHE1 activity is regulated by activation of G protein coupled receptors (GPCRs) induced by various extracellular receptor agonists (Figure 1.2). GPCRs are seven transmembrane helices, with an extracellular domain involved in ligand binding and an intracellular domain involved in the recognition and activation of G (guanine-nucleotide

binding) proteins[88]. G-proteins consist of α, β, and γ subunits. Upon GPCR coupling, the G-protein converts GTP to GDP on its α subunit, resulting in the dissociation of the Gα from the Gβγ subunits to mediate downstream signaling[89,90]. The four primary families of Gα-proteins include $G\alpha_s$, $G\alpha_i$, $G\alpha_q$, and $G\alpha_{11/12}$[89]. Activation of $G\alpha_q$ has been shown to stimulate NHE1 activity, while activation of $G\alpha_s$ and $G\alpha_i$ have been shown to inhibit NHE1 activity (reviewed in[61]). A simplified diagram of GPCR receptor regulation of NHE1 is illustrated in Figure 1.3.

$G\alpha_q$ is activated by various hormones and paracrine/autocrine stimuli. α_1-adrenoreceptors (ARs) activate $G\alpha_q$ signaling upon stimulation with α_1-AR agonists such as phenylephrine (PE), thus translating chemical messages from the sympathetic nervous system into cardiovascular responses. Angiotensin II (Ang II), a peptide that stimulates vascular smooth muscle contraction, aldosterone release, and production of extracellular matrix proteins, also signals via $G\alpha_q$ and is coupled to Ang II receptor type 1[91]. Endothelin-1 (ET-1), a powerful vasoconstrictor, a chronotropic, inotropic, and hypertrophic promoting growth factor, also signals via the $G\alpha_q$ and is coupled to the ET-1 receptor type A[92]. Stimulation with α_1-AR agonists[93,94], or Ang II[95,96], or with ET-1[97,98] shifts the pH_i/NHE1 activity relationship to the right, thus raising the pH_i threshold for NHE1 activation. In the myocardium, regulation of NHE1 mediated by α_1-ARs is the most characterized.

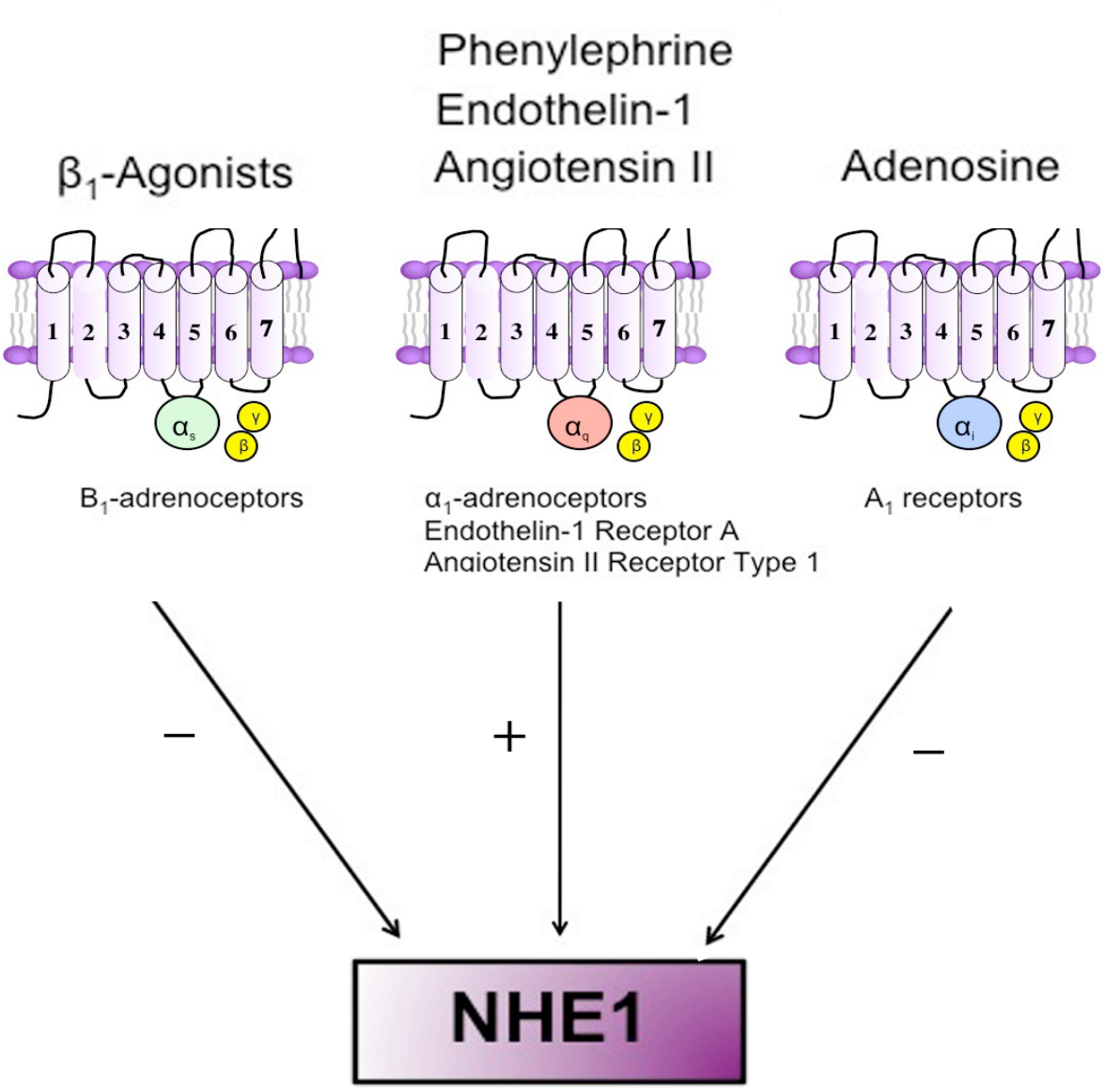

Figure 1.3. G protein coupled receptor regulation of NHE1 in the myocardium. NHE1 activity is stimulated (+) by activation of $G\alpha_q$ coupled receptors (α_1-adrenoreceptors. endothelin-1 receptor A, angiotensin II receptor type 1) upon activation with corresponding agonists (phenylephrine, endothelin-1 and angiotensin II). NHE1 activity is inhibited (-) by activation of $G\alpha_s$ and $G\alpha_i$ coupled receptors (β_1-adrenoreceptors, adenosine receptors (A_1 receptors), respectively) upon stimulation with corresponding agonists (β_1-agonists and adenosine, respectively).

1.5.1.2 Other Receptors

In addition to the effects mediated by GPCRs on NHE1 stimulation in the myocardium, a number of other less characterized receptor mediated pathways have been identified. These receptor mediated pathways are stimulated by aldosterone, thrombin and lysophosphatidic acid (LPA).

Aldosterone has traditionally been seen as a key regulator of fluid and electrolyte balance, acting via the mineralocorticoid receptor, a member of the steroid hormone receptor family found in non-epithelial (vessel, heart, and brain) and epithelial tissue[103]. In addition to identifying mineralcorticoid receptors in the heart, aldosterone has been shown to be synthesized in the hearts of patients with heart failure or hypertension[104,105]. NRVMs stimulated with aldosterone increase NHE1 activity and expression.

Thrombin induces a variety of cellular responses in addition to its established role in blood coagulation and thrombus formation, through the thrombin receptor[106]. A number of cell types within the cardiovascular system including platelets, endothelial cells, and vascular smooth muscle cells have been shown to express the thrombin receptor[61]. With respect to the cardiac myocyte, thrombin was shown to increase sarcolemmal NHE1 activity[106].

LPA is a bioactive phospholipid that mediates its signal through the LPA receptor. It is a cardiotoxic metabolite that has been shown to stimulate NHE1 activity[107]. Inhibition of NHE1 in isolated rat hearts subjected to low concentrations of LPA protected the myocardium against mechanical, biochemical and ultrastructural impairments[108].

1.5.2 Receptor Independent Regulation of NHE1

In addition to the receptor dependent mechanisms, NHE1 is also regulated by a number of receptor independent pathways. The receptor independent regulation of NHE1 involves protein-protein interactions, either directly or indirectly, with the C-terminal tail of NHE1 (Figure 1.2).

1.5.2.1 NHE1 Regulation Mediated by Direct Cofactor and Protein-Protein Interactions with the C-terminal Tail of NHE1

Phosphatidylinositol 4, 5-bisphosphate (PIP_2), which converts to inositol 1,4,5-triphosphate and diacylglycerol, has been identified as a stimulator of NHE1. It has been suggested that association of NHE1 with PIP_2 is required for optimal NHE1 activity[109]. PIP_2 has two binding motifs at amino acids 509-516 and 552-560 in the C-terminal tail of NHE1[109].

Calcineurin homologous proteins (CHP) are Ca^{2+}-binding proteins, which share a 40% identity with the protein phosphatase calcineurin[110]. Three isoforms of CHP have been identified, CHP1-3, which exhibit approximately a 29-61% identity to each other[110]. The CHP family is crucial for basal as well as regulated activity of NHE1[110,114]. CHP1 is present in most tissues, and binds to the proximal region of the cytoplasmic C terminus of NHE1. CHP1 plays a significant role in setting the resting pH_i and activating NHE1 in response to various stimuli[111]. Our laboratory has shown that the CHP1 protein is present in the myocardium, and that NHE1 activity was not increased in NRVMs over-expressing CHP1 (unpublished data). CHP2 is largely restricted to normal intestinal epithelia and is highly expressed in tumor cells[112]. CHP2 interacts with the same region of NHE1 as

CHP1, and results in a marked elevation in steady state pH_i. Although CHP2 mRNA has been detected in the myocardium, the role of CHP2 in the myocardium remains unknown[112]. CHP3 is detected predominantly in the adult mouse heart, brain and stomach. In adult human tissues, CHP3 appears to be restricted to the heart[113]. CHP3 was also found to bind to the same region of the cytoplasmic C terminus of NHE1 as CHP1 and CHP2, and is crucial for optimal NHE1 function[110]. The role of CHP3 in the myocardium remains unknown.

Calmodulin (CaM) is another Ca^{2+} binding protein found in many cell types, including the heart[115]. Two CaM binding sites have been identified on the C-terminal tail of NHE1[115]. The high affinity site consists of residues 636-656, and the low affinity site consists of residues 657-700. In the absence of CaM bound Ca^{2+}, the high affinity CaM binding site interacts with another region of NHE1, resulting in autoinhibition of NHE1[116]. Addition of CaM bound Ca^{2+} reverts this interaction and produces an active NHE1[115]. Deletion of the high affinity CaM binding site has been shown to stimulate NHE1 and mimics elevated intracellular Ca^{2+}[115]. Additionally, there are seven conserved amino acids in the distal region of NHE1's cytoplasmic tail 753-759 (EEDEDDD) that play a role in modulating CaM binding[117]. Mutation of these acidic residues results in decreased NHE1 activity and decreased CaM binding.

Carbonic anhydrase II (CAII) is an enzyme that catalyzes the production of HCO_3^- and H^+ from the hydration of CO_2. CAII is expressed in the myocardium[118]. It has been reported that CAII associates with NHE1, *in vivo* and *in vitro,* at residues 790-802 of the NHE1 C-terminal tail resulting in enhanced NHE1 activity[118]. Pharmacological inhibition of CAII has been shown to reduce myocardial NHE1 activity[119].

1.5.2.2 NHE1 Regulation Mediated by Indirect Cofactor and Protein-Protein Interactions with the C-terminal Tail of NHE1

NHE1 does not use ATP directly, however the presence of physiological levels of ATP is required for optimal NHE1 activity[120-122]. It has been shown that depletion of PIP_2 is concurrent with ATP depletion, and contributes to inhibition of NHE1[109].

1.5.3 NHE1 Regulation by Phosphorylation

Residues 636-815 of the NHE1 C-terminal tail have been identified as major sites of *in vivo* phosporylation[123]. Deletion of this region results in a 50% loss of NHE1 stimulatory effects (Figure 1.2). Phosphorylation has been suggested to alter the association of the C-terminal tail with the H^+ sensor, enabling the H^+ sensor to be more sensitive, thus activating NHE1[124]. However, the pathways leading to the phosphorylation of NHE1 are complex and involve a number of signaling molecules, second messengers, binding proteins and protein kinases.

1.5.3.1 Direct Phosphorylation of NHE1

The C-terminal tail of NHE1 has several serine/threonine residues, which are directly phosphorylated by a number of serine/threonine protein kinases. The first serine/threonine kinase identified to act directly on NHE1 was the Ca^{2+}/Calmodulin-dependent protein kinase (CaM Kinase II), a protein that regulates many Ca^{2+} homeostatic proteins in the myocardium[125]. CaM Kinase II has three consensus sequence sites on the C-terminal tail of NHE1[125]. In the myocardium, NHE1 activity was significantly greater in CaM Kinase II over-expressing cardiomyocytes vs. controls, thus

demonstrating the stimulatory effects of CaM Kinase II on NHE1[126]. The mitogen-activated protein kinase (MAPK) family, which includes extracellular signal-regulated kinases (ERK) 1/2, c-Jun N-terminal kinases (JNK) 1/2/3, p38 MAPK (p38), belongs to a highly conserved family of serine/threonine protein kinases and have also been implicated in NHE1 regulation in the myocardium (Figure 1.2). MAPKs are ubiquitously expressed, and their specific functions in the heart have been the focus of numerous studies for more then a decade (reviewed in[127]). *In vitro,* ERK 1/2 has been shown to phosphorylate specific sites on the C-terminal tail of NHE1 in NRVMs[86,128]. p38 phosphorylation sites on the C-terminal tail of NHE1 have also been identified[129]. p^{90} ribosomal s6 kinase (RSK), a downstream kinase of ERK, has also been shown to directly phosphorylate NHE1 and stimulate NHE1 activity in the myocardium[130]. ERK 1/2 and RSK have been implicated as signaling mechanisms for NHE1 activity induced by GPCRs, particularly receptors coupled to $G\alpha_q$ (as described in Section 1.5.1.1). In ARVMs, inhibition of α_1-AR agonist stimulation resulted in inhibition of ERK 1/2, RSK and NHE1 activity[131]. In addition, amino acids phosphorylated by ERK 1/2 in the C-terminal of NHE1 following stimulation with a α_1-AR agonist were identified in NRVMs[86].

Adenosine monophosphate-activated protein kinase (AMPK), another serine/threonine protein kinase expressed in the heart, has also been suggested to contribute to NHE1 activity[132,133]. AMPK acts as a cellular fuel gauge, which stimulates energy-producing processes and inhibits energy-requiring processes in times of metabolic stress in effort to maintain or restore intracellular ATP levels[335]. Recent reports have suggested that AICAR, an AMPK activator, inhibits NHE1 activity/expression[133].

However, no direct link has been identified between NHE1 and AMPK. NHE1 has also been shown to be regulated by protein kinase B (PKB), another serine/threonine kinase expressed in the myocardium. A recent report has suggested that PKB directly phosphorylates NHE1 at a site that resides in the middle of the high-affinity CaM binding region (as described in Section 1.5.2.1), thus inhibiting binding of CaM bound Ca^2 to the NHE1 regulatory domain and NHE1 activity[134].

1.5.3.2 Indirect Phosphorylation of NHE1

Protein kinase C (PKC) is another serine/threonine protein kinase that has been identified as a regulator of NHE1. PKC produces its effects through indirect interactions with NHE1. Inhibition of PKC pathways blocks activation of NHE1[135-137]. In addition, PKC inhibitors have been shown to inhibit NHE1 stimulation in response to stimuli such as α_1-AR agonists in cardiomyocytes, thus implicating that the stimulatory effect of α_1-AR agonists on NHE1 activity is mediated by PKC[94,131]. However, NHE1 does not express phosphorylation consensus sites for PKC[125,138].

1.5.3.3 Dephosphorylation of NHE1

The effects of phosphorylation on NHE1 were confirmed by examining phosphatases, which remove phosphates from phosphorylated amino acids. Dephosphorylation occurs via serine/threonine protein phosphatases (PP), which play a regulatory role in many physiological processes (reviewed in[139]). PP1, PP2A, calcineurin (PP2B), and PP2C, members of the PP family, have all been found in the myocardium and recognized as regulators of NHE1 in the myocardium[140,141]. *In vitro* and *in vivo*

studies using PP1 and PP2A demonstrated that upon binding to NHE1, basal level of NHE1 activity was reduced in NRVMs[142,143], thus emphasizing the importance of phosphorylation mediated NHE1 regulation.

1.5.4 Developmental Regulation of NHE1 Expression

Levels of NHE1 mRNA and protein expression itself vary during development. In the newborn heart, NHE1 mRNA expression and activity were greater in comparison to adult hearts[144-147]. NHE1 protein expression has also been shown to be elevated during heart development and immediately after birth[148,149]. This is of particular interest considering that CH (as described in Section 1.7.4), often characterized by reactivation of the fetal gene program, also shows elevated NHE1 message and activity[150-152]. Postnatally, NHE1 protein expression and activity have also been shown to decline in the myocardium[148,153].

1.6 Physiological Roles of NHE1

NHE1 has many important physiological roles (reviewed in[36]), many of which could be used as tools to understanding the role of NHE1 in the myocardium.

1.6.1 Intracellular pH and Volume Regulation

The most important role of the mammalian NHE1 is to regulate pH_i (as described in Section 1.3). NHE1 protects cells from intracellular acidification, as evidenced by the fact that mutant cell lines devoid of NHE1 activity are extremely sensitive to acidosis[154,155]. When acidosis occurs, NHE1 activity increases, thus returning pH_i to

resting values.

NHE1 also serves as a major Na^+ entry pathway in many cell types (as described in Section 1.1.2), and as such it regulates both Na^+ flux and cell volume after osmotic shrinkage[124,156,157]. NHE1 functions to increase the [Na^+] within the cytoplasm and cytoplasmic alkalinization. This elevated pH_i subsequently activates the AE, which concurrently increases the [Cl^-] within the cytoplasm. The net gain of Na^+ and Cl^- causes osmotically obliged water to enter the cell, resulting in cell swelling[156].

1.6.2 Cell Growth, Progression, Differentiation and Apoptosis

NHE1 activation is implicated in many other cell functions apart from modulation of pH_i and cell volume including cell growth, progression, differentiation and apoptosis. The role of NHE1 in cell growth was demonstrated in NHE1 null mice, which demonstrated decreased postnatal growth[158,159]. NHE1 has also been implicated in cell cycle progression. In cells expressing an inactive NHE1 mutant, cell proliferation is significantly reduced[160]. NHE1 activity is also important for cell differentiation[161-163]. During the differentiation of various non-myocardial cells lines, transcription of the NHE1 gene increases[164,165]. Taken together, the role of NHE1 in cell growth, proliferation and differentiation suggests that NHE1 is critical in several cellular processes. NHE1 has also been implicated in apoptosis. Apoptosis results in cell shrinkage and intracellular acidification, processes that are opposed by NHE1. In addition, the NHE1 C-terminal tail has been suggested to be a caspase-3 substrate[166]. However, its role in apoptosis is cell type specific[129,167-168]. In both renal proximal tubule cell lines and human leukemic cell lines, NHE1 activity serves to protect cells from apoptosis[167,168]. However, in two

cytokine-dependent cell lines, NHE1 mediates an elevation in pH_i that triggers apoptosis. More research must be done in this area to fully understand the role of NHE1 in apoptosis.

1.6.3 Maintenance of Cytoskeletal Structure, Focal Adhesion and Cell Migration

Ezrin, radixin and moesin (ERM) are actin binding proteins that are closely related, and important components of cell structure. They have been identified as cytoskeleton cross linkers, which form links between actin filaments of the cytoskeleton and integral proteins of the plasma membrane[169]. Interestingly, the NHE1 C-terminal tail contains 2 ERM protein-binding motifs within amino acids 553-564[170] (Figure 1.2). Structural links between NHE1 and ERM proteins control the integrity of the cortical cytoplasm[171,172]. Cells that are NHE1-deficient or expressing NHE1 and unable to interact with ERM demonstrate reduced actin stress fiber organization, irregular cell shape and impaired migration[173-175]. In addition, the interaction between NHE1 and ERM directs NHE1 localization in the lamellipodia of migrant cells[176]. In fibroblasts, wild type NHE1 localizes to the distal margin of membrane protrusions or lamellipodia, but a mutant NHE1 lacking binding sites for ERM is mislocalized. Taken together, it is quite clear that the NHE1-ERM interaction facilitates cell migration and the formation of cell signaling complexes. The importance of ERM in the myocardium was recently investigated. In a recent report, activated ERM proteins were shown to mediate the effects of acid-induced NHE1 activation in cardiomyocytes, with PKB acting as a downstream target[177].

1.7 NHE1 in the Myocardium

Heart failure is estimated to account for 29% of the yearly total mortality worldwide with approximately 16.7 million deaths per annum[178-180]. Heart failure can be defined as the inability of the heart to pump blood sufficiently to meet the demands of the body[181] due to deficiencies in contraction of the affected ventricles and the single cardiomyocyte[182]. A number of abnormalities have been described at various steps of the excitation-contraction coupling of cardiomyocytes, which regulate force and shortening, and Ca^{2+} dysregulation[31,182]. These abnormalities can result from a number of etiologies including I/R injury, hypertension, and neurohormonal activation[31,183]. In response to these pathologies the heart initially undergoes physiological hypertrophy, whereby cardiomyocytes grow in size to increase ventricular wall thickness in order to adapt to the increased wall stress[181]. The enlarged ventricles then contract more strongly and pump more blood. This adaptation becomes increasingly ineffective and leads to pathological hypertrophy and cardiac dysfunction associated with fibrosis and apoptosis. Investigating the mechanisms that contribute to the development of heart failure leads to the development of novel therapeutic approaches. NHE1 has been implicated in a number of etiologies resulting in the development of heart failure.

1.7.1 NHE1 and I/R Injury

Myocardial ischemia occurs when there is an imbalance between the oxygen requirement of the contracting muscle and the oxygen supply to the heart by the coronary. Reperfusion is the restoration of blood flow. The cellular and molecular mechanisms of I/R injury are multifaceted and are manifested as both reversible and

irreversible injury, ranging from cardiac stunning and arrhythmias to cardiomyocyte death in the form of apoptosis and necrosis[383]. I/R injury predisposes the heart to heart failure. Since the 1990s, the role of NHE1 in I/R injury has been extensively studied. NHE1 activity and mRNA expression were shown to be increased during I/R[184,185]. This increase in NHE1 activity/expression during I/R has been proposed to represent a major component of I/R injury (reviewed in[186]). Whether I/R injury is a result of NHE1 expression or activity or both expression and activity has not been compared, and requires further investigation. Ischemia-induced acidosis is a major stimulus for NHE1 activation. In addition to ischemia-induced acidosis, NHE1 activation is further stimulated by LPA, as well as paracrine and autocrine factors acting through phosphorylation-dependent processes (as described in Section 1.5). The basis for the involvement of NHE1 in myocardial I/R injury reflects a close interaction between ion-regulatory processes, particularly NHE1, NCX and NKA (as described in Section 1.1) (Figure 1.1). Briefly, during ischemia, anaerobic glycolysis produces H^+, which decreases cardiac pH_i and activates NHE1. Reperfusion also requires the restoration of pH_i, and therefore also activates NHE1. Activation of NHE1 results in increased exchange of intracellular H^+ for extracellular Na^+, leading to a rapid accumulation of intracellular Na^+ in the cell. Ischemia induced energy deprivation inhibits the activity of NKA, resulting in Na^+ accumulation within the cell. This Na^+ accumulation increases intracellular Ca^{2+} via NCX, working in reverse mode. This increase in intracellular Ca^{2+} triggers various detrimental pathways, such as arrhythmias and cell deterioration. The detrimental effects of increased $[Ca^{2+}]_i$ are clearly demonstrated in single ventricular cardiomyocytes from transgenic (TG) mice expressing elevated NHE1 expression and subjected to metabolic inhibition and recovery, which displayed augmented cell

contractility[187]. An alternative hypothesis to the mechanism of NHE1 induced I/R injury includes the loss of ATP during I/R. This has been proposed to result in phospholipase and protease activation, which in turn results in cell membrane injury and death[188,189]. In addition, the changes that occur during I/R have also been suggested to stimulate the formation of mitochondrial membrane permeability transition, which results in depression of ATP resynthesis[189].

The role of NHE1 in I/R injury was confirmed for the first time in 1988. Karmazyn et al. demonstrated that NHE1 inhibition prevented I/R injury[190]. Since this initial report, extensive evidence has been published in regards to the protective effects of NHE1 inhibitors during I/R injury, in various animal models and with an unusual degree of conformity between different investigators (reviewed in[191]). Treatment with NHE1 inhibitors during I/R results in enhanced contractility, reduced contracture, fewer incidences of arrhythmias, and improvements in biochemical and ultrastructural indices. The cardioprotective role of NHE1 inhibitors during I/R injury were confirmed in a mouse model in which NHE1 was genetically ablated[192]. The cardioprotective effects of NHE1 inhibitors have also been suggested to be superior to ischemic preconditioning, the gold standard among cardioprotective interventions[75,193,194]. The cardioprotective effects of NHE1 inhibitors have been associated with diminished tissue content of Na^+ and Ca^{2+}[195,196], thus supporting the concept that NHE1 mediated increases in Na^+ and Ca^{2+} are involved in I/R injury. Inhibition of NHE1 has also been shown to protect the heart from metabolites produced by the ischemic myocardium such as LPA (as described in Section 1.5.1.2), which may further activate the antiporter[188], thus supporting the role of NHE1 activation by NHE1 regulators in I/R injury. NHE1 inhibitors also inhibit

ventricular arrhythmias in the reperfused ischemic myocardium induced by α_1-AR agonists, another well known regulator of NHE1 activity[197]. The mechanisms by which NHE1 inhibitors induce cardioprotection is a subject of on going investigation. A means to identify targets that regulate NHE1 activity and potentiate I/R injury is a great area of interest. Another identified regulator of NHE1 activity is RSK. Inhibition of RSK reduced cardiomyocyte apoptosis in intact hearts subjected to I/R, and this was attributed to the reduced activation of NHE1[198].

Recent reports using TG mice expressing elevated NHE1 levels have demonstrated surprising results. They have shown that elevated NHE1 expression in TG mice can reduce the susceptibility to I/R injury[204,205]. In one study it was shown that TG mice expressing NHE1 have a minor improvement in recovery of pH_i and ATP levels, perhaps contributing to the cardioprotective effects[204]. In another study, activation of the ER stress response was suggested to contribute to the cardioprotective effects of elevated expression of NHE1[205]. Further investigations are required to determine the mechanism of NHE1 induced cardioprotection.

1.7.1.1 NHE1 Inhibitor Clinical Trials

The clinical development and testing of NHE1 inhibitors quickly progressed from the bench to the bedside, reflecting the excellent cardioprotection demonstrated in various animal models[199]. The first experimental data with cariporide, a member of benzoylguanidine derivative NHE1 inhibitors (as described in Section 1.4), was published in 1995. By 1997, cariporide was being used in the first clinical trial[195]. The first clinical trial, GUARD During Ischemia Against Necrosis (GUARDIAN), a phase

II/phase III study with more than 11,590 patients assessed cariporide in patients with acute coronary syndromes[200]. The benefits of cariporide were only observed in a subset of patients who underwent coronary artery bypass graft[195]. The Evaluation of the Safety and Cardioprotective effects of eniporide in the Acute Myocardial Infarction (ESCAMI) was another clinical trial on NHE1 inhibitors. It was a phase II trial where eniporide, another benzoylguanidine derivative NHE1 inhibitor (as described in Section 1.4), was assessed in patients undergoing thrombolysis or angioplasty for acute myocardial infarctions (MI)[201]. In this study, the administration of eniporide did not demonstrate any significant findings[202]. The lack of beneficial effects seen in the clinical trials were attributed to suboptimal dosing (GUARDIAN), and the timing in which NHE1 inhibitors were administered (ESCAMI)[191]. Another clinical trial using cariporide was conducted, the Na^+/H^+ Exchange inhibition to Prevent coronary Events in acute cardiac conDITIONs (EXPEDITION), which examined the effects of cariporide on mortality and the incidence of MI in high-risk patients undergoing coronary artery bypass graft surgery. In this study, cariporide reduced MIs, however, this was paralleled by negative cerebrovascular events[77,203]. The lack of cardioprotective effects seen by NHE1 inhibitors in the clinical trials is in agreement with recent reports, in which NHE1 is expressed in TG mice. Two different studies have shown that TG mice expressing elevated NHE1 reduced the susceptibility to I/R injury rather than inducing detrimental effects, as would be expected based on previous experiments in which NHE1 inhibitors were used[204, 205]. An additional report demonstrated that NHE1 inhibition has no benefits on the postischemic functional recovery of the aging myocardium[206]. The mechanisms by which this occurs requires further investigation.

1.7.2 NHE1 and Hypertension

Hypertension is a chronic medical condition characterized by elevated blood pressure. Hypertension is classified as either essential or secondary hypertension[207]. No medical causes have been identified to explain the elevated blood pressure in essential hypertension, which accounts for about 90-95% of hypertension. Secondary hypertension is high blood pressure induced by endocrine diseases, kidney diseases or tumors. Hypertension is particularly important since it leads to pathological hypertrophy and strongly enhances the risk of future cardiovascular events[208].

Interestingly, enhanced NHE1 activity has been demonstrated in a variety of cell types obtained from essential hypertensive patients[35]. Over-activation of NHE1 in vascular smooth muscle cells (VSMCs) has been suggested to induce hypertension. This results in $[Na^+]_i$ accumulation, which in turn activates NCX in reverse mode, thus increasing cytosolic Ca^{2+} concentrations[33]. The involvement of over-active NHE1 was confirmed in a study in which spontaneous hypertensive rats with pathological hypertrophy were treated with NHE1 inhibitors. This regressed CH, normalized NHE1 activity, and decreased systolic blood pressure[209].

NHE1 has also been implicated in pulmonary hypertension, which is caused by chronic lung diseases and results in right ventricular hypertrophy and heart failure[210,211]. NHE1 inhibition reduces right ventricular hypertrophy in a model of pulmonary hypertension[212]. Deficiency of the NHE1 gene prevented the development of hypoxia-induced pulmonary hypertension and vascular remodeling, thus confirming the role of NHE1 in pulmonary hypertension[213].

There is no definitive evidence documenting an NHE1 defect in human hypertension, however, it is quite obvious that NHE1 is a plausible candidate and more studies are needed to clarify its involvement.

1.7.3 NHE1 and Neurohormonal Activation

Neurohormonal disorders, which include persistent activation of the renin-angiotensin-aldosterone axis and the sympathetic nervous system, contribute to the development of heart failure[214]. A decrease in cardiac output induces homeostatic mechanisms that activate the renin-angiotensin-aldosterone axis and the sympathetic nervous system, and the resultant effect is the development of a vicious cycle characterized by excessive neurohormonal stimulation[215]. This in turn is responsible for myocardial remodeling. NHE1 activity has been shown to be regulated by neurohormones (as described in Section 1.5), which in turn contributes to I/R injury (as described in Section 1.7.2) and CH (as described in Section 1.7.4). Inhibition of NHE1 has been demonstrated to protect the heart against I/R injury and CH in hearts subjected to neurohormonal stimuli (as described in Section 1.7.2 and 1.7.4).

1.7.4 Cardiac Hypertrophy

CH is heart growth in response to environmental demands, and a variety of hormonal, paracrine and autocrine stimuli. It is a means to reduce stress on the ventricular wall[216]. CH could be classified as either physiological or pathological hypertrophy. Exercise, pregnancy, and postnatal growth promote physiological hypertrophy of the heart[216,217] (Figure 1.4). I/R injury, hypertension and neurohormonal

activation could cause pathological hypertrophy. Pathological hypertrophy is a major risk factor for cardiac death, and commonly precedes the development of heart failure[218] (Figure 1.4).

Distinct structural and molecular bases have been identified in physiological and pathological hypertrophy in animal models. Consistent markers of pathological hypertrophy include activation of the fetal gene program (atrial natriuretic peptide (ANP) and B-type natriuretic peptide, and genes for fetal isoforms of contractile proteins such as skeletal α-actin and β-myosin heavy chain (MHC), increase in cell size, protein synthesis, and heightened organization of sarcomere assembly[219,220]. Fibrous tissue accumulation is another feature of the structural remodeling of the myocardium. A fine network of collagen fibers surrounds cardiomyocytes under normal conditions to provide a supporting framework. During pathological insults, excessive cardiac fibroblasts and extracellular matrix proteins accumulate, leading to myocardial stiffness, diastolic and systolic dysfunction[221]. Exercised rats showed down regulation of hypertrophic markers and are typically not accompanied by accumulation of myocardial collagen[222,223].

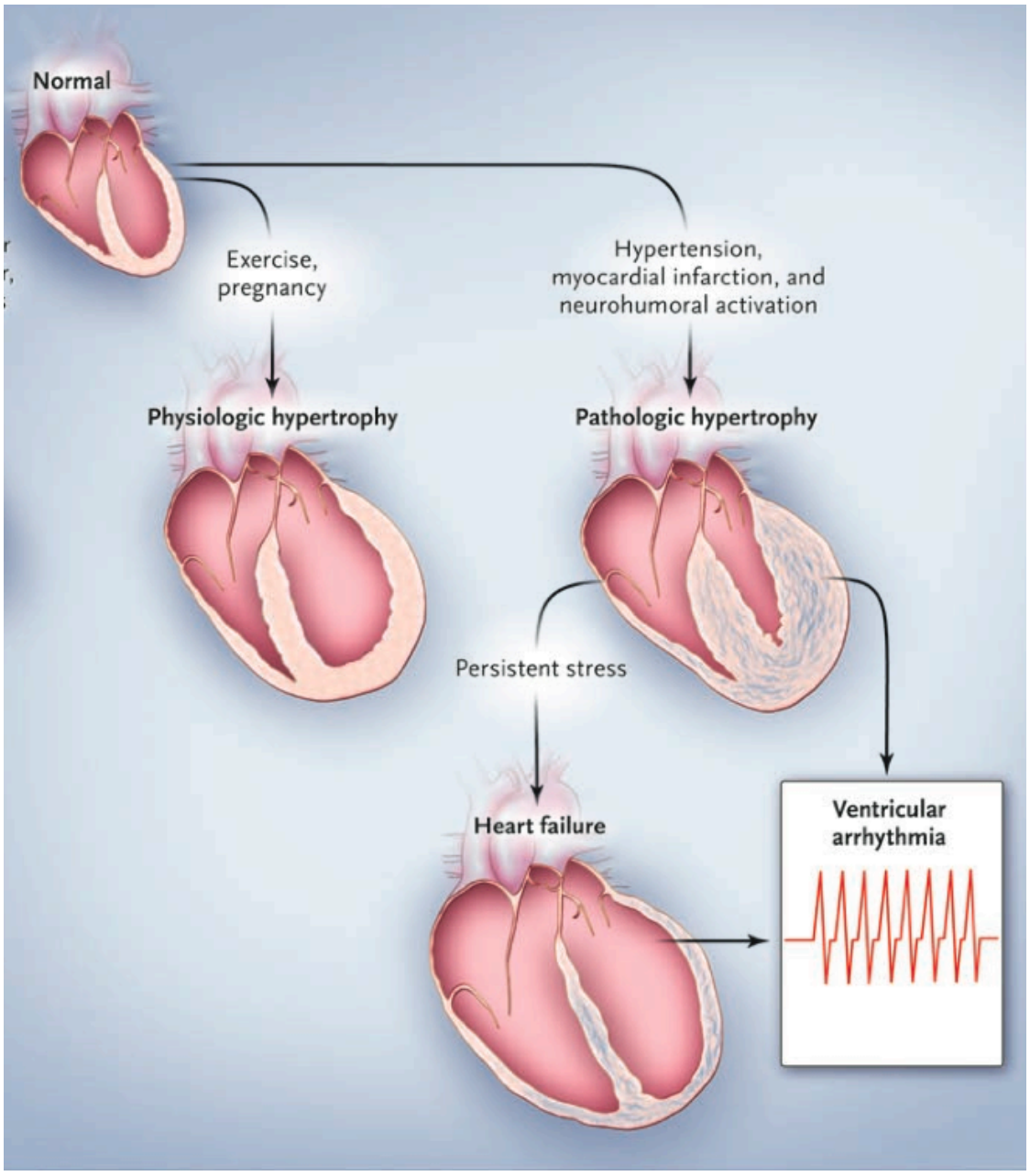

Figure 1.4. Schematic representation of physiological and pathological cardiac hypertrophy. Exercise, pregnancy, and postnatal growth promote physiological hypertrophy of the heart, which does not compensate into dilated cardiomyopathy or heart failure. I/R injury, neurohormonal activation and hypertension could cause pathological hypertrophy. (The figure was adopted from Hill et al.,[216])

CH is further classified into concentric and eccentric hypertrophy. Concentric hypertrophy, the predominant form of CH, is characterized by an increase in the thickness of the ventricular wall caused by parallel addition of sarcomeres, re-expression of the fetal gene program and little or no chamber dilatation. Myocyte length is less than the increase in myocyte width, and leads to reduced left ventricular volume and increased wall thickness. Systemic hypertension, aortic stenosis and MIs often induce concentric hypertrophy[224]. Eccentric hypertrophy is an increase in cardiac mass with increased chamber volume[216] and is common under conditions of isotonic exercise or volume overload following MIs[216]. Eccentric hypertrophy is distinguished by the addition of sarcomeres in series and longitudinal cell growth[216]. The increase in myocyte length is greater than the increase in myocyte width, causing dilatation and thinning of the heart wall.

1.7.4.1 NHE1 and Cardiac Hypertrophy

NHE1 mRNA expression, protein expression or activity have been shown to be elevated in various *in vivo* models of CH[225,226,238,239,240]. Interestingly, in some CH models NHE1 protein expression and activity are increased[238,239], while in others NHE1 activity is increased in the absence of any alterations in NHE1 expression[240]. The degree of hypertrophy obtained with varying NHE1 expression and activity has not been investigated.

1.7.4.1.1 Direct Inhibition of Cardiac Hypertrophy by NHE1 Inhibitors

NHE1 inhibitors have been shown to attenuate CH directly in a number of *in vivo*

models. Chronic inhibition of NHE1 attenuated the development of CH in rabbits subjected to volume and pressure over-load and prevented further development of heart failure[227]. NHE1 inhibitors have also been shown to reduce right and left ventricular hypertrophy in models subjected to MIs[228-230]. Mice expressing active human NHE1 have provided further evidence of NHE1 mediated CH, contractile dysfunction and heart failure[231]. In this study, the hypertrophic phenotype was associated with activation of CaM Kinase II, and increases in Ca^{2+}[231]. Additionally, these TG mice displayed increased expression of activated ERK 1/2 and p38[231].

1.7.4.1.2 Inhibition of Autocrine, Paracrine and Hormonal Induced Cardiac Hypertrophy by NHE1 Inhibitors

The cellular mechanistic base for NHE1 induced CH is not known with certainty. Since NHE1 activation occurs through receptor dependent mechanisms induced by neuroendocrine disorders and cardiac dysfunction (as described in Section 1.5, 1.7.2 and 1.7.3), NHE1 has been suggested to be a target of multiple signaling pathways, which mediate the CH response[199]. In a number of studies, inhibition of NHE1 attenuated CH in models induced by autocrine, paracrine or hormonal stimuli. *In vitro*, HOE 694, a selective NHE1 inhibitor was shown to block norepinephrine-induced protein synthesis in NRVMs[232]. *In vivo*, NHE1 inhibition suppressed the hypertrophic effect of isoproterenol[233].

In addition, MAPKs, important pathways leading to CH and kinases involved in NHE1 regulation (as described in Section 1.5), have been implicated in NHE1 induced CH[131,234-236]. The MAPK pathway has been suggested to be a downstream target of autocrine, paracrine and hormonal stimuli, particularly those acting through GPCRs (as

described in Section 1.5.3.1). Treatment with NHE1 inhibitors reversed the MAPK pathway induced NHE1 stimulation and CH[237].

1.7.4.1.3 Inhibition of Genetically Induced Cardiac Hypertrophy by NHE1 Inhibitors

Inhibition of NHE1 in genetic models of CH has been effective in regressing the hypertrophic response. NHE1 expression and activity were increased in a model of human hereditary cardiomyopathy, which was accompanied by increased $[Na^+]_i$ and $[Ca^{2+}]_i$ levels, all of which were prevented by NHE1 inhibitors[238]. NHE1 inhibition also reversed CH, fibrosis and heart failure in TG mice over-expressing β_1-adrenergic receptors[239]. Another genetic model studied was ANP deficient mice, which were associated with hypertension, marked CH, enhanced NHE1 activity, subsequent alkalinization, and increased $[Ca^{2+}]_i$. All of these symptoms were attenuated with NHE1 inhibition[240].

1.7.4.1.4 NHE1 and Diabetes-Induced Cardiac Hypertrophy

The prevalence of cardiovascular diseases, including left ventricular hypertrophy, in the diabetic population is many times higher than in the non-diabetic population[241,242]. The common consequence of all diabetes is hyperglycemia due to either abnormalities of insulin secretion by pancreatic β-cells (type 1 diabetes) or inefficiency of insulin[243]. Hyperglycemia encountered during diabetes triggers abnormalities of vascular function associated with cell acidosis and Ca^{2+} overload. This leads to different pathologies such as ischemic heart disease and left ventricular hypertrophy[243]. It is quite interesting to note that the role of NHE1 is also translated to models of diabetes-induced CH. Left ventricular myocytes from a type 2 diabetes rat model demonstrated a marked increase in

NHE1 activity[244]. In addition, glucose-induced CH has been shown to be attenuated by NHE1 inhibitors[245]. The benefits of NHE1 inhibition extend to the extent of protecting the coronary endothelium against deleterious effects of hyperglycemia induced by streptozotocin, therefore preventing future MIs[243]. Targeting NHE1 therefore represents an attractive therapeutic approach in diabetic induced CH.

1.7.4.2 NHE1 and Apoptosis

Apoptosis is initiated by the death receptor/extrinsic pathway, the mitochondrial/intrinsic pathway or the endoplasmic reticulum (ER)-stress death pathway[249]. Understanding the mechanisms by which apoptosis occurs is very important since apoptosis has been demonstrated to play a role in the transition from CH to heart failure[246]. It has been reported that patients with advanced heart failure have higher rates of cardiomyocyte apoptosis[247,248]. Since recent reports show that NHE1 inhibition delays the transition from CH to heart failure (as described in Section 1.7.3) and apoptosis plays a key role in this process, numerous studies have investigated the role of NHE1 on CH and apoptosis. *In vitro*, enhanced NHE1 was shown to be associated with apoptosis in a hypoxia/reoxygenation model[251]. *In vivo*, chronic NHE1 inhibition decreased both CH and apoptosis in the spontaneously hypertensive rat heart[250]. The anti-apoptotic effect has been suggested to be a result of the inhibition of cytosolic Na^+, Ca^{2+} and the opening of the mitochondrial permeability transition pore[250]. The role of the mitochondrial transition pore in inducing NHE1 mediated apoptosis is further supported in another model. In this model, NHE1 inhibition protects against IR injury by attenuating the opening of the mitochondrial transition pore, apoptosis and the resultant mitochondrial dysfunction[252].

1.7.4.3 NHE1 and Congestive Heart Failure

In congestive heart failure (CHF), the reduced efficiency of the heart causes blood to back up in the circulatory system leading to the build up of fluid in tissue (edema). Over time, untreated CHF worsens and affects virtually every organ in the body. NHE1 was also investigated in hearts with CHF. In hearts samples from patients with CHF, NHE1 activity was increased relative to normal human donor hearts, suggesting that NHE1 activity and expression are maintained throughout pathological hypertrophy and its progression to CHF[253]. CHF commonly coexists with atrial fibrillation, which often exacerbates CHF[254]. In the left atrium from 29 patients undergoing mitral valve replacement, NHE activity and expression were significantly greater in tissue with atrial fibrillation and severe heart failure vs. other groups, which had atrial fibrillation with mild heart failure or normal sinus rhythm with mild heart failure[255].

1.7.5 NHE1 and Stem Cells

Despite all the therapeutic interventions available, the prognosis for most patients with heart failure remains poor[181]. Stem cells and their ability to generate cardiomyocytes and to promote local repairs provides a new therapeutic strategy for treatment of the failing heart[181]. Recent studies have employed various techniques to enhance the specificity and amount of differentiated stem cells, since differentiated cardiomyocytes account for a minor portion of cells present within embryoid bodies of embryonic stem cells[256-258]. It has been suggested that NHE1 is required for differentiation of embryoid bodies into cardiomyocytes[259,260]. Treatment of P19 stem cells with NHE1 inhibitors

prevented differentiation of embryoid bodies into cardiomyocytes[259], thus emphasizing the importance of NHE1 in the differentiation of embryoid bodies into cardiomyocytes. Inhibition of NHE1 activity was also shown to inhibit cardiomyocyte differentiation of CGR8 stems cells, indicated by the decreased message of transcription factors Nkx2-5 and Tbx5 and the decreased levels of α-MHC[260]. This further confirms the role of NHE1 in the differentiation of embryoid bodies into cardiomyocytes. CGR8 stem cells were also reported to have expressed elevated NHE1 expression and activity, which facilitated cardiomyocyte differentiation [260]. These results demonstrate that NHE1 is important in facilitating stem cell differentiation to cardiomyocytes, and further emphasizes that NHE1 is an essential target in understanding heart failure.

1.8 Other Pathophysiological Roles of NHE1

NHE1 has number of pathophysiological roles. Understanding its function or regulation in other systems has often been used as a means to provide insights into the role or regulation of NHE1 in the myocardium.

1.8.1 NHE1 and Cancer

Cancer is estimated to account for 13% of the yearly total mortality worldwide[261]. Most cancer-induced deaths are the sequel of metastatic diseases rather than of primary tumor growth[262]. Tumor cells display alkaline pH_i and the maintenance by NHE1 has been shown to be a key mechanism in the oncogenic transformation and maintaining the tumor cells in a transformed state[263]. NHE1 inhibitors have been proposed as potential therapeutic agents against metastasis and multi-drug resistant cancers[264]. Interestingly,

paclitaxel, a chemotherapy agent for leukemia and lymphoma has been shown to activate pathways that inhibit NHE1 and cancer cell apoptosis[265]. The potential for use of NHE1 inhibitors in the treatment of cancer is gaining more attention.

1.8.2 NHE1 and Central Nervous System

NHE1 is the most abundant isoform in the rat central nervous system. Targeted disruption of the murine NHE1 locus results in severe neurodegenerative disorders[266]. In addition, brain ischemia activates NHE1, and infusion with NHE1 inhibitors results in beneficial neurological outcomes[267].

1.8.3 NHE1 and Chronic Kidney Disease

Chronic kidney disease is characterized by a lack of renal tubular epithelial cells (tubular atrophy)[268,269]. The absence of renal tubular epithelial cells has been attributed to ischemia[269]. NHE1 inhibitors protect against cellular stress such as streptozotocin-induced diabetes renal tubule epithelial cell apoptosis and renal dysfunction[270].

1.8.4 NHE1 and Skeletal Muscle

NHE1 is known to be present in rat and human skeletal muscle[271,272]. Skeletal ischemia occurs as a result of prolonged ischemia due to unpredictable complications, such as thrombosis and/or vasospasm occurring perioperatively in selective reconstructive surgery or delayed surgical interventions in trauma surgery[273]. Recent reports have suggested than inhibition of NHE1 attenuates skeletal muscle infarctions when administered before ischemia or reperfusion[273].

1.9 Thesis Objectives

Understanding the fundamental underlying mechanisms in the development of heart failure, particularly during pathological hypertrophy and I/R injury, likely holds the key for potentially effective heart failure management. The purpose of this study was to understand how NHE1 upregulation affects the myocardium's susceptibility to pathological CH and I/R injury using a gain-of-function model. This was done by (1) using an *in vivo* and an *in vitro* gain-of-function model. Our *in vivo* model involved TG mice expressing cardiac specific NHE1, in the wild type (N-line) or active form (K-line). Our *in vitro* model involved NRVMs infected with adenoviruses containing wild type (IRM) or constituitively active (K-IRM) NHE1. In these studies we were also able to determine whether the involvement of NHE1 in CH is a result of protein expression, activity or a combined effect. It is uncertain whether enhanced expression of NHE1 alone has detrimental effects without the activation that shifts it to greater activity at more alkaline pH. Such activation could occur in more pathological situations, since numerous regulators of NHE1 increase in the diseased myocardium. In order to determine whether enhancement of NHE1 activity increases the susceptibility to stimuli that causes CH, both our *in vivo* and *in vitro* models were stimulated with PE. PE is a hormonal α_1-AR agonist that induces hypertrophy and activates NHE1. Both models were then assessed for CH. (2) In the second part of the study, our *in vivo* gain-of-function model was used to determine whether elevation of NHE1 expression mediates I/R injury and whether this response is enhanced when NHE1 is active. (3) The third part of the study was to confirm that the NHE1 induced cardiac phenotype was not gender dependent. The NHE1 transgenic male mice where characterized for CH and compared to its female

counterpart. Our **hypothesis** is that enhanced NHE1 expression in the myocardium makes the myocardium more susceptible to CH and I/R injury and this is accentuated further with activation of the exchanger.

Chapter 2

Materials and Methods

2.1 Transgenic Mice Expressing Cardiac-Specific NHE1

Two types of TG mice were created, the N-line, which express wild type human NHE1 and K-line, which express an active human NHE1. NHE1 was tagged with hemagglutinin (HA) and directed to the myocardium under the control of the α-MHC.

2.1.1 Construction of Wild Type Human NHE1-HA Tagged Plasmid

The wild type human NHE1-HA plasmid used for the construction of N-line TG mice was made from the plasmid pYN4$^+$. pYN4$^+$ contains the human complementary deoxyribonucleic acid (cDNA) of the entire coding region of NHE1 and is HA tagged at the NHE1 C-terminal tail. Expression of the plasmid is driven by the Rous Sarcoma Virus promoter. The plasmid contains an ampicillin (Amp) resistance cassette for selection[274]. pYN4$^+$ was digested with SmaI and NdeI restriction enzymes to yield a 2551 base pair (bp) segment that contained HA tagged-wild type human NHE1. The NdeI site was blunted with the Klenow enzyme. HA tagged-wild type human NHE1 was cloned to a plasmid containing the 5.5-kilobase (kb) mouse cardiac α-MHC promoter, which was digested with SalI and also filled with a Klenow fragment. The α-MHC promoter was used to direct cardiac specific expression. After the correct orientation was confirmed, linear DNA containing α-MHC-wild type NHE1-HA tag was excised from the plasmid using the enzyme NotI[275].

2.1.2 Construction of Active Human NHE1-HA Tagged Plasmid

The second transgenic mouse line, the K-line, which contained the active human NHE1-HA tagged construct, was also constructed from the plasmid pYN4$^+$ (as described

in Section 2.1.1). The active NHE1-HA tagged plasmid represented by the following notation, 1K3R4E, was made by mutating specific regions of the NHE1 C-terminal tail (Figure 1.2). Amino acids lysine (K) 641, arginine (R) 643, arginine (R) 645, and arginine (R) 647 were all mutated to glutamic acid (E)[115]. Mutation of the CaM binding site has been shown to stimulate NHE1 and mimics the effects of elevated $[Ca^{2+}]_i$ (as described in Section 1.5.2.1) (Figure 1.2). This occurs because in the absence of CaM bound to Ca^{2+}, the high affinity CaM binding site causes autoinhibition of NHE1[116]. Addition of CaM bound to Ca^{2+}, which occurs when $[Ca^{2+}]_i$ is elevated, reverses this inhibition and produces an actived NHE1[115]. Deletion or mutation of regions of the high affinity CaM binding site prevents autoinhibition of NHE1, and stimulates NHE1 activity and mimics elevated $[Ca^{2+}]_i$[115]. This results in an NHE1 protein that is alkaline shifted in its pH dependence and is more active at a given pH.

To make the 1K3R4E muations, amplification was carried out with PWO DNA polymerase (Roche Applied Science; Laval, Quebec), followed by use of the Stratagene QuikChange™ site-directed mutagenesis kit (Roche Applied Science; Laval, Quebec). Site-specific mutagenesis was carried out using the following forward and reverse synthetic oligonucleotide sequence, 5'-CGCAAAATCCTGAGGAACAACTTGCAGgAGACCgaGCAGgaGCTcgaGTCCTAC AACAGACACACGCTGG-3', with lower case letters indicating mutations. SacI and XhoI sites were introduced to facilitate mutant identification by restriction enzyme digestion. The resulting polymerase chain reaction (PCR) product was used to transform XL1-Blue cells by electroporation. DNA was isolated from randomly selected XL1-Blue colonies and positive colonies were identified by restriction enzyme digestion using SacI

and XhoI. The accuracy of the mutated plasmid was confirmed by sequencing. Oligonucleotides used as PCR primers and for sequencing were synthesized by either Qiagen or MWG Biotech, Inc. DNA samples were sent to the University of Alberta, Department of Biochemistry, DNA Core Services lab for DNA sequencing.

The 1K3R4E plasmid was constructed with the α-MHC promoter as described in Section 2.1.1. After the correct orientation was confirmed, linear DNA containing α-MHC-active type NHE1-HA tag was excised from the plasmid using the enzyme NotI and this construct was used for generation of NHE1 TG K-line mice (as described in Section 2.1.4).

2.1.3 Characterization of NHE1 Plasmid with the 1K3R4E Mutation

2.1.3.1 Cell Culture and Transient Transfection of AP-1 Cells

AP-1 cells, derived from a Chinese hamster ovary cell line, lack endogenous NHE1 and are used to characterize wild type NHE1 or mutant (1K3R4E) constituitively active NHE1 plasmids (as described in Section 2.1.1 and 2.1.2). AP-1 cells were grown in modified Eagle's medium, alpha modification (α-MEM) supplemented with 10% fetal bovine serum (FBS), 25 mM N-2-hydroxyethylpiperazine-N'-2-ethanesulfonic acid (HEPES), 0.25 mM glutamine, penicillin (100 U/mL), streptomycin (100 U/mL) and gentamicin (4 mg/mL) in a humidified atmosphere containing 95% O_2-5% CO_2. For transfection, 1×10^6 cells were seeded in a 60 mm petridish and grown overnight without antibiotics. Cells were transfected with LIPOFECTAMINE™ 2000 Reagent (LF 2000) according to the manufacturer's protocol. Briefly, the DNA-LF 2000 containing solution

was prepared using 10 μg of plasmid DNA, Opti-MEM and LF 2000. During this time the media of the cells to be transfected was replaced with media containing no antibiotics or FBS and 1 mL of the DNA-LF 2000 containing solution. Cells were then incubated at 37°C for 24 hours, and were supplemented with 10% FBS 4 hours following transfection.

2.1.3.2 Western Blot Analysis of NHE1 in AP-1 Cells

Expression of the NHE1 protein was confirmed by western blot analysis of total cell lysates obtained from AP-1 transfected cells. The cells were extracted in the presence of lysis buffer containing [(mM) (50 Tris, pH 7.4, 150 NaCl, 1 ethylene glycol-bis(b-aminoethylether)-N,N,N',N'-tetraacetic acid (EGTA), 0.1 benzamidine, 0.1 phenylmethylsulfonyl fluoride), 0.25% (w/v) sodium deoxycholate, 0.1% (v/v) Triton X-100, 0.1% (v/v) protease inhibitor cocktail and 1% (v/v) Nonidet P-40][276]. The cell lysates were centrifuged at 16 000 x *g* for 5 minutes at 4°C and the pelleted cell debris was discarded. The protein concentration of each lysate was determined using a Bio-Rad D_C Protein Assay. 50 μg of total protein was resolved on a 10% SDS-PAGE gel and transferred onto a nitrocellulose membrane. The nitrocellulose membrane was incubated with anti-HA (12CA5) antibody (Boehringer Mannheim; Burlington,Ontario) in 1% milk/TBS for 2 hours at room temperature with constant rocking and then incubated with peroxidase-conjugated goat anti-mouse antibody in 1% milk/TBS for 1.5 hours. Blots were developed by the Amersham ECL Western blotting and detection system, as described by the manufacturer.

2.1.3.3 Measurement of NHE1 Activity in Mammalian Cells

NHE1 activity, the ability of the wild type or active NHE1 (1K3R4E mutant) to exchange Na^+ and H^+ across the plasma membrane was estimated by the rate at which cells recover following an acid load. Transfected AP-1 cells (as described in Section 2.1.3.1) were grown to 80-90% confluence on glass coverslips and were loaded with 3 μg/mL 2,7-bis(carboxyethyl)-5(6)-carboxyfluorescein acetoxymethyl ester (BCECF-AM) (EMD Chemicals Inc.; Gibbstown, NJ) in AP-1 growth medium (as described in Section 2.1.3.1) without FBS. BCECF-AM is a cell permeable and non-fluorescent pH sensing dye that is cleaved to BCECF once inside the cell by cellular esterases, which makes the dye impermeable and fluorescent[277]. NHE1 activity was measured using a PTI Deltascan spectrofluorometer (Photon Technology International; London, Ontario). The excitation wavelengths used were 452 and 503 nm, which coincide with the excitation ratios of BCECF, one of which is pH independent (452nm) and one of which is pH dependent (503nm)[235]. The emission wavelength used was 524 nm, and the ratio of the two emissions at this wavelength gives a measurement of pH_i that is independent of the dye concentration[278]. Following incubation with BCECF-AM, the coverslip was placed in a cuvette containing Na^+-normal buffer [(mM) (135 NaCl, 5 KCl, 1.8 $CaCl_2$, 1 $MgSO_4$, 5.5 Glucose, 10 HEPES) warmed to 37°C and adjusted to pH 7.3 using KOH and HCl], until a steady pH_i was obtained. The cells were then acid loaded with 50 mM ammonium chloride for 3 minutes, followed by a brief incubation in Na^+-free buffer [(mM) (135 N-Methyl glucamine, 5 KCl, 1.8 $CaCl_2$, 1 $MgSO_4$, 5.5 Glucose, 10 HEPES) warmed to 37°C and adjusted to pH 7.3 using KOH and HCl], allowing a steady acidic pH_i to be obtained. The cells were then transferred into fresh Na^+-normal buffer for 3 minutes. A

three-point pH calibration was carried out for each coverslip by placing the cells in calibration buffers [(mM) (135 N-Methyl glucamine, 135 KCl, 1.8 $CaCl_2$, 1 $MgSO_4$, 5.5 Glucose, 10 HEPES) warmed to 37°C and adjusted to pH 8, 7 or 6 using KOH and HCl] and 10 μM nigericin, a K^+ ionophore[44]. Using this calibration data, a standard curve was generated and used to calculate the rate of recovery and resting pH_i. The rate of recovery was taken in the first 20 seconds of linear recovery following an acid load, with final units of ΔpH/second. For measurements of resting pH_i, readings were taken 3 minutes following stabilization in Na^+-normal buffer and prior to the acid load.

2.1.4 Construction of NHE1 Transgenic Mice

Linearized α-MHC-wild type or active NHE1-HA tagged DNA (as described in Section 2.1.1 and 2.1.2) was microinjected into fertilized oocytes, which were then transferred into the oviduct of pseudopregnant FVB/N mice. This procedure was performed by the Health Sciences Laboratory Animal Services at the University of Alberta, Edmonton, AB, Canada. Founder mice were identified, bred with wild-type FVB/N, and maintained in a pathogen-free environment.

2.1.4.1 Identification of NHE1 Transgenic Mice

TG mice were identified by PCR analysis of ear genomic DNA. Ear notch biopsies from NHE1 TG mice, 3 weeks of age, were extracted by personel from the Health Sciences Laboratory Animal Services at the University of Alberta. Genomic DNA was extracted from the ear notches using the REDExtract-N-Amp™ Tissue PCR kit (XNAT) (Sigma) according to the manufacture's instructions. The PCR reaction mix

consisted of 5 μL of 10x PCR buffer, 2 mM deoxyribonucleoside triphosphate (dNTPs), 0.5 μL Taq polymerase, 1μM forward and reverse primers, 3 mM $MgCl_2$ and 4 μL DNA, diluted to a final volume of 50 μL dH_2O. The forward primer corresponded to the 3' end of the α-MHC promoter sequence (5'-GCCCAGCTGCCCGGCACTCTTAG-3') and the reverse primer corresponded to the 5' end of the NHE1 cDNA sequence (5'-GCCCCACCAAAGCAACCACCAC-3'). Each PCR set contained a negative and positive control. A step down PCR program was used. PCR samples were diluted in 6x DNA loading buffer and run on 1% agarose gel (ultrapure agarose dissolved in 1xTBE) containing ethidium bromide at 70 V for 1 hour. Gels were exposed to UV, which reacts with ethidium bromide, to illuminate bands of appropriate size for mice that are TG.

2.2 *In Vivo* Studies of NHE1 Transgenic Mice

All experimental procedures involving animals presented in this study were used in accordance with guidelines set out by the University of Alberta Animal Policy and Welfare Committee and by the Canadian Council on Animal Care. In the following study control, N-line and K-line male and female mice, 10-12 weeks of age, were used. Female (Chapter 3) and male (Chapter 5) mice were characterized for CH and female mice were used for our I/R studies (Chapter 4). All TG mice used in our study were heterozygous. Mice were housed in a conventional facility at the University of Alberta Health Sciences Laboratory Animal Services with free access to standard mouse chow and tap water. In some studies, the standard mouse chow contained N-(4,5-Bis-methansulfony-2-methyl-benzoyl) guanidine (EMD 87580/EMD), an NHE1 inhibitor, which was made by Harlan Laboratories (Madison, WI). EMD 87580 was a generous gift from Dr. N. Beier (Merck

KGaA; Frankfurt, Germany). In these studies, the EMD 87580 enriched chow was administered for 14 days or 3 months. In parallel control experiments, animals were fed the standard chow.

2.2.1 Isolation of Adult Ventricular Cardiomyocytes from NHE1 Transgenic Hearts

Adult ventricular cardiomyocytes (AVMs) were isolated from control and TG mice by collagenase digestion[281]. Mice were heparinized and then anesthetized using euthanyl. Hearts were excised and placed in ice-cold Ca^{2+}-free perfusion buffer [(in mM) (113 NaCl, 4.7 KCl, 0.6 KH_2PO_4, 0.6 Na_2HPO_4, 1.2 $MgSO_4 \cdot 7H_2O$, 12 $NaHCO_3$, 12 $KHCO_3$, 20 D-glucose, 10 Na^+-HEPES, 2 creatine, 2 carnitine, 30 taurine, 10 2,3-butanedione monoxime), pH 7.2 at 37°C]. Non-cardiac tissue was quickly removed, and the heart was cannulated via the aorta. The heart was then perfused with continuously gassed (95% O_2-5% CO_2) Ca^{2+}-free perfusion buffer for 4 minutes at 37°C, followed by perfusion with an enzymatic digestion buffer (Ca^{2+}-free perfusion buffer, 0.08% collagenase Type II Worthington (Worthington Biochemical Corporation; Lakewood, NJ), 25 μM Ca^{2+}, and 0.1% bovine serum albumin (BSA), continuously equilibrated with 95% O_2-5% CO_2 at 37°C) for 3 minutes. By the end of the digestion period, the heart became soft and flaccid, and the ventricles were removed and cut into five to six pieces and placed in storage buffer (Ca^{2+}-free perfusion buffer, 100 μM $CaCl_2$, and 0.1% BSA). This suspension was dispersed by gentle trituration using a wide-bore disposable serological pipette. The cell suspension was maintained in storage buffer at 25°C for at least 2 hours before use.

2.2.1.1 Intracellular pH Measurements of Isolated Adult Ventricular Cardiomyocytes

pH_i was monitored in single AVMs using the pH-sensitive fluorescent dye BCECF-AM (as described in Section 2.1.3.1.3*)*. Two hours following the isolation of the AVMs, 500 μL of the cell suspension was placed on a coverslip that was mounted on the stage of an inverted Leica DMLA microscope (Leica Microsystems Bannockburn, IL), which contained an adjustable aperture and a single photomultiplier tube (Photon Technology International; London, Ontario). The coverslip was coated with 10 μg/mL laminin (Collaborative Biomedical Products; Mississauga, Ontario). The stage was set at a temperature of 37°C. The cell suspension was loaded with 12 μM BCECF-AM for 30 minutes. A single healthy cardiomyocyte was chosen for the remaining experiment. The cells were superfused (1 mL/min) with normal buffer solution [(in mM) (135 NaCl, 4.5 KCl, 2 $CaCl_2$, 1 $MgCl_2$, 20 HEPES, and 10 glucose), adjusted to pH 7.4 with NaOH at 37°C]. The cells were excited with light at 490 and 440 nm, and the resulting fluorescence emission intensity from a single cardiomyocyte was measured simultaneously at 530 nm. After an initial measurement period of resting pH_i, cells were acidified by using 50 mM NH_4Cl and the remaining procedure was as described earlier in Section 2.1.3.1.3.

2.2.1.2 Cell Area of Isolated Adult Ventricular Cardiomyocytes

Cell area of AVMs isolated by retrograde perfusion was measured using Image ProPlus Version 4.5 software (Media Cybermetics Inc. Silver Spring, MD). Digitized images were gathered using a Photometrics $CoolSNAP_{fx}$ camera (Photometrics Surrey,

BC) equipped to a Leica DMIRB microscope (Leica Microsystems Bannockburn, IL) using 20X magnification. 100 cells were measured from each perfusion, representing an n=1.

2.2.2 Western Blot Analyses of Tissue from NHE1 Transgenic Mice

2.2.2.1 Immunoblot Analysis of Various Transgenic Tissues for Total and Exogenous NHE1 Protein Expression

Hearts used for examining NHE1 protein expression were isolated from control and NHE1 TG mice and added to a homogenization buffer [(mM) (120 NaCl, 10 Tris (pH 7.4), 0.1 phenylmethylsulfonyl fluoride, 0.1 benzamidine), 37.5 μM ALLN (calpain I inhibitor) and a proteinase inhibitor cocktail]. Samples were homogenized at 4°C for 30 seconds, incubated on ice for 30 seconds, and then homogenized again for 30 seconds by using an Omni International 2000 electric homogenizer (OMNI International, Kennesaw, GA). The crude membrane fractions were obtained by subjecting the homogenates to a series of centrifugation steps. The initial centrifugation was for 10 minutes at 735 x *g*. The resulting pellet was discarded and the supernatant was centrifuged at 8 200 x *g* for 15 minutes. The resulting pellet was again discarded and the supernatant was centrifuged for the last time at 40 000 x *g* for 1 hour. The supernatant was discarded and the pellet containing the membrane fraction was resuspended in the homogenization buffer with the addition of 1% SDS, to aid in solubilization. Total protein was quantified using the Bio-Rad D_C Protein Assay kit as described by the manufacturer. 100 μg of each sample was resolved on 10% SDS-PAGE and transferred to nitrocellulose membranes. For western

blots examining NHE1 tissue expression in NHE1 TG mice, lysates were prepared using lungs, liver, kidney, brain or hearts as described above. For western blots examining the time course of expression of the NHE1 transgene in the intact myocardium, hearts were isolated at various ages ranging from 1-18 weeks, and lysates were prepared as described above. Nitrocellulose membranes were blocked in blocking buffer solution (LI-COR Biosciences, Lincoln, Nebraska) overnight at 4ºC, with gentle rocking. Membranes were incubated with anti-HA (Y11) antibody (sc-805) (Santa Cruz Biotechnology; Santa Cruz, Ca) or anti-NHE1 antibody (BD Biosciences Pharmingen; San Diego, CA) overnight. Anti-NHE1 was used to examine total (endogenous and exogenous) NHE1 protein expression. Anti-HA was used to examine expression of exogenous NHE1. Anti-actin antibody (H-300) (Santa Cruz) was used as a loading control. The primary antibodies were diluted 1:1000 in TBS + 0.1% Tween-20 and incubated overnight. The membrane was then washed with TBS + 0.1% Tween-20 4x for 5 minutes each at room temperature. Species and wavelength specific LI-COR secondary antibodies including goat anti-mouse (GAM) IRDye 800CW and goat anti-rabbit (GAR) IRDye 680 (LI-COR Biosciences; Lincoln, Nebraska) were diluted 1:10 000 in TBS + 0.1% Tween-20. The membrane was incubated in secondary antibody for 1 hour in a dark box at room temperature. The membrane was then washed 4 x for 5 minutes each in TBS + 0.1% Tween-20 and stored in TBS. The Odyssey® Infrared Imaging System was used to visualize and quantify immunoreactive proteins. Total NHE1 or exogenous NHE1 expression was quantitated and corrected with the total protein expression of actin. Protein expression of the exogenous NHE1 protein was slightly larger in apparent molecular weight, likely due to the HA tag[275].

2.2.2.2 Immunoblot Analysis of Transgenic Heart Lysates for Ion Regulatory Membrane Proteins

For some experiments, heart lysates were prepared to examine protein expression of membrane proteins involved in ion regulation of cardiomyocytes in hearts of NHE1 TG and control mice. Heart lysates and protein concentration were prepared as described in Section 2.2.2.1 and blots were run as described in described in Section 2.2.2.1. The primary antibodies used included; NKA (05-369) (Millipore; Billerica, Massachusetts), NCX (from Dr. Jonathan Lytton; University of Calgary, Calgary, AB), sarcoendoplasmic reticulum Ca^{2+}-ATPase (SERCA) (from Dr. Marek Michalak; University of Alberta, Edmonton, AB), NBC Isoform 1 (AB3208) (Millipore) and AE 1 and 3 (from Dr. Joe Casey, University of Alberta, Edmonton, AB). Primary and secondary antibodies were incubated as described in Section 2.2.2.1. Total expression of NKA, NCX, SERCA NBC1, AE1 or AE3 was quantified and expressed as % of controls.

2.2.2.3 Immunoblot Analysis of Transgenic Heart Lysates for MAPK and RSK

Heart lysates were prepared to examine phosphorylated ERK (pERK) 1/2 (Thr^{202}/Tyr^{204}) and total ERK 1/2, phosphorylated-p38 ($Thr^{180/182}$) (pp38) and total p38 or p38 α, phosphorylated JNK (pJNK) (Thr^{183}/Tyr^{185}) and total JNK Isoform 1/2/3 and phosphorylated RSK (pRSK)(Ser^{380}) and total RSK 1 and 2 immunoblots. Heart tissue was homogenized at a high setting with an OMNI 2000 homogenizer in lysis buffer [(mM)(50 HEPES, 100 NaCl, 50 NaF, 1 ethylene glycol tetraacetic acid (EGTA), 1 ethylenediaminetetraacetic acid (EDTA), 4 phenylmethylsulfonyl fluoride, 0.8 Na_3VO_4), (μM) (0.6 aprotinin, 8.6 leupeptin, 5.8 pepstatin A), and 1% Triton X-100]. The homogenate was centrifuged at 100 000 x *g* for 10 minutes at 4ºC and then the

supernatant was isolated[282]. Protein concentration of the supernatant was measured and blots were run as described in Section 2.2.1.1. Table I is a list of primary antibodies, corresponding secondary antibodies and cataolog number of the primary antibodies used for the MAPK and RSK western blots. Phosphorylated protein kinase expression was normalized to expression of the corresponding total protein kinase for control, N-line and K-line hearts and expressed as a % of controls.

Table I: Primary and secondary antibodies for the analysis of protein kinases.

	Primary Antibody	Secondary Antibody	Company and Catalog #
pERK	Phosphorylated-ERK (Thr^{202}/Tyr^{204}) Goat polyclonal	Donkey anti-goat IRDye 800CW	Cell Signaling Technology (#9106)
ERK	ERK 1/2 (p44/p42 MAPK) Rabbit polyclonal	Goat anti-rabbit IRDye 680	Cell Signaling Technology (#9102)
pp38	Phosphorylated-p38 ($Thr^{180/182}$) Rabbit polyclonal	Goat anti-rabbit IRDye 680	Santa Cruz (sc-17852)
p38 (α)	p38 (α) Goat polyclonal	Donkey anti-goat IRDye 800CW	Santa Cruz (N20) (sc-728) or (C20) (sc-535)
pJNK	Phosphorylated-JNK (Thr^{183}/Tyr^{185}) Goat polyclonal	Donkey anti-goat IRDye 800CW	Santa Cruz (sc-12882)
JNK	JNK 1/2/3 Rabbit polyclonal	Goat anti-rabbit IRDye 680	Santa Cruz (sc-581)
pRSK	Phosphorylated-RSK (Ser^{380}) Rabbit polyclonal	Goat anti-rabbit IRDye 680	Cell Signaling Technology (#9323)
RSK	RSK 1 and 2 Goat monoclonal	Donkey anti-goat IRDye 800CW	Santa Cruz (C21) (sc-231) and (C18) (sc-1430)

2.2.2.4 Immunoblot Analysis of Transgenic Heart Lysates for Markers of Apoptosis

Markers of apoptosis, apoptosis-inducing factor (AIF), cytochrome C (Cyt c) and poly (ADP-ribose) polymerase (PARP), were measured in both the cytosolic and mitochondrial fraction of hearts from TG and control mice[283]. Heart tissues were homogenized in sucrose buffer [(mM) (300 sucrose, 10 Tris-HCl, 2 EGTA; pH 7.4, 0.5% BSA], then centrifuged at 2 000 x *g* for 2 minutes at 4°C, and then the supernatant was centrifuged at 10 000 x *g* for 5 minutes at 4°C. The remaining pellet, the mitochondrial fraction, was then washed three times at 10 000 x *g* for 5 minutes at 4°C and resuspended in sucrose buffer. The latter was centrifuged at 100 000 x *g* for 60 minutes at 4°C and the supernatant was used as the cytosolic fraction. Protein concentrations of both the mitochondrial and cytosolic fractions were measured as described in Section 2.2.2.1. The purity of the mitochondrial fraction was tested by immunoblotting with anti-histone antibody (H5100-02B, US Biological; Swampscott, MA), a nuclear marker, following the same immunoblotting procedure described in Section 2.2.2.1. The purity of the mitochondrial fraction was based on the absence of nuclear markers in the mitochondrial fraction. Cytosolic or mitochondrial lysates were immunoblotted with Cyt c (#4272, Cell Signaling Technology) and AIF (#4642, Cell Signaling Technology) antibodies. Cleaved PARP protein expression, detected by anti-PARP antibody (#9542, Cell Signaling Technology), was only examined in the cytosolic fraction. Mitochondrial superoxide dismutase (MnSOD) (SOD -110, Stressgen; Ann Arbor, MI) was used as a loading control for protein measured in the mitochondrial fraction. Glyceraldehyde 3-phosphate dehydrogenase (GAPDH) (ab9485, Abcam; Cambridge, MA) was used as a loading

control for proteins measured in the cytosolic fraction. Actin was used as a loading control for heart lysates immunoblotted with anti-PARP antibody. Heart lysates immunobloted with anti-Cyt c antibody were resolved on 8% SDS-PAGE, whereas all others were resolved on 10% SDS-PAGE (as described in Section 2.2.2.1). Table II is a list of primary antibodies and corresponding secondary antibodies used to detect proteins that represent markers of apoptosis.

Table II: Antibodies used to detect markers of apoptosis. Protein expression of AIF and Cyt c were examined in the mitochondrial and cytosolic fractions. PARP was examined in the cytosolic fraction. MnSOD was used as a loading control for proteins examined in the mitochondrial fraction. GAPDH was used as a loading control for proteins examined in the cytosolic fraction. Actin was used as a loading control in the cytosolic fraction blotted for cleaved PARP. The source of the primary antibodies is indicated below the specified antibody.

Fraction		**Primary Antibody**	**Secondary Antibody**	*Loading Control*
Mitochondria	AIF	AIF Rabbit polyclonal	Goat anti-rabbit IRDye 680	**MnSOD** Rabbit polyclonal Goat anti-rabbit IRDye 680
	Cyt c	Cyt c Rabbit polyclonal	Goat anti-rabbit IRDye 680	**MnSOD** Rabbit polyclonal Goat anti-rabbit IRDye 680
Cytosol	AIF	AIF Rabbit polyclonal	Goat anti-rabbit IRDye 680	**GAPDH** Rabbit polyclonal Goat anti-rabbit IRDye 680
	Cyt c	Cyt c Rabbit polyclonal	Goat anti-rabbit IRDye 680	**GAPDH** Rabbit polyclonal Goat anti-rabbit IRDye 680
	PARP	PARP Rabbit polyclonal	Goat anti-rabbit IRDye 680	**Actin** Rabbit polyclonal Goat anti-rabbit IRDye 680

2.2.2.5 Immunoblot Analysis of Transgenic Heart Lysates for GSK-3β

Phosphorylated-glycogen synthase kinase-3β (pGSK-3β) (Ser9) (5B3, Cell Signaling Technology) and total GSK-3β (27C10, Cell Signaling Technology) protein expression were measured in the cytosolic and mitochondrial fractions. The cytosolic and mitochondrial fractions were prepared as described in Section 2.2.2.4. Protein concentrations were measured as described in Section 2.2.2.1. Blots were run as described in Section 2.2.2.1. GSK-3β and pGSK-3β were normalized for MnSOD in the mitochondrial fraction, and were normalized for GAPDH in the cytosolic fraction. pGSK-3β/MnSOD, pGSK-3β/GAPDH, GSK-3β/MnSOD or GSK-3β/GAPDH were expressed as a % of controls. Table III lists primary antibodies and corresponding secondary antibodies used to detect pGSK-3β and GSK-3β protein expression.

Table III: Antibodies used for the detection of pGSK-3β and GSK-3β. Total and phosphorylated GSK-3β were analyzed in heart lysates from NHE1 TG and control mice. The source of the antibodies is indicated below the specified antibody. Primary antibodies used include GSK-3β and pGSK-3β, which were normalized for MnSOD in the mitochondrial fraction and GAPDH in the cytosolic fraction.

Fraction		**Primary Antibody**	**Secondary Antibody**	*Loading Control*
Mitochondria	pGSK-3β	pGSK-3β Rabbit polyclonal	Goat anti-rabbit IRDye 680	**MnSOD** Rabbit polyclonal
	GSK-3β	GSK-3β Rabbit polyclonal	Goat anti-rabbit IRDye 680	Goat anti-rabbit IRDye 680
Cytosol	pGSK-3β	pGSK-3β Rabbit polyclonal	Goat anti-rabbit IRDye 680	**GAPDH** Rabbit polyclonal
	GSK-3β	GSK-3β Rabbit polyclonal	Goat anti-rabbit IRDye 680	Goat anti-rabbit IRDye 680

2.2.2.6 Immunoblot Analysis of Transgenic Heart Lysates for ER Stress Response Proteins

Anti-calreticulin and anti-protein disulfide isomerase (PDI) antibodies were a generous gift from Dr. Marek Michalak (University of Alberta; Edmonton, Alberta). Heart lysates from control, N-line and K-line hearts were prepared as described in Section 2.2.2.1. Protein concentrations were measured as described in Section 2.2.2.1. Blots were run as described in Section 2.2.2.1. Calreticulin and PDI protein expression were normalized with actin protein expression and expressed as % of controls.

2.2.3 Collection of NHE1 Transgenic Heart Specimens

Mice were euthanized with halothane and hearts were isolated for the following analyses, and used as markers of cardiac hypertrophy; *1*) Heart Weight to Body Weight ratio (HW/BW), *2*) Histological studies, *3*) ANP mRNA expression.

2.2.3.1 HW/BW of NHE1 Transgenic Mice

CH was evaluated by measuring the HW/BW, in mg/g. Body weight of control, N-line and K-line hearts was measured, and then the hearts were excised. All extracardiac structures were then removed. The hearts were then washed in PBS, blotted and weighed[284]. To examine whether changes in the heart weight were due to edema, water content was evaluated in the isolated hearts. This was ensured by the dry weight to wet weight ratio. The initial weight of the freshly isolated heart is the wet weight. Dry weight is the weight after incubation at 100ºC for 24 hours. The dry weight to wet weight ratio was calculated according to the formula: Dry tissue weight /Wet tissue weight[285].

2.2.3.2 Expression of ANP mRNA in Hearts from NHE1 Transgenic Mice

ANP mRNA expression was measured by real-time PCR[286]. Heart tissues were homogenized in Trizol reagent according to the manufacturer's instructions. 1 μg of the isolated RNA was transcribed to cDNA using Superscript™ III First-Strand Synthesis SuperMix (Invitrogen) according to the manufacturer's instructions. Real-time PCR was performed using SYBR Green JumpStart *Taq* ReadyMix (Sigma) and fluorescence was measured with a DNA Engine Opticon 2 system (MJ Research; Waltham, MA). The 18S ribosomal RNA (18S rRNA) gene has been demonstrated to be highly stable and conserved, and selected as a reference gene[287]. The primer sequences and PCR conditions for ANP and 18S rRNA are shown in Table IV and Table V, respectively[286, 287]. For each reaction tube, the fluorescence signal of the reporter dye (SYBR) of each unknown sample containing ANP primers was divided by the fluorescence signal of the reporter dye (SYBR) of each unknown sample containing 18S rRNA to obtain a ratio, which is defined as indirect quantified data. This ratio was normalized to a standard curve, which was created using varying concentrations of the pooled sample set. A negative control, containing individual ANP or 18S rRNA forward and reverse primers, was run for each experiment.

Table IV: Synthetic oligonucleotide primer sequences for real-time PCR analysis of ANP and 18S rRNA. ANP and 18S rRNA primer sequences were as described by Xia et al. 2007[286].

Gene		Primer Sequence
ANP	Sense	5′—CTGCTAGACCACCTGGAGGA—3′
	Antisense	5′—AAGCTGTTGCAGCCTAGTCC—3′
18S rRNA	Sense	5′—GTAACCCGTTGAACCCCATT—3′
	Antisense	5′—CCATCCAATCGGTAGTAGCG—3′

Table V: Real-time PCR conditions for ANP and 18S rRNA. Fluorescence was measured with a DNA Engine Opticon 2 system under the following conditions[286].

Gene	Initial Denaturation	Cycles	Denaturation	Annealing	Extension	Prolonged Extension
ANP	94°C, 15 min	35	94°C, 20 sec	59°C, 20 sec	72°C, 30 sec	72°C, 5 min
18S rRNA	94°C, 15 min	35	94°C, 20 sec	59°C, 20 sec	72°C, 30 sec	72°C, 5 min

2.2.3.3 Histology of Hearts from NHE1 Transgenic Mice

Isolated hearts were fixed overnight in 10% buffered formalin, then embedded in paraffin, and serially sectioned into 5-μm thick slices[208,288]. These heart cross sections were stained with hematoxylin and eosin (H&E) to evaluate gross morphology and cross sectional area or with picrosirius red (PSR) to assess fibrosis[289]. The nuclei in the heart cross sections were stained with hematoxylin (haematin binds to nuclear histones) and then counterstained with eosin to view the cellular details. PSR stains for collagen. In bright-field microscopy, collagen is red on a pale yellow background. Interstitial fibrosis (IF) was measured from digitized images using Open lab 3.5 (Improvision Inc;Waltham, MA) and digitized images were gathered using a QImaging camera (QImaging; Surrey, BC) equipped to a Leica DMLA microscope. 3-4 cross sections were used from each heart with ten fields randomly selected. The maximum fibrosis observed for any section was calculated (areas occupied by red stained connective tissue) x 100/ (areas occupied by connective tissue plus cardiac myocytes). Intramural vessels, the perivascular collagen, the endocardium and the trabeculae were excluded from these measurements[290]. Cross sectional area (CSA) was measured from digitized images using Image ProPlus Version 4.5. Digitized images were gathered using a Photometrics CoolSNAP$_{fx}$ camera equipped to a Leica DMIRB microscope. Dimensions of at least 100 cells from 3-4 cross sections per heart were measured. Visual fields were accepted for quantification if nuclei were visible and cell membranes were intact[208, 289].

2.2.3.4 Calcineurin Phosphatase Activity of Hearts from NHE1 Transgenic Mice

Calcineurin phosphatase activity in hearts from control, N-line and K-line mice were assayed using the BIOMOL Green Cellular Calcineurin Assay Kit Plus (BIOMOL Research Laboratories, Plymouth Meeting, PA)[291,292]. The assay was conducted according to the manufacture's instructions. Briefly, hearts were homogenized at 4°C in lysis buffer containing a protease inhibitor, and then the supernatant was collected. Free phosphates were removed by passing the supernatant through centri-spin 10 columns (Princeton Separations, Freehold, NJ). To discriminate between the contributions of other phosphatases, total phosphatase activity was measured in the presence of EGTA (to inhibit PP2B (calcineurin)), or in the presence of 100 nM okadaic acid (to inhibit PP1 and PP2A), or in the presence of EGTA and okadaic acid (to inhibit PP1, PP2A and PP2B (calcineurin), not PP2C). The reaction was carried out in a 96 well microtiter plate. It was initiated by the addition of the sample, and terminated by the addition of BIOMOL green reagent. The color was allowed to develop for 30 minutes and then the optical density was measured at 620nm. Calcineurin activity was calculated for each group using the following equation, calcineurin activity = (total activity in the presence of okadaic acid) – (total activity in the presence of okadaic acid and EGTA)**.**

2.2.3.5 Electron Microscopy of Hearts from NHE1 Transgenic Mice

Hearts were perfusion fixed with 2% paraformaldehyde-2% glutaraldehyde. Tissue from the hearts were then sectioned and stained by the conventional osmium-uranium lead method[291].

2.2.3.6 Measurement of Terminal Deoxynucleotidyl Transferase Mediated dUTP Nick End Labeling Staining in Hearts from NHE1 Transgenic Mice

Terminal deoxynucleotidyl transferase mediated dUTP nick end labeling (TUNEL) staining was performed on paraffin-embedded heart cross sections using DeadEnd™ Fluorometric TUNEL System (Promega, Madison, WI) as per manufacture's instructions[288,293]. Heart cross sections were deparaffinized and treated with Proteinase K, which permeabilizes the tissue to the staining reagents. The heart cross sections were then equilibrated with equilibration buffer [(mM) (200 potassium cacodylate (pH 6.6 at 25ºC), 25 Tris-HCl (pH 6.6 at 25ºC), 0.2 DTT, 2.5 cobalt chloride) and 0.25mg/mL)] and then incubated with terminal deoxynucleotidyl transferase (Tdt). To distinguish TUNEL positive nuclei from TUNEL negative nuclei, heart cross sections were counterstained with 4'-6-Diamidino-2-phenylindole (DAPI). For negative controls, heart cross sections were treated similarly, but in the absence of the Tdt enzyme. For positive controls, heart cross sections were treated with DNase I, which fragments the DNA. TUNEL-positive cells were measured from digitized images using Image ProPlus Version 4.5. Digitized images were gathered using a Photometrics CoolSNAP$_{fx}$ camera equipped to a Leica DMIRB microscope with filters set to view the green fluorescence of TUNEL stained cells (520 nm) and blue DAPI stained cells (460 nm). TUNEL-positive cells were counted in five randomly selected fields per slide and three cross sections per heart and averaged for statistical analysis to represent an n=1. The percentage of nuclei labeled by TUNEL per unit of cells stained with DAPI reflected the apoptotic index. The observer was blinded to the treatment group.

2.2.3.7 Caspase-3 Activity of Hearts from NHE1 Transgenic Mice

For measurement of caspase-3 activity, freshly collected hearts were homogenized at 4ºC in 1 mL of 10x PBS, pH 7.4, and then centrifuged with 10 000 x *g* for 20 minutes. 10 μL of the supernatant was mixed with 40 μL of assay buffer [(mM) (100 NaCl, 50 HEPES, 10 DTT, 1 EDTA), 10% Glycerol, 0.1% CHAPS (3-[(3-cholamidopropyl)dimethylammonio]-1-propanesulfonate), pH 7.4)]. 50 μL of the caspase-3 substrate I, which contains 200 μM of acetyl-Aspartic-Glutamic-Valine-Aspartic p-nitroanilide (Ac-DEVD-pNA) (Alexis Biochemical's, Farmingdale NY), was added to the mixture. The absorbance was measured at 405 nm. This caspase-3 colorimetric assay is based on the hydrolysis of Ac-DEVD-pNA by caspase-3, which results in the release of p-nitroaniline and its absorbance is read at 405 nm[288].

2.2.4 Echocardiography of NHE1 Transgenic Mice

Echocardiography was performed on isoflurane anesthetized mice using a Vevo 770 ultrasound unit (VisualSonics Inc., Toronto, ON) equipped with a 35MHz transducer. The short axis M-mode analysis, at the level of the papillary muscle, was used for measurements of diastolic and systolic diameters of the left ventricle and wall thickness. Pulsed wave doppler was used at the level of the left ventricular outflow tract, the right ventricular outflow tract and the mitral valve tip, to monitor flow patterns and velocity. The myocardial performance index or Tei index was calculated using the equation: (isovolumic contraction time + isovolumic relaxation time)/(ejection time)[294].

2.2.5 In Vivo Stimulation of NHE1 Transgenic Mice Using Alzet Osmotic Mini Pumps

2.2.5.1 Preparation of Alzet Osmotic Mini Pumps

Alzet osmotic mini pumps are miniature implantable pumps, which continuously deliver reagents at controlled rates for a set duration of time. Alzet osmotic mini pump model 1002 (Alzet Osmotic Pumps; Cupertino, CA) were used in some of our studies. They had a mean pump rate of 0.25μL±0.1/hour and the test reagent was administered over a two-week period. For studies in which EMD 87580 was infused using Alzet osmotic mini pumps, Alzet osmotic mini pumps model 1004 were used. The mean pump rate was also 0.25μL±0.1/hour and was administered over twenty-eight days. Alzet osmotic mini pumps attached to their flow modulators were weighed before being filled and were then filled using the appropriate test reagent. The pumps were weighed again after being filled, to ensure that the pumps have been filled to greater or equal to 90% of the mean fill volume, determined by the manufacture's set values. Preparation of the sterile test reagent were based on average basal body weight of the animal set being used during the experiment, as well as the mean pump rate set by the manufacture. The following equation was used in preparation of sterile test reagents:

$$C_d \text{ (concentration of solution, in } \mu g/\mu L) = \frac{K_o \text{ (compound delivered/hour, in } \mu gC)}{Q \text{ (mean pumping rate, } \mu L/\text{ hour)}}$$

K_o is calculated by multiplying the desired concentration [(ng/μg/mg)/kg/duration (seconds/minutes/hours/days)] by the average mouse basal body weight. Q, the mean

pumping rate, was 0.25μL±0.1/hour for Alzet pumps 1002 and 1004. Alzet osmotic mini pumps were filled with 50mg/kg/day PE (dissolved in phosphate buffered saline (PBS)) or PBS (vehicle). The concentration of PE used in our experiments was based on our own preliminary experiments and the work of others[295-297]. In our preliminary experiments, male control mice, 10-12 weeks of age, were infused with PBS (control) or 50mg/kg/day PE. Hearts from these mice were used to isolate AVMs (as described in Section 2.2.1), and cell area was measured (as described in Section 2.2.1.2). For studies in which EMD 87580 was administered using Alzet osmotic mini pumps, NHE1 TG mice and controls were treated with 10mg/kg/day of EMD 87580[71,298,299]. EMD 87580 was dissolved in PBS. PBS was used as a control in parallel experiments. HW/BW (as described in Section 2.2.3.1) and CSA (as described in Section 2.2.3.3) were measured in NHE1 TG and control mice infused with EMD 87580. Delivery of test reagent through Alzet osmotic mini pumps was verified by measuring the residual volume in the Alzet osmotic mini pumps after being explanted from the animal. The residual volume was aspirated using the filling tube and the volume obtained was measured. This value corresponded with the predicted residual volume = [actual fill volume - (mean pump rate x infused duration (hours)].

2.2.5.2 Surgical Implantation of Alzet Osmotic Mini Pumps

All animal surgeries were performed in an asceptic certified surgery room at the University of Alberta, Health Sciences Laboratory Animal Services facility. Mice were anesthetized with a cocktail containing a mixture of 100 mg/kg ketamine and 2.5 mg/kg acepromazine. The anesthesia was maintained using 1% isoflurane. Mice were kept on

an asceptic heating pad throughout the surgery. A small incision was made in the mid scapular region of the mice, using sterilized surgical tools. By spreading apart the subcutaneous tissue, a small pocket was created and an Alzet osmotic mini pump filled with the desired test reagent was inserted. The incision was closed with sutures and animals were left overnight in the surgery room to recover. Drug-treated mice were paired with vehicle-treated mice, and housed in a conventional facility. In all studies, mice were matched for age and body weight, and were housed together throughout the duration of the experiment. Alzet mini osmotic pumps were removed two weeks following implantation. At this time, animals were sacrificed and hearts were removed and used to measure the HW/BW (as described in Section 2.2.3.1), ANP mRNA expression (as described in Section 2.2.3.2), IF and CSA (as described in Section 2.2.3.3). For experiments using Alzet osmotic mini pumps model 1004, pumps were removed twenty-eight days following implantation.

2.3 *Ex Vivo* Working Heart Experiments of NHE1 Transgenic Mice

2.3.1 Ex Vivo Working Mouse Heart Perfusions

Hearts from control, N-line and K-line hearts were perfused using an *ex vivo* working heart model[300]. Mice were anesthetized with 12 mg of pentobarbital sodium, and then hearts were excised. Excised hearts were immediately immersed in ice-cold Krebs-Henseleit bicarbonate (KHB) solution [(mM) (118.5 NaCl, 25 $NaHCO_3$ 4.7 KCl, 1.2 $MgSO_4$ 1.2 KH_2PO_4 2.5 $CaCl_2$, 0.5 EDTA, 5 glucose, 1.2 palmitate bound to 3% fatty acid-free BSA) and 100 μU/mL insulin]. The aorta and pulmonary vein were cannulated

and the hearts were perfused with KHB containing either [5-^{3}H/U-^{14}C] (GE Healthcare (Amersham); Baie d'Urfe, Quebec) labeled glucose and unlabeled palmitate for glycolysis and glucose oxidation measurements, or [U-^{14}C] (GE Healthcare (Amersham); Baie d'Urfe, Quebec) labeled glucose and [9,10-^{3}H] (PerkinElmer; Waltham, MA) labeled palmitate for glucose and palmitate oxidation measurements. Hearts were perfused aerobically for 30 minutes, and then subjected to 20 minutes of global no-flow ischemia, and this was followed by 40 minutes of aerobic reperfusion. Pressure and flow measurements were obtained every 10 minutes and 2.5 mL samples of perfusate were taken every 10 minutes for determination of metabolite content (glycolysis, glucose oxidation and palmitate oxidation). At the end of the experiment, hearts were frozen in liquid nitrogen and stored at -80ºC. To correct for variations in heart size, the dry weight to wet weight ratio was measured. Metabolic rates, ATP production rates and tricarboxylic acid (TCA) cycle acetyl CoA production rates were normalized to the total dry mass of the heart, calculated from the dry weight to wet weight ratio (as described in Section 2.2.3.1).

2.3.1.1 Measurement of Cardiac Function in Working Perfused Mouse Hearts

Cardiac function was measured in the *ex vivo* working perfused hearts[300]. Heart rate and pressure (peak systolic pressure and developed pressure) were detected by a pressure transducer in the aortic outflow line (Harvard apparatus; Massachusetts). Data was collected with an MP100 and analyzed using Acqknowledge (BIOPAC Systems Inc, California). Cardiac output (mL/min) and aortic outflow (mL/min) were obtained by measuring the flow detected by the transonic flow probe in the preload (set at 11.5

mmHg) and afterload line (set at 50 mmHg), respectively. Cardiac work (mL x mmHg/minute) = peak systolic pressure (mmHg) x cardiac output (mL/minute); Coronary flow (mL/minute) = cardiac output (mL/minute) - aortic flow (mL/minute); Cardiac power (mL x mmHg/minute) = developed pressure (mmHg) x cardiac output (mL/minute).

2.3.1.2 Measurement of Glycolysis, Glucose Oxidation and Fatty Acid Oxidation Rates in Working Perfused Mouse Hearts

Glycolysis, glucose oxidation and fatty acid (FA) oxidation rates were measured in the *ex vivo* working perfused hearts[300]. Glycolytic rates (nmol x g dry wt^{-1} x min^{-1}) were determined by measuring the amount of ^3H_2O, which is released from the metabolism of [5-^{3}H] glucose at the enolase step of glycolysis. Glucose oxidation rates (nmol x g dry wt^{-1} x min^{-1}) were determined by measuring the amount of $^{14}CO_2$ released from the metabolism of [U-^{14}C] glucose at the level of the pyruvate dehydrogenase complex and in the TCA cycle. Palmitate oxidation rates (nmol x g dry wt^{-1} x min^{-1}) were determined by measuring the amount of ^3H_2O derived from the metabolism of [9,10-^{3}H] palmitate. Specific activities of each tracer were determined by adding 10 μL of the buffer in the appropriate window (^{3}H or ^{14}C) of the scintillation counter. Metabolic rates were also compared after normalization for differences in contractile performance (cardiac power). Metabolic rates were divided by cardiac power [(nmol x g dry wt^{-1} x min^{-1})/(mL x mmHg/min)].

2.3.1.3 Measurement of ATP Production Rates and TCA Cycle Acetyl CoA Production Rates in Working Perfused Mouse Hearts

The ATP production rates (μmol x g dry wt^{-1} x min^{-1}) from glucose oxidation, glycolysis and palmitate oxidation of the *ex vivo* working perfused hearts was calculated by multiplying the respective rates of oxidation to the amount of ATP (2 moles of ATP per mole of glucose passing through glycolysis, 30 moles of ATP per mole of glucose being oxidized and 105 moles of ATP per mole of palmitate oxidized)[300]. For TCA cycle acetyl CoA production rates (μmol x g dry wt^{-1} x min^{-1}), the respective rates of palmitate oxidation and glucose oxidation were multiplied by the amount of TCA cycle acetyl CoA (oxidation of 1 mole of glucose produces 2 moles of acetyl CoA and oxidation of 1 mole of palmitate produces 8 moles of acetyl CoA)[300]. Cardiac efficiency was determined by dividing cardiac power by ATP production rates or TCA cycle acetyl CoA production rates [(mL x mmHg/min)/(μmol x g dry wt^{-1} x min^{-1})].

2.3.1.4 Measurement of Proton Production in Working Perfused Mouse Hearts

The rates of H^+ production were derived from the rates of glucose oxidation and glycolysis in the *ex vivo* working perfused hearts[301,302]. The rates of glucose oxidation were subtracted from the rates of glycolysis and multiplied by 2. Proton production was calculated using this method and has previously been demonstrated to correlate well with pH_i in a global ischemia model[303].

2.3.2 Western Blot Analyses of Hearts Subjected to Ex Vivo Perfusions

pERK/ERK, pp38/p38, pJNK/JNK, pRSK/RSK, pGSK-3β/GSK, phosphorylated AMPK (Thr172) (#2531) (Cell Signaling Technology) and total AMPK α (#2532) (Cell Signaling Technology) protein expression were examined in heart lysates subjected to I/R as described in Section 2.3.1. Heart lysates were homogenized at a high setting with an OMNI 2000 homogenizer in lysis buffer [(mM) (50 Tris-HCl (pH 8 at 4°C), 1 EDTA, 1 DTT), 10% (wt/vol) glycerol, 0.02% (vol/vol) Brij-35, protease inhibitors and phosphatase inhibitors][304]. The homogenates were centrifuged at 10 000 x *g* for 20 minutes at 4°C, and the resultant supernatant was used for immunoblotting as described in Section 2.2.2.1 and Table I.

2.4 *In Vitro* Experimentation using Isolated Neonatal Rat Ventricular Cardiomyocytes

2.4.1 Isolation of Neonatal Rat Ventricular Cardiomyocytes

Primary cultures of cardiomyocytes were prepared from 5-to 6-day-old neonatal Sprague-Dawley rat heart ventricles[86,305]. Hearts were removed from 5-6 day old rats under aseptic conditions, followed by removal of the atria and any extracardiac tissue. The ventricles were gently minced in solution I (5 mL 10x hanks buffered salt solution (HBSS), 1 mL 1M HEPES, and 1 mL 1% penicillin/streptomycin mixed stock solution). The tissue was then digested in three separate treatments of collagenase solution II (0.1% Type II Worthington collagenase in combination with solution I). The

collagenase digestion was carried out 3 times with 20, 15 and 8 mLs of collagenase soution, each treatment lasted 20 minutes and was maintained at 37°C with gentle stirring under sterile conditions. Upon completion of each treatment, the digested tissue was neutralized with ice cold solution III (20% FBS, 5 mL 10x HBSS, and 1 mL 1% penicillin/streptomycin mixed stock solution). At the end of all 3 treatments, all suspensions were combined and filtered using a 70 μm cell strainer to remove debris, and centrifuged for 8 minutes at 2 000 rpm at room temperature. The supernatant was discarded and the remaining pellet containing cardiomyocytes was resuspended in solution IV (Dulbecco's modified Eagle's medium (DMEM/F12), 0.25 mg/mL fetuin, 5 μg/mL transferrin, 5 μg/mL insulin, 5 ng/mL selenium, 50 U/mL penicillin, 50 μg/mL streptomycin, 0.72 mM calcium chloride, 0.11 mM L-ascorbic acid, 10 mg/mL BSA, 0.1 mM MEM non-essential amino acids, 10% MEM vitamin, pH 7.4). Dissociated cells were incubated in T-75 flasks at 37°C in a humidified atmosphere (95% O_2-5% CO_2) for 45 minutes. During this time, fibroblasts, endothelial cells, and smooth muscle cells attach and the majority of cardiomyocytes remain in suspension. Isolated cardiomyocytes were then plated on to appropriate sized cell culture dishes according to the experimental procedure, and maintained for 2 days in solution V (DMEM/F12 supplemented with 10% FBS, 10 μg/mL transferrin, 10 μg/mL insulin, 10 ng/mL selenium, 50 U/mL penicillin, 50 μg/mL streptomycin, 2 mg/mL BSA, 5 μg/mL linoleic acid, 3 mM pyruvic acid, 0.1 mM MEM nonessential amino acids, 10% MEM vitamin, 0.1 mM bromodeoxyuridine, and 30 mM HEPES (pH 7.4)). Previous studies have shown that cardiomyocytes were able to maintain their morphology and characteristic cross striations for up to two weeks and were free of non-myocardial cells[185].

Adenoviruses were chosen as a tool to express NHE1 in NRVMs because in previous studies primary cultures were shown to be refractory to lipid or Ca^{2+} transfections[306, 307]. On the other hand, infection of NRVMs with adenoviruses resulted in almost 100% efficiency[308].

2.4.2 Construction of Adenoviruses Expressing NHE1

Adenoviral vectors containing HA tagged-wild type NHE1 (IRM) resistant to NHE1 inhibition or HA tagged-active NHE1 (K-IRM) resistant to NHE1 inhibition used for infection of NRVMs. The GFP protein was co-expressed in all adenoviral vectors. Use of adenoviruses expressing inhibitor resistant NHE1, allowed us to study the effects of just exogenous NHE1 expression, while inhibiting endogenous NHE1.

2.4.2.1 Construction of NHE1 Inhibitor Resistant Plasmid

The $pYN4^+$ plasmid, which contains the human cDNA of NHE1-HA tagged (as described in Section 2.1.1), was used as the template for the development of the IRM plasmid. The IRM plasmid contains a double mutation, leucine (L) 163 to phenylalanine (F) and glycine (G) 174 to serine (S) in $pYN4^+$. Figure 1.1 depicts the NHE1 TM segment with the following mutations. This mutation has previously been shown to increase the resistance to NHE1 inhibitors[309]. The DNA mutations were introduced into the $pYN4^+$ plasmid by PCR. The primers for this mutant were, $pYN4^+$L163F*f*-GACGTCTTCTTCtTCTTCCTcCTcCCGCCCATCATCC, $pYN4^+$L163F*r*-GGATGATGGGCGGgAGgAGGAAGAaGAAGAAGACGTC and $pYN4^+$G174S*f* -CATCCTGGATGCtagCTACTTCCTGCCAC, $pYN4^+$G174S*r*-

GTGGCAGGAAGTAGctaGCATCCAGGATG. Mutations (lower case) were also introduced to add restriction enzyme sites (Nhe1 and BseR1) used for screening plasmids. The PCR reaction contained: 1.5 mM MgSO4, 250 μM dNTPs, 5 μL High Fidelity 10x PCR buffer, 10 μM forward primer, 10 μM reverse primer, 750 ng template DNA, 2.5 Unit of Platinum® Taq Polymerase High Fidelity (Invitrogen), and were brought to a final volume of 50 μL with ddH_20. PCR was performed using one cycle of 94˚C for 3 minutes, 16 cycles of 94˚C for 1 minute, one cycle of 55˚C for 2 minutes and one cycle of 72˚C for 15 minutes. All PCR products were digested with 1 Unit of the restriction enzyme Dpn1 (New England Biolabs; Toronto, Ontario) for 1 hour at 37˚C to remove methylated template DNA. This DNA (approximately 1 μL) was used to transform into DH5α competent cells (Invitrogen) by electroporation, using 1.8 kV, 25 μF capacitance and 150 Ω resistance (Biorad Gene Pulser®II). Transformed bacterial cells were transferred to Luria-Bertani (LB) medium and placed in a 37˚C shaker for 1 hour, and then plated on LB agarose plates containing 100 μg/mL Amp and incubated at 37˚C for 18 hours. Transformed colonies were picked and cultured in LB media containing 100 μg/mL Amp and incubated at 37˚C for 18 hours. Bacterial cells were harvested by centrifugation at 12 000 rpm for 2 minutes. Bacterial cell pellets were resuspended in Solution A [(mM)(50 Glucose, 25 Tris pH 8.0, 10 EDTA), followed by addition of Solution B (0.2 M NaOH and 1% SDS), followed by addition of solution C (3 M Potassium-Actetate and 1.5% glacial acetic acid). The cell suspension was then centrifuged at 12 000 rpm for 5 minutes. Plasmid DNA was extracted from the supernatant using PCI (as described in Section 2.4.2.2). In this case, the DNA pellet was resuspended in 50 μL TE buffer solution (10 mM Tris pH 8.0, 1 mM EDTA pH 8.0, and

20 μg/mL RNase) and incubated at 37˚C for 30 minutes. Restriction enzyme digests were performed to confirm that the PCR reaction introduced the proper mutations. The digestion reaction contained: 10x buffer, 10 U of enzyme (Nhe1 and BSeI), template DNA (purified plasmid DNA), all brought to volume with ddH_20. Samples from the digestion reaction were then run on 1% agarose gel to confirm the PCR product was correct, and of proper size. The plasmid DNA was further purified using the Qiagen Plasmid Maxi kit (Qiagen; Mississauga, Ontario) according to the manufacture's instructions. This resulted in the NHE1 inhibitor resistant plasmid DNA (IRM).

In NRVMs, 10 μM of EMD 87580, the NHE1 inhibitor, inhibited endogenous NHE1 but not exogenous NHE1 with the L163F/G174S mutations (as described in Section 2.4.2.1)[275]. This concentration was used in our *in vitro* studies to study the exogenous NHE1 expression.

2.4.2.2 Construction of Active NHE1 Inhibitor Resistant Plasmid

Construction of the active NHE1 DNA (1K3R4E) was described in Section 2.1.1. Construction of IRM was described in Section 2.4.2.1. For construction of K-IRM, which contains both the IRM and the 1K3R4E plasmid, restriction enzyme digests were performed, which moved the resistance-containing region in the IRM plasmid into the 1K3R4E plasmid. Both plasmids were digested with the enzymes AgeI and SpeI. The 50 μL digestion reactions contained: 5 μL 10x buffer reaction, 10 U of enzyme, 1 μL of purified plasmid DNA, and was brought to volume with ddH_20. The digests were resolved on a 1% low melting point agarose gel (low melting point agarose, 1xTBE and ethidium bromide), and the specific bands were viewed on a UV box and excised. DNA

fragements were purified by placing frozen gel slices between clean parafilm and gently squeezing out the DNA. The liquid containing DNA was collected and purified by adding PCI (as described in Section 2.4.2.2). DNA was precipitated with 100% ethanol, washed with 70% ethanol and the DNA pellet was resuspended in 10 μL ddH_20. Purified DNA fragments were ligated using T4 DNA ligase (New England Biolabs). The ligation reaction mixture contained 2 μL 10x T4 DNA ligase buffer, 20 U of T4 DNA ligase, 9 μL insert DNA and 1 μL vector DNA. The ligase reaction was incubated at 16˚C for 16 hours. Ligated DNA (approximately 1 μL) was used to transform into DH5α competent cells and obtain purified plasmid DNA as described in Section 2.4.2.1.

2.4.2.3 Subcloning (Transferring) the cDNA of IRM and K-IRM into the pAdTrack-CMV Plasmid

PCR was used to transfer the cDNA of both the IRM and K-IRM into a new template plasmid, the pAdTrack-CMV. The pAdTrack-CMV plasmid is driven by the cytomegalovirus (CMV) promoter and contains a kanamycin (Kan) resistance cassette for selection, and is used as a backbone vector for constructing GFP trackable viruses. The PCR reaction mix contained plasmid DNA from either IRM or K-IRM and the following primers, MackPyn*f* -CCGGGGTACCGCCACCATGGTTCTGCGGTCTGG and MackPyn*r* –GGAAGCTTAAGCTTCTACTGAGCAGCGTAATCTGGAAC, which flanked the insert with Kpn I and Hind III restriction sites, respectively. The remaining contents of the PCR reaction and the conditions of the PCR reaction were as described in Section 2.4.2.1. The IRM or K-IRM plasmids were ligated with the pAdTrack-CMV plasmid as previously described in Section 2.4.2.2. Ligated DNA (approximately 1 μL)

was used to transform DH5α competent cells and obtain purified plasmid DNA as described in Section 2.4.2.1. The restriction enzymes used for this plasmid were KpnI and Hind III. This resulted in pAdTrack-CMV containing either the IRM or K-IRM plasmids.

2.4.2.3.1 Characterization of pAdTrack-CMV Containing IRM or K-IRM Plasmids Transfected in AP-1 cells

The pAdTrack-CMV containing IRM or K-IRM plasmids were characterized in AP-1 cells as described in Section 2.1.3. NHE1 protein expression (as described in Section 2.1.3.2) and NHE1 activity (as described in Section 2.1.3.3) were examined in AP-1 cells transfected with the pAdTrack-CMV containing IRM or K-IRM plasmids or the pAdTrack-CMV plasmid, which was the control. For some NHE1 activity assays, EMD 87580, an NHE1 inhibitor, was used to confirm the inhibitor resistant effects of the plasmids. 10 μM of EMD 87580 was added at the beginning of the assay and maintained throughout the experiment.

2.4.2.4 Generation of the Recombinant Adenoviral Plasmids Containing NHE1

The pAdTrack-CMV containing IRM or K-IRM plasmids were cloned into the pAdEasy-1 vector, which contained the adenovirus 5 genome in the absence of the E1 and E3 gene, two recombinant arms, and an Amp resistance cassette for selection. Initially, the pAdTrack-CMV-IRM or K-IRM plasmids were linearized with Pme1, a restriction enzyme. The contents of the restriction enzyme digestion were as described in Section 2.4.2.1. DNA fragements were purified by running them on 1% low melting point agarose followed by extraction, purification and precipitation as described in

Section 2.4.2.1. The Pme1 cut shuttle vector (300 ng) was used to transform into *E. coli* strain BJ5183 (Stratagene; La Jolla, CA) as previously described in Section 2.4.2.1. BJ1583, which contains the pAdEasy-1 vector, allows for recombination between the pAdEasy-1 vector and the pAdTrack-CMV shuttle vector containing the IRM or K-IRM plasmids. Purified plasmid DNA was obtained as described in Section 2.4.2.1. The identity of the isolated plasmid DNA was confirmed by digestion with the restriction enzyme Pac1, and seperation was on a long 1% agarose gel. Non-recombined pAdEasy-1 was ~23 kb, properly recombined pAdEasy-1 and pAdTrack-CMV have two Pac 1 sites, ~20 kb and 3 or 4.5 kb, with the smaller band of 3 or 4.5 kb resulting from differences in recombination sites. The newly produced recombinant DNA was retransformed into XL-1 Blue *E. Coli*. . Unlike BJ1583, XL-1 Blue *E. Coli*., is a bacterial strain with relatively low recombinase levels, which could result in unwanted recombination events. The bacterial plasmid DNA was then extracted, purified and precipitated (as described in Section 2.4.2.1). Recombinants were checked using Pac1, BamH1 and EcoR1. The plasmid DNA was further purified using the Qiagen Plasmid Maxi kit (Qiagen) according to the manufacture's instructions. The plasmids were screened again for correct sizes by digestion with PacI, BamHI and EcoRI. Prior to transfection of the recombinant plasmid, 8 μg of the plasmid DNA was digested with Pac1 for 18 hours at 37°C, and then heat inactivated at 65°C for 20 minutes.

2.4.2.5 Expansion, Precipitation, Purification, and Titration of Adenoviruses Containing NHE1

For the production of adenoviruses in mammalian cells, HEK 293A cells, a

human embryonic kidney cell line were used. The HEK 293A cells express the adenovirus 5 virus with the E1 gene, which is essential to complete the growth of E1 defective adenovirus vectors. HEK 293A cells were grown in α-MEM, 10% FBS and 10 μg/mL gentimicin to 70% confluency, at which time they were transfected with 8 μg of heat inactivated Pac1 digested recombinant plasmid using LF 2000 as described in Section 2.1.3.1. Four hours following transfection, the transfection medium was aspirated and replaced with medium containing α-MEM, 5% horse serum (HS) and 10 μg/mL of gentimicin, and cells were incubated at 37°C in a humidified atmosphere (95% O_2-5% CO_2). The transfection was monitored by GFP and the medium was exchanged with fresh medium every 2-3 days, until viral lysis occurred. When viral lysis reached ~70%, cells were harvested, then were frozen in liquid nitrogen, then thawed at 4°C, then centrifuged for 5 minutes at 5 000 rpm at room temperature, and then used to infect another plate of HEK 293A cells to expand the production of the adenoviruses. The HEK 293A cells were maintained as described above and harvested upon viral lysis. This procedure was repeated using a large scale of 24 plates of HEK 293A cells. Following infection, cells were harvested upon viral lysis and subjected to 3x freeze-thaw cycles. The lysates were then thawed at 37°C, and then vortexed and refrozen in liquid nitrogen. Lysates were then centrifuged for 15 minutes at 4 000 rpm at 4°C and the supernatants were transferred to a 500 mL sterile glass beaker in which ammonium sulfate was added, to precipitate the adenovirus. The lysate-ammonium chloride solution was centrifuged for 15 minutes at 1 614 x *g* at room temperature. The remaining pellet was dissolved in PBS and centrifuged for 15 minutes at 4 000 rpm at room temperature. The adenovirus was purified using a cesium chloride (CsCl) gradient made in ultracentrifugation tubes,

using 1.5 g/mL, 1.35 g/mL and 1.25 g/mL CsCl dissolved in ddH_2O solutions, to which the supernatant from the ammonium sulfate precipitation was transferred to. The ultracentrifugation tubes were balanced and centrifuged at 150 000 x *g* for 22 hours at 10°C in a Ti60 rotor (Beckman L-80 Ultracentrifuge). The adenovirus was isolated from the CsCl gradient and placed in a sterile 50 mL conical. CsCl was removed from the isolated adenovirus by overnight dialysis of the adenovirus stored in the Pierce Slide-A-Lyzer dialysis cassette (10 000 MW, 3-15 mL capacity) (Pierce; Rockford, IL) and placed in a beaker containing 1xPBS and 10% glycerol at 4°C. The adenovirus was collected and centrifuged at 1 620 x *g* for 5 minutes at 4°C, aliquoted and stored at 4°C for use.

2.4.2.6 Determination of the Adenoviral Titer

The concentration of the active adenoviruses was determined using a plaque assay. The adenoviruses were diluted to various concentrations varying from 10^3 to 10^{11} in a final volume of 1 mL of α-MEM, 5% HS and 10 μg/mL gentimicin. HEK 293A cells were infected with these samples and cells were incubated at 37°C for 4 hours in a humidified atmosphere (95% O_2-5% CO_2). After 4 hours, the adenovirus was removed and an agar solution (1x α-MEM with bicarbonate, 5% HS, and 0.5% agar) was added and allowed to solidify at room temperature. Dishes were maintained at 37°C and 95% O_2-5% CO_2 for 4-5 days, adding 1.5 mL of fresh agar overlay solution on top of existing agar each day. On day 4, visible plaques were visible and counted every day for 2 weeks. From the number of fluorescent cells and the dilution of the adenovirus, a fluorescent titer was calculated. A plaque titer was calculated from the total number of plaques per

dish. All titers were performed in duplicates with two different sets of diluted adenovirus.

2.4.3 Characterization of Neonatal Rat Ventricular Cardiomyocytes Infected with IRM or K-IRM Adenoviruses

2.4.3.1 Adenoviral Infection of Neonatal Rat Ventricular Cardiomyocytes

The estimated number of cardiomyocytes plated was measured prior to adenoviral infections using a hemocytometer. NRVMs were prepared as described in Section 2.4.1. A 35 mm petri dish was plated with 1 mL of the cardiomyocyte cell suspension for each experiment and used as a counting dish. The cardiomyocytes were trypsinized with 1 mL of 0.25% Trypsin EDTA (Invitrogen) and incubated at 37ºC for 10 minutes. Cardiomyocytes were then tritrated and diluted with 5 mL of solution V (as described in Section 2.4.1). 20 μL of the cardiomyocyte suspension was added to the hemocytometer and cells were counted. The calculations were performed as follows: number of cells/mL x mL cells/dish results in number of cells/dish and then multiplied by the multiplicity of infection (MOI), the number of plaque formation units (PFU)/cell, which results in PFU required/dish. The PFU/dish is divided by the viral titer, PFU/mL, which determines the volume, mL of stock virus required for infection. The appropriate volume of stock virus was added to cardiomyoctyes nourished with solution V containing 0.5% FBS. Cells were then incubated at 37°C in a humidified atmosphere (95% O_2-5% CO_2).

2.4.3.1.1 Determination of Adenoviral MOI for Neonatal Rat Ventricular Cardiomyocytes

Various adenoviral MOIs, including an MOI of 10, 20 and 30 were tested in NRVMs to determine an MOI that provides high expression of NHE1 without injury to the cultured cardiomyocytes. In addition, tests were run to determine the appropriate duration. NRVMs were infected with an MOI of either 10, 20 or 30 for 24, 36 or 48 hours. NRVMs were prepared as described in Section 2.4.1. Immunoblot analysis was performed on cardiomyocyte lysates prepared as described in Section 2.1.3.2. Total protein was quantified using the Bio-Rad D_C Protein Assay kit. 100 μg of each sample was resolved on 10% SDS-PAGE and transferred to nitrocellulose membranes as described in Section 2.2.2.1. Membranes were incubated with anti-HA (12CA5) antibody. The Li-COR fluorescence labeling and detection system was used to visualize and quantify immunoreactive proteins. The amount of GFP fluorescence was also examined. In all subsequent experiments, NRVMs were infected with IRM, K-IRM or GFP adenovirus using an MOI of 20 for 24 hours.

2.4.3.2 Infection of Neonatal Rat Ventricular Cardiomyocytes with Adenoviruses

NRVMs were prepared as described in Section 2.4.1. After 48 hours of culturing of NRVMs at 37ºC in a humidified atmosphere (95% O_2-5% CO_2), NRVMs were placed in solution V containing 0.5% FBS and 10 μg/ml gentamicin and then infected with one of three adenoviruses; the IRM, K-IRM or GFP. The GFP containing adenovirus was used as a control adenovirus at a MOI of 20. After infection for 4 hours, cells were treated with vehicle, 10 μM PE or 10 μM EMD 87580 for 24 hours[310]. In some

experiments NRVMs were treated with 10 μM PE and 10 μM EMD 87580. EMD 87580 was added 30 minutes prior to the addition of PE[311].

2.4.3.2.1 NHE1 Protein Expression of Infected Neonatal Rat Ventricular Cardiomyocytes

NRVMs were prepared as described in Section 2.4.1 and plated at a concentration of $4x10^6$ cells/60 mm. Immunoblot analysis was performed on cardiomyocyte lysates prepared as previously described in Section 2.1.3.2. Membranes were incubated with anti-NHE1 antibody or anti-HA (12CA5) antibody and β-tubulin was used as a loading control as described in Section 2.2.2.1. The Li-COR fluorescence labeling and detection system was used to visualize and quantify immunoreactive proteins.

2.4.3.2.2. Measurement of Cell Surface Area of Infected Neonatal Rat Ventricular Cardiomyocytes

NRVMs were prepared as described in Section 2.4.1. Cells were plated at an average density of $1x10^4$/35 mm, which allowed for clear distinction of cells. After 24 hours of infection/treatment as described in Section 2.4.3.2, cells were washed 2x with PBS. Cell area was measured from digitized images using Image ProPlus Version 4.5. Digitized images were gathered using a Photometrics $CoolSNAP_{fx}$ camera equipped to a Leica DMIRB microscope. At least 50 cells were averaged from three dishes and represented as one n value[286].

2.4.3.2.3 Protein Synthesis Rate Measurements of Infected Neonatal Rat Ventricular Cardiomyocytes

Protein synthesis rate measurements were estimated by the amount of [^{3}H] phenylalanine incorporated. For measurement of [^{3}H] phenylalanine incorporation, NRVMs were prepared as described in Section 2.4.1 and plated in 12 well plates at a density of $3.3x10^5$. [^{3}H] Phenylalanine (Amersham Biosciences, Piscataway, NJ) (1μCi/mL) was added four hours after viral infection, and at the same time as PE or EMD 87580 treatment (as described in Section 2.4.3.2). Cells were left for 24 hours at 37ºC in a humidified atmosphere (95% O_2-5% CO_2). Cell suspensions were prepared using the following protocol[310]; cells were washed 3x with ice-cold 1x PBS and then incubated at 4ºC for 1 hour in 10% trichloroacetic acid. The precipitates were washed twice with 95% ethanol, dissolved in 1M NaOH, scraped and neutralized with 1M HCl. Radioactivity was measured with a liquid scintillation counter. Protein synthesis was corrected with DNA synthesis measured by hoescht 33258 (Sigma)[312]. Hoescht 33258 was diluted to 0.1μg/mL in ddH_2O containing Tris pH 7.4, EDTA, NaCl and added to cell suspension. The amount of DNA present was measured through fluorescence using a PTI Deltascan spectrofluorometer. The excitation filter was set at 360nm and the emission filter was set at 450nm. Final results were expressed as counts per minute/μg of DNA[312].

2.5 Statistical Analysis

Various sets of data were compared by both Student t-test and Wilcoxon signed-rank test. Statistical differences were considered significant when *P* values were less than 0.05.

Chapter 3

Activated NHE1 Induces Cardiac Hypertrophy in Female NHE1 Transgenic Mice Independent of Calcineurin and Mitogen Activated Protein Kinases

My role in this project involved planning and conducting experiments (unless otherwise indicated in the figure legend), data analysis and writing a manuscript.

3.1 Introduction

NHE is a ubiquitously expressed plasma membrane glycoprotein. It is associated with versatile biological functions, including cell proliferation, differentiation, apoptosis and regulation of cytoskeletal organization and migration (reviewed in[36]). One of its key functions is the regulation of pH_i, which is done by extruding one intracellular H^+ in exchange for one extracellular Na^+, thus protecting the cell from intracellular acidification (reviewed in[313]). Ten isoforms of NHE have been identified, NHE1-NHE10, all with distinct tissue expression, membrane localization and inhibitor sensitivity (reviewed in[36,44,16])[37]. NHE1 is the only cardio-specific plasma membrane isoform of the ten isoforms described so far. NHE1 consists of an N-terminal membrane associated domain, involved in ion transport, and a C-terminal cytoplasmic regulatory tail (Figure 1.1). NHE1 is active at acidic pHs, but inactive at physiological pHs[68]. NHE1 activity is regulated via various agonists such as ET-1, Ang II, α_1-AR agonists, thrombin, and protein kinases such as the MAPKs, all of which act on the C-terminal tail of NHE1 and change the set point so that the protein is more active at more alkaline pHs (reviewed in[87])[68]. In addition, neurohormonal activation, myocardial I/R, cardiotoxic metabolites released during I/R and stimuli inducing CH, lead to increasing levels of NHE1 mRNA and protein expression.

In the myocardium, NHE1 plays a critical role in mediating the damage that occurs during I/R (reviewed in[186]) and is an important mediator of CH (reviewed in[87]). CH is the natural response of the myocardium to various stressors, including neurohormonal activation, I/R injury and hypertension (reviewed in[216]) (Figure 1.4). Continued stress progresses to pathological hypertrophy, which commonly precedes

apoptosis, the development of fibrosis and heart failure[218]. Numerous signaling pathways have been implicated in stress-induced remodeling of the heart, including intracellular $[Ca^{2+}]_i$ homeostasis, several Ca^{2+}-dependent signaling molecules and MAPKs[234,314]. Many of the same pathways have been implicated in NHE1 regulation[61]. The signaling pathways leading to CH are very complex, but recent studies have shown that NHE1 expression/activity were increased in several *in vivo* and *in vitro* models of CH (reviewed in[87]). *In vitro*, NHE1 mRNA and protein expression were shown to be elevated in NRVMs following stimulation with aldosterone, a hypertrophic stimulator[103]. *In vivo*, mice over-expressing β_1-adrenergic receptors displayed both the phenotypes of CH and upregulation of NHE1[239]. Similarly, in other models of CH, such as the monocrotaline-induced ventricular hypertrophic model[212] and in the diabetes induced hypertrophic model[244], NHE1 activity was enhanced. The involvement of NHE1 in CH has been further supported with the use of NHE1 inhibitors. NHE inhibition has been beneficial in the prevention/regression of several models of CH (reviewed in[87]). These reports, along with others, suggest that NHE1 inhibition maybe used as a therapeutic strategy for cardiac failure. Inhibiting early maladaptive hypertrophy and understanding the determinants involved in the progression from hypertrophy to heart failure is the key to prevention. However, the direct role of NHE1 in CH and the effects of elevation of NHE1 activity and expression, both *in vivo* and *in vitro*, have not been fully defined. Because the unstimulated protein NHE1 is relatively quiescent at resting physiological pHs, it is questionable whether elevation of the non-activated protein alone is detrimental to the myocardium without the activation that shifts it to a greater activity at more alkaline pH, which occurs under more pathological situations.

The present study sought to confirm the direct link between NHE1 and CH both *in vitro* and *in vivo,* using a gain of function model. *In vivo*, we characterized female N-line mice, which express wild type NHE1 and female K-line mice, which express active NHE1 in the myocardium. In parallel experiments *in vitro*, we characterized NRVMs infected with IRM or K-IRM adenoviruses, which contain wild type NHE1 or active NHE1, respectively. Our models allowed us to study whether NHE1, in its wild type or active form, directly acts on the myocardium to potentiate CH. We demonstrate that NHE1 expression with elevated activity potentiates CH independent of calcineurin and MAPKs pathways, which have been suggested to be important in mediating CH[87,141,325,326,381]. Furthermore, activation of NHE1 activity with elevated neurohormonal stimulation enhances the hypertrophic response *in vivo,* partially due to enhanced edema of the heart.

3.2 Results

3.2.1 NHE1 Transgene Expression in N-line and K-line Hearts

To study the direct role of NHE1 in CH and I/R injury (Chapter 4), two gain-of-function mouse lines that express exogenous wild type (N-line) or active (K-line) NHE1 protein in the myocardium were created (as described in Section 2.1). Figure 3.1 illustrates the transgene used in the construction of NHE1 TG mice. It consisted of a full length NHE1 cDNA flanked at the 5' end by the cardiac specific α-MHC promoter and an HA-tag at the 3' end. The 1K3R4E mutation (as described in Section 2.1.2), which induces an active NHE1, was absent in the N-line mice and present in K-line mice.

Figure 3.1. Gene construct used for the expression of the NHE1 protein in the mouse myocardium. α-MHC, alpha myosin heavy chain promoter; HA, hemagglutinin tag; ±1K3R4E indicates that DNA may have contained the mutation of lysine (K) 641, arginine (R) 643, arginine (R) 645 and arginine 647 (R) to glutamic residues. The 1K3R4E mutation was absent in the N-line mice expressing HA tagged-wild type NHE1and present in the K-line mice expressing HA tagged-active NHE1. A version of this figure appears in Coccaro E et al. 2007 (275).

3.2.2 Characterization of Constitutively Active NHE1 in AP-1 Cells

The 1K3R4E mutant expressed active human NHE1 tagged to HA. It was constructed using the pYN4$^+$ NHE1 containing plasmid (as described in Section 2.1.1), which was mutated at amino acids K641, R643, 645 and 647 to amino acid E. This mutant was used to construct the K-line mice and the K-IRM adenovirus. This mutation has been shown to cause a defect in the CaM regulation of NHE1 and results in an NHE1 protein that is alkaline shifted in its pH dependence, and therefore more active than the control at a given pH[115]. After the 1K3R4E plasmid was made and confirmed by DNA sequencing, and prior to being used to construct the NHE1 TG mice, we confirmed that this mutation did indeed produce an active NHE1. The 1K3R4E and the wild type pYN4$^+$ plasmids were transfected into NHE1-deficient AP-1 cells. Figure 3.2 is a representative western blot of two stable cells lines of AP-1 cells transfected with HA tagged-wild type NHE1 (lane 1*)* or HA tagged-constituitively active NHE1 (1K3R4E plasmid) (lane 2*)*. Both the wild type NHE1 and the 1K3R4E mutant express NHE1 in AP-1 cells as detected by anti-HA tag antibody. The predominant immunoreactive species is at 110 kDa, whereas a more minor secondary band of 90 kDa was also found. This immunoreactive band has previously been suggested to represent the unglycosylated or partially glycosylated NHE1 protein[315].

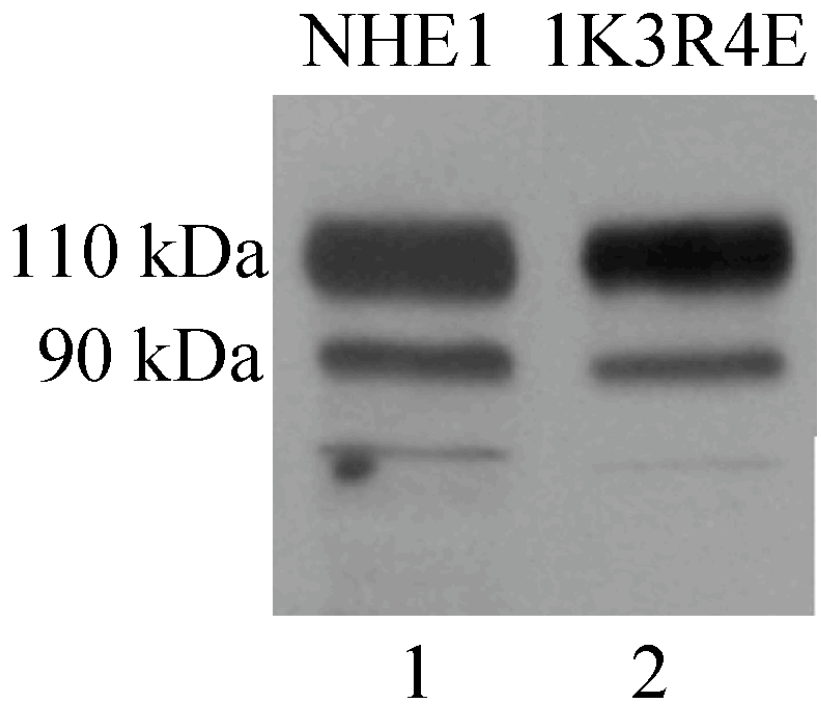

Figure 3.2. NHE1 protein expression of HA tagged-NHE1 in AP-1 cells. Representative western blot of cell extracts from a stable cell line of AP-1 cells transfected with either pYN4^{+} containing HA tagged-wild type NHE1 (NHE1) (*lane 1)* or from AP-1 cells transfected with 1K3R4E plasmid containing the HA tagged-active NHE1 (1K3R4E) *(lane 2)*. Cell extracts were immunoblotted with anti-HA tag antibody. The predominant immunoreactive species was at 110 kDa and a secondary band was found at 90–95 kDa. Bonnie Bullis performed this experiment. A version of this figure appears in Imahashi K et al. 2007 (204).

We also measured the resting pH_i of AP-1 cells transfected with either HA tagged-wild type NHE1 or the 1K3R4E plasmid in bicarbonate-free medium after loading with BCECF-AM, a pH sensing dye (as described in Section 2.1.3.3). The results are shown in Figure 3.3. AP-1 cells transfected with the 1K3R4E plasmid had an elevated resting pH_i of 0.25 pH units greater than AP-1 cells transfected with HA tagged-wild type NHE1. These results confirmed that the 1K3R4E mutation was functional and active, as described earlier by others[316]. The 1K3R4E plasmid (as described in Section 2.1.2) was used to create the K-line mice. The $pYN4^+$ plasmid, containing HA tagged-wild type NHE1, was used to create the N-line mice (as described in Section 2.1.1).

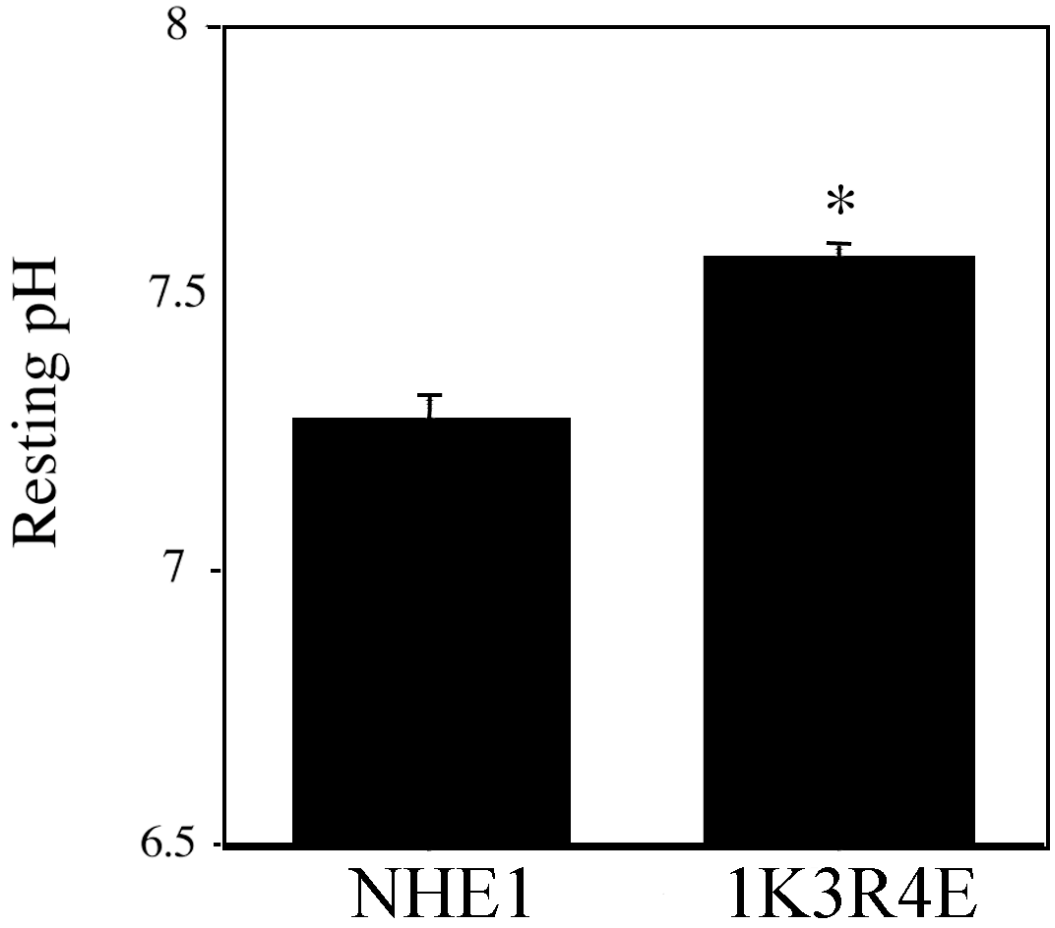

Figure 3.3. Resting pH_i of AP-1 cells transfected with wild type NHE1 or constitutively active NHE1 (1K3R4E). AP-1 cells were transfected with either the pYN4$^+$ plasmid, which contains wild type NHE1 (NHE1) or the 1K3R4E plasmid, which contains wild type NHE1 mutated at amino acids K641, R643, 645 and 647 to amino acid E resulting in a constituitively active NHE1. AP-1 cells were incubated with BCECF-AM, a fluorescent pH sensing dye and fluorescence was measured using a PTI deltascan. Resting pH_i was measured during a 3 minute incubation period in Na^+ normal buffer as described in Section 2.1.3.3. Results are displayed as mean±SEM. $^*P<0.05$ vs. NHE1; n=8/group. Bonnie Bullis performed this experiment. A version of this figure appears in Imahashi K et al. 2007 (204).

3.2.3 Characterization of N-line and K-line NHE1 Transgenic Mice

Prior to characterizing our NHE1 TG mice for CH, we examined NHE1 expression in various tissues to ensure that NHE1 was present and specific to the heart. Figure 3.4 illustrates representative western blots that examine tissue-specific expression of NHE1 in the N-line and K-line mice. The upper panel is a representative western blot of lysates from N-line mice and the bottom panel is a representative western blot of lysates from K-line mice. The antibody used for this blot was anti-HA tag. Therefore, only exogenous NHE1, which carries the HA-tag, was detected. The NHE1 protein was found at 110 kDa and a second band was found at 90 kDa. They were present exclusively in the heart lysates (lane 3). There was no detectable expression of NHE1 in the lung, liver, kidney, or brain (lanes 4-7, respectively) in both N-line and K-line mice. Lane 1 is from a control heart and lane 2 is a positive control of AP-1 cells transfected with HA tagged-wild type NHE1 (pYN4^{+} NHE1 containing plasmid).

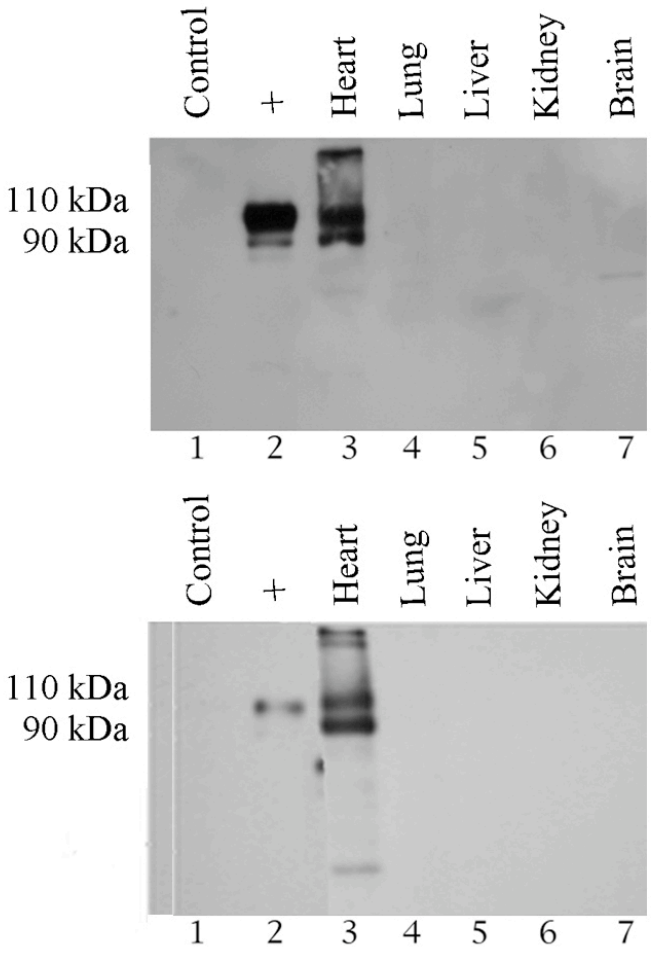

Figure 3.4. Tissue-specific protein expression of NHE1 in N-line and K-line mice. Representative western blots illustrating NHE1 protein expression in various tissue. Lane 1, control heart lysate; lane 2, positive control (+), cell extract from AP-1 cells transfected with HA tagged-wild type NHE; lanes 3–7 are lysates from the heart, lung, liver, kidney, and brain, respectively of N-line (**upper panel**) or K-line (**bottom panel**) mice. The antibody used for this blot was anti-HA tag. The immunoreactive band was found at 110 kDa and a second band was found at 90 kDa. Bonnie Bullis performed this experiment. A version of this figure appears in Imahashi K et al. 2007 (204).

3.2.4 Developmental Expression of NHE1 in Mouse Hearts

We then examined the developmental expression of the NHE1 transgene in the intact myocardium, which was used to help us determine at what age to conduct our experiments. Figure 3.5 shows a representative western blot of a time course of expression of the NHE1 transgene in hearts from N-line and K-line mice. NHE1 protein expression was detected using anti-HA tag antibody, and was examined in heart lysates obtained from hearts 1 week to 26 weeks of age. NHE1 protein expression was detected and the immunoreactive band was found at 110 kDa and a secondary band was found at 90 kDa. NHE1 was found as early as 1 week post birth and expression continued until several months past birth. Quantitation of a series of experiments (data not shown) demonstrated that NHE1 protein expression was greatest at 13 weeks of age in N-line mice and 8 weeks of age in K-line mice. Based on these results, N-line and K-line mice were characterized in all upcoming experiments at 10-12 weeks of age.

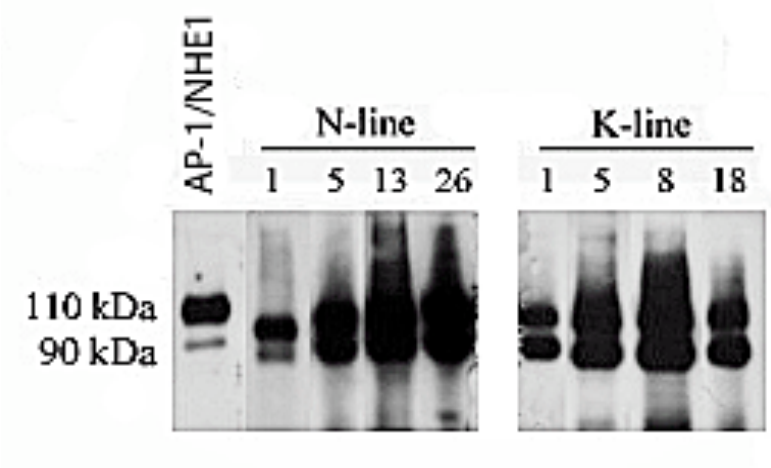

Figure 3.5. Developmental expression of the NHE1 transgene in the intact myocardium of N-line and K-line hearts. Hearts lysates were made from the intact myocardium of either N-line **(left panel)** or K-line **(right panel)** mice isolated at the age indicated (in weeks). The antibody used for this blot was anti-HA tag. The predominant immunoreactive band was found at 110 kDa and a second band was found at 90 kDa. AP-1/NHE-1 is a positive control, lysates were AP-1 cells transfected with HA tagged-wild type NHE1. This experiment was performed by Bonnie Bullis.

3.2.5 NHE1 Activity of Isolated Adult Ventricular Cardiomyocytes from NHE1 Transgenic Hearts

We measured NHE1 activity using a single freshly isolated AVM from control, N-line and K-line TG hearts. The AVMs were isolated by retrograde perfusion and incubated with BCECF-AM, a fluorescent pH sensing dye (as described in Section 2.1.3.3). Fluorescence was measured using a PTI deltascan fluorometer. Figure 3.6 compares the rate of recovery of pH_i in a single isolated AVM subjected to an ammonium chloride-induced acid load, which is indicative of NHE1 activity. NHE1 activity increased approximately 2- and 3 fold in the single AVMs of N-line and K-line hearts, respectively ($P<0.05$).

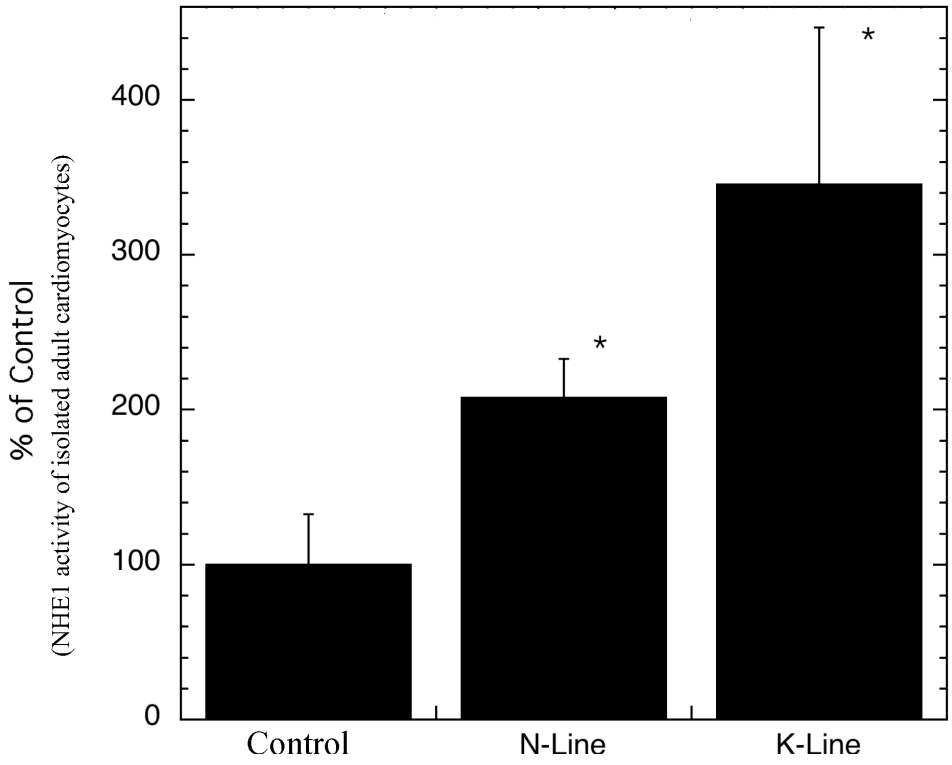

Figure 3.6. NHE1 activity of single isolated adult ventricular cardiomyocytes from control, N-line and K-line hearts. Intracellular pH was measured in a single adult ventricular cardiomyocyte isolated by retrograde perfusion from control, N-line and K-line hearts. The cardiomyocyte was then incubated with BCECF-AM and subjected to an ammonium chloride-induced acid load. The rate of recovery following the acid load was indicative of NHE1 activity. **Upper panel,** representative isolated mouse ventricular cardiomyocyte. **Bottom panel,** quantification of a series of experiments. NHE1 activity was expressed as a % of controls±%SEM. $^{*}P<0.05$ vs. controls; n=6/group.

3.2.6 Total Endogenous and Exogenous NHE1 Protein Expression of Hearts from NHE1 Transgenic Mice

To further confirm that the NHE1 protein was expressed and to provide a quantitative value of NHE1 expression in our NHE1 TG mice relative to controls, total (exogenous and endogenous) NHE1 protein expression in control, N-line and K-line heart lysates were quantitated by immunoblotting against the NHE1 protein (Figure 3.7). All three samples contained NHE1 protein, with the relative amount increasing in controls (lanes 1-3) vs. N-line (lanes 4-6) and in K-line (lanes 7-9) (Figure 3.7, upper panel). Quantification of a series of experiments measuring the protein expression of total NHE1 (Figure 3.7, bottom panel) shows that there was a marked increase of approximately 2.5 and 3.5 fold in total NHE1 protein expression in N-line and K-line mouse hearts vs. control mouse hearts, respectively ($P<0.05$).

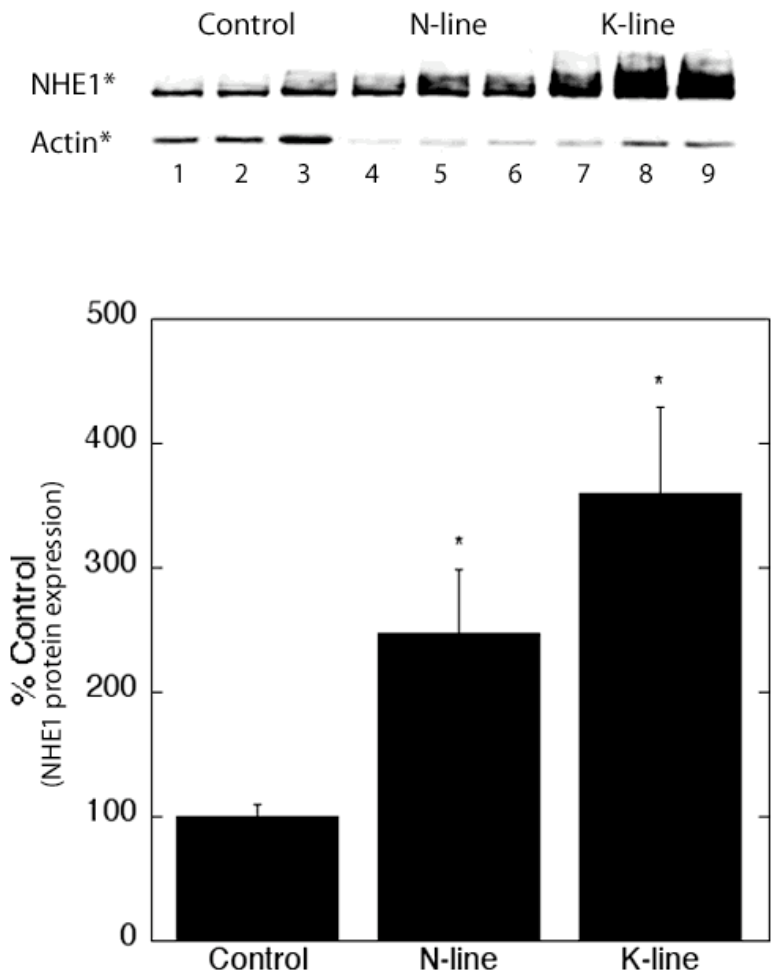

Figure 3.7. Immunoblot analysis of total (endogenous and exogenous) NHE1 protein expression in control, N-line and K-line hearts. Immunoblot analysis of NHE1 protein expression was detected using anti-NHE1 antibody. **Upper panel,** representative western blot of total NHE1 (90-110 kDa) and actin (40 kDa) protein expression. Lanes 1-3, 4-6, and 7-9 represent heart lysates from control, N-line and K-line mice, respectively. **Bottom panel,** quantification of a series of experiments. NHE1 protein levels were normalized to actin and are expressed as a % of controls±%SEM. $^{*}P<0.05$ for control vs. N-line or K-line; n=3-4.

3.2.7 Exogenous NHE1 Protein Expression in Hearts from NHE1 Transgenic Mice

Exogenous NHE1 protein expression was also measured. Heart lysates from control, N-line and K-line mice were immunoblotted for HA tagged-NHE1 with anti-HA tag antibody (Figure 3.8). Exogenous NHE1 protein was present in the N-line (lanes 4-6) and K-line (lanes 7-9) samples, but not in the control (lanes 2-3) hearts (Figure 3.8, upper panel). The HA tag was not detected in control hearts, which confirmed the specificity of the anti-HA antibody. A sample of AP-1 cells transfected with HA tagged-wild type NHE1 (lane 1) served as a positive control. Quantification of a series of experiments measuring protein expression of exogenous NHE1 (Figure 3.8, bottom panel) showed no significant differences in exogenous NHE1 protein expression between hearts from N-line and K-line mice.

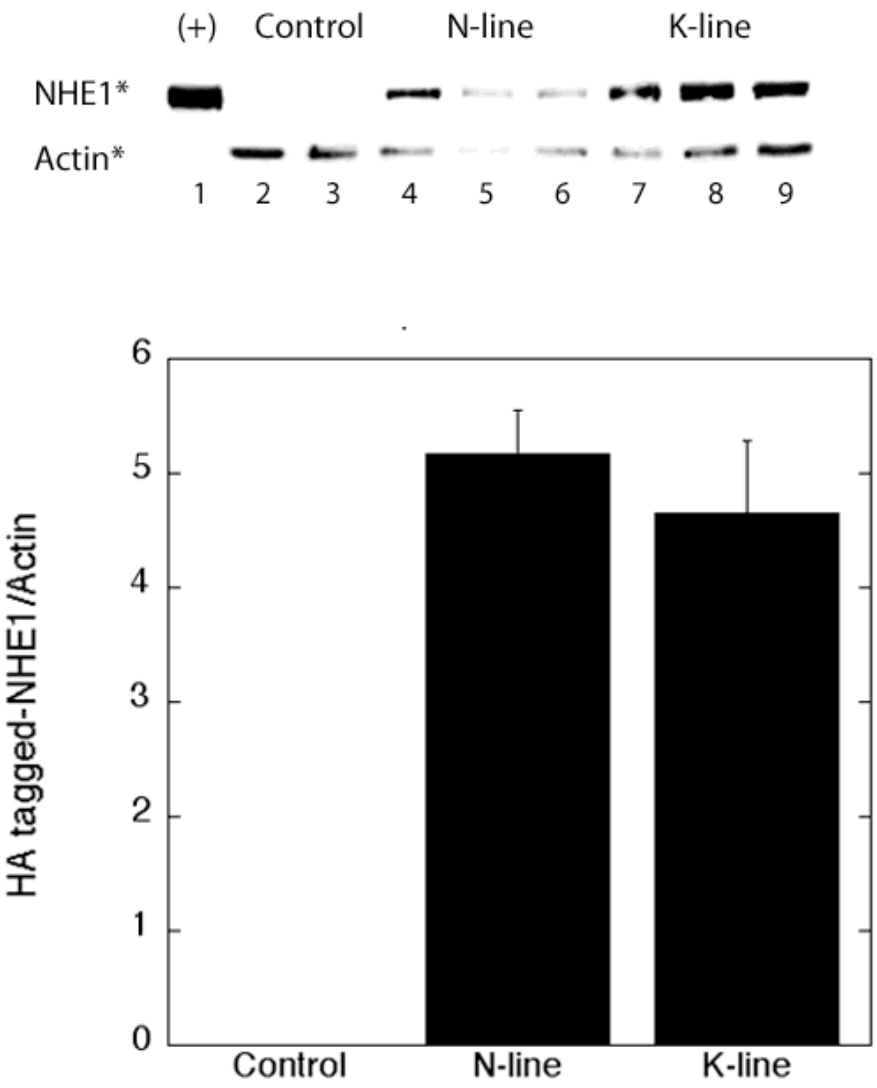

Figure 3.8. Immunoblot analysis of exogenous HA tagged-NHE1 protein expression in control, N-line and K-line hearts. Upper panel, representative western blot of NHE1 (90-110 kDa) and actin (40kDa) protein expression. Lane 1, positive control (+) of AP-1 cells transfected with HA tagged-wild type NHE1. Lanes 2-3, 4-6 and 7-9 represent heart lysates from control, N-line and K-line mice, respectively. **Bottom panel,** quantification of a series of experiments. NHE1 protein expression was quantified and normalized to actin for each group and expressed as a ratio, HA tagged-NHE1/Actin±SEM. (n=3-4 hearts/group).

3.2.8 In Vivo Characterization of Intact N-line and K-line Mouse Hearts for Cardiac Hypertrophy

To evaluate the effects of varying levels of NHE1 protein expression and activity on the degree of CH, various hypertrophic indices were measured including the HW/BW, ANP mRNA expression, CSA and IF. Initially, we qualitatively examined the whole hearts and the transverse cross sections stained with H&E of control, N-line and K-line mice (Figure 3.9). The K-line heart appeared to be enlarged and the left ventricle appeared dilated (Figure 3.9).

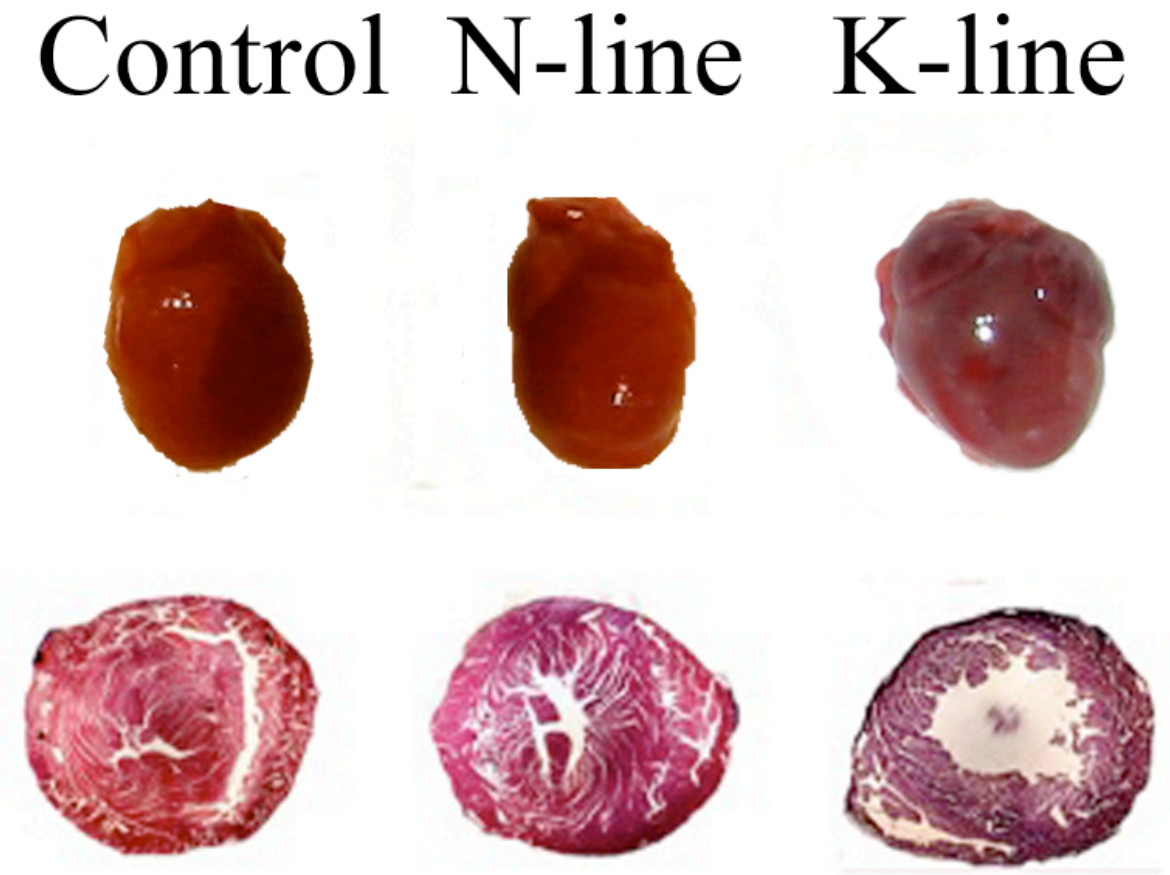

Figure 3.9. Qualitative comparison of whole hearts and transverse heart cross sections stained with H&E from control, N-line and K-line mice. Upper panel, representative whole hearts from control, N-line and K-line mice. **Bottom panel,** representative transverse heart cross sections stained with H&E from control, N-line and K-line hearts.

The heart weight normalized by body weight, the HW/BW, was significantly greater in both N-line (126.0±9.4%, $P<0.05$) and K-line (142.6±9.2%, $P<0.005$) mice vs. control mice, and more so in the K-line mice (Figure 3.10). The variations seen in the HW/BW between groups were a result of changes in the heart weight (100.0±4.4% controls vs. 126.0±12.3% N-line vs. 157.0±10.3% K-line, $P<0.05$), as there were only small changes in the body weight (100.0±2.9% controls vs. 98.2±3.8% N-line vs. 109.6±2.1% K-line). This change in the heart weight was due to an increase in heart mass, not edema. This was indicated by the dry weight to wet weight ratio measured in hearts from control (0.15±0.01) and K-line (0.14±0.009) mice, which showed no significant differences between the two groups.

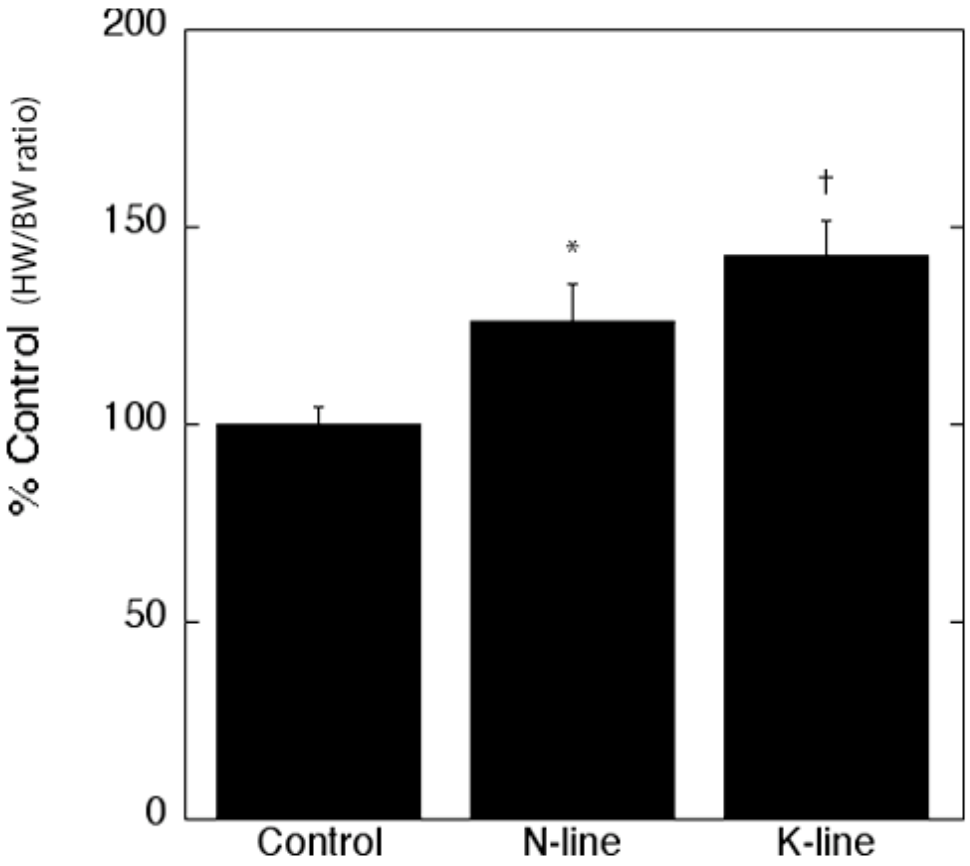

Figure 3.10. Analysis of the HW/BW ratio in control, N-line and K-line mice. The HW/BW ratio was expressed as a % of controls±%SEM. $^{*}P<0.05$ for controls vs. N-line, $^{\dagger}P<0.005$ for controls vs. K-line mice; n=7-9 hearts/group.

Another index of CH that was measured in control, N-line and K-line hearts was the expression of ANP mRNA (as described in Section 1.7.4). Hearts from N-line and K-line mice had significantly greater ANP mRNA expression in comparison to hearts from control mice (100.0±43.5% controls vs. 1226.0±386.5% N-line vs. 2067.0±359.8% K-line; $P<0.05$) (Figure 3.11).

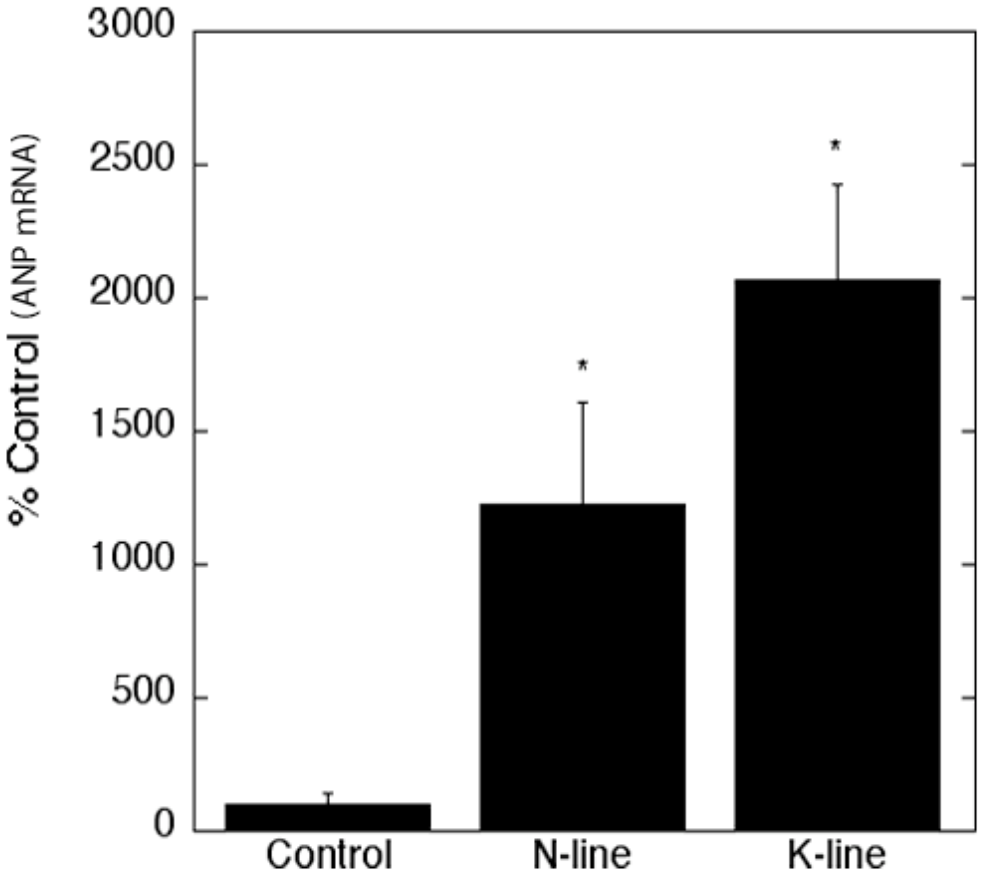

Figure 3.11. Analysis of ANP mRNA expression in hearts from control, N-line and K-line mice. ANP mRNA levels were expressed as a % of controls±%SEM. $^{*}P<0.05$ for controls vs. N-line or K-line mice; n=3 hearts/group.

In addition to fetal gene re-expression, CH is also associated with changes in histology. Figure 3.12, upper panel, illustrates representative images of heart cross sections stained with H&E for measurement of CSA and heart cross sections stained with PSR for IF measurements from control, N-line and K-line mice. Accumulated CSA from K-line hearts, not N-line hearts, were significantly different from control and N-line hearts (100.0±15.0% controls vs, 103.2±1.6% N-line vs. 164.0±20.0% K-line, $P<0.05$) (Figure 3.12, bottom panel). Similarly, measurements of IF from heart cross sections stained with PSR demonstrated that K-line hearts had significantly increased IF vs. controls or N-line (100.0±6.3% controls vs. 137.1±24.9% N-line vs. 305.0±63.1% K-line, $P<0.05$) (Figure 3.12, bottom panel). N-line hearts did not show any significant increases in IF vs. controls.

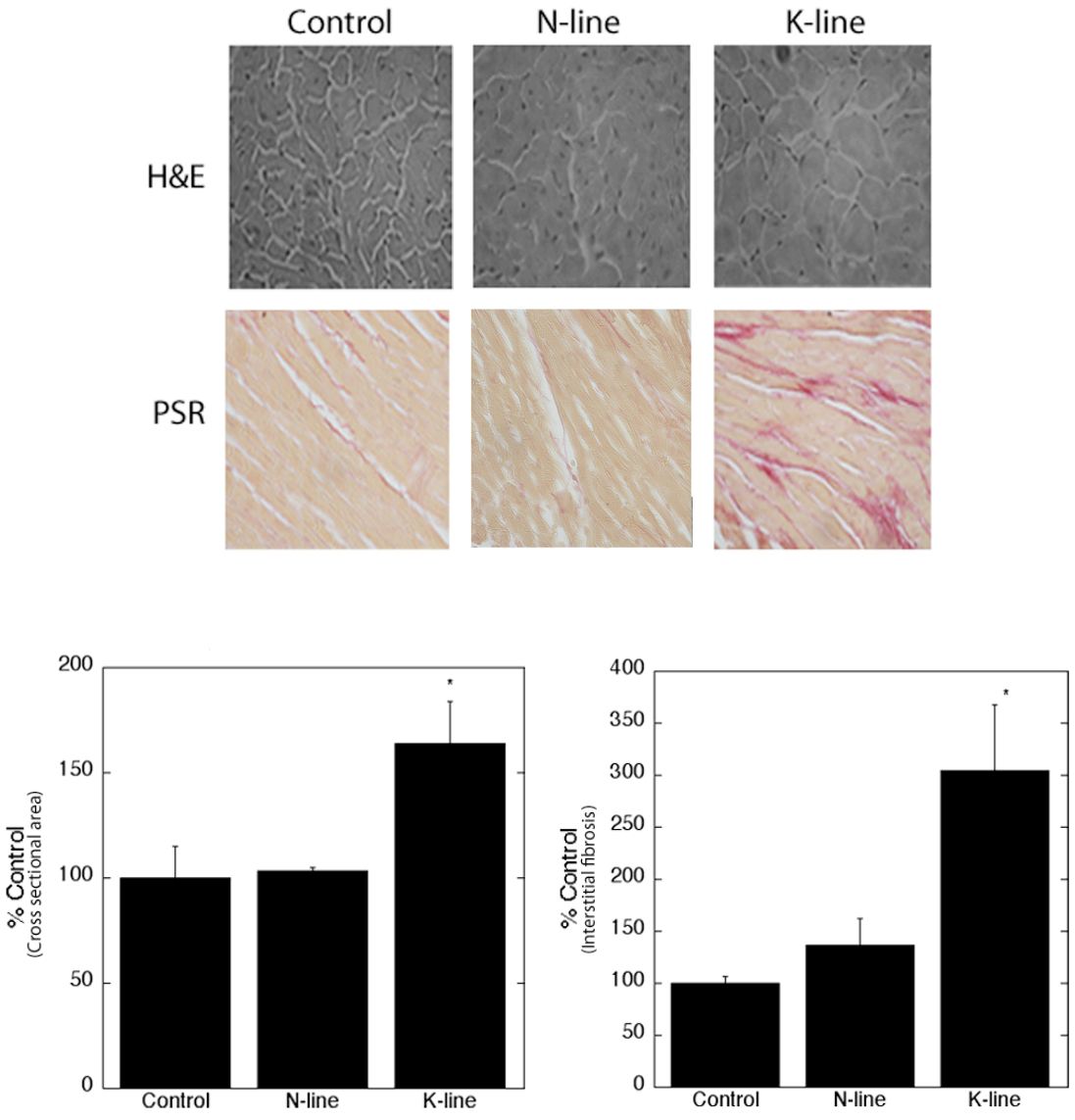

Figure 3.12. Cross sectional area and interstitial fibrosis of control, N-line and K-line hearts. Upper panel, representative heart cross sections of control, N-line and K-line hearts stained with H&E or PSR. For CSA, visual fields were accepted for quantification if nuclei were visible and cell membranes were intact. The maximum fibrosis observed for any section was calculated as the area occupied by red stained connective tissue x 100/areas occupied by connective tissue plus cardiac myocytes. **Bottom panel,** quantitative analysis of CSA and IF. Results are expressed as a % of controls±%SEM. For CSA, $^{*}P<0.05$ for K-line vs. control or N-line mice; n=4-6 hearts/group. For IF, $^{*}P<0.05$ for K-line vs. control or N-line mice; n=4 hearts/group.

3.2.9 Cardiac Function and Myocardial Remodeling of Control, N-line and K-line Mice

Cardiac function and myocardial remodeling were assessed in control, N-line and K-line mice. Echocardiographic measurements of cardiac function and morphology of control, N-line and K-line mice are summarized in Table VI. Compared to control hearts (or hearts from N-line mice), hearts from K-line mice exhibited significant ventricular hypertrophy, which confirms our previous indication of NHE1 dependent CH. Left ventricular mass (LVM) of K-line mice was significantly elevated as were diastolic inter-ventricular septal wall thickness (IVSTd) and diastolic left ventricular posterior wall thickness (LVPWd). N-line mice were not significantly elevated in any of these parameters relative to controls. Both diastolic and systolic cardiac function were significantly affected, principally in the K-line mice and to a lesser degree in the N-line mice. In K-line mice the decrease in systolic function was demonstrated by a decrease in percent left ventricular ejection fraction (EF). The decrease in diastolic function was demonstrated by the increase in the ratio of peak E wave mitral valve velocity to peak A wave mitral valve velocity (E/A). This decrease in systolic and diastolic function in K-line mice was associated with ventricular dilation, as indicated by the increase in LV internal diameter (LVID) during systole (s) or diastole (d) *(P*<0.05 vs. control or N-line mice). The global deterioration in myocardial performance in K-line mice is further confirmed by the significant increase in the Tei index.

In N-line hearts, the decrease in systolic and diastolic function is also associated with ventricular dilation. N-line hearts displayed increased LVID during systole. However, this was significantly less than the LVID during systole in K-line mice.

Similarly, N-line mice had a significant decrease in percent left ventricular FS and EF and increase in the E/A ratio, however the changes observed were not as pronounced as those observed in K-line mice. N-line mice did not show an increase in TEI index. The changes in the Tei index, left ventricular FS and EF were significantly greater in K-line mice compared to N-line.

Table VI: Cardiac morphology and contractile function of control, N-line and K-line mice. IVSTd, diastolic inter-ventricular septal wall thickness; LVPWd, diastolic left ventricular posterior wall thickness; LVM, left ventricular mass; LVIDd and LVIDs, left ventricular internal diameter during diastole and systole; FS, left ventricular % fractional shortening; EF, left ventricular % ejection fraction; MV E/A ratio, ratio of peak E wave mitral valve velocity to peak A wave mitral valve velocity. Values are expressed as mean ±SEM. $^{*}P<0.05$ vs. controls, $^{\dagger}P<0.005$ vs. controls, $^{\S}P<0.05$ for N-line vs. K-line, $^{¥}P<0.005$ for N-line vs. K-line; n=7-8/group.

n=7-8/group	**Controls**	**N-line**	**K-Line**
IVSTd, mm	0.71 ± 0.01	0.77 ± 0.02	0.83± 0.03*
LVPWd, mm	0.74 ± 0.02	0.74 ± 0.02	0.84 ± 0.02*,§
LVM , mg	81.3 ± 2.1	85.9 ± 3.0	103.4 ± 4.6†,§
LVIDd, mm	3.98 ± 0.08	3.98 ± 0.06	4.10 ± 0.08
LVIDs, mm	2.44 ± 0.06	2.69 ± 0.07*	3.12 ± 0.09*,§
FS, %	38.8 ± 0.7	32.4 ± 1.1†	24.0 ± 1.2$^{\dagger,¥}$
EF, %	69.8 ± 0.9	61.2 ± 1.6†	48 .1 ± 2.1$^{\dagger,¥}$
MV E/A ratio	1.95 ± 0.1	2.65 ± 0.2*	4 .04 ± 0.6*
Tei index	0.457 ± 0.02	0.5 1 ± 0.02	0.70 ± 0.03$^{\dagger,¥}$

3.2.10 NHE1 expression in IRM and K-IRM Adenoviruses

Adenoviruses containing NHE1 were created to infect NRVMs with varying levels of NHE1. Using this *in vitro* gain-of-function model, we were able to study the direct effects of varying levels of NHE1 in myocytes. Figure 3.13 illustrates the NHE1 gene construct used for production of the NHE1 containing adenoviruses. The IRM NHE1 cDNA, which is resistant to NHE1 inhibition, has the L163F/G174S mutation. It is flanked by the CMV promoter on the 5' end and a long terminal repeat (LTR) and a polyadenylation (PA) signal at the 3' end. The plasmid also has a GFP DNA sequence driven by the CMV promoter to allow for easy confirmation of infection and a HA tag at the 3' end of the NHE1 cDNA, which was used to monitor NHE1 expression. The HA tag has previously been shown not to interfere with NHE1 expression or activity[274]. The K-IRM NHE1 cDNA, which expresses an active NHE1 resistant to NHE1 inhibition, contains the mutations L163F/G174S and 1K3R4E, an HA tag, a PA signal and a LTR at the 3'end.

Figure 3.13. Adenovirus constructs used for the expression of NHE1 in neonatal rat ventricular cardiomyocytes. The IRM adenovirus contains HA tagged-wild type NHE1 resistant to NHE1 inhibitors. The IRM plasmid contains the mutations L163F/G174S. The K-IRM adenovirus contains HA tagged-active NHE1 resistant to NHE1 inhibitors. The K-IRM plasmid was created by ligating two DNA fragements, one containing the L163F/G174S NHE1 cDNA and the other containing the 1K3R4E NHE1 cDNA. 1K3R4E indicates that the DNA contained the mutation of lysine (K) 641, arginine (R) 643, 645 and 647 to glutamic acid (E) residues and is indicated by (+). CMV, cytomegalovirus promoter; GFP, green fluorescent protein; HA, hemagglutinin tag; polyadenylation (PA) signal; LTR, long terminal repeat.

3.2.11 Characterization of the pAdTrack CMV Plasmids in AP-1 Cells

To confirm that the mutations of the IRM and K-IRM plasmids were successful and that the mutant NHE1 retained activity when moved into the pAdTrack CMV vector for production of the adenovirus, we stably transfected AP-1 cells with the pAdTrack CMV-IRM or pAdTrack CMV-K-IRM plasmid (as described in Section 2.4.2.3). Western blot analysis (Figure 3.14) demonstrates NHE1 expression in AP-1 cells transfected with pAdTrack CMV-IRM/K-IRM. The NHE1 immunoreactive band was present at 90-110 kDa. Lane 2 is representative of a lysate from AP-1 cells transfected with the pAdTrack CMV, not containing the HA tagged-NHE1 protein. Lanes 3 and 4 represent lysates from AP-1 cells transfected with pAdTrack CMV-IRM and lanes 5 and 6 represent lyastes fom AP-1 cells transfected with pAdTrack CMV-K-IRM. Lane 1 is a positive control of AP-1 cells transfected with the $pYN4^{+}$ plasmid, which contains HA tagged-wild type NHE1.

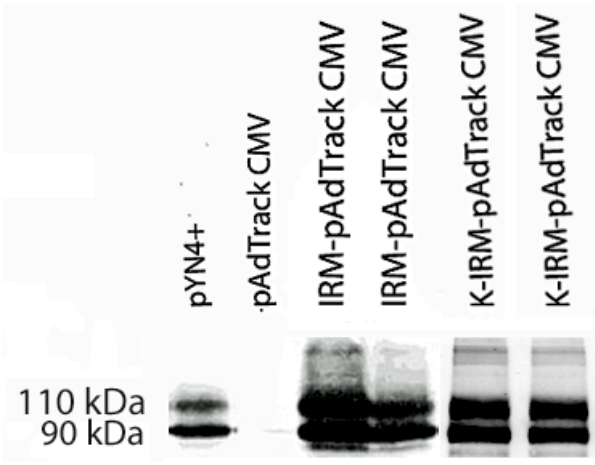

Figure 3.14. Western blot analysis of AP-1 cells transfected with pAdTrack CMV-IRM or pAdTrack CMV-K-IRM plasmids. Representative western blot of AP-1 cells transfected with pAdTrack CMV-IRM or pAdTrack CMV-IRM K-IRM plasmids and immunoblotted with anti-HA tag antibody. Lane 1, $pYN4^+$, is AP1 cells transfected with the $pYN4^+$ plasmid, which contains an HA tagged-wild type NHE1 protein. Lane 2 represents AP-1 cells transfected with pADTrack CMV, which contains no HA tag. Lanes 3 and 4 represent lysates from AP-1 cells transfected with pAdTrack CMV-IRM, which contains the HA tagged-inhibitor resistant wild type NHE1. Lanes 5 and 6 represent lysates from AP-1 cells transfected with pAdTrack CMV-K-IRM, which contains the HA tagged-inhibitor resistant active NHE1.

We also measured the NHE1 activity of AP-1 cells transfected with either pAdTrack CVM-IRM or pAdTrack CMV-K-IRM. The results are shown in Figure 3.15. In AP-1 cells transfected with pAdTrack CMV-IRM, NHE activity was comparable to AP-1 cells transfected with the pYN4^{+} plasmid, containing wild type NHE1 (NHE1) and significantly increased in comparison to AP-1 cells transfected with pAdTrack CMV (P<0.05) (Figure 3.15, *A*). Treatment with 10 μM EMD 87580 did not decrease the NHE1 activity of AP-1 cells transfected with pAdTrack CVM-IRM. Similarly, in AP-1 cells transfected with pAdTrack CMV-K-IRM, NHE1 activity increased vs. AP-1 cells transfected with pAdTrack CMV (P<0.05) (Figure 3.15, *B*). Treatment with 10 μM EMD 87580 did not decrease the activity of AP-1 cells transfected with pAdTrack CVM-K-IRM. The lack of inhibitory effects on NHE1 activity by EMD 87580 demonstrates that the inhibitor resistant protein was expressed in both the pAdTrack CMV-IRM and pAdTrack CMV-K-IRM plasmids.

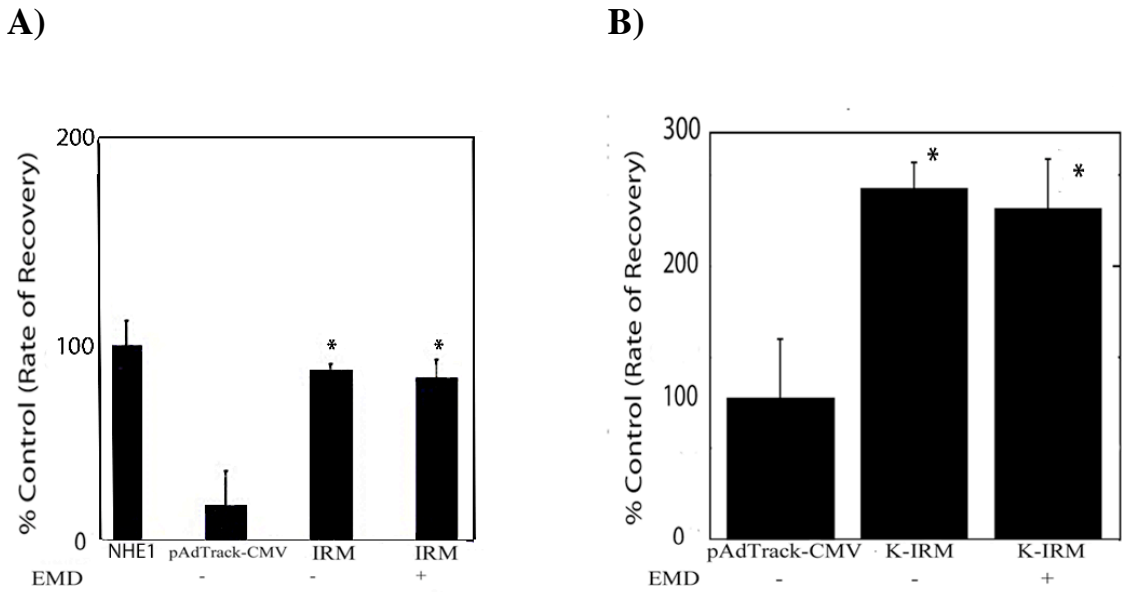

Figure 3.15. NHE1 activity of AP-1 cells transfected with pAdTrack CMV-IRM or pAdTrack CMV-K-IRM in the presence (+) or absence (-) of EMD 87580. (–), not treated with EMD; (+), treated with EMD. **A),** AP-1 cells transfected with pAdTrack CMV-IRM (IRM), pAdTrack-CMV, $pYN4^{+}$ plasmid containing wild type NHE1 (NHE1). Results are expressed as a % of controls±%SEM, with controls being AP-1 cells transfected with NHE1. $^{*}P<0.05$ vs. pAdTrack CMV; n=8/group. **B),** AP-1 cells were transfected with pAdTrack CMV-K-IRM (K-IRM) or pAdTrack CMV. Results are expressed as a % of controls±%SEM, with controls being AP-1 cells transfected with pAdTrack CMV. $^{*}P<0.05$ vs. pAdTrack CMV; n=8/group.

3.2.12 Determination of the IRM and K-IRM Adenoviruses MOI

Prior to the characterization of our IRM and K-IRM adenoviruses, we identified the ideal MOI (as described in Section 2.4.3.1.1) and duration of viral infection in NRVMs. This was done to ensure 100% efficiency of the adenoviral infections and maintenance of cell viability. Figure 3.16 illustrates representative western blots (middle and bottom panel) and representative pictures of GFP fluorescence (upper panel) of NRVMs during various times following infection with the K-IRM adenovirus at an MOI of 10, 20 and 30. NHE1 expression, detected by anti-HA antibody, was present as early as 24 hours after infection and continued 48 hours post infection. NHE1 protein expression declined slightly with the time of infection. Both the glycosylated and the deglycosylated form of the NHE1 protein are substantially visible at a MOI of 20 following 24 hours of infection. Similar experiments were conducted using the IRM adenovirus and a MOI of 20 for 24 hours also gave the best conditions (data not shown). NRVMs were infected with GFP at an MOI of 20 for 24 hours to confirm the specifity of the HA-tagged antibody and no immunoreactivity was detectected. In all subsequent experiments, NRVMs were infected with the IRM or K-IRM adenoviruses using an MOI of 20 for 24 hours. The conditions of GFP, the control adenovirus, paralled the experimental conditions of the IRM and K-IRM adenoviruses.

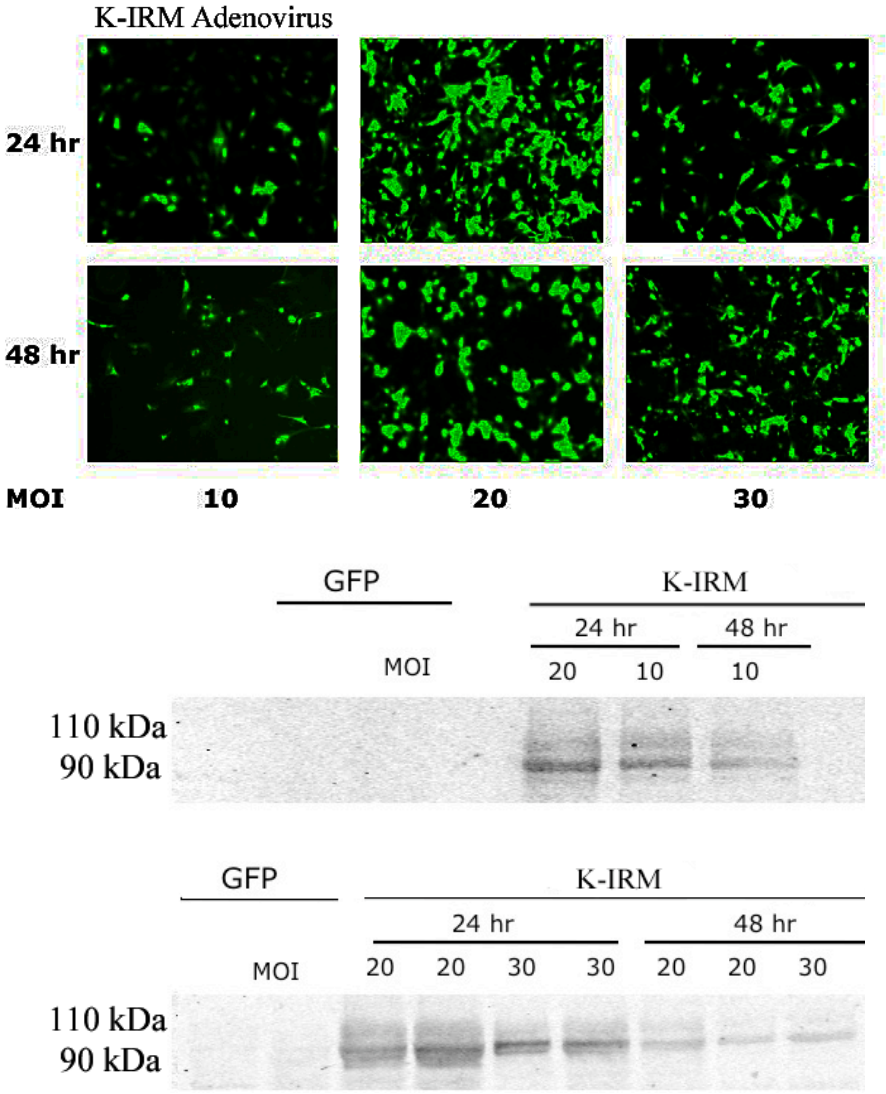

Figure 3.16. MOI and time course of NHE1 protein expression in neonatal rat ventricular cardiomyocytes infected with the K-IRM adenovirus. NRVMs were infected with the K-IRM adenovirus (HA tagged-inhibitor resistant active NHE1) or GFP and the time course of expression was examined by western blotting against the anti-HA tag. **Upper panel,** representative picture of NRVMs infected with the K-IRM adenovirus using an MOI of 10, 20 or 30 for 24 and 48 hours (hr). **Middle and bottom panel,** representative western blots of NRVMs infected the K-IRM adenovirus using an MOI of 10, 20 or 30 of and were examined at 24 and 48 hours (hr) post infection with anti-HA tag antibody. NRVMs were also infected the GFP adenovirus using an MOI of 20 for 24 hours and blotted with anti-HA tag antibody.

3.2.13 In Vitro Characterization of IRM and K-IRM Adenoviruses for Myocyte Hypertrophy

We compared the effects of *in vivo* expression of NHE1 in mice with *in vitro* expression of NHE1 in NRVMs. NRVMs were infected with one of three adenoviruses. One expressed GFP and was used as a control. A second expressed wild type NHE1 (IRM). The third adenovirus expressed NHE1 with the same mutations as in the K-line mice, creating an active NHE1 (K-IRM). To confirm that the infection of NRVMs with the IRM or K-IRM adenoviruses led to expression of the NHE1 protein and to determine the total amount of NHE1 protein expressed, we measured total (exogenous and endogenous) NHE1 protein expression using a commercial antibody against NHE1 (Figure 3.17). Figure 3.17, upper panel, is a representative immunoblot of NRVMs infected with GFP (lanes 1-3), IRM (lanes 4-6) or K-IRM (lanes 7-9) adenoviruses. Quantification of a series of experiments measuring total NHE1 protein expression (Figure 3.17, bottom panel) shows that there was a marked increase (≈ 70 and 90 fold, $P<0.05$) in total NHE1 protein expression in NRVMs infected with the IRM and K-IRM adenoviruses vs. NRVMs infected with the GFP adenovirus, respectively. Total NHE1 protein expression was not significantly in NRVMs infected with the IRM or K-IRM adenoviruses, however, K-IRM infected NRVMs had a slightly greater expression.

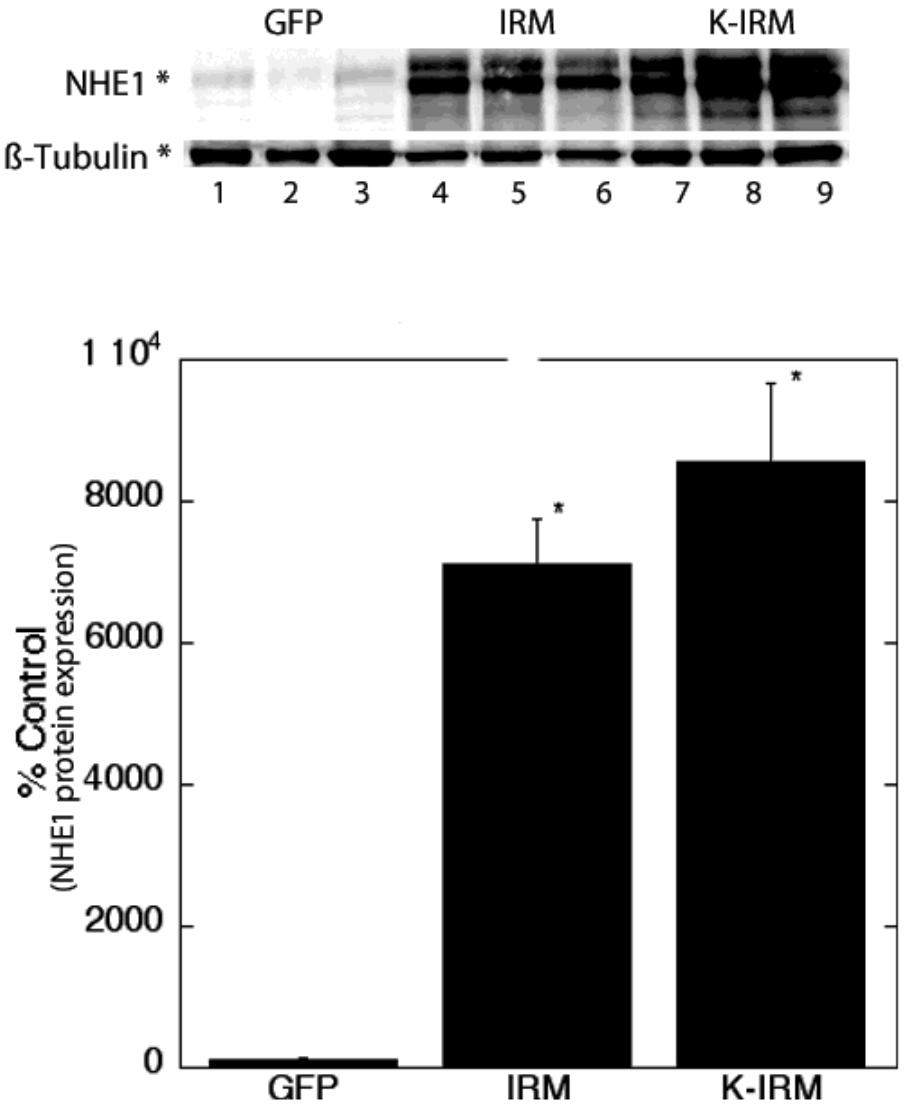

Figure 3.17. Western blot analysis of NHE1 protein expression in neonatal rat ventricular cardiomyocytes infected with IRM, K-IRM or GFP (control) adenoviruses. NRVMs were infected with a MOI of 20 of GFP, IRM or K-IRM adenoviruses for 24 hours. **Upper panel,** representative immunoblot analysis of total (exogenous and endogenous) NHE1 protein expression in lysates isolated from NRVMs. NHE1 was detected by a mouse monoclonal anti-NHE1. NHE1, at 90-110 kDa, is indicated by * and β-Tubulin, the loading control, at 50 kDa, is indicated by the *. Lanes 1-3 represent lysates from NRVMs infected with the GFP adenovirus, lanes 4-6 represent lysates from NRVMs infected with the IRM adenovirus and lanes 7-9 represent lysates from NRVMs infected with the K- IRM adenovirus. **Bottom panel,** is a quantification of a series of experiments measuring total NHE1 protein expression. NHE1 protein levels were quantified and normalized to β-Tubulin for each group and calculated as a % of GFP (control)±%SEM. $^{*}P<0.05$ for control (GFP) vs. IRM or K-IRM; n=4-5/group.

Total exogenous NHE1 protein expression was also measured by immunoblotting for HA tagged-NHE1 with anti-HA tag antibody (12CA5) (Figure 3.18). Exogenous NHE1 protein was present in NRVMs infected with either the IRM (lanes 2-5) or K-IRM (lanes 6-9) adenovirus, but not in NRVMs infected with the GFP adenovirus (lane 1). Quantification of a series of experiments measuring the levels of exogenous NHE1 (Figure 3.18, bottom panel) showed that NRVMs infected with the K-IRM adenovirus had a higher level of NHE1 protein expression than NRVMs infected with the IRM adenovirus. The level of NHE1 protein expression between IRM and K-IRM infected NRVMs were not significantly different.

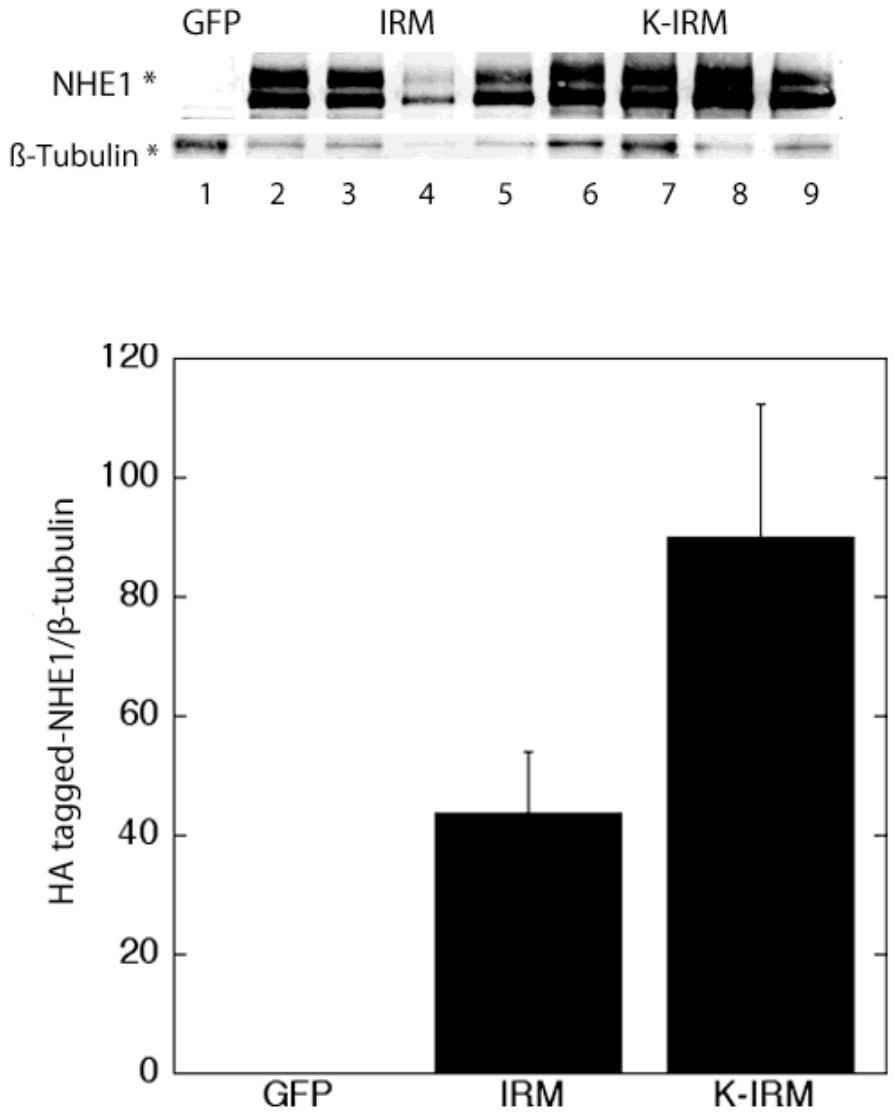

Figure 3.18. Immunoblot analysis of exogenous HA tagged-NHE1 protein expression in lysates of neonatal rat ventricular cardiomyocytes infected with GFP, IRM or K-IRM adenoviruses. NRVMs were infected with a MOI of 20 of GFP, IRM (HA tagged-wild type NHE1) or K-IRM (HA tagged- active NHE1) adenoviruses for 24 hours. NHE1 was detected by western blotting with a mouse monoclonal anti-HA (12CA5). **Upper panel,** is a representative western blot of NHE1 detected at 90-110 kDa and 50 kDa β-Tubulin, a loading control. Lane 1 represents lysates of NRVMs infected with the GFP adenovirus, lanes 2-5 represent lysates of NRVMs infected with the IRM adenovirus and lanes 6-9 represent lysates of NRVMs infected with the K-IRM adenovirus. **Bottom panel,** quantification of a series of experiments. NHE1 protein expression was quantified and normalized to β-Tubulin for each group. Results are expressed as mean±SEM. (n=4 /group).

To evaluate the effects of varying types of NHE1 protein expression on the degree of CH *in vitro*, hypertrophic indices were measured in NRVMs infected with GFP, IRM or K-IRM adenoviruses. Cells were infected with IRM, K-IRM or GFP control adenoviruses in the presence or absence of 10 μM EMD 87580 and cell area and protein synthesis were monitored. We previously determined that 10 μM EMD 87580 inhibits all endogenous NHE1 and not exogenous NHE1 activity (as described in Section 2.4.2.1), therefore allowing us to compare the hypertrophic effects of NHE1 due to expression of endogenous and exogenous NHE1 or expression of exogenous NHE1 alone. We found that endogenous NHE1 makes up approximately 50% of the measureable activity present in NRVMs[86,275]. Figure 3.19 illustrates that only NRVMs infected with the K-IRM adenovirus in the absence of EMD 87580 (113.7±2.9%, $P<0.005$) showed a significant increase in cell area vs. NRVMs infected with the GFP adenovirus (100.0±3.4%), IRM (95.6±1.8%) or NRVMs infected with the K-IRM adenovirus in the presence of EMD 87580 (90.4±2.1%). NRVMs infected with the IRM adenovirus in the presence (96.6±2.4%) or absence of EMD 87580 (95.6±1.8%) did not show any significant increase in cell area vs. NRVMs infected with the GFP adenovirus (100.0±3.4%).

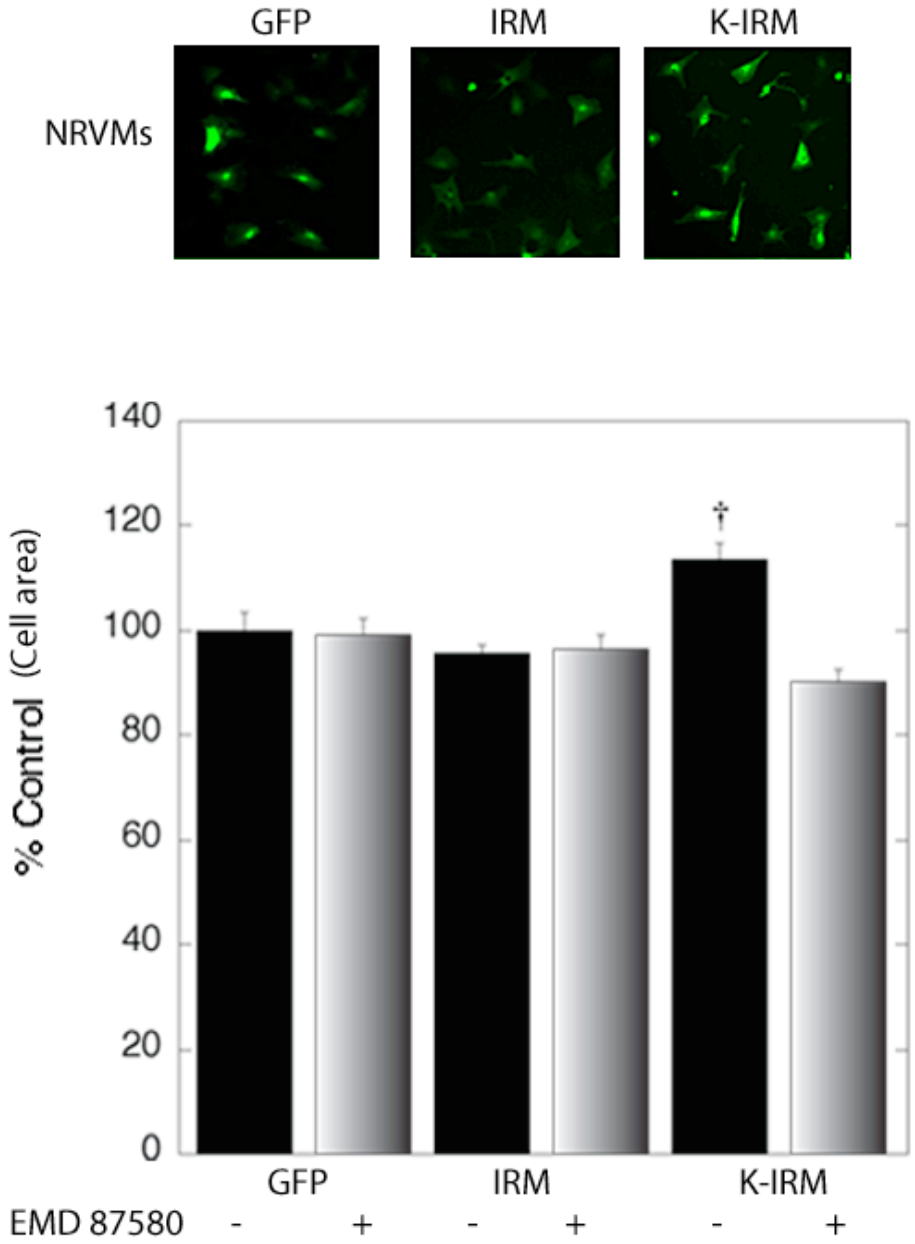

Figure 3.19. Analysis of cell area of neonatal rat ventricular cardiomyocytes infected with IRM, K-IRM or GFP adenoviruses in the presence (+) or absence (-) of 10 μM EMD 87580. NRVMs were infected with a MOI of 20 of GFP, IRM or K-IRM adenoviruses for 24 hours. EMD 87580 was added 4 hours following adenoviral infection; (-) EMD 87580 was not present, (+) EMD 87580 was present. **Upper panel,** representative images of fluorescence microscopy of NRVMs infected with GFP, IRM or adenoviruses. **Bottom panel,** quantitative analysis of cell area. Results are expressed as % GFP±%SEM. $^{\dagger}P<0.005$ for K-IRM vs. GFP, IRM, or K-IRM in the presence of EMD 87580; n=4-7. At least 50 cells were measured from three individual dishes to represent one n value.

We also examined proteins synthesis of NRVMs. Protein synthesis is another index of CH. Figure 3.20 shows that only NRVMs infected with the K-IRM adenovirus in the absence of EMD 87580 had a significant increase in protein synthesis ($P<0.005$ for K-IRM vs. GFP, IRM or K-IRM in the presence of EMD 87580). When NRVMs were infected with the IRM adenovirus either in the presence or absence of EMD 87580, they did not show a significant increase in protein synthesis vs. NRVMs infected with the GFP adenovirus (Figure 3.20).

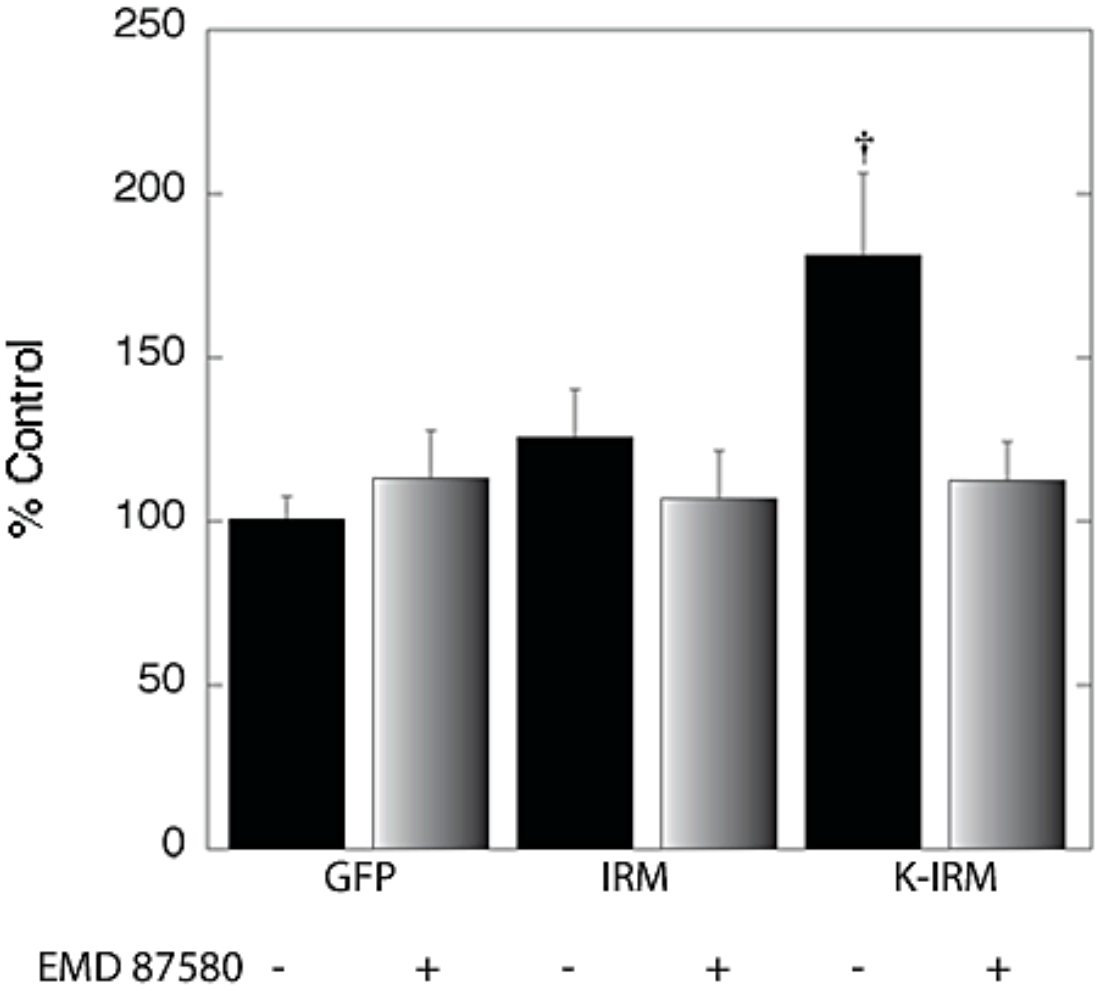

Figure 3.20. Analysis of the rate of protein synthesis in neonatal rat ventricular cardiomyocytes infected with IRM, K-IRM or GFP adenoviruses in the presence (+) or absence (-) of 10 μM EMD 87580. NRVMs were infected with a MOI of 20 of GFP, IRM or K-IRM adenoviruses for 24 hours. [^{3}H] Phenylalanine (1μCi/mL) was added 4 hours following adenoviral infection and at the same time as EMD 87580. Quantitative analysis of the rate of protein synthesis was measured by the amount of [^{3}H] phenylalanine incorporated. Protein synthesis was corrected with DNA synthesis and was expressed as % GFP±%SEM. $^{\dagger}P<0.005$ for K-IRM vs. GFP, IRM or K-IRM in the presence of EMD 87580; n=20-30 plates, 5-8 experiments.

3.2.14 Signaling Pathways Contributing to NHE1 Induced Cardiac Hypertrophy

Based on our *in vivo* and *in vitro* studies, active NHE1 expression induces CH. Experiments were done to ensure that the phenotype we examined was NHE1-dependent and not due to altered expression of other regulatory membrane proteins involved in ion regulation (as described in Section 1.1). Heart lysates were made and western blotting was used to examine protein expression of NKA, NCX, SERCA, NBC1, and AE3. The results are shown in Figure 3.21. The upper panel shows one example of each type of western blot for these proteins from control, N-line and K-line heart lysates. The bottom panel shows quantification of a series of western blots for each protein. There were no significant changes in protein expression of any of these proteins in the N-line and K-line hearts compared with controls. A preliminary experiment also examined protein expression of AE1 in the myocardium of N-line and K-line hearts vs. controls. These levels were very low and difficult to quantify, but there were no apparent differences between NHE1 TGs and controls (data not shown).

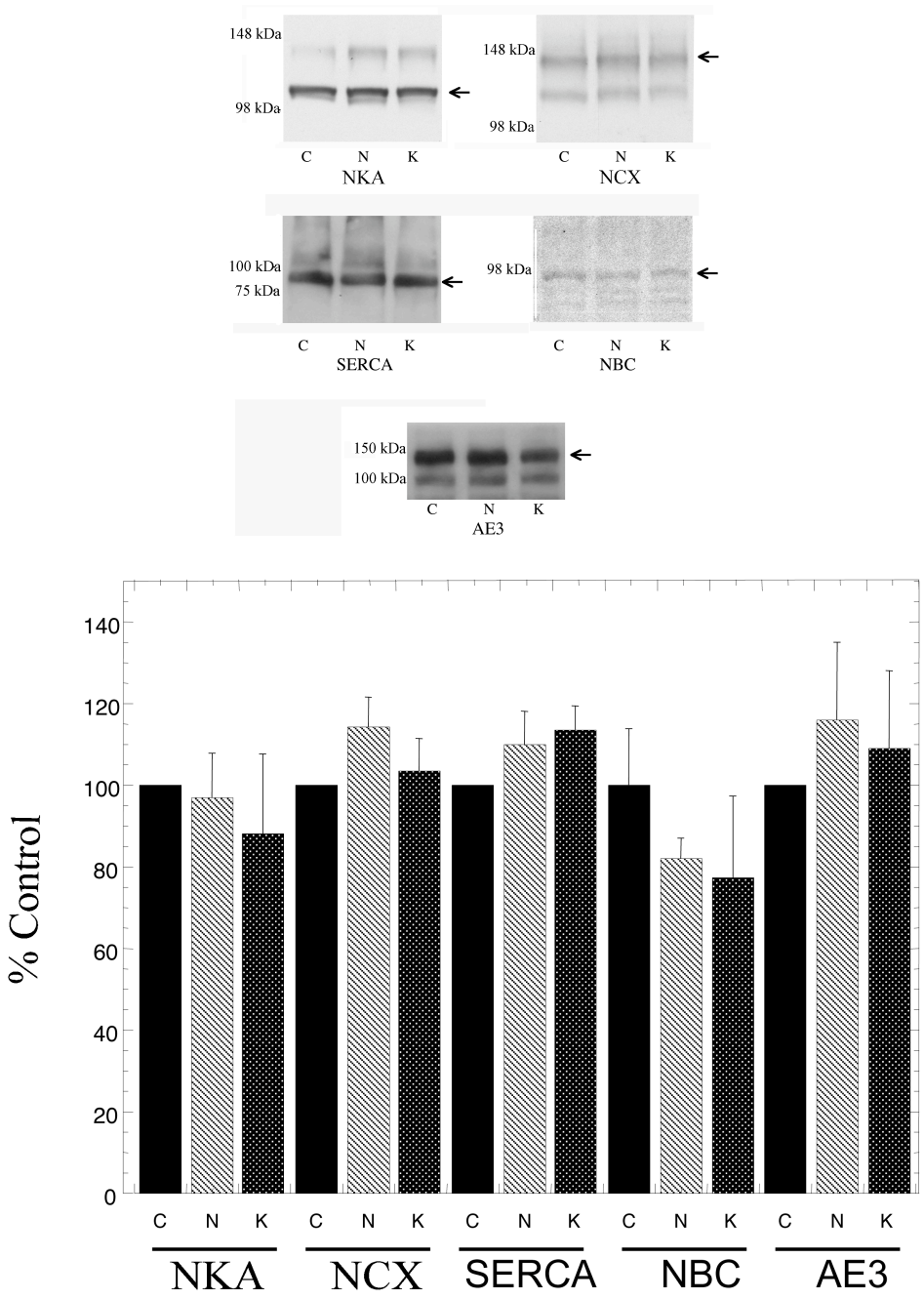

Figure 3.21. Western blot analysis of protein expression of ion transport and pH regulatory proteins in hearts from control, N-line and K-line mice. C, controls; N, N-line; K, K-line. **Upper panel,** representative western blots of heart lysates immunoblotted with antibodies directed against NKA, NCX, SERCA, NBC and AE3. Arrows indicate the cross-reactive species of the predicted molecular weight. **Bottom panel,** quantitative analysis of western blot protein expression of ion transport and pH regulatory proteins. Results are displayed as % of control±%SEM within each group. (n= 4-7/group). Heather Vanier-Vandertol performed these experiments.

We also examined expression and activation of signaling pathways that have been implicated in stress-induced remodeling of the heart to determine whether these pathways were involved in NHE1-mediated remodeling of the heart. Prohypertrophic signaling pathways were examined. These include: ERKs, JNKs, p38 and RSK, which are regulated by phosphorylation-dephosphorylation, with phosphorylation being in its active form. The levels of pERK, pp38 or pJNK were not elevated in heart lysates from N-line and K-line mice when compared to controls (Figure 3.22). Further studies were done using antibodies specific to p38α, the most abundant p38 isoform in the myocardium[127], and no differences were seen in protein expression between heart lysates from control, N-line and K-line mice (Figure 3.22). Similarly, the ratio of pRSK to total RSK did not change in heart extracts from N-line and K-line mice when compared to controls (Figure 3.22).

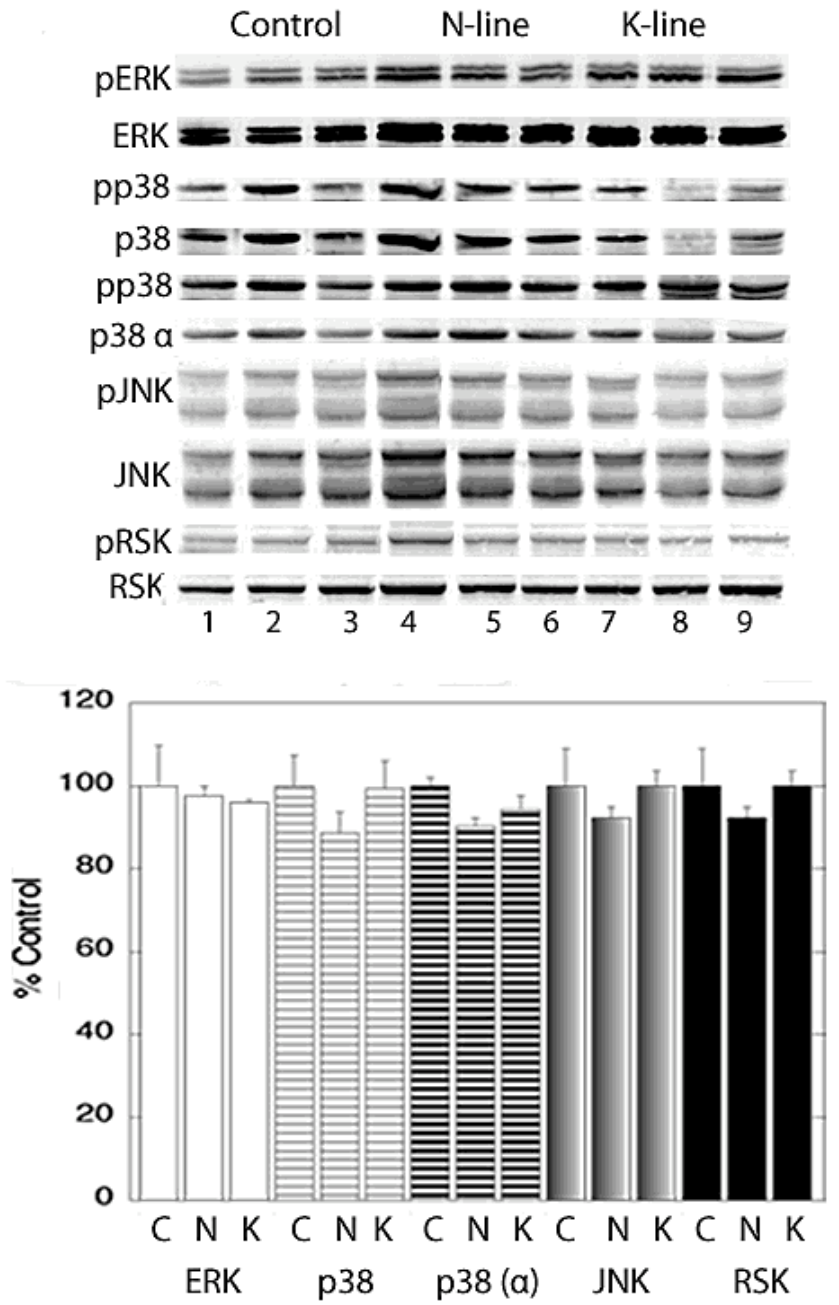

Figure 3.22. Western blot analysis of protein expression of MAPKs and RSK in hearts from control, N-line and K-line mice. C, controls; N, N-line; K, K-line. **Upper panel,** representative western blots of relative amounts of phosphorylated and total pro-hypertrophic kinases, ERK, p38, p38(α), JNK and RSK. Lanes 1-3 represent control heart lysates, lanes 4-6 represent N-line heart lysates, and lanes 7-9 represent K-line heart lysates. **Bottom panel,** quantification of a series of experiments measuring the ratio of phosphorylated to total protein for pERK/ERK, pp38/p38(α), pJNK/JNK and pRSK/RSK. Results are calculated as a % of control (for each group)±%SEM. (n=3 hearts/group).

Catalytically-active GSK-3β has been implicated in anti-hypertrophic signaling[380]. It is regulated by phosphorylation-dephosphorylation, with phosphorylation being inhibitory. GSK-3β is located predominantly in the cytosol and is also found in the mitochondria. To determine whether GSK-3β is involved in the cardiac phenotype of the N-line and K-line mice, we examined the total amount of GSK-3β and phosphorylated GSK-3β expressed in both the cytosolic and mitochondrial fractions of heart lysates from control, N-line and K-line mice (Figure 3.23). No significant changes were observed in GSK-3β protein levels in the cytosolic and mitochondrial fractions of heart lysates of N-line and K-line mice vs. controls. Phosphorylated GSK-3β was not detected in heart lysates from control, N-line and K-line mice in both the cytosolic and mitochondrial fractions (data not shown).

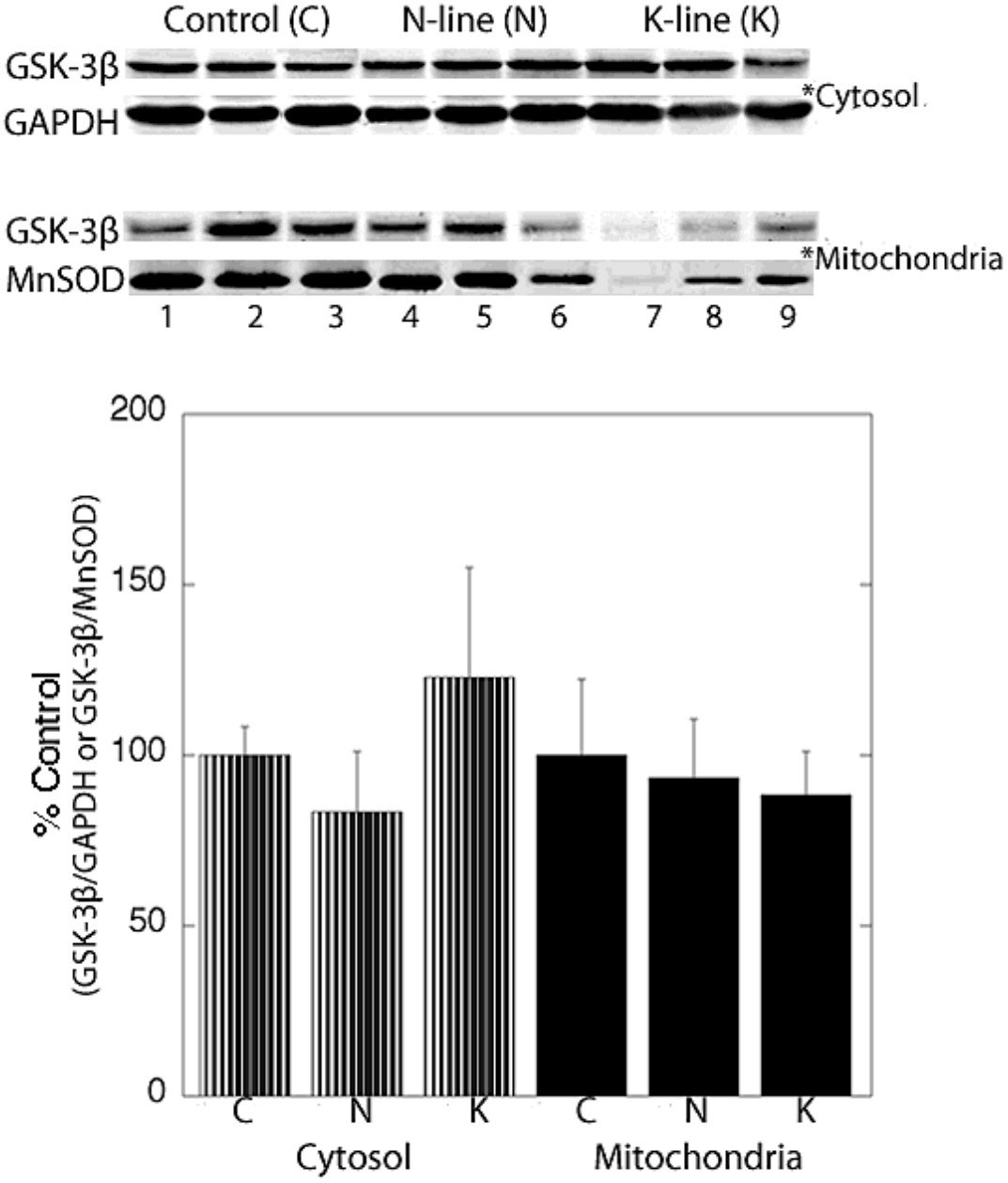

Figure 3.23. Western blot analysis of protein expression of GSK-3β in the cytosolic and mitochondrial fractions of hearts from control, N-line and K-line mice. C, controls; N, N-line; K, K-line. **Upper panel,** representative western blot of GSK-3β and GAPDH in the cytosolic fraction of heart lysates. **Middle panel,** representative western blot of GSK-3β and MnSOD in the mitochondrial fraction of heart lysates. **Bottom panel,** quantification of a series of experiments measuring the ratio of GSK-3β to GAPDH or MnSOD in the cytosolic or mitochondrial fractions. Results are expressed as a % of control (for each group)±%SEM. (n=5-6 hearts/group).

Finally, we examined calcineurin activity in heart lysates from control, N-line and K-line mice (Figure 3.24). Calcineurin is a prohypertrophic serine-threonine protein phosphatase that is activated in response to sustained elevation of $[Ca^{2+}]_i$[381,141]. Calcineurin's prohypertrophic effects have also been implicated in NHE1 induced CH[141]. We found that there were no differences in calcineurin activity in heart lysates from control, N-line and K-line mice.

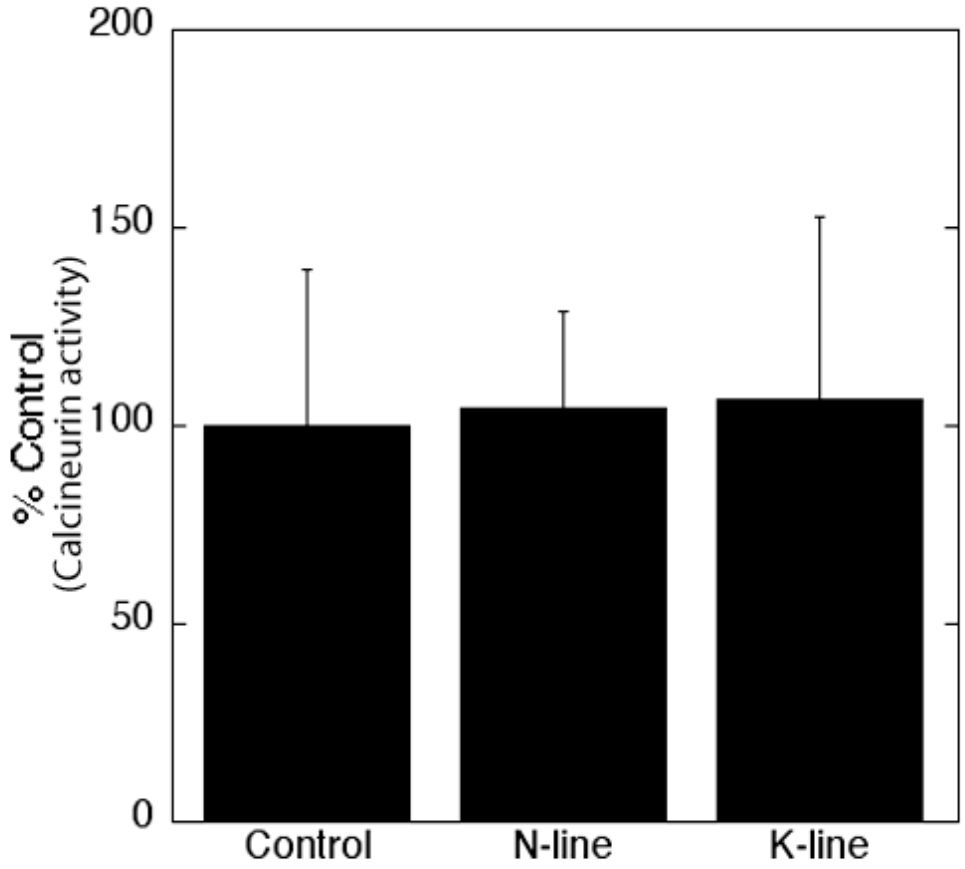

Figure 3.24. Calcineurin phosphatase activity in control, N-line and K-line mouse hearts. Calcineurin activity was calculated for each group using the following equation; calcineurin activity = total calcineurin activity detected in the presence of 100 nM okadaic acid - total calcineurin activity detected in the presence of okadaic acid and EGTA. Okadaic acid inhibits PP1 and PP2A, EGTA inhibits PP2B. Results are expressed as a % of control±%SEM. (n=5 hearts/group).

3.2.15 Measurement of Indices of Apoptosis in Hearts from NHE1 Transgenic Mice

Hypertrophied cardiomyocytes have been shown to be more susceptible to apoptosis as described in Section 1.7.4.3. Many key events in the apoptotic machinery are linked to the mitochondria. The mitochondria is a central integrator and transducer for proapoptotic signals due to its storage of several critical proapoptotic activators, such as Cyt c and AIF[319]. Release of Cyt c and AIF from the mitochondria into the cytoplasm initiates caspase-dependent and caspase-independent cell death pathways, respectively[283,293,319].

We examined apoptosis in hearts from N-line and K-line mice. Initially, we examined left ventricular sections from control and K-line mice using transmission electron microscopy. The mitochondria appeared swollen in K-line vs. controls (Figure 3.25, upper panel). We then measured the level of apoptosis in cross sections of these hearts stained with TUNEL. Hearts from K-line mice showed a significant increase in the ratio of TUNEL-stained positive cells to DAPI (0.45±0.014 vs. 0.37±0.025 controls; $P<0.05$) (Figure 3.25, middle and bottom panel). Hearts from N-line mice showed no statistical significance in the ratio of TUNEL-stained positive cells to DAPI when compared to controls (0.37±0.025 controls vs. 0.36±0.068 N-line).

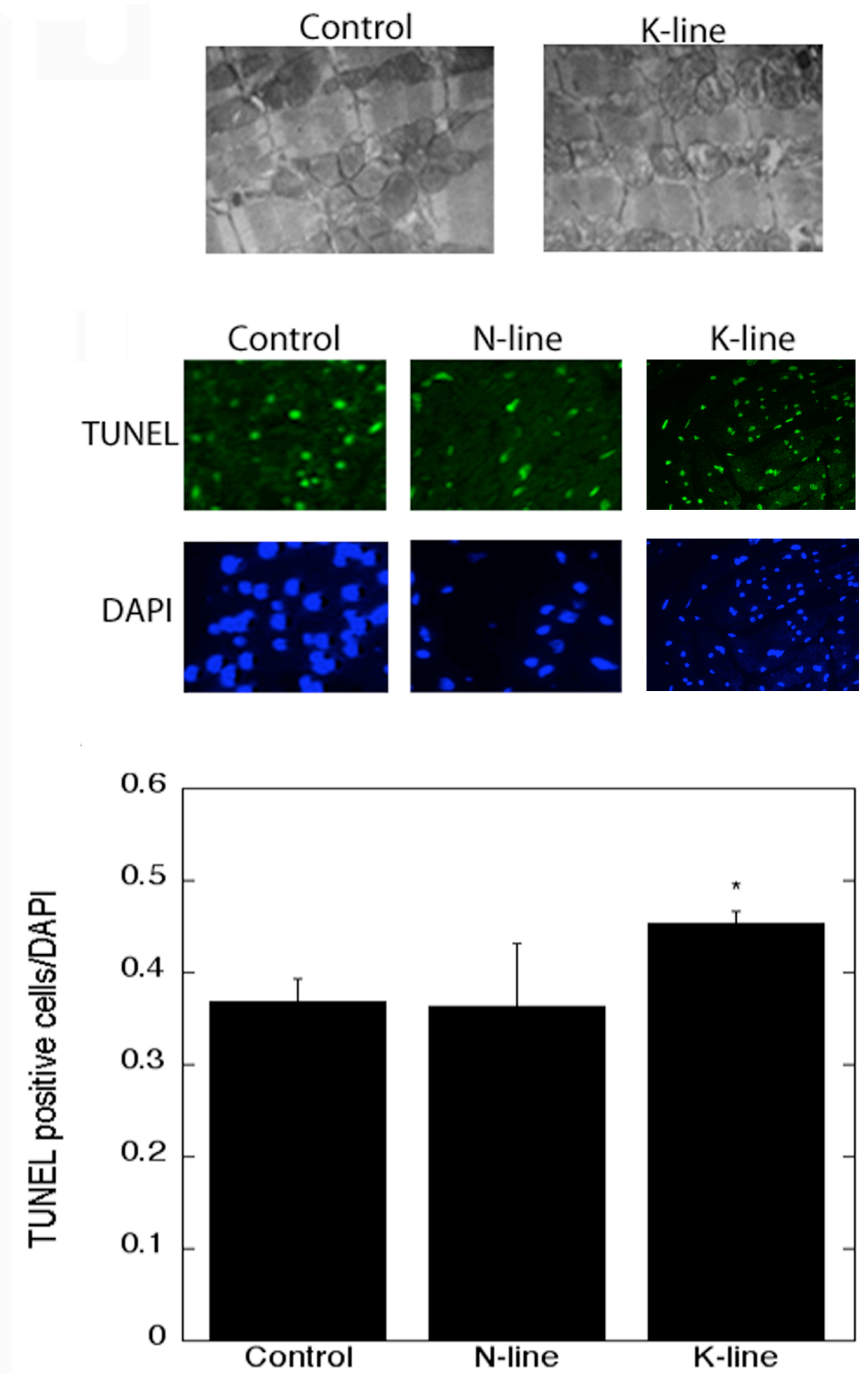

Figure 3.25. Examination of TUNEL and electron microscopy in the left ventricles of control, N-line and K-line hearts. Upper panel, representative electron micrographs of control and K-line left ventricles. **Middle panel,** representative heart cross sections of control, N-line and K-line hearts stained with TUNEL (top) and DAPI (bottom). **Bottom panel,** quantification of experiments measuring the ratio of TUNEL-positive cells to DAPI staining in control, N-line and K-line left ventricles. Results are expressed as the ratio of TUNEL positive cells/DAPI±SEM. $^{*}P<0.05$ for controls vs. K-line; n=3-4 hearts/group.

To further understand the mechanism by which apoptosis occurred, we looked at markers involved in both the caspase-dependent and caspase-independent pathways in the cytosolic and mitochondrial fractions of hearts from control, N-line and K-line mice. Caspase-3 an indicator of the caspase dependent pathway was measured activity in the cytosolic fraction. Cyt c, another marker of the caspase dependent pathway, was measured in the mitochondria and cytosolic fractions. This was done to determine whether NHE1 induced apoptosis was mediated through the caspase-dependent pathway. Caspase-3 activity in the cytosolic fraction of heart lysates from N-line or K-line mice was not significantly different (100±8.8% controls vs. 75.0±17.2 N-line vs. 116±22.6% K-line) (Figure 3.26).

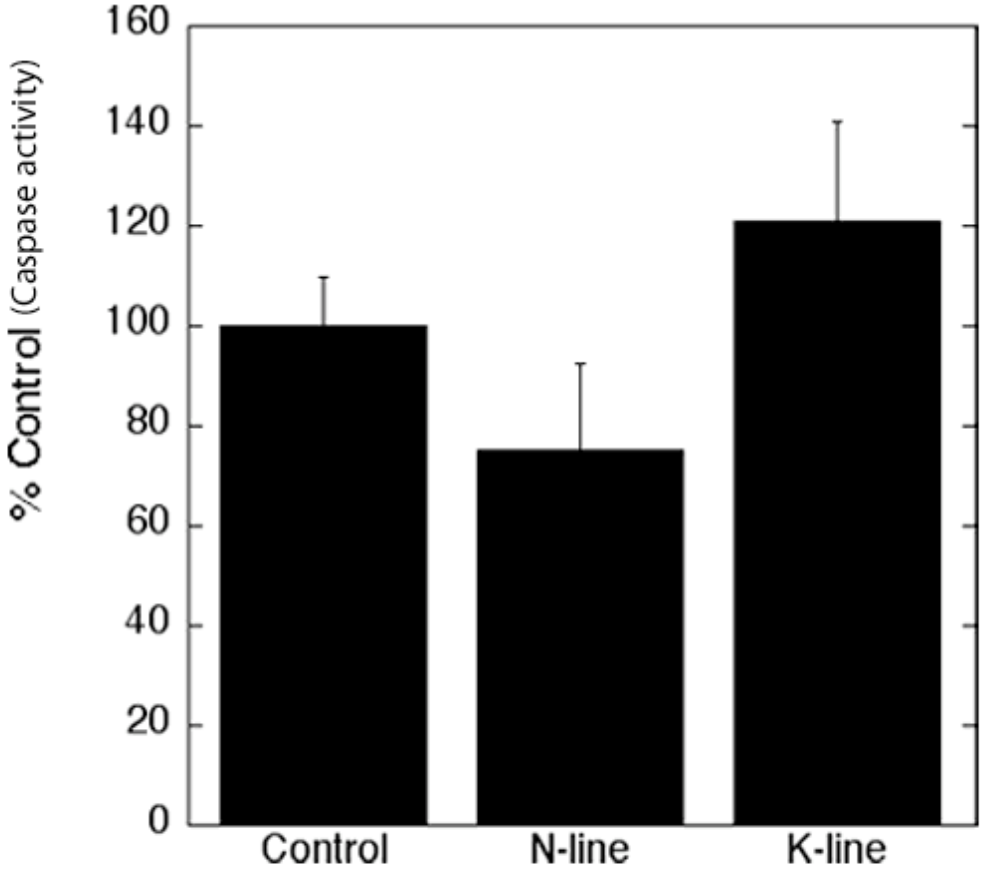

Figure 3.26. Analysis of caspase-3 activity of hearts from control, N-line and K-line mice. Caspase-3 activity was measured in the cytosolic fraction of hearts from control, N-line and K-line mice. Results are expressed as a % of controls±%SEM. (n=4 hearts/group).

Immunoblot analysis of Cyt c protein expression in the mitochondrial and cytosolic fractions of control and NHE1 TG mice were examined (Figure 3.27). There were no significant changes in protein expression of Cyt c in both the cytosolic (100.0±8.1% controls vs. 81.1±3.5% N-line vs. 86.7±15.2% K-line) and mitochondrial (100±15.7% controls vs. 67.0±24.8% N-line vs. 114.7±47.3% K-line) fractions of hearts from control vs. N-line and K-line mice.

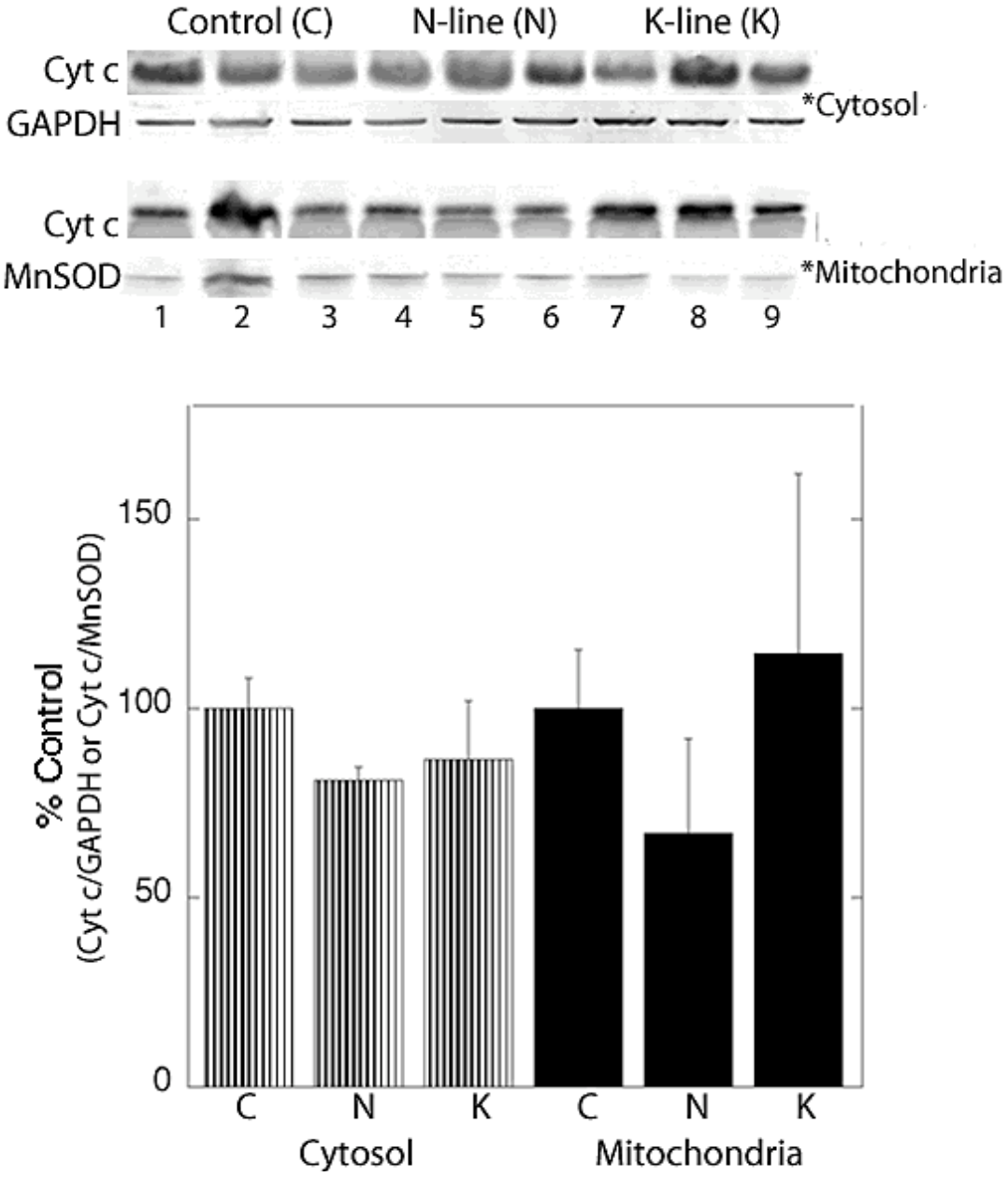

Figure 3.27. Analysis of Cyt c protein expression in the mitochondrial and cytosolic fractions of hearts from control, N-line and K-line mice. C, controls; N, N-line and K, K-line. **Upper Panel,** representative western blots of total Cyt c protein expression in the cytosolic fraction (normalized to GAPDH) and mitochondrial fraction (normalized to MnSOD) of hearts from control, N-line and K-line mice. Lanes 1-3 represent controls, lanes 4-6 represent N-line mice and lanes 7-9 represent K-line mice. **Bottom panel,** quantification of a series of experiments quantified for Cyt c and normalized to GAPDH in the cytosol or MnSOD in the mitochondria. Results are expressed as a % of controls for each group±%SEM. (n=6 hearts/group).

To further investigate whether the caspase-dependent pathway was involved in NHE1 mediated apoptosis, we examined the amount of PARP cleaved by caspase-3. Caspase-3 cleaves PARP of 116 kDa to produce cleaved fragment of 89 kDa size. As shown in Figure 3.28, control (100.3±28.3%), N-line (168.0±33.3%) and K-line (131.8±14.0%) mice had comparable levels of cleaved PARP (89kDa).

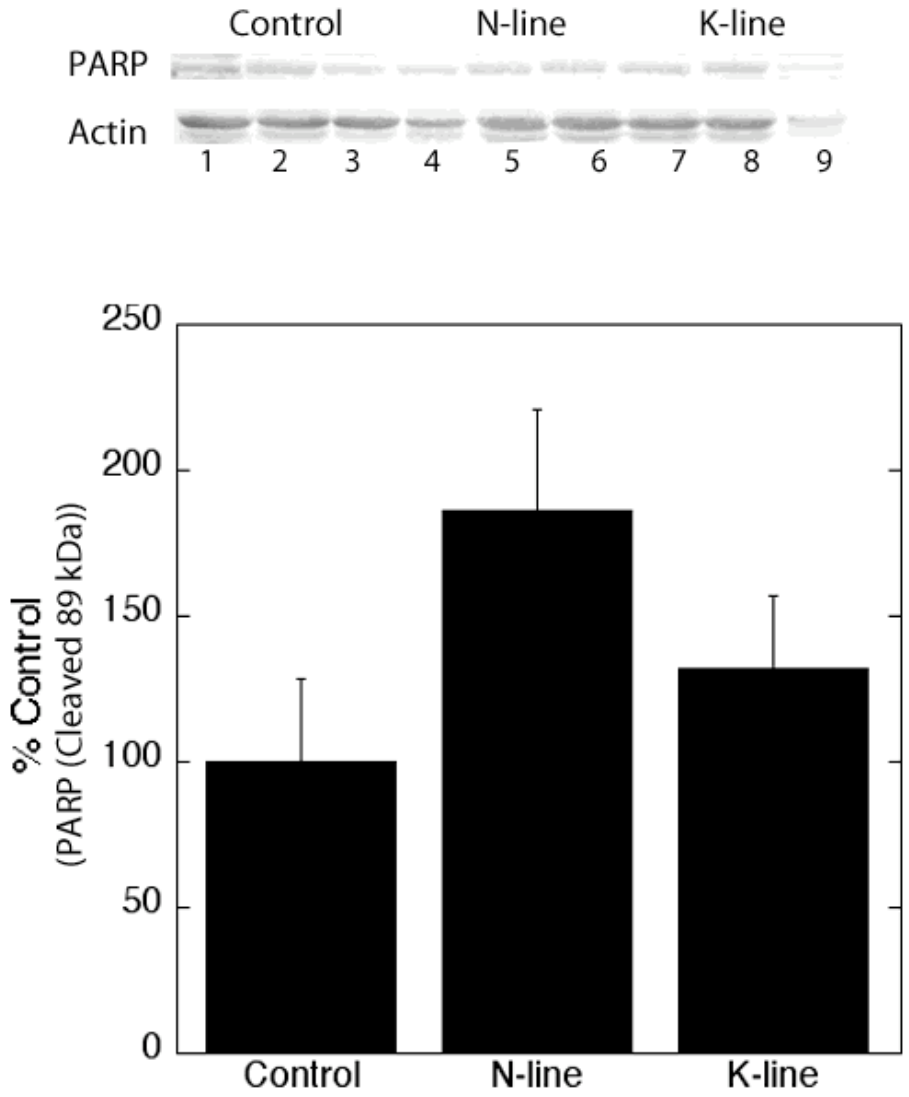

Figure 3.28. Analysis of cleaved PARP protein expression in the cytosolic fraction of hearts from control, N-line and K-line mice. Caspase-3 cleaves PARP leaving a fragement of 89 kDa size. **Upper panel,** representative western blot of cleaved PARP (89kDa) in the cytosolic fraction of hearts from control, N-line and K-line mice, normalized to actin. Lanes 1-3 represent controls, lanes 4-6 represent N-line mice and lanes 7-9 represent K- line mice. **Bottom panel,** quantification of a series of experiments measuring the level of 89 kDa cleaved PARP normalized to actin. Results are expressed as a % of controls±%SEM. (n=5-6 hearts/group).

Additionally, we investigated the contribution of the caspase-independent pathway in NHE1 mediated apoptosis. AIF protein expression was measured in the mitochondrial and cytosolic fractions (Figure 3.29). Immunoblot analysis showed that AIF protein expression (normalized to MnSOD) was significantly greater in the mitochondrial fraction of hearts from K-line mice (165.0±13.6% K-line vs. 100.0±16.3% controls; $P<0.05$). No significant differences were found in AIF protein expression in the mitochondrial fraction of hearts from control (100.0±16.3%) and N-line (151.7±19.1%) mice. In the cytosolic fraction of hearts from control (100.0±1.6%), N-line (100.5±3.9%) and K-line (98.8±3.5%) mice, AIF expression (normalized to GAPDH) was comparable.

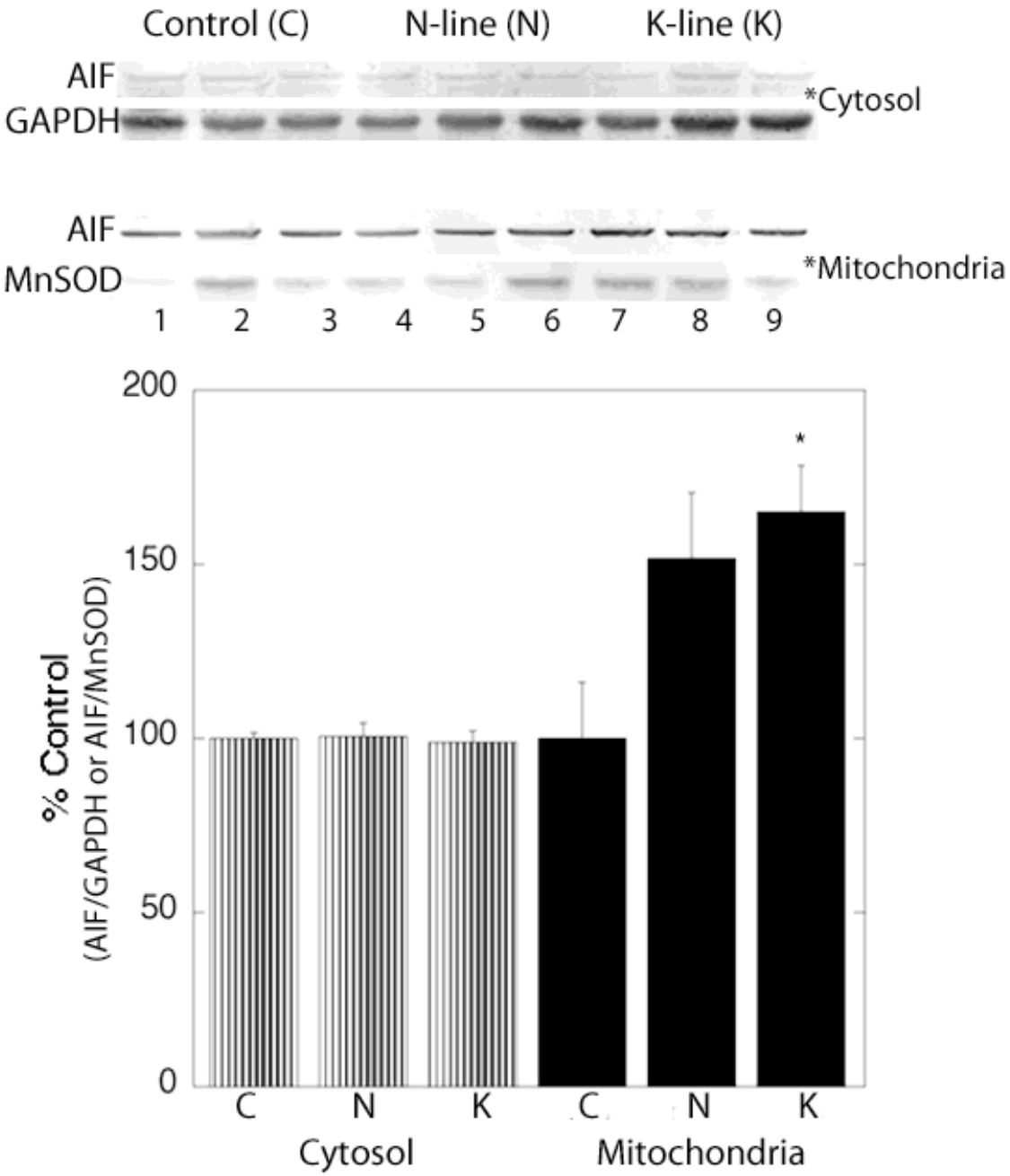

Figure 3.29. Analysis of AIF protein expression in hearts from control, N-line and K-line mice. C, controls; N, N-line; K, K-line. **Upper panel,** representative western blots of total AIF protein expression in the cytosolic (normalized to GAPDH) and mitochondrial (normalized to MnSOD) fractions of hearts from control, N-line and K-line mice. Lanes 1-3 represent control, lanes 4-6 represent N-line and lanes 7-9 represent K- line. **Bottom panel,** quantification of a series of experiments measuring AIF levels normalized to GAPDH in the cytosolic fraction or MnSOD in the mitochondria. Results are expressed as a % of controls±%SEM in each group. (n=6 hearts/group).

3.2.16 Characterization of NHE1 Transgenic Mice Following Neuroendocrine Stimulation

Increased sympathetic activity mediated by agonists such as PE has been implicated in the development of CH in animal models[233,320] and in humans[321]. In addition to mediating the sympathetic activity, PE has been shown to activate NHE1 (reviewed in[61]) (Figure 1.3).

To test the susceptibility of control, N-line and K-line mice to CH mediated by increased sympathetic activity/NHE1 activation, PE was administered using Alzet osmotic mini pumps for a period of two weeks. The dosage of PE administered, 50mg/kg/day, was based on previous studies[295-297]. We performed some preliminary studies to confirm that 50mg/kg/day PE induces CH. We measured cell area of isolated AVMs of male control mice treated with PE or PBS using Alzet osmotic mini pumps (Figure 3.30). The cell area of AVMs isolated from control hearts stimulated with PE (134.9±5.9%, $P<0.001$) was significantly greater than the cell area of AVMs from hearts treated with PBS (100.0±3.6%). Therefore, we proceeded with our experiments using the dosage of 50mg/kg/day PE.

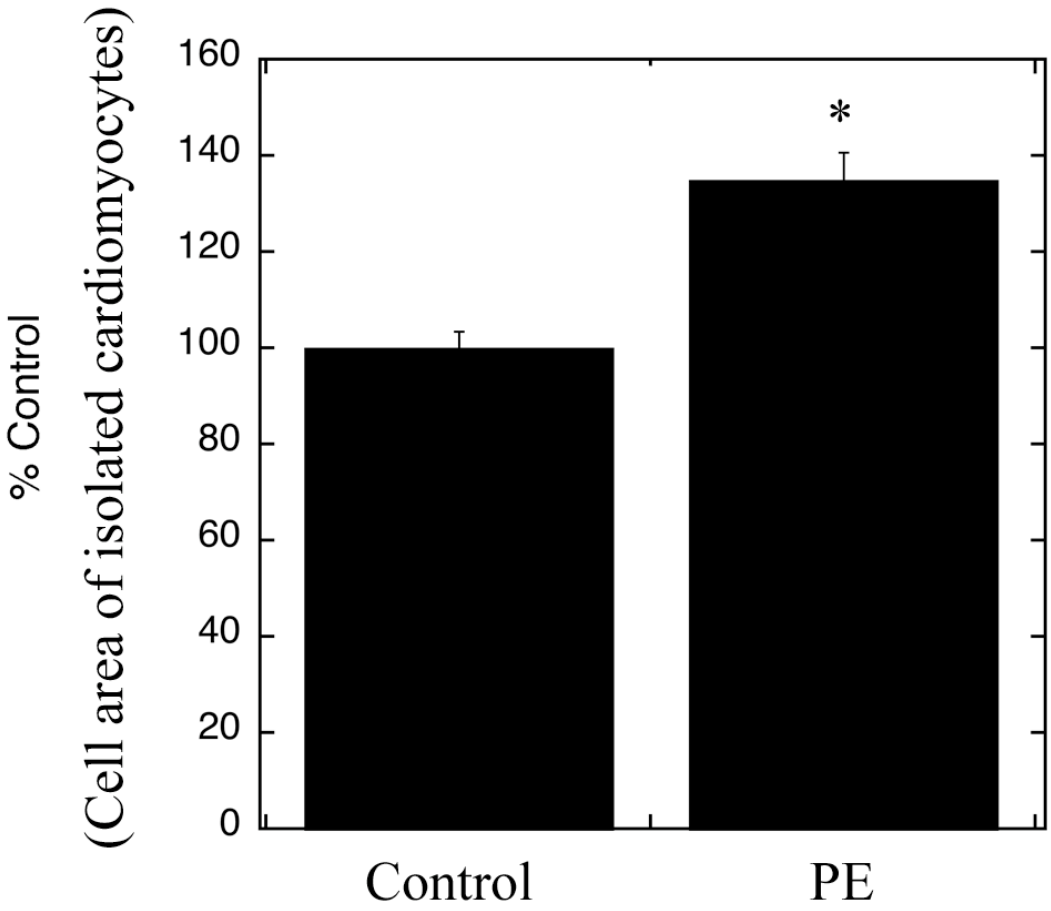

Figure 3.29. Cell area of isolated adult ventricular cardiomyocytes from hearts isolated from control male mice treated with PBS (control) or PE. Control, are control male hearts treated with PBS; PE, are control male hearts stimulated with 50 mg/kg/day PE. Control male mice were treated with PBS or PE using Alzet osmotic mini pumps over a period of two weeks. AVMs were isolated using retrograde perfusion. Results are expressed as a % of controls±%SEM. $^{*}P<0.001$ vs. control; n=2.

NHE1 TG mice stimulated with PE were then characterized for CH. The same hypertrophic indices measured in previous experiments including the HW/BW ratio, ANP mRNA expression, CSA and IF were measured in mice subjected to PE treatment. K-line mice stimulated with PE (133.0±11.0%, $P<0.05$) had a significantly greater HW/BW vs. K-line treated with PBS (100.0±6.4%) (Figure 3.31). Control mice stimulated with PE (112.1±8.1% PE vs. 100.0±4.6% PBS) also showed a trend towards increase in the HW/BW, although this was not significant. Surprisingly, N-line hearts stimulated with PE (100.0±7.5%) showed no differences vs. N-line hearts treated with PBS (98.7±2.8%). The variations seen in the HW/BW of controls and K-line mice stimulated with PE were the result of changes in the heart weight (100.0±4.4% PBS vs. 112.3±8.7% PE controls and 100.0±6.6% PBS vs. 118.2±7.1% PE K-line, $P<0.05$), as there were no significant changes in the body weight (100.0±2.8% PBS vs. 99.8±2.2% PE controls and 100.0±1.9% PBS vs. 90.3±2.2% PE K-line).

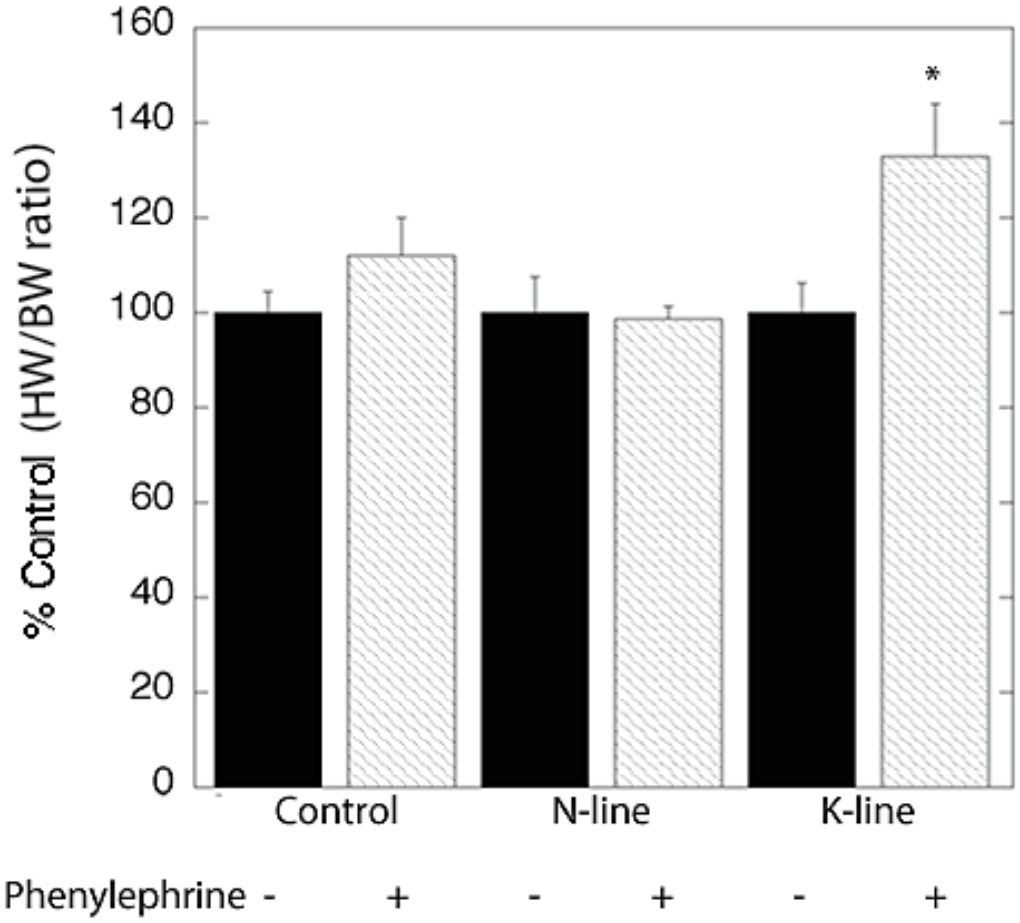

Figure 3.30. HW/BW ratio of control, N-line and K-line mice treated with PE or PBS control. + or – indicates the presence of absence of 50mg/kg/day PE administered using Alzet osmotic mini pumps over a two week period. The results are expressed as % of values obtained for the each control group (treated with vehicle, PBS)±%SEM. $^{*}P<0.05$ for K-line treated with PBS vs. K-line stimulated with PE; n=7-11 hearts/group.

This change in heart weight in the K-line hearts was at least in part due to edema. When we examined the dry weight to wet weight ratio of control and K-line hearts, we found a decrease in the dry weight to wet weight ratio of K-line hearts stimulated with PE (69.4±9.8%, $P<0.05$, Figure 3.32). For control hearts stimulated with PE, the changes in heart weight were due to an increase in heart mass, not edema. This was indicated by the dry weight to wet weight ratio measured in control hearts stimulated with PE (104.4±4.5%). There was no significant difference when compared to hearts treated with PBS.

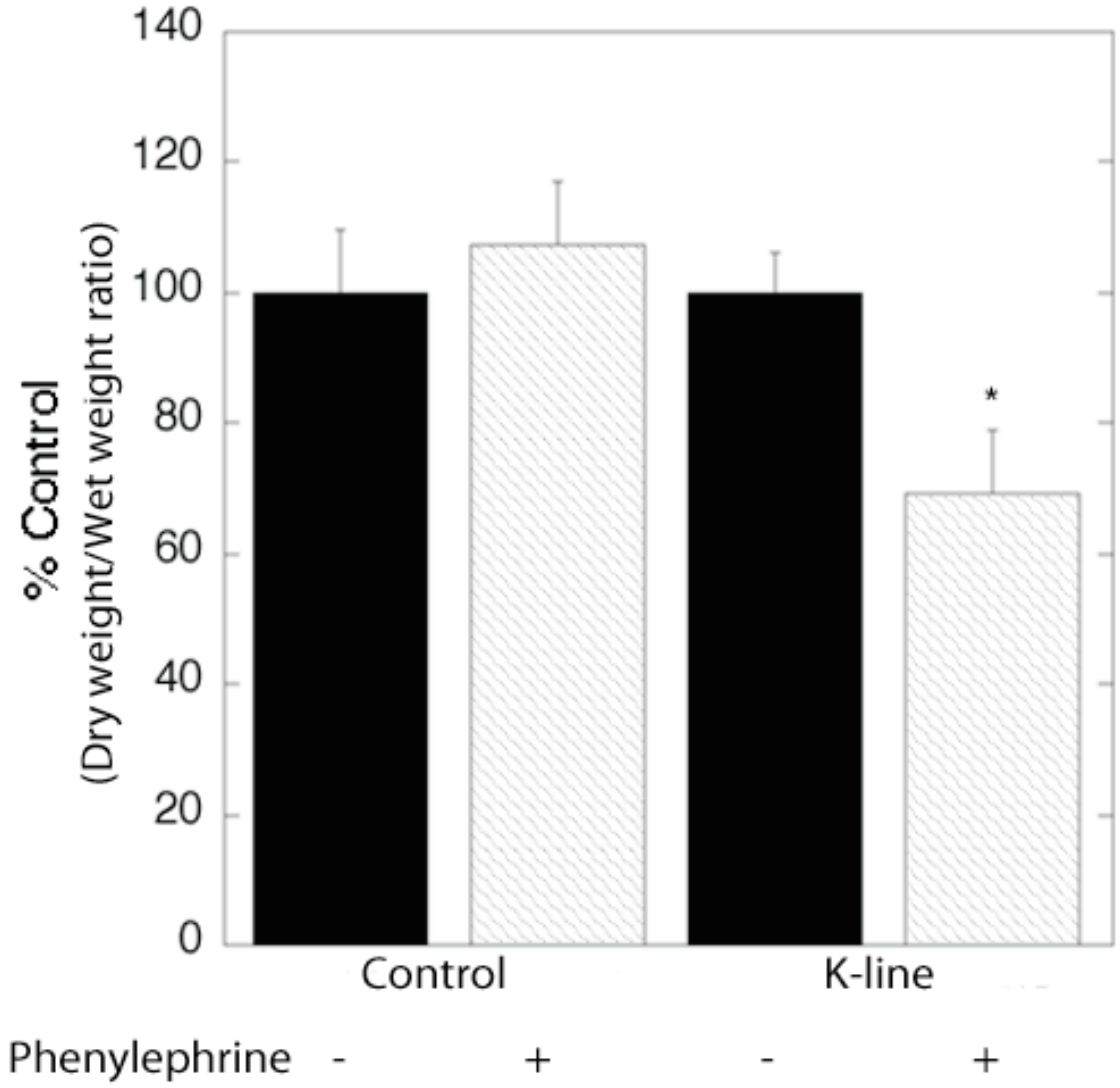

Figure 3.31. Dry tissue weight to wet tissue weight ratio of hearts from control or K-line mice stimulated with PE or PBS. + or – indicates the presence of absence of 50mg/kg/day PE administered using Alzet osmotic mini pumps over a two week period. Results are expressed as % of controls (treated with vehicle PBS)±%SEM. $^{*}P<0.05$ for K-line stimulated with PE vs. K-line treated with PBS; n=3-4 hearts/group.

We also examined another CH marker, ANP mRNA expression. We compared the ANP mRNA levels of control, N-line and K-line mice stimulated with PE to PBS treatment, a parallel control for each group. As shown in Figure 3.34, ANP mRNA expression was only elevated in K-line mice stimulated with PE (468.1±128.1%, $P<0.05$).

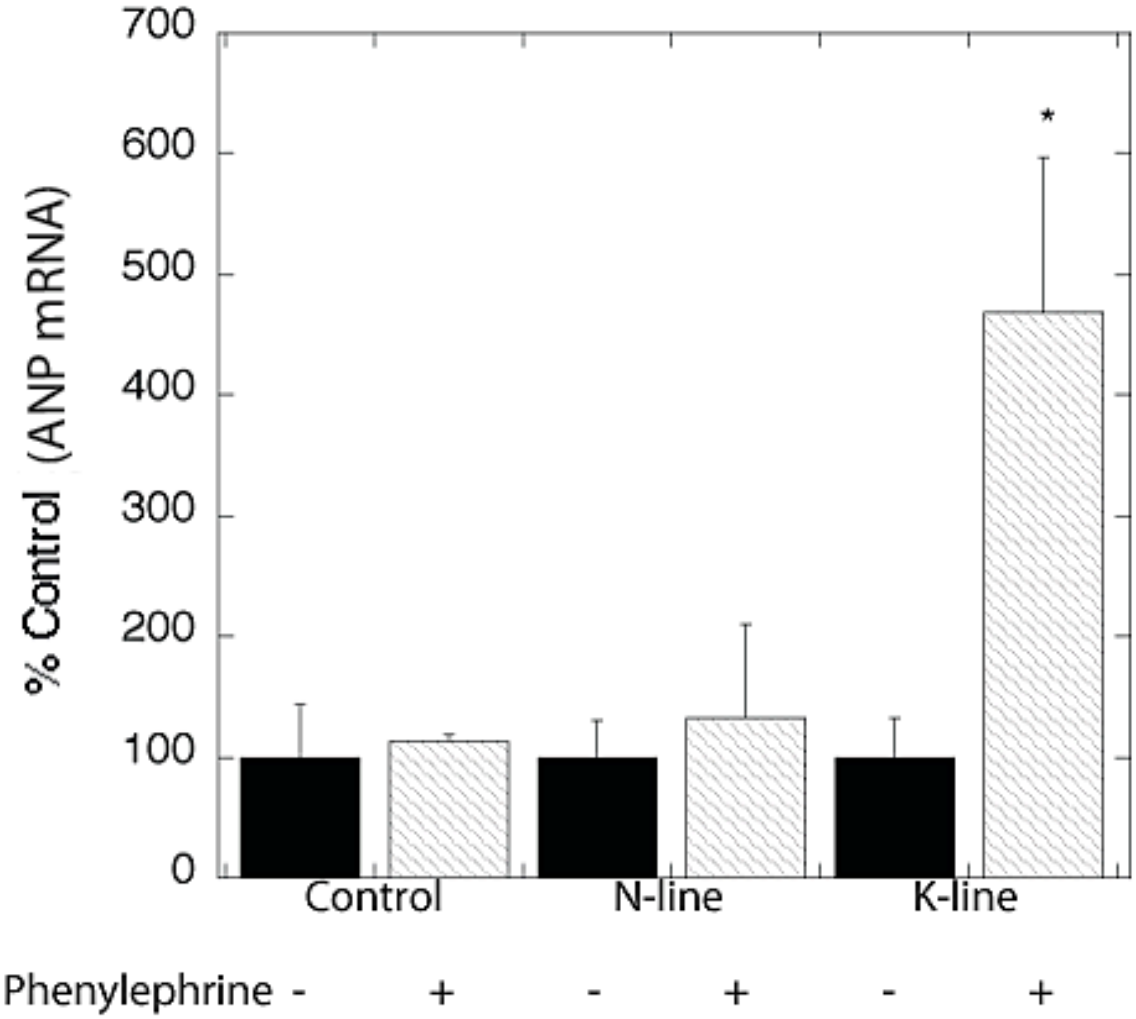

Figure 3.32. Analysis of ANP mRNA expression in hearts from control, N-line and K-line mice treated with PE or PBS. + or – indicates the presence of absence of 50mg/kg/day PE administered using Alzet osmotic mini pumps over a two week period. Results are the ratio of ANP to 18S rRNA and are expressed as % of controls (group treated with vehicle PBS)±%SEM. $^{*}P<0.05$ for K-line stimulated with PE vs. K-line treated with PBS; n=3 hearts/group.

Finally, *in vivo*, we also examined CSA and IF, histological markers of CH, in hearts of NHE1 TG mice stimulated with PE. Stimulation with PE had no significant effects on CSA (Figure 3.35, A) and IF (Figure 3.35, B) in hearts from control, N-line and K-line mice.

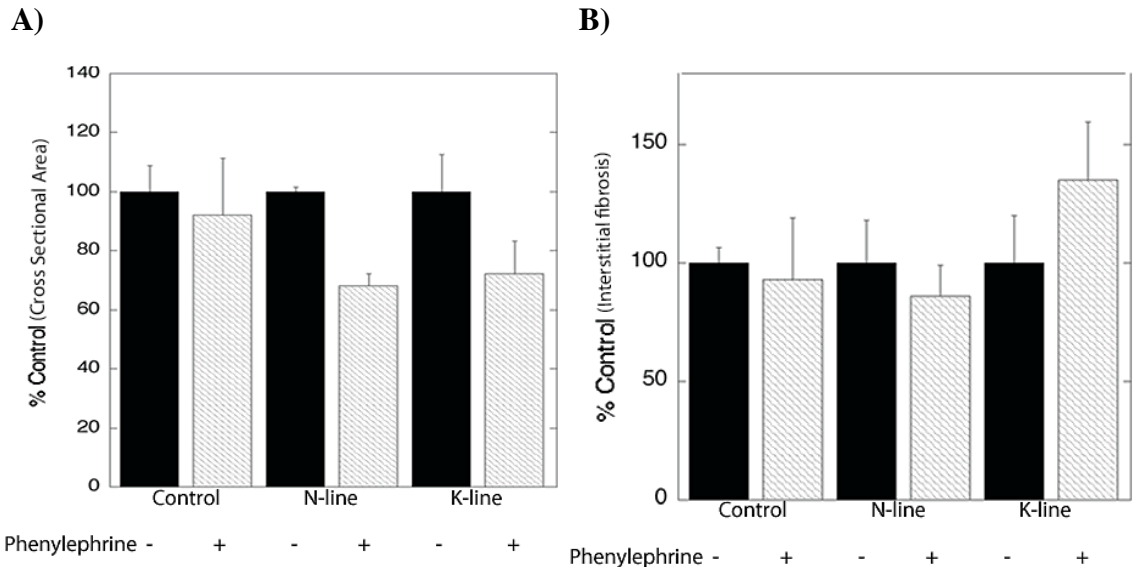

Figure 3.33. Analysis of CSA and IF in hearts from control, N-line and K-line mice stimulated with PE or PBS. + or – indicates the presence of absence of 50mg/kg/day PE administered using Alzet osmotic mini pumps over a two week period. **A),** quantitative analysis of CSA from heart cross sections stained with H&E and expressed as % of controls (individual group treated with vehicle PBS)±%SEM. (n=4-6 hearts/group). **B),** quantitative analysis of IF from heart cross sections stained with PSR. The maximum fibrosis observed for any section was calculated as the area occupied by red stained connective tissue divided by the areas occupied by connective tissue plus cardiac myocytes. Accumulated IF area per group, expressed as % of controls±%SEM. (n=4 hearts/group).

3.2.17 Characterization of Cardiac Hypertrophy Following Neuroendocrine Stimulation in Neonatal Rat Ventricular Cardiomyocytes Infected with IRM or K-IRM Adenoviruses

Since we found that the K-line mice exhibited increased CH and an increased sensitivity to hypertrophic stimuli, we also examined the effect of this same constitutively active NHE1 protein in NRVMs in the presence of PE. We measured indices of CH in NRVMs infected with wild type NHE1 (IRM), K-IRM (equivalent to K-line mice) or GFP (control) adenoviruses in the presence or absence of PE. In our *in vitro* studies, NRVMs were some times treated with 10 μM EMD 87580, which was added four hours following adenoviral infections. The addition of 10 μM EMD 87580 allowed us to study the effects of exogenous NHE1, since at this concentration EMD 87580 has been shown to inhibit endogenous NHE1 expression. We found (Figure 3.36) that NRVMs infected with the K-IRM adenovirus induced a relatively small, but significant increase in cell size relative to NRVMs infected with the control adenovirus ($P<0.005$) (as described in Section 3.2.14, Figure 3.19). Addition of PE produced a similar significant increase in cell size in NRVMs infected with control, GFP adenovirus (3219.9±110.4 arbitrary units GFP vs. 3760.2±110.2 arbitrary units GFP+PE, $P<0.005$) but not in NRVMs infected with the IRM adenovirus (3077.4±56.4 arbitrary units IRM vs. 3226.0±114.0 arbitrary units IRM+PE). In NRVMs infected with the K-IRM adenovirus, there was no further increase with addition of PE and in fact there was a slight decrease in the cell area relative to cells not treated with PE (3662.0±93.3 arbitrary units K-IRM vs. 3512.4±110.0 arbitrary units K-IRM+PE). The addition of EMD 87580 decreased the cell area of NRVMs infected with GFP and stimulated with PE

(3760.2±110.2 arbitrary units GFP+PE vs. 3328.3±61.1 arbitrary units GFP+PE+EMD, $P<0.005$) and of K-IRM infected NRVMs stimulated with PE (3512.4±110.0 arbitrary units K-IRM+PE vs. 3115.0±124.0 arbitrary units K-IRM+PE+EMD).

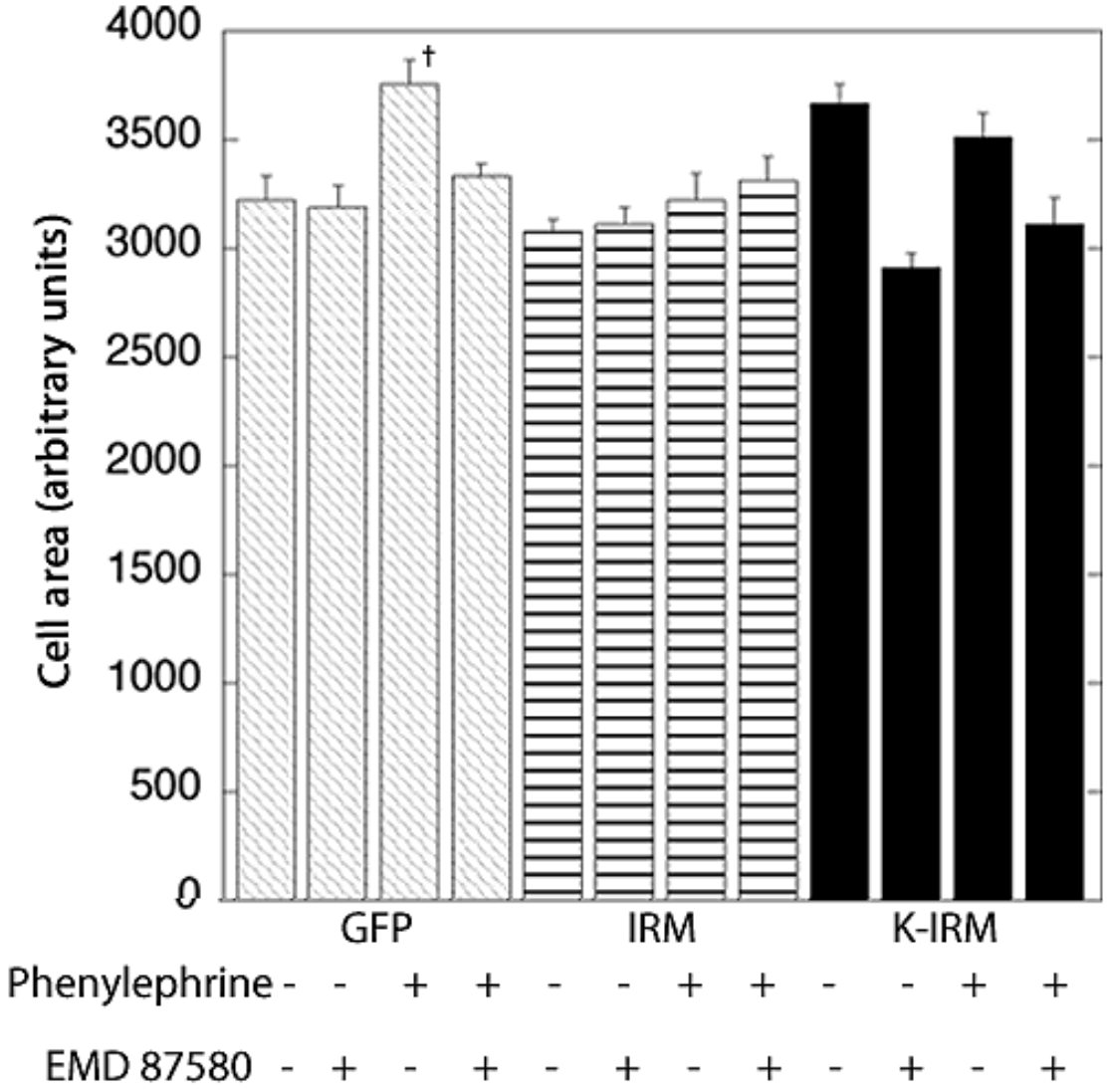

Figure 3.34. Analysis of cell area in neonatal rat ventricular cardiomyocytes infected with IRM, K-IRM or GFP (control) adenoviruses in the presence (+) or absence (-) of 10 μM EMD 87580 and 10 μM PE. NRVMs were infected with a MOI of 20 of GFP, IRM or K-IRM adenoviruses for 24 hours. PE was added 4 hours after infection and 30 minutes after the addition of EMD 87580. Quantitative analysis of cell area was expressed as a mean (arbitrary units)±SEM. $^{\dagger}P<0.005$ for GFP controls vs. GFP+PE or GFP+PE vs. GFP+PE+EMD 87580; n=4-7 experiments.

When we monitored the effects of NHE1 expression on protein synthesis of NRVMs infected with NHE1 containing adenoviruses and the results were similar to those seen with cell area (Figure 3.37). PE increased protein synthesis of NRVMs infected with the GFP adenovirus (100.0±7.0% GFP vs. 176±25.4% GFP+PE, $P<0.005$). Similarly, NRVMs infected with the K-IRM adenovirus also significantly increased the protein synthesis relative to NRVMs infected with the GFP adenovirus (100.0±7.0% GFP vs. 181±24.5% K-IRM, $P<0.01$) (described in Section 3.2.14) (Figure 3.20). In NRVMs infected with K-IRM adenovirus, there was no further increase with addition of PE and in fact there was a slight decrease in the rate of protein synthesis relative to cells not treated with PE (181.6±24.5% K-IRM vs. 167.5±32.3% K-IRM+PE). PE did not elevate protein synthesis of NRVMs infected with the IRM adenovirus (126.0±14.3% IRM vs. 112.9±13.4% IRM+PE). EMD 87580 did not significantly reverse the effects of PE stimulation in NRVMs infected with the GFP adenovirus (176.5±25.7% GFP+PE vs. 132.7±23.3% GFP+PE+EMD) and NRVMs infected with the K-IRM adenovirus (167.5±32.3 K-IRM+PE vs. 144.1±22.9% K-IRM+PE+EMD).

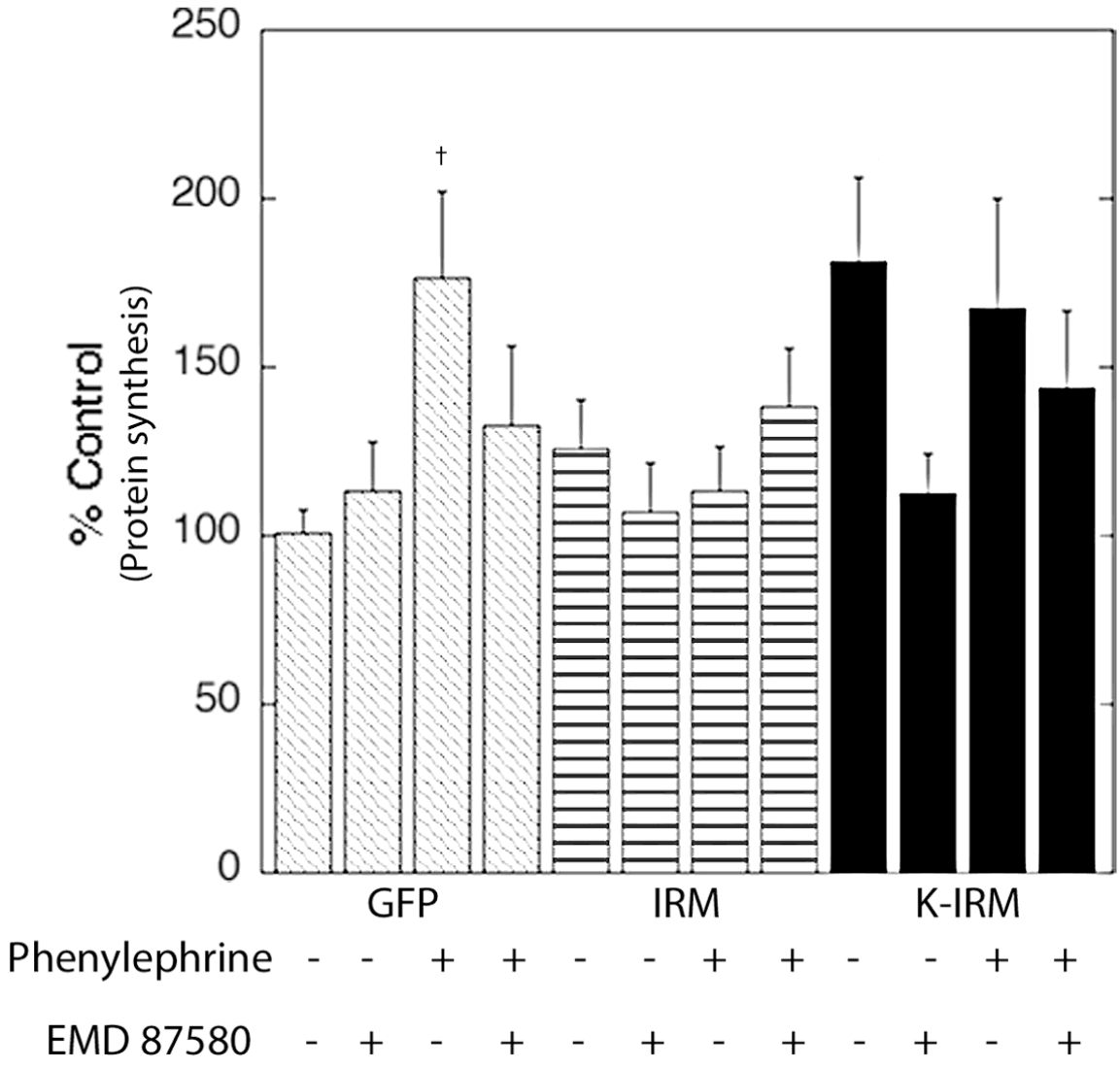

Figure 3.35. Protein synthesis of neonatal rat ventricular cardiomyocytes infected with IRM, K-IRM or GFP (control) adenoviruses in the presence (+) or absence (-) of 10 μM EMD 87580 and 10 μM PE. NRVMs were infected with a MOI of 20 of GFP, IRM or K-IRM adenoviruses for 24 hours. PE was added 4 hours following adenoviral infection and 30 minutes after the addition of EMD 87580. Quantitative analysis of the protein synthesis rate was measured by the amount of [^{3}H] phenylalanine incorporated. Protein synthesis was corrected with DNA synthesis measured by hoescht 33258. Protein synthesis was expressed as % GFP±%SEM. $^{\dagger}P<0.005$ for GFP vs. GFP + PE or GFP vs. K-IRM, n=20-30 plates; 5-8 experiments.

3.3 Discussion

We examined the effects of elevated expression of wild type and active NHE1 on the myocardium both *in vivo* and *in vitro*. *In vivo,* mice expressing cardiac specific NHE1 were characterized. The use of animal models to study cardiovascular disease is of particular importance since similar genes and signaling pathways in mice and humans regulate the development of the heart and vasculature, thus allowing for the translation of research from the bench to the bedside[322]. For our *in vitro* studies, we used NRVMs, one of the most well used experimental models. This approach allows us to precisely study the direct hypertrophic response to relevant stimuli (NHE1) in the absence of other contributing factors[323]. The NRVMs were infected with adenoviruses containing NHE1 and characterized for CH. Our *in vitro* studies provided a confirmation of our *in vivo* reports. Caution was applied when interpreting the *in vitro* data using NRVMs, since these cells likely possess different receptor subtypes or cell signalling mechanisms from adult tissues[323].

The direct effects of expression of an active form of NHE1 compared with the wild type have not been examined. This is a physiologically relevant question as increased NHE1 expression and activity are reported in several *in vivo* and *in vitro* models of cardiac disease (reviewed in[87,186]). Protein kinases that phosphorylate NHE1 also have increased activity in the diseased myocardium, as do many hormonal, autocrine and paracrine stimuli that induce CH. In addition, in some CH models, NHE1 protein expression and activity are increased[238,239], while in others NHE1 activity is increased in the absence of any alterations in NHE1 expression[240]. The degree of hypertrophy obtained with varying NHE1 expression and activity has not been

investigated. The implications of our results are several fold:

NHE1 requires enhanced activity to lead to rapid remodeling and myocardial dysfunction.

NHE1 generated a pro-hypertrophic effect, but the effect was principally in mice expressing an active form of NHE1 (K-line mice) (Figure 3.38). K-line mice demonstrated increased HW/BW, ANP mRNA expression, IF and CSA. N-line mice, expressing wild type NHE, only showed elevated HW/BW and ANP mRNA expression. The accumulation of fibrillar collagen seen in K-line mice has been suggested to be a major determinant of impaired stiffness and pump dysfunction. Progressive accumulation of collagen accounts for a spectrum of ventricular dysfunction that first appears during diastole and subsequently involves systole[218], which is illustrated by echocardiography in our K-line mice. N-line mice, which express wild type NHE1, developed systolic and diastolic dysfunction, however not severe enough to cause global deterioration and accumulation of IF. Active NHE1 was required to induce global deterioration of the heart. Echocardiography revealed that K-line mice had a number of morphological defects and global myocardial deterioration, while N-line mice were generally similar to control, with mild functional abnormalities. The results with the K-line mice are largely in agreement with a recent study[231] that also expressed active NHE1 in the myocardium. However, their study used a large deletion of the NHE1 C-terminal tail (637-656 base pair region), as opposed to the specific point mutations in the CaM binding region used in the present study (as described in Section 2.1.2). In addition, we examined 10-12 week old mice as opposed to 40 day-old mice. Our findings also directly distinguish between the effects of increased expression of wild type NHE1 (N-line) vs.

expression of active NHE1 (K-line), which was not shown in the earlier work[231]. We showed that expression of the active NHE1 causes strong hypertrophic effects while expression of the wild type NHE1 causes milder effects. Our results were confirmed by *in vitro* studies. NRVMs infected with adenovirus containing constituitively active NHE1 significantly increased cell area and protein synthesis, whereas NRVMs infected with adenoviruses containing wild type NHE1 showed no such differences. Inhibition of endogenous NHE1 with EMD 87580 inhibited expression of CH, thus suggesting that the total activity of both endogenous and exogenous active NHE1 are required to induce CH *in vitro*. Thus, the active form of NHE1 was required to induce CH in the whole animal and at the level of cardiomyocytes - expression of wild type NHE1 had milder effects *in vivo* and no effect *in vitro*, thus suggesting that *in vivo* factors maybe contributing to the cardiac phenotype. Our results with the N-line mice did not agree with a previous report. Cook et al,[324] demonstrated that enhanced expression of wild type NHE1 results in spontaneous development of heart failure, premature mortality, increased apoptotic cell death and cardiac remodeling. However, their results were for much older mice, 8-11 months of age, as opposed to ours at 10-12 weeks of age. The differences in the time used between both studies could account for this discrepancy. This cardiac phenotype appears to accumulate and cause more severe pathological changes with age. Another report has suggested that age effects the efficacy of NHE1 inhibitors, which may modify their usefulness in treating ischemia in the human myocardium[206].

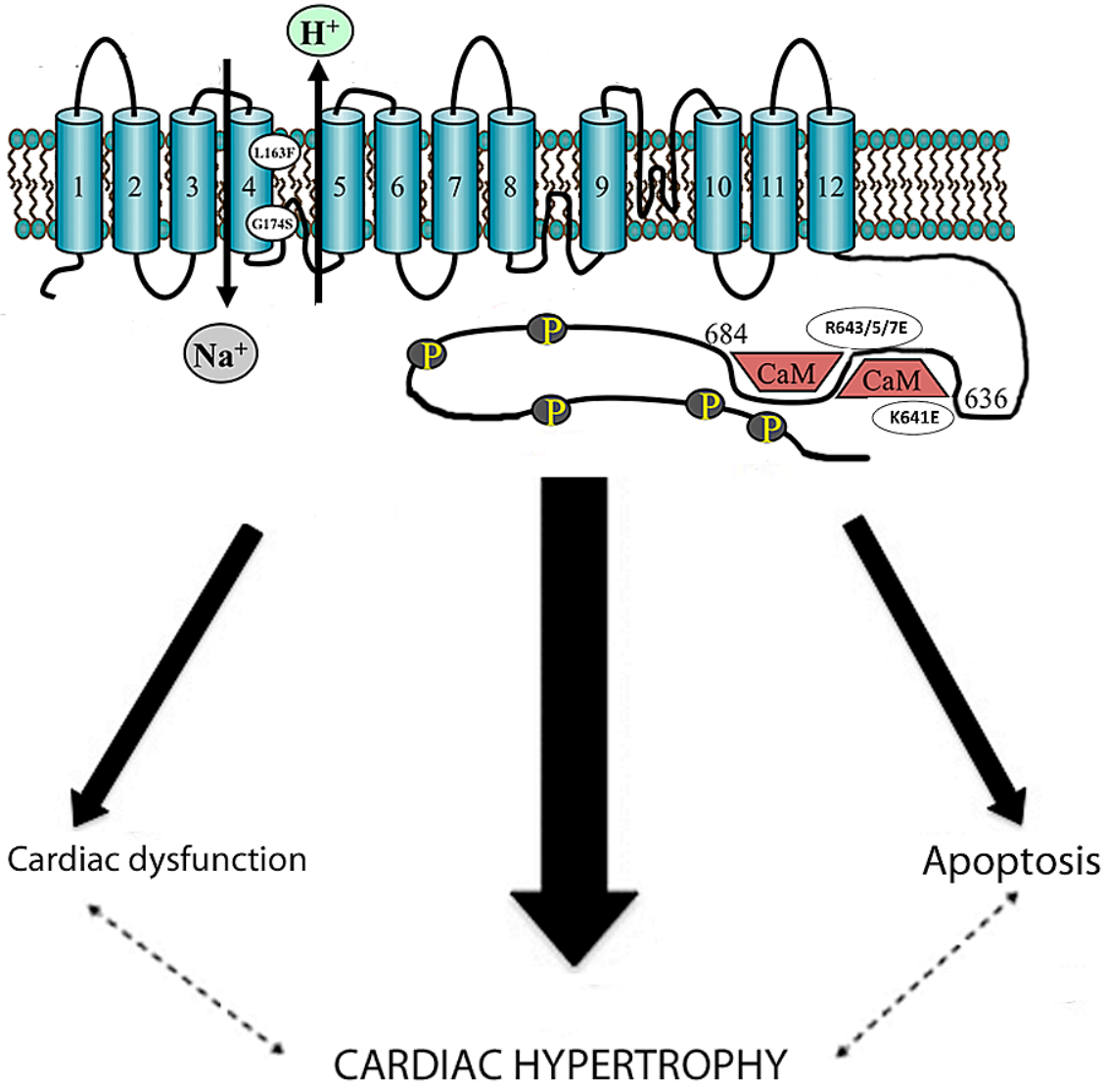

Figure 3.36. Schematic diagram of the role of active NHE1 expression in the myocardium. Active NHE1 induces cardiac hypertrophy, apoptosis and cardiac dysfunction independent of calcineurin, MAPKs, RSK and GSK-3β. *In vivo,* cardiac hypertrophy, cardiac function and apoptosis were assessed in TG mice expressing cardiac specific active NHE1. The active NHE1 transgene was created by site specific mutations at the C-terminal tail of NHE1 (1K3R4E; lysine (K) 641, arginine (R) 643, R645 and R647 all mutated to glutamic acid (E)). *In vitro*, active NHE1 was assessed in NRVMs infected with adenoviruses containing active NHE1 resistant to NHE1 inhibitors. Active NHE1 plasmid DNA was created as described above.

Signaling pathways leading to CH

Numerous signaling pathways have been implicated in the development of CH including MAPKs (ERK, p38 and JNK)[325] and RSK[326]. Many of these pro-hypertrophic signaling pathways have also been implicated in regulation of NHE1[87,326]. We found no significant differences in the level of phosphorylated ERK, p38, JNK, RSK in hearts from N-line and K-line mice when compared to controls (Figure 3.38). A previous report[231] in which active NHE1 was expressed found that p38 and ERK were significantly activated. This discrepancy could be due in part to the differences in regions mutated on the C-terminus of NHE1. Deletion of amino acids 637 to 656 may have caused a more extreme activation of the NHE1 protein, inducing further stress and perhaps contributing to the activation of MAPKs. The early and more severe effects of NHE1 expression shown in that study[231] support this suggestion. If activation of these kinases only occurs with later severe stages of the pathology, the activation of these pathways are likely a later consequence of heart failure, rather than being causal. We also did not find any differences in total GSK-3β and calcineurin activity in hearts from N-line and K-line mice (Figure 3.38). This suggested that these pathways are also not involved in mediating the pathology that we observed. It has been suggested that alterations of Ca^{2+} cycling[231] mediate NHE1 induced CH. We demonstrated that Ca^{2+} cycling (NCX, SERCA and NKA) and pH regulatory proteins (AE3 and NBC1) were not altered in hearts from N-line and K-line mice. However, other proteins that are regulated by Ca^{2+} such as CaM Kinase II could not be ruled out and require further investigation.

Apoptosis and NHE1

Apoptosis can be initiated by the death receptor/extrinsic pathway, the mitochondrial/intrinsic pathway[327], and unresolved ER stress[324]. In previous reports, the expression of C/EBP homologous protein, which mediates the induction of pro-apoptotic pathways during unresolved ER stress was significantly elevated in mice expressing wild type NHE1[324]. This suggested that enhanced NHE1 expression and unresolved ER stress may contribute to elevated apoptosis. However, the mitochondrial/intrinsic pathway was not investigated nor ruled out as means of inducing apoptosis in NHE1 TG mice. This pathway has been implicated in NHE1 mediated apoptosis in the myocardium[327]. The mitochondrial/intrinsic pathway is of particular importance. Recent reports have shown that NHE1 inhibitors induce an anti-apoptotic effect by prevention of cytosolic Na^+ and Ca^{2+} over-load and a direct mitochondrial effect preventing mitochondrial permeability transition pore opening[250]. In our study we showed swollen mitochondria in our K-line mice. In addition, they had significantly elevated apoptosis in the left ventricular myocardium, as indicated by the TUNEL positive myocytes (Figure 3.38). Apoptosis was not demonstrated in N-line mice. Cook et al.[324] found that wild type NHE1 induces apoptosis, however they examined much older mice, which again suggests that the effects of elevated NHE1 expression with age. We further investigated the pathway contributing to the NHE1 induced apoptosis. Initially we examined the caspase dependent pathway that mediates apoptosis. We observed no differences in Cyt c and PARP protein expression in both the cytosolic and mitochondrial fractions of hearts from control vs. N-line and K-line mice. We further studied the direct apoptotic effects of NHE1 by determining whether AIF was released from the mitochondria into the cytoplasm. AIF has been shown to translocate into the cytoplasm with further induction

into the nuclei to induce caspase-independent DNA fragmentation[328]. Our results demonstrate that AIF appears to be significantly greater in the mitochondrial fraction of our K-line mice, but does not appear to be released into the cytosol. Release of AIF from the mitochondria is normally thought to trigger the cell death program. However, AIF is also known for its role as a mitochondrial flavoprotein important for mitochondrial energy-generating processes and is required for oxidative phosphorylation and for the assembly and or/stabilization of respiratory complex I[329]. Further investigation of the effects of enhanced AIF and resulting energy generating processes in mice expressing active NHE1 is required. Overall, our results suggest that cell death is likely not mediated through the mitochondrial pathway. Although it is evident that expression of active NHE1 induces apoptosis, the mechanism by which this occurs seems less likely to involve the mitochondrial/intrinsic pathway, supporting the suggestion that other pathways are involved[324].

Perhaps subjecting these mice to further cardiac insults, such as ischemia or MIs will allow us to further understand the mechanisms inducing apoptosis. The ipsilateral hemisphere from NHE1 over-expressing brains was investigated following cerebral ischemia and was shown to contribute to mitochondrial damage and ischemic apoptosis[293]. Further studies ruling out activation of membrane death receptors such as FasL/Fas may aide in our understanding of the mechanism in which apoptosis is induced.

NHE1 expression sensitizes the myocardium to neurohormonal stimulation

Neurohormonal activation, myocardial I/R, cardiotoxic metabolites released during I/R and numerous autocrine and paracrine factors lead to increasing levels of NHE1

mRNA and protein expression (reviewed in[87]). We noticed that K-line mice appeared to be particularly sensitive to the stress induced by pregnancy, causing a relatively high rate of mortality during gestation that was associated with cardiovascular failure (data not shown). We therefore examined whether these mice were more sensitive to the cardiovascular stress of neurohormonal stimulation, which both causes CH and stimulates NHE1 activity. In heart failure, chronic neurohormonal stimulation of ARs have been linked to pathological cardiac remodeling including cardiomyocyte apoptosis and hypertrophy[330]. We found that stimulation of K-line mice with PE led to a further increase in the HW/BW and a further increase in ANP mRNA expression. In contrast, NRVMs infected with the K-IRM (active NHE) adenovirus appeared resistant to further PE stimulation, possibly because they had already reached a maximal level of stimulation. The effect of PE on K-line mice was associated with myocardial edema, possibly indicating a later stage of chronic heart failure. The large elevation of ANP mRNA expression by PE in the K-line mice indicates that there was further progression of the hypertrophic response. CSA and IF were not further elevated, as they may have already been elevated near a maximal level for this pathology. The results suggest that the presence of active NHE1 causes an increase in the sensitivity to PE stimulation, particularly *in vivo*.

Conclusion

Our data is in agreement with previous reports that suggest that increased NHE1 expression is stimulatory for CH. A novel finding is that increased expression of active NHE1 protein is much more detrimental than expression of the wild type protein both *in*

vivo and *in vitro*. Expression of active NHE1 is associated with CH, cardiac dysfunction and apoptosis, as illustrated in Figure 3.38. Elevated expression of wild type NHE1 only caused relatively minor increases in indices of CH. With time, these may cause more detrimental effects. Our model did not show increases in ERK, p38, JNK, RSK phosphorylation or calcineurin levels, suggesting that these are not causal in the early stages of the pathology. Thus suggesting that the pathology induced by NHE1 expression was independent of these factors as illustrated in Figure 3.38. Expression of activated NHE1 protein increased sensitivity to neurohormonal stimuli in intact mice. The requirement of active NHE1 expression in CH was further confirmed *in vitro*.

Chapter 4

Elevated Levels of Activated NHE1 Protect the Heart and Improve Myocardial Metabolism Following Ischemia/Reperfusion Injury

My role in this work involved data analysis, investigating signaling pathway experiments and writing a manuscript. Heart perfusions and metabolic assays were performed by Cory Wagg in Dr. Gary Lopaschuk's lab.

4.1 Introduction

NHE is a ubiquitously expressed plasma membrane glycoprotein, which extrudes one intracellular H^+ in exchange for one extracellular Na^+ and thus regulates pH_i[313]. NHE1, the only cardio-specific plasma membrane isoform (reviewed in[36])[37], has been implicated in mediating the damage that occurs during I/R injury (reviewed in[186]). NHE1 protein expression and activity increase in response to various stimuli, including acidosis[185,331], cardiotoxic metabolites released during I/R (reviewed in[188]) and CH (reviewed in[87]). In numerous *in vitro* and *in vivo* studies, NHE1 inhibitors have been shown to prevent or reduce I/R injury (reviewed in[186]).

The lack of specificity of NHE1 inhibitors and the critical physiological role of NHE1 necessitates an understanding of the effects of varying NHE1 expression and has encouraged the development of TG mouse models expressing altered NHE1 levels and activity. Initial studies in which NHE1 was genetically ablated in TG mice demonstrated cardioprotective effects against I/R injury[192]. However, recent reports using TG mice expressing elevated NHE1 levels have demonstrated surprising results. They have shown that elevated NHE1 expression in TG mice can reduce the susceptibility to I/R injury[204,205]. However, the effects of expression of an active form of NHE1 compared with the wild type using the working heart perfusion model were not examined. In addition, the cardiac energy metabolism of hearts with varying NHE1 levels has not been studied in detail. This is of particular importance since it was earlier shown[204] that TG mice expressing NHE1 have a minor improvement in recovery of pH_i and ATP levels.

Variations in substrate utilization occur during I/R, and energy substrate preference has a significant impact on both contractile function and efficiency of O_2 use,

particularly following severe ischemia[303,332]. In previous studies, the effects of varying NHE1 levels were examined in hearts perfused with only glucose as a substrate[204,205]. However, this is not representative of the physiological substrate used by the myocardium. FAs are the main source of ATP production in normal hearts and during reperfusion following ischemia[333].

The purpose of this study is to examine cardiac energy metabolism and cardiac function in hearts from (female) TG mice expressing cardio-specific wild type NHE1 or active NHE1. The hearts were perfused using the more physiological substrate of FAs. In addition, these hearts were subjected to *ex vivo* working heart perfusions[334]. Rates of glycolysis, glucose oxidation and FA oxidation were directly measured in both the preischemic and postischemic periods in the myocardium. Our results demonstrate that increased expression of activated NHE1 protein is cardioprotective in the myocardium subjected to I/R. This was accompanied by increased FA oxidation, glycolysis and ATP production rates, as well as a more energetically efficient myocardium.

4.2 Results

4.2.1 Preischemic and Postischemic Cardiac Function in Ex Vivo Mouse Hearts

Initially, we assessed baseline cardiac function of NHE1 TG hearts. To assess the baseline functional consequences of elevated NHE1 expression, cardiac function was measured in control, N-line and K-line mouse hearts subjected to *ex vivo* aerobic perfusion for 30 minutes. During aerobic perfusion, N-line and K-line mice displayed no

significant differences in mechanical function compared to controls (72±4.2 controls vs. 64±4.1 N-line vs. 66±4.1 K-line mLxmmHg/min, Figure 4.1). Similarly, no significant differences existed in cardiac output, aortic outflow, coronary flow and cardiac work between control, N-line and K-line mice (Table VII). However, peak systolic pressure was significantly depressed in N-line ($P<0.005$) and K-line ($P<0.05$) hearts compared to controls. In spite of this, hearts expressing either wild type or active NHE1 did not have any significant differences in cardiac power when examined during *ex vivo* aerobic perfusion (preischemia).

When hearts were subjected to 20 minutes of global no flow ischemia followed by 40 minutes of reperfusion, surprisingly, K-line hearts recovered to a much greater extent than N-line and control hearts (49±4.6 K-line vs. 12±4.3 N-line vs. 9.7±3.6 control, mLxmmHg/min, $P<0.0001$)(Figure 4.1). K-line hearts recovered to almost 75% of their preischemic values and mechanical function was significantly improved in all parameters measured (Table VI). No significant differences were found between control and N-line hearts during postischemia.

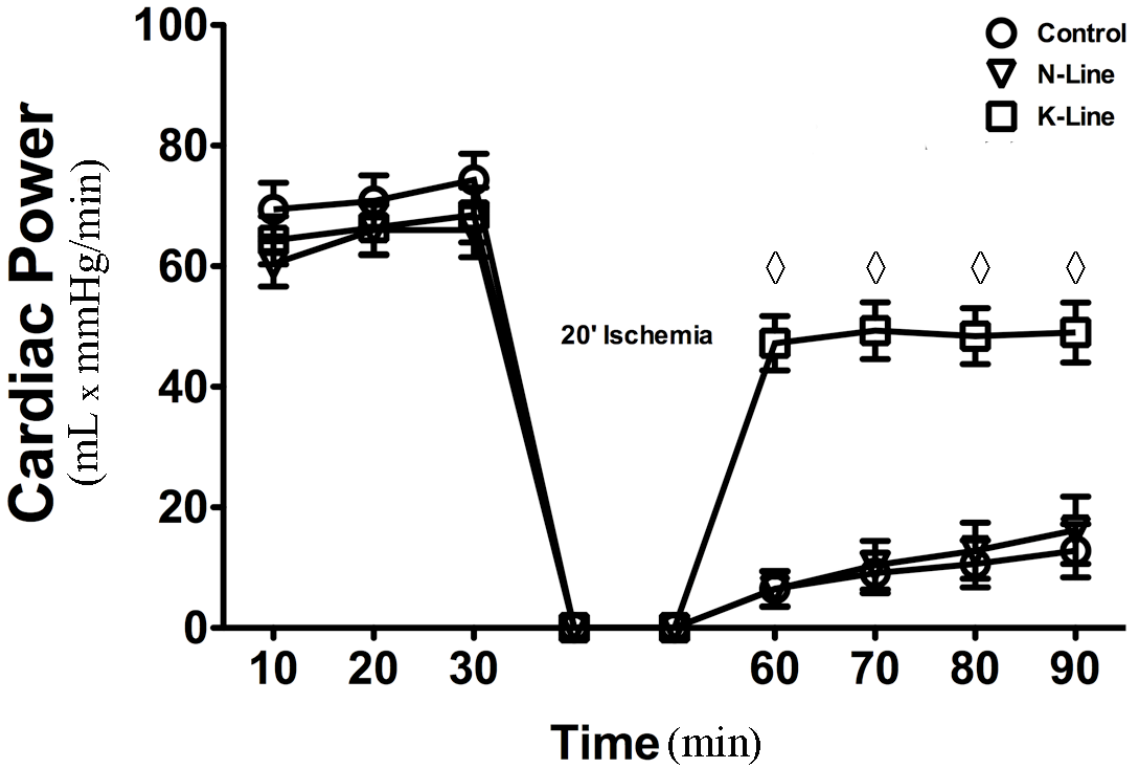

Figure 4.1. Effects of wild type or active NHE1 expression on cardiac function in the *ex vivo* aerobically perfused and reperfused working mouse heart. Controls (circle); N-line, TG mice that express wild type NHE1 (upside down triangle); K-line, TG mice that express active NHE1 (square). Hearts were subjected to 30 minutes of aerobic perfusion, followed by 20 minutes of global no-flow ischemia and 40 minutes of aerobic reperfusion. Cardiac power was the product of developed pressure (mmHg) and cardiac output (mL/min), which were measured at 10 minute intervals (on the x-axis). Values are mean (at each time point)±SEM. $^{\lozenge}P<0.0001$ for controls or N-line vs. K-line mice during postischemia; n=10-14 hearts/group.

Table VII: Parameters of cardiac function in *ex vivo* working mouse hearts during aerobic perfusion (preischemia) and reperfusion (postischemia). Mean average values measured over a period of 30 minutes (preischemia) and over a period of 40 minutes following 20 minutes of global no flow ischemia (postischemia). Cardiac work (mLxmmHg/min)=peak systolic pressure x cardiac output; Coronary flow=cardiac output – aortic flow. Values represent means±SEM. Significantly different from the corresponding preischemic group, $^{\lozenge}P<0.0001$, $^{*}P<0.05$, $^{\dagger}P<0.005$; n=12-16 hearts/group.

		Preischemia			**Postischemia**	
	Control	**N-line**	**K-line**	**Control**	**N-line**	**K-line**
Peak systolic pressure, mmHg	76 ± 1.0	68 ± 1.0†	71 ± 1.0*	47 ± 4.0$^{\lozenge}$	47 ± 4†	68 ± 1.0
Cardiac output, mL/min	8.4 ± 0.5	8.4 ± 0.4	8.4 ± 0.5	1.6 ± 0.4$^{\lozenge}$	1.8 ± 0.6$^{\lozenge}$	6.3 ± 0.5*
Aortic outflow, mL/min	5.7 ± 0.3	6.7 ± 0.5	6.3 ± 0.3	0.4 ± 0.2$^{\lozenge}$	0.8 ± 0.5$^{\lozenge}$	3.6 ± 0.4$^{\lozenge}$
Coronary flow, mL/min	2.6 ± 0.3	2.0 ± 0.5	2.2 ± 0.2	1.2 ± 0.3†	1.0 ± 0.3	2.7 ± 0.3
Cardiac work, mLxmmHg/min	6.3 ± 0.4	5.8 ± 0.4	6.0 ± 0.4	0.9 ± 0.3$^{\lozenge}$	1.1 ± 0.4$^{\lozenge}$	4.4 ± 0.4*

4.2.2 Preischemic and Postischemic Rates of Glycolysis, Palmitate Oxidation and Glucose Oxidation in Ex Vivo Working Mouse Hearts

When comparing control, N-line and K- line hearts, significant changes in cardiac energy metabolism were evident during the preischemic and postischemic periods (Figure 4.2). During preischemia, glucose oxidation rates were significantly decreased in N-line hearts vs. controls (1184±196 N-line vs. 2058±247 controls, nmol x g dry wt^{-1} x min^{-1}, $P<0.05$) (Figure 4.2A). In K-line hearts, glucose oxidation showed a trend towards decrease vs. controls (1469± 179 K-line vs. 2058±247 controls, nmol x g dry wt^{-1}x min^{-1}), but the change was not significant. During postischemia reperfusion, glucose oxidation rates were not significantly different between control, N-line and K-line hearts. However, the rate of glucose oxidation during postischemia was depressed in control and N-line hearts vs. preischemic values ($P<0.05$, Figure 4.2A). In contrast, glucose oxidation was not significantly altered in preischemic K-line hearts vs. postischemic K-line hearts.

During preischemia, palmitate oxidation rates were comparable between control and N-line hearts (Figure 4.2*B*). However, K-line hearts had a significantly greater rate of palmitate oxidation vs. controls (380±31 controls vs. 513±26 K-line nmol x g dry wt^{-1} x min^{-1}, $P<0.05$, Figure 4.2B). Palmitate oxidation remained significantly greater in K-line hearts during postischemia reperfusion (215±37 controls vs. 399±21 K-line nmol x g dry wt^{-1} x min^{-1}, $P<0.05$, Figure 4.2B). When compared to preischemic values, the postischemic levels of palmitate oxidation were significantly depressed for both control and K-line hearts ($P<0.05$, Figure 4.2B). In N-line hearts postischemia, palmitate

oxidation levels were not significantly different than control hearts and remained comparable to preischemic levels (Figure 4.2B).

Preischemic levels of glycolysis were significantly elevated in K-line hearts vs. N-line hearts (8,065±876 controls vs. 6,105±905 N-line vs. 10,366± 936 K-line, nmol x g dry wt^{-1} x min^{-1}, $P<0.05$, Figure 4.2C). There was no significant difference between N-line and control hearts in preischemic levels of glycolysis. During the postischemic reperfusion period, glycolytic rates remained significantly elevated in the K-line hearts compared to N-line (2,326±595 N-line vs. 7,538±1,352 K-line nmol x g dry wt^{-1} x min^{-1}, $P<0.01$, Figure 4.2C). In N-line hearts postischemia, glycolysis was not significantly different than control hearts, but was significantly depressed vs. preischemic values (6,105±905 preischemia vs. 2,326±595 postischemia, nmol x g dry wt^{-1} x min^{-1}, $P<0.05$, Figure 4.2C). The rate of glycolysis in control and K-line hearts remained comparable during presichemia and postischemia.

Since cardiac work is an important determinant of metabolic rates, glucose oxidation and palmitate oxidation, and glycolysis were normalized for cardiac power (Figure 4.2D-F). During preischemia there was little difference in cardiac power (Figure 4.1), and thus the rates of glucose oxidation and palmitate oxidation and glycolysis normalized for function varied little. However, mechanical function during postischemia varied notably and was elevated in K-line hearts (Figure 4.1). With correction, it was notable that in K-line hearts, both glucose oxidation and palmitate oxidation relative to cardiac power, were greatly decreased. The same trend occurred for both N-line and K-line hearts with regards to glycolysis. Preischemic vs. postischemic rates of palmitate oxidation, glucose oxidation and glycolysis normalized to cardiac power were

comparable in K-line hearts. In contrast, during postischemia, the rates of glucose oxidation and palmitate oxidation were elevated in control and N-line hearts vs. presischemia. Similarly, the glycolytic rate normalized for cardiac power was elevated in control hearts when preischemic rates vs. postischemic rates were compared.

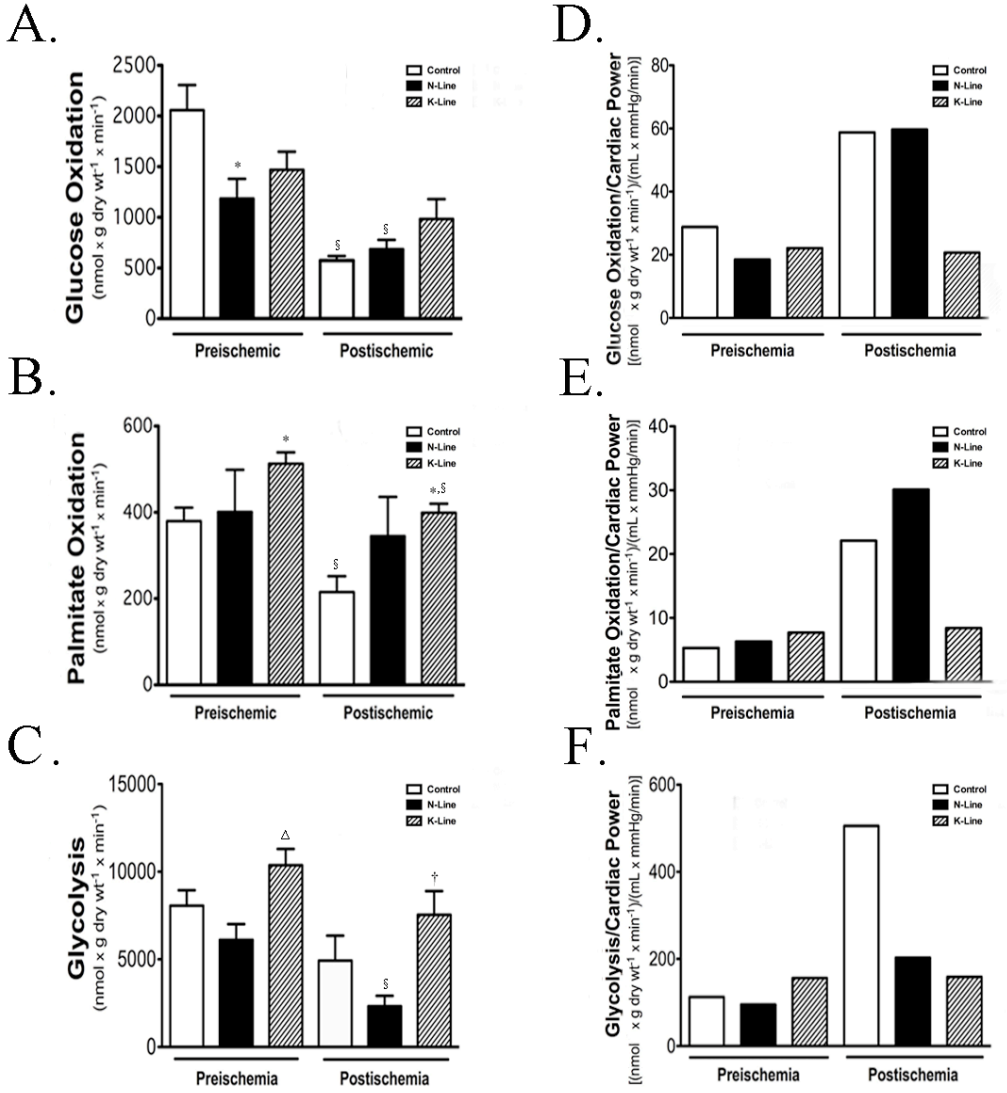

Figure 4.2. Rates of glucose oxidation, palmitate oxidation, and glycolysis in control, N-line and K-line hearts during preischemic and postischemic periods of the *ex vivo* working perfused hearts. White bar graph, control mice; black bar graph, N-line mice and grey bar graph, K-line mice. Preischemic values were obtained during 30 minutes of aerobic perfusion. Postischemic values were obtained following 20 minutes of global no flow ischemia and during 40 minutes of aerobic reperfusion. Glucose oxidation rates **(A),** palmitate oxidation rates **(B),** glycolytic rates **(C),** glucose oxidation **(D),** palmitate oxidation **(E),** and glycolysis **(F)** normalized for cardiac power. Values represent the mean±SEM. For corresponding control, $^{*}P<0.05$ for controls vs. N-line or K-line and $^{\Delta}P<0.05$, $^{\dagger}P<0.01$ for N-line vs. K-line. For preischemic vs. postichemic values $^{\S}P<0.05$; n=5-10 hearts/group.

4.2.3 Preischemic and Postischemic ATP Production Rates in Ex Vivo Working Mouse Hearts

Using measured steady state rates of glycolysis, glucose oxidation and palmitate oxidation, we calculated the relative contribution of each of these substrates to ATP production rates during preischemia and postischemia (Figure 4.3A-C). During preischemia, palmitate oxidation accounted for a greater amount of energy production in K-line hearts (53.4±2.7μmol x g dry wt^{-1} x min^{-1}) vs. both control (39.5± 3.2μmol x g dry wt^{-1} x min^{-1}) and N-line (41.7±10.2μmol x g dry wt^{-1} x min^{-1}) hearts (P<0.05, Figure 4.3A). During preischemia, ATP derived from glycolysis in K-line hearts was significantly greater vs. N-line hearts (12.2±1.8 N-line vs. 20.7±1.9 K-line, μmol x g dry wt^{-1} x min^{-1}, P<0.05, Figure 4.3A). However, ATP production rates derived from glucose oxidation were relatively similar in control and K-line hearts and significantly depressed in N-line hearts (P<0.05, Figure 4.3A). Total ATP production rates were significantly greater in control and K-line hearts vs. N-line hearts, suggesting that N-line hearts were energetically compromised during preischemia. TCA cycle acetyl-CoA production rates during preischemia reflected trends similar to that seen with ATP production rates. The contribution of glucose oxidation to TCA cycle acetyl CoA was significantly decreased in N-line hearts (P<0.05, Figure 4.3D) and TCA cycle acetyl CoA from palmitate oxidation was significantly greater in K-line hearts vs. controls (P<0.05, Figure 4.3D). This resulted in greater total TCA cycle acetyl CoA production rates in control and K-line vs. N-line hearts (Figure 4.3D).

During postischemia reperfusion, palmitate oxidation predominated as the source of ATP production rates and TCA cycle acetyl CoA production rates in control, N-line

and K-line hearts, as was seen during preischemia (Figure 4.3B,E). During postischemia, total ATP production rates and total TCA cycle acetyl CoA production rates in K-line hearts were greater vs. controls ($P<0.05$, Figure 4.3A,D). The contribution of glucose oxidation and palmitate oxidation to TCA cycle acetyl CoA production rates and ATP production rates were similar in control and N-line hearts (Figure 4.3A). However, in K-line hearts the contribution of palmitate oxidation to TCA cycle acetyl CoA production rates (1.7±0.3 controls vs. 3.2±0.2 K-line μmol x g dry wt^{-1} x min^{-1}, $P<0.05$, Figure 4.3D-E), as it was for ATP production rates (22.5±3.9 controls vs. 41.4±2.2 K-line, $P<0.05$, Figure 4.3A), was significantly greater than controls. Part of the higher levels of ATP production rates in postischemic K-line hearts were also a result of glycolysis derived ATP, as this was also significantly greater in K-line hearts vs. N-line (15.1±2.7 K-line vs. 4.65±1.2 N-line, μmol x g dry wt^{-1} x min^{-1}, $P<0.01$, Figure 4.3A). Postischemia, a notable change from preischemia was that the efficiency of energy utilization, indicated by total ATP production rates and TCA cycle acetyl CoA production rates normalized to cardiac power, was greater in K-line hearts vs. controls (Figure 4.3C,F).

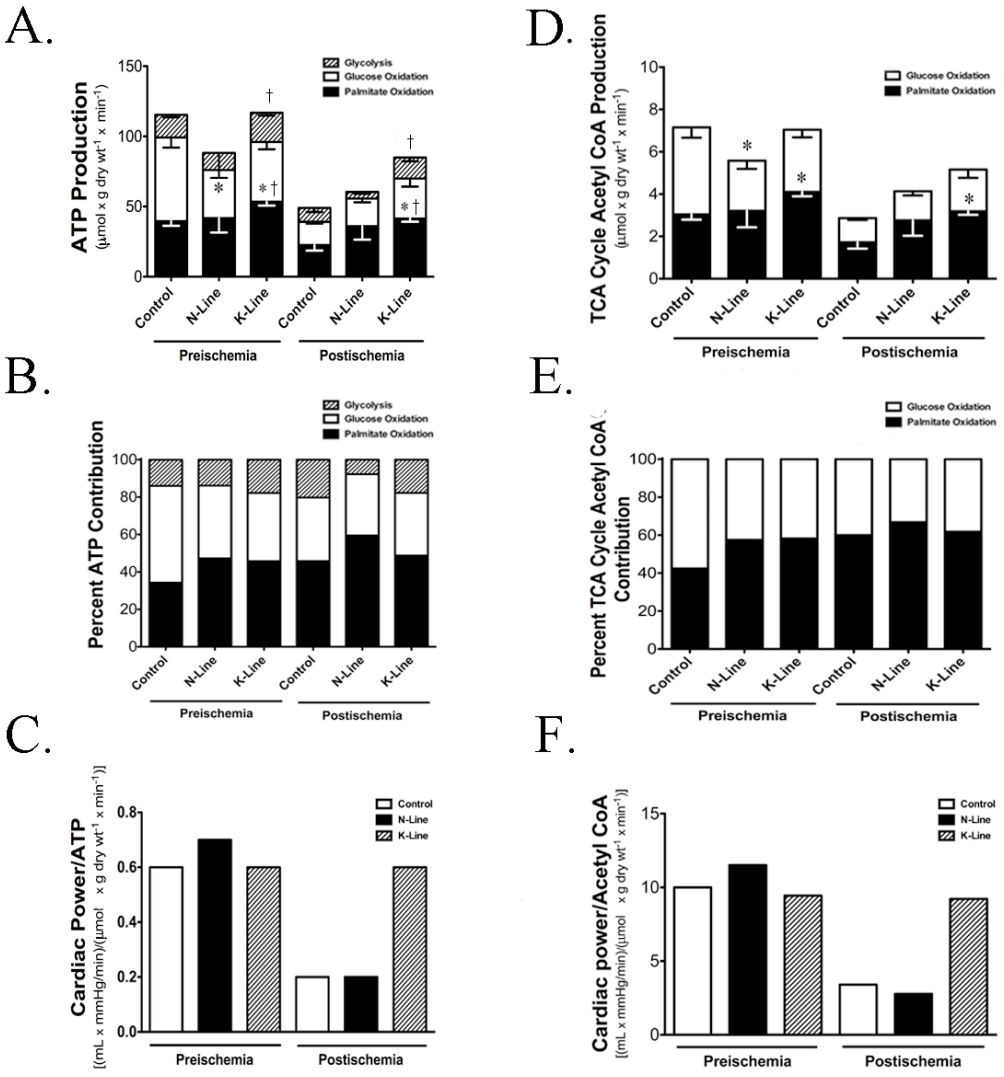

Figure 4.3. Total ATP production rates and TCA cycle acetyl CoA production rates in control, N-line and K-line hearts during preischemic and postischemic periods of the *ex vivo* working perfused hearts. White bar graph, control mice; black bar graph, N-line mice and grey bar graph, K-line mice. Preischemic values were obtained during 30 minutes of aerobic perfusion. Postischemic values were obtained following 20 minutes of global no flow ischemia and during 40 minutes of aerobic reperfusion. **(A),** ATP production was calculated from the rates of palmitate oxidation and glucose oxidation and glycolysis. **(B),** Percentage of ATP production rates contributed by palmitate oxidation, glucose oxidation or glycolysis. **(C),** Total ATP production rates normalized to cardiac power. **(D),** TCA cycle acetyl CoA production rates from palmitate oxidation and glucose oxidation. **(E),** Percentage of TCA cycle acetyl CoA contributed by palmitate oxidation or glucose oxidation. **(F),** TCA cycle acetyl CoA production rates normalized to cardiac power. Values are expressed as mean±SEM. $^{*}P<0.05$ for controls vs. N-line or K-line, $^{\dagger}P<0.05$ for N-line vs. K-line; n=5-10 hearts/group.

4.2.4 Preischemic and Postischemic Proton Production in Ex Vivo Working Mouse Hearts

We also examined the rates of H^+ production, which were derived from the degree of uncoupling of glucose oxidation from glycolysis[304]. A greater reliance on glucose as a source of mitochondrial acetyl-CoA production, suggests that more pyruvate and protons are being consumed aerobically in the TCA cycle. This was not the case in N-line and K-line hearts (Figure 4.3D), thus suggesting that protons are being produced. In addition, ATP derived from glycolysis, which is significantly elevated in K-line mice (Figure 4.3A), leads to the production of H^+[301]. During preischemia, K-line hearts produced 1.5-fold more protons than controls (17.8 K-line vs. 12.0 controls, μmol x g dry wt^{-1} x min^{-1}), whereas in N-line hearts, proton production remained relatively comparable to controls (9.84 N-line vs. 12.0 controls, μmol x g dry wt^{-1} x min^{-1}). During postischemia reperfusion, we found that the rates of H^+ production in K-line hearts remained elevated and were greater than proton production in control and N-line hearts (13.1 K-line vs. 8.7 controls vs. 3.3 N-line, μmol x g dry wt^{-1} x min^{-1}).

4.2.5 Signaling Pathways Contributing to the NHE1 Induced I/R Effects in NHE1 Transgenic Mouse Hearts

We examined protein expression and activation of various signaling pathways *in vivo* to determine their contribution, if any, to the NHE1-mediated cardioprotection or lack of it following I/R. Initially, we examined protein expression of AMPK and its phosphorylated counterpart of heart lysates subjected to I/R (as described in Section 2.3.1). AMPK is an important regulator of myocardial energy metabolism during I/R

injury[335]. AMPK is a heterotrimeric serine/threonine kinase that acts as a cellular fuel gauge, which stimulates energy-producing processes and inhibits energy-requiring processes in times of metabolic stress in effort to maintain or restore intracellular ATP levels[335]. AMPK is activated by AMP and upon binding of AMP, it becomes a better substrate for its upstream kinase, AMPK kinase. This results in an increase in AMPK phosphorylation (reviewed in[336]). During ischemia, AMPK has been shown to promote glycolysis[337,338], thus producing an anaerobic source of ATP and improving the cardiac energy balance by stimulating ATP-generating pathways[335]. During reperfusion, AMPK has been shown to accelerate FA oxidation, which has been suggested to exacerbate I/R injury. An increase in FA oxidation occurs at the expense of glucose oxidation, therefore increasing myocardial acidosis and subsequent postischemic contractile dysfunction[302,303,339]. Western blot analysis of protein expression of pAMPK relative to AMPK, indicated that there were no differences between control, N-line and K-line mice (Figure 4.4).

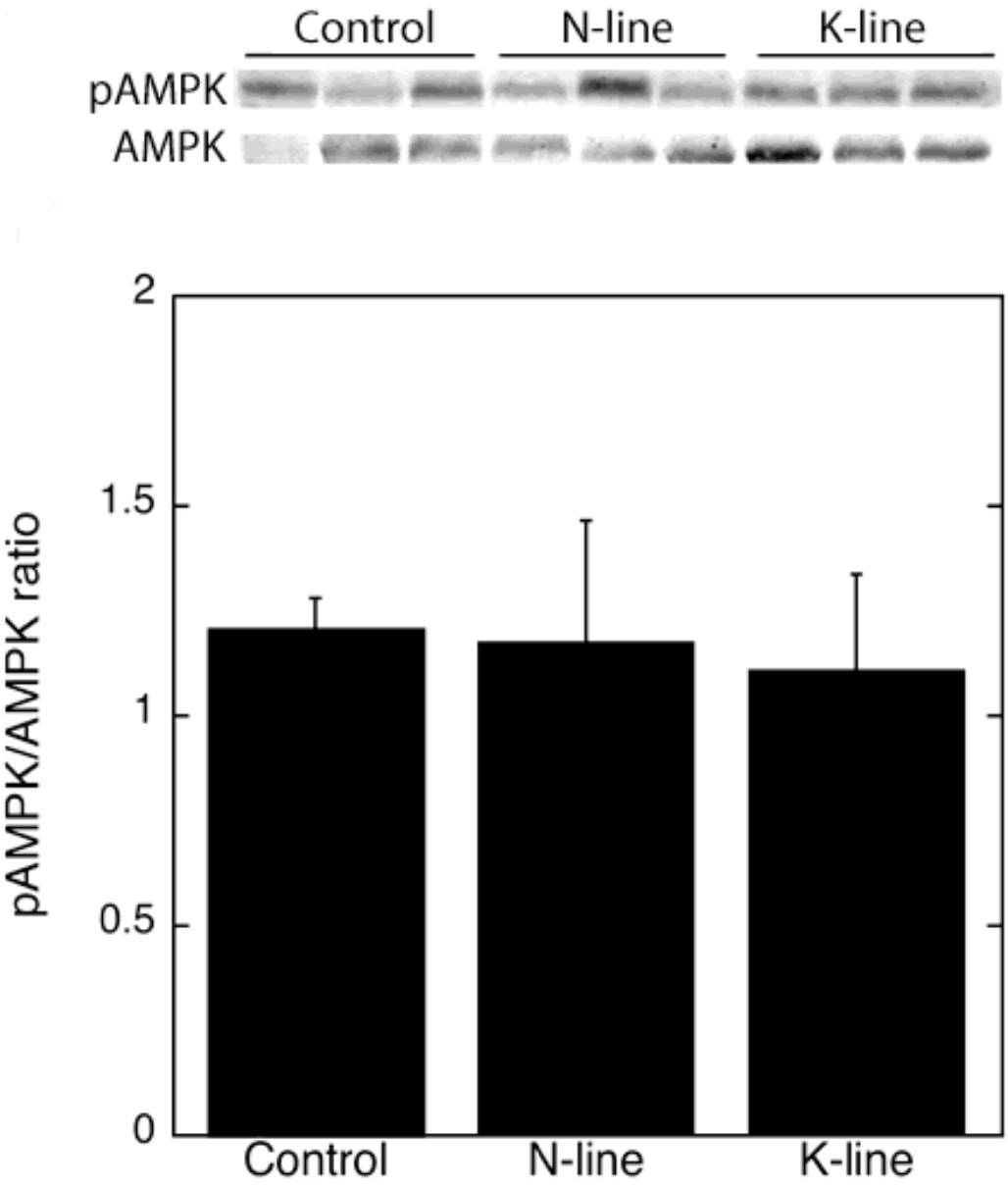

Figure 4.4. Immunoblot analysis of total and phosphorylated AMPKα protein expression in control, N-line and K-line mouse hearts subjected to I/R. Heart lysates were from hearts subjected to 30 minutes of aerobic perfusion, 20 minutes of global no flow ischemia and 40 minutes of aerobic perfusion. Blots were immunoblotted with pAMPK and AMPKα. **Upper panel,** representative western blot of total phosphorylated AMPK and total AMPK protein expression. **Bottom panel,** quantification of a series of experiments. Results are expressed as a ratio of phosphorylated AMPK to total AMPK. (n=5-6 hearts/group).

We then examined protein expression of the MAPKs (ERK, JNK, p38) and RSK, pathways that are potentially activated by I/R[340] (Figure 4.5). ERK, JNK, p38, and RSK are regulated by phosphorylation-dephosphorylation, with phosphorylation being in its active form. Protein expression of pERK, pp38 and pRSK, normalized to total ERK, p38 and RSK, respectively, were not elevated in heart lysates from N-line and K-line hearts subjected to I/R (as described in Section 2.3.1) when compared to controls (Figure 4.5). However, protein expression of pJNK normalized to total JNK was significantly attenuated in K-line hearts vs. controls ($P<0.05$, Figure 4.5).

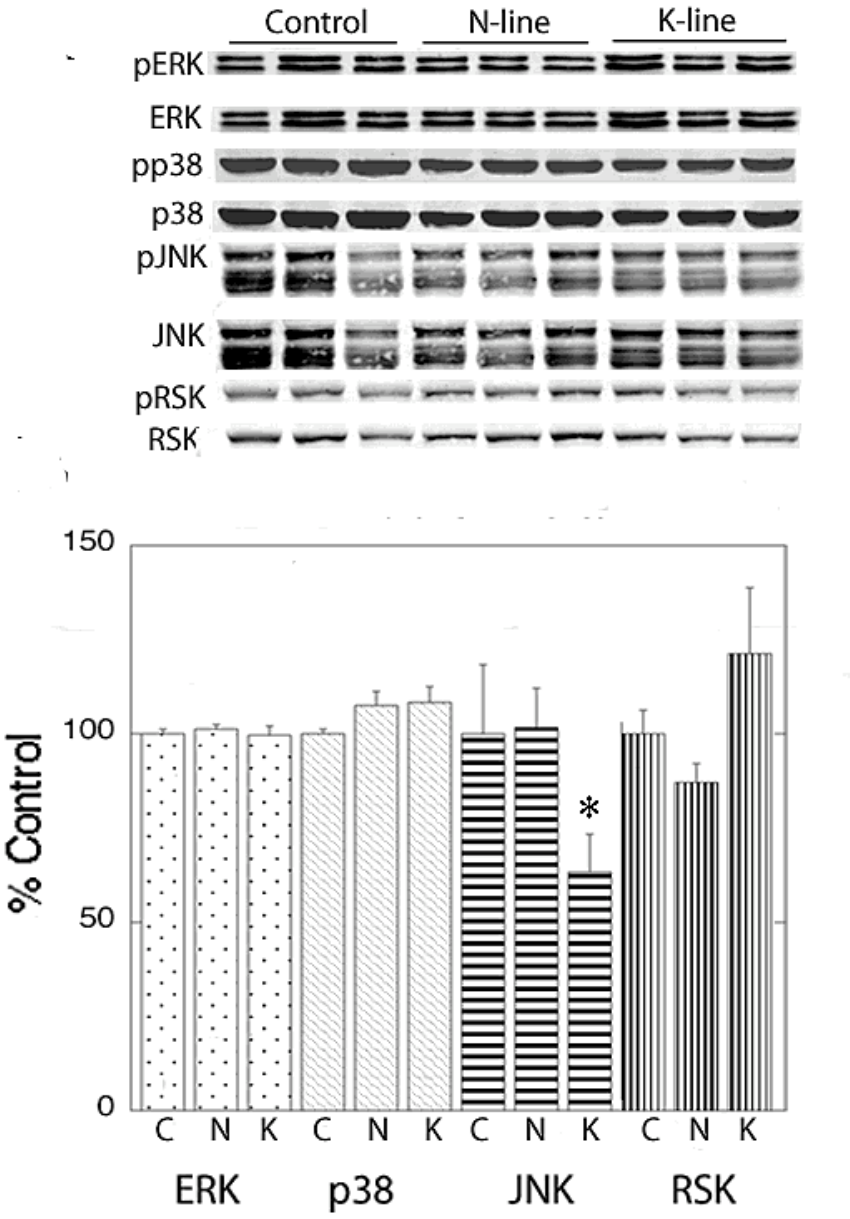

Figure 4.5. Western blot analysis of MAPKs and RSK in control, N-line and K-line mouse hearts subjected to I/R. C, control mice; N, N-line mice and K, K-line mice. Heart lysates were prepared from hearts subjected to 30 minutes of aerobic perfusion, 20 minutes of global no flow ischemia and 40 minutes of aerobic reperfusion. **Upper panel,** representative western blots of relative amounts of phosphorylated and total protein expression of ERK, p38, JNK and RSK. **Bottom panel,** quantification of a series of experiments measuring the ratio of phosphorylated to total protein for pERK/ERK, pp38/p38, pJNK/JNK and pRSK/RSK. Results are expressed as a % of controls (for each group)±SEM. $^{*}P<0.05$ for K-line vs. controls or N-line; n=5-6 hearts/group.

GSK-3β, a serine/threonine kinase, was originally identified as an enzyme that phosphorylates and downregulates glycogen synthase, the rate-limiting enzyme of glycogen metabolism[341,342]. Unlike most kinases, GSK-3β is highly active in the unstimulated state and usually exerts a negative inhibitory effect on its downstream pathways upon phosphorylation. Ischemic preconditioning has been suggested to result in phosphorylation and hence inhibition of GSK-3β. In addition, pharmacological inhibition of GSK-3β has been shown to protect against I/R injury[343]. Protein expression of GSK-3β and its phosphorylated counterpart were therefore investigated in control, N-line and K-line hearts subjected to I/R (as described in Section 2.3.1). However no significant changes were evident in N-line and K-line mouse hearts vs. controls (Figure 4.6).

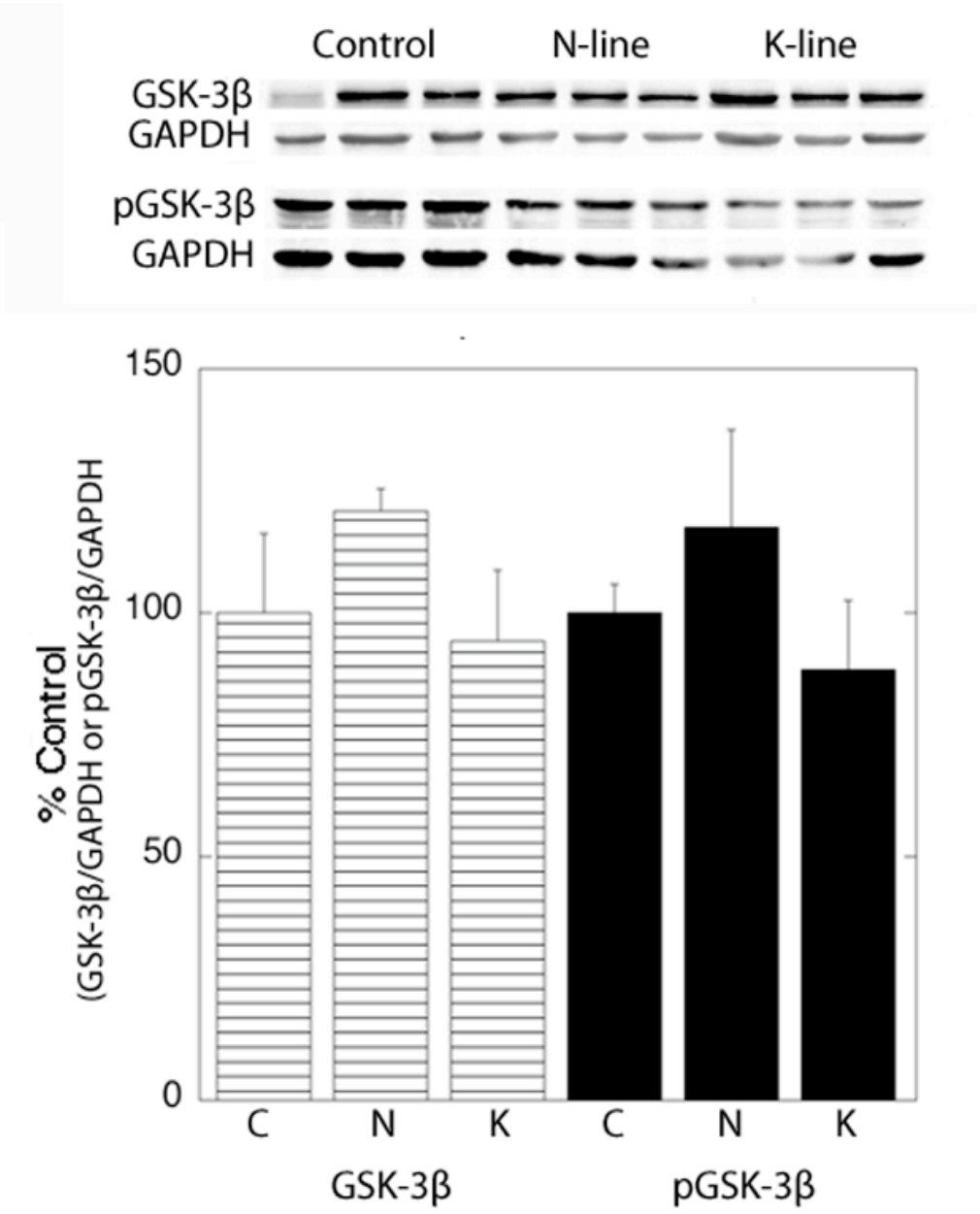

Figure 4.6. Western blot analysis of total and phosphorylated GSK-3β in control, N-line and K-line mouse hearts subjected to I/R. C, control mice; N, N-line mice and K, K-line mice. Heart lysates were prepared from hearts subjected to 30 minutes of aerobic perfusion, 20 minutes of global no flow ischemia and 40 minutes of aerobic reperfusion. **Upper panel,** representative western blots of relative amounts of phosphorylated and total GSK-3β normalized to GAPDH. **Bottom panel,** quantification of a series of experiments measuring the ratio of phosphorylated or total GSK-3β protein to GAPDH. Results are expressed as a % of controls±%SEM. (n=5-6 hearts/group).

The ER has also been suggested to contribute to cardioprotection following I/R injury. The ER senses oxidative stress, maintains Ca^{2+} homeostasis and can trigger apoptotic signaling[344,345]. I/R injury has been suggested to affect the ability of the ER to synthesize, fold, and sort proteins, which in turn leads to ER stress and activation of the unfolded protein response (UPR). The UPR results in decreased protein synthesis, increased expression of chaperone proteins that promote proper ER function and homeostasis. The UPR response has been suggested to contribute to the protective effects of hearts subjected to I/R[346]. In a previous report, upregulation of ER stress response proteins, calreticulin and PDI, were implicated in the cardioprotective effect of TG mice expressing elevated NHE1 following stimulation with I/R[205]. Therefore, we examined protein expression of calreticulin and PDI in control, N-line and K-line hearts (Figure 4.7). In agreement with previous reports, heart lysates from N-line mice had significantly greater levels of calreticulin and PDI protein expression vs. controls ($P<0.005$, Figure 4.7). Heart lysates from K-line mice also had significantly greater calreticulin and PDI protein expression vs. controls ($P<0.005$, Figure 4.7). PDI protein expression in K-line heart lysates was also significantly greater than PDI protein expression in heart lysates from N-line mice ($P<0.05$, Figure 4.7).

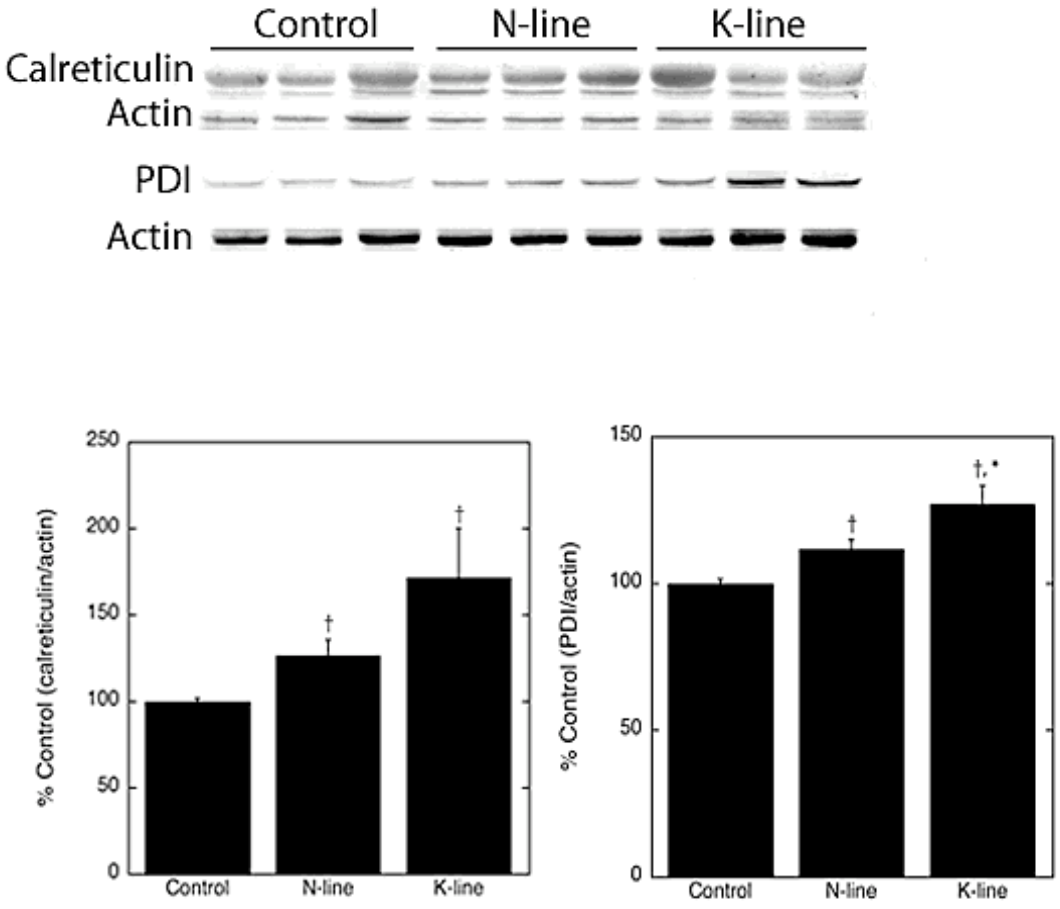

Figure 4.7. Immunoblot analysis of calreticulin and PDI in control, N-line and K-line mouse hearts. Upper panel, representative western blots of calreticulin and PDI protein expression normalized to actin. **Bottom panel,** quantification of a series of experiments measuring the ratio of calreticulin or PDI to actin. Results are expressed as a % of control±%SEM. $^{\dagger}P<0.005$ for controls vs. N-line or K-line, $^{*}P<0.05$ for N-line vs. K-line; n=5-6 hearts/group.

4.3 Discussion

Although many studies have suggested that inhibition of NHE1 attenuates I/R-injury, recent reports in two different TG mouse models have suggested that elevated expression of NHE1 induces cardioprotective effects in hearts subjected to I/R[204, 205]. The role that NHE1 plays in the cardioprotection of hearts subjected to I/R is still unclear. In addition, the effects of expression of an active form of NHE1 compared with the wild type have not been investigated using a working heart perfusion model. A previous report suggested that in mice expressing elevated NHE1, a minor improvement in recovery of pH_i and ATP were evident following I/R injury[204]. This observation led to the more detailed examination, in a more physiologically relevant model, of cardiac energetics in aerobic and reperfused ischemic hearts from mice expressing elevated NHE1.

Energy metabolism of hearts with varying NHE1 levels has not been studied in detail. We used the *ex vivo* isolated working heart model with the inclusion of FAs as a substrate. This model was used because it has a higher and more physiological energy demand compared with the Langendorff perfused hearts[347], which were used earlier[204,205]. In addition, the KHB perfusate used in this study contained both glucose and FAs as a substrate, making it more representative of normal human plasma in the setting of ischemia[348]. Palmitate is the preferred energy substrate of the normal perfused heart[332] and is used by the myocardium in reperfusion following ischemia[301].

A number of important findings were made. Firstly, similar to a previous report[204], cardiac specific expression of wild type (N-line) or activated NHE1 (K-line) does not functionally compromise the heart function during aerobic perfusion

(preischemia). On the contrary, we found that expression of NHE1 during I/R produced a marked cardioprotection during reperfusion of the ischemic hearts. However, in the present study, only activated NHE1 (K-line) was cardioprotective. Earlier it was found that cardioprotection occurred in both hearts that expressed wild type NHE1 and constituitively active NHE1[204]. Cook et al.[205] also demonstrated that elevated NHE1 expression in TG mice induces a cardioprotective effect in hearts subjected to I/R injury. The difference between this and previous reports is likely due to the difference in the perfusion conditions. Either inclusion of FAs or the greater workload of the present study was likely accountable. In any case, our results further verify that elevated expression of NHE1 can be cardioprotective under appropriate conditions. In addition, since the difference between the N-line and K-line mice is that K-line mice have an activated NHE1, our results suggest that elevation of NHE1 activity or its downstream effects enhances the cardioprotection.

Why would addition of an activated NHE1 protein be more effective at cardioprotection in comparison with increased levels of the non-activated protein? The NHE1 protein is regulated by a proton sensor[65]. At more alkaline pH's, the activity of NHE1 is minimal. Activation of the protein shifts the pH dependence to the more alkaline range[36]. It may be that increased levels of the wild type protein provides minimal benefit if the protein is not activated. Shifting the activity to the more alkaline range, such as with the K-line mutation may provide a more functional protein at a critical pH.

To gain further insights into the mechanisms of NHE1 mediated cardioprotection, we examined cardiac energy metabolism, signaling pathways and the expression of the

ER stress response proteins. The notable metabolic differences in K-line hearts in comparison to the controls and N-line were: (1), an elevation in FA oxidation, preischemia and postischemia; (2), an elevation in glycolysis, preischemia and postischemia, (3), a lack of postischemia reduction in glucose oxidation, (4), significantly greater levels of total ATP production rates and TCA cycle derived acetyl CoA production rates.

Recently, approaches to the treatment of cardiovascular disease have concentrated on minimization of FAs as a fuel, while increasing glucose oxidation. This is believed to minimize the degree of acidosis associated with I/R injury[349,350]. However, in our study, we found that FA oxidation was elevated in K-line hearts relative to control hearts, and this occurred with an improvement in contractile function. While the mechanism by which this occurred is uncertain, it is evident in our study that increasing availability of FA substrate (palmitate) in the presence of activated NHE1 increases FA oxidation and ATP production and improves recovery of function following I/R. This could reflect that increased activity of the K-line NHE1 protein aids in removal of excess acid and minimize acidosis.

In K-line *ex vivo* working hearts, glycolysis was significantly elevated during both preischemic and postischemic periods, which contributed to higher rates of ATP production. Increasing glucose oxidation has been shown to have a beneficial effect on functional recovery of hearts[339]. Elevated glycolysis could also be protective during and following myocardial ischemia[351]. However, if glycolysis is increased to a greater extent than glucose oxidation an increased proton load on the heart can occur, which can contribute to a decrease in cardiac efficiency and a decrease in functional recovery

postischemia[339]. In K-line hearts, proton production from uncoupled glycolysis to glucose oxidation was actually increased. Despite this, these hearts showed the best recovery of function postischemia. Opie[352] has suggested that enhanced glycolysis is more beneficial to the myocardium when pH_i is maintained appropriately. It maybe that elevated activity of the K-line NHE1 protein coupled with enhanced, but "pH managed" glycolysis, were responsible for at least part of the protective effects that were observed. This data challenges the widely held belief that excessive NHE1 activity contributes to I/R injury, but rather suggests that maintenance of pH is more important in postischemic recovery.

We also examined a number of signaling pathways and ER stress related proteins in this experimental model. Numerous signaling pathways are activated during I/R injury, contributing to either I/R injury or protecting the heart from further injury. In this study, we determined whether such pathways contribute to the cardioprotective effect seen. AMPK has been shown to be rapidly activated during myocardial ischemia and is associated with an increase in FA oxidation, as well as an increase in glycolysis[338,353]. However, no differences were seen in N-line and K-line hearts vs. controls, suggesting that AMPK activation was not responsible for the increase in metabolic rates. We also investigated the primary protein kinase pathways activated by myocardial I/R injury, which include, the MAPKs (ERK, JNK, p38) and RSK[340]. No significant differences were seen between control and NHE1 TG hearts in activation of ERK, p38 and RSK. However, phosphorylated JNK (normalized to total JNK) was significantly decreased in K-line hearts vs. control and N-line hearts. JNK is activated in response to various cellular stresses including inflammatory cytokines, ischemia, reversible ATP depletion, heat shock, endotoxin, and genotoxic stress[354]. The decrease in phosphorylated JNK

protein expression in hearts subjected to I/R provides further evidence that our K-line hearts were not as energetically or functionally stressed as control and N-line hearts. Another kinase we examined was GSK-3β, which has been suggested to be crucial to cardioprotection of hearts subjected to I/R[341]. In our study, no differences were seen in pGSK-3β or GSK-3β protein expression in control, N-line and K-line hearts, suggesting that the cardioprotection seen in K-line hearts is not mediated through this mechanism.

We also investigated the involvement of the ER stress response, which has previously been suggested to contribute to the cardioprotective effects of elevated expression of NHE1[205]. Induction of multiple ER stress associated genes have been reported to lead to a dramatic reduction in infarct size following I/R injury[346]. In our studies we found that both N-line and K-line mouse hearts expressed elevated levels of the ER stress response proteins, calreticulin and PDI. K-line mouse hearts expressed significantly more PDI than N-line hearts. This could account for the improved cardiac performance with exposure to I/R.

Conclusion

Elevated expression of activated NHE1 protein results in cardioprotection of the myocardium (Figure 4.8). This is accompanied by increased ER stress response protein levels, a decrease in active JNK, increased rates of glycolysis, and increased rates of FA oxidation. Increased levels of NHE1 may be beneficial in coping with elevated proton production that occurs with elevated use of FA and glycolysis.

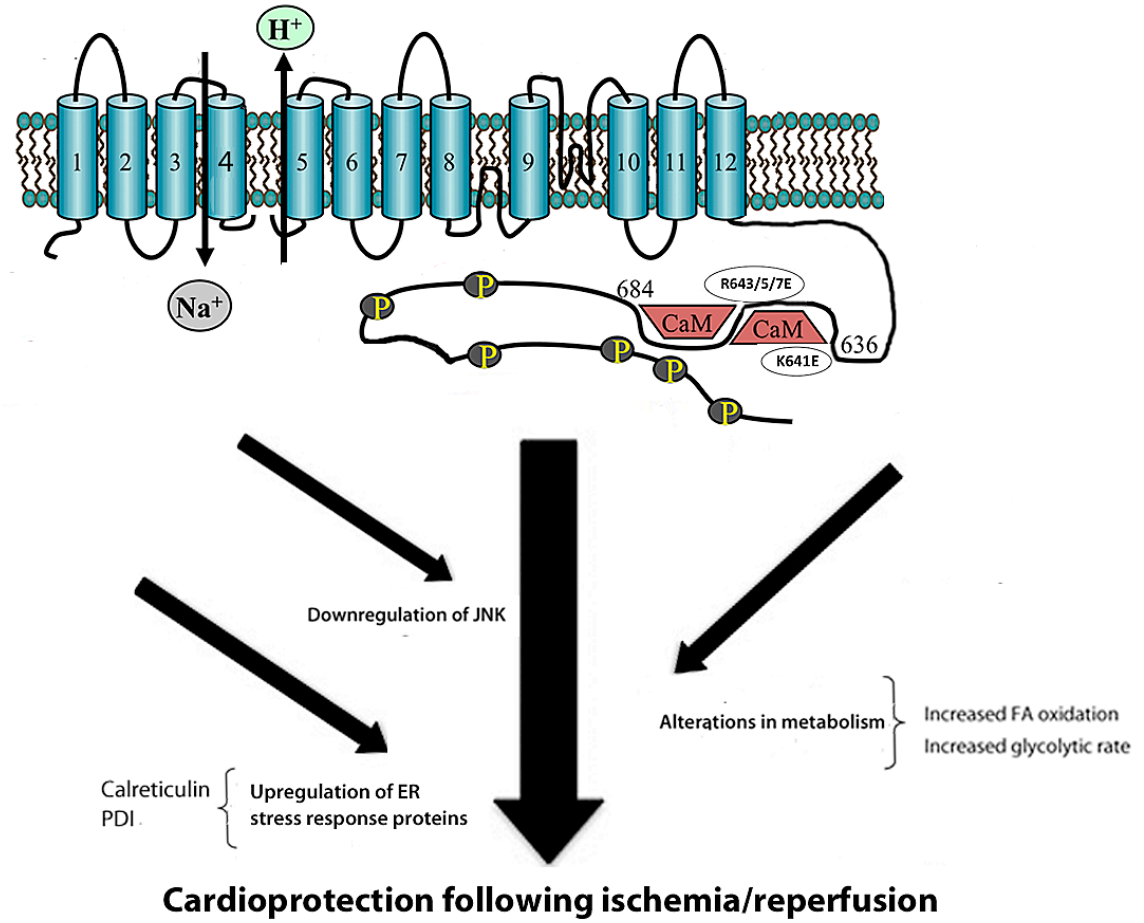

Figure 4.8. Schematic representation of the role of active NHE1 expression during I/R. Expression of active NHE1 in transgenic mice induces cardioprotection in hearts subjected to I/R. This cardioprotective effect occurs in association with altered metabolism (increased FA oxidation and glycolytic rates), upregulation of ER stress response proteins (calreticulin and PDI), downreguation of JNK and independent of ERK, p38, RSK and GSK-3β. The active NHE1 transgene was created by site specific mutations at the C-terminal tail of NHE1 (1K3R4E; lysine (K) 641, arginine (R) 643/645/647 mutated to glutamic acid (E)).

Chapter 5

Characterization of Male Transgenic Mice with Elevated NHE1 Expression

5.1 Introduction

The mortality and morbidity rate of heart failure is different in men and women, with the prognosis for women being significantly better than for men[355,356]. Similarly, in animal models, murine/or rat models, heart failure is accelerated in males[357,358]. Less cardiac remodeling, ventricular dysfunction, pathological change and an increased survival advantage is seen in females[359-362]. An example of the male/female differences is clearly demonstrated in the guanylyl cyclase-A knockout mice. CH and expression of hypertrophy-associated genes are more pronounced in males vs. females[361]. In addition to the differences in the degree of hypertrophy observed in male vs. female animal models, it has also been noted that in some animal models, the entire cardiac phenotype is gender dependent[362]. For example FKBP12.6 is a sarcoplasmic reticulum membrane protein that regulates gating of ryanodine receptors, which are important for Ca^{2+}-induced-Ca^{2+} release[363]. In FKBP12.6 null mice, only males developed CH, and gender was suggested to be an independent variable[362,364].

In the myocardium, NHE1 plays a critical role in CH (reviewed in[87]). NHE1 has been shown to be activated/expressed in several *in vivo* and *in vitro* models of CH. An *in vitro* study done by our group showed that NRVMs stimulated with aldosterone elevated NHE1 mRNA and protein expression[103]. *In vivo*, NHE1 expression/activity has been shown to be upregulated in models in which CH has been experimentally induced and in genetically modified models with phenotypic expression of CH (reviewed in[87]). Specific inhibition of NHE1 has resulted in prevention/regression of CH (reviewed in[87]). We have also shown, using a gain of function model, that female mice which express

constituitively active NHE1 develop pathological CH (Chapter 3). Increased expression of wild type NHE1 induces moderate levels of pathological CH (Chapter 3).

NHE1 activity is regulated by some sex hormones. The sex steroids, progesterone and testosterone, have been suggested to be ineffective in stimulating NHE1, as indicated by their inability to increase cell volume[367]. However, *in vitro*, low levels of estrogen were shown to activate NHE1[365]. *In vivo*, chronic deprivation of female sex hormones induced by ovariectomization modulated $[Ca^{2+}]_i$ by stimulating NHE1[366]. Kilic et al.[365] has also shown that activation of NHE1 with low concentrations of estrogen induced cardiomyocyte hypertrophy. This suggests that the phenotypes induced by NHE1 may vary with gender.

In the present study, we sought to determine whether male NHE TG mice, expressing either wild type NHE1 (N-line) or constituitively active NHE1 (K-line) at 10-12 weeks of age exhibited the same phenotype as their female counterparts. In addition, we examined the degree of the phenotype in males relative to females. We demonstrate that elevated NHE1 expression and activity potentiates CH in male mice. The NHE1 induced CH phenotype was not specific to female mice. In addition, we demonstrate that indicators of myocardial remodeling including the HW/BW and LVM, LVID are greater in male mice vs. female mice. Inspite of this, the degree of hypertrophy was not significantly different between males and females.

5.2 Results

5.2.1 NHE1 Protein Expression of Male vs. Female NHE1 Transgenic Mice

We measured total (exogenous and endogenous) NHE1 protein expression to confirm that the NHE1 protein was expressed in our male N-line and K-line mice. Figure 5.1 upper panel illustrates a representative western blot of total NHE1 protein expression of male control, N-line and K-line mice. This was detected using a commercial antibody against the NHE1 cytoplasmic tail. Lane 1 represents a heart lysate from control mice, lane 2 represents a heart lysate from N-line mice, and lane 3 represents a heart lysate from K-line mice. Quantification of a series of experiments measuring the total NHE1 protein expression is shown in Figure 5.1, bottom panel. The results show that there was a marked increase of approximately 5 and 14 fold in total NHE1 protein expression in N-line and K-line hearts vs. controls, respectively. Total NHE1 protein expression in male K-line hearts was significantly elevated vs. male N-line hearts ($P<0.05$). A different western blot confirmed the presence of exogenous NHE1 protein in male control, N-line and K-line hearts (Figure 5.2). Immunoblotting with anti-HA tag antibody showed that the exogenous NHE1 protein was present in hearts from N-line (lane 2) and K-line (lane 3) mice, but not in the controls, which lack the HA tag. A sample of AP-1 cells transfected with HA tagged-NHE1 (lane 1) served as a positive control.

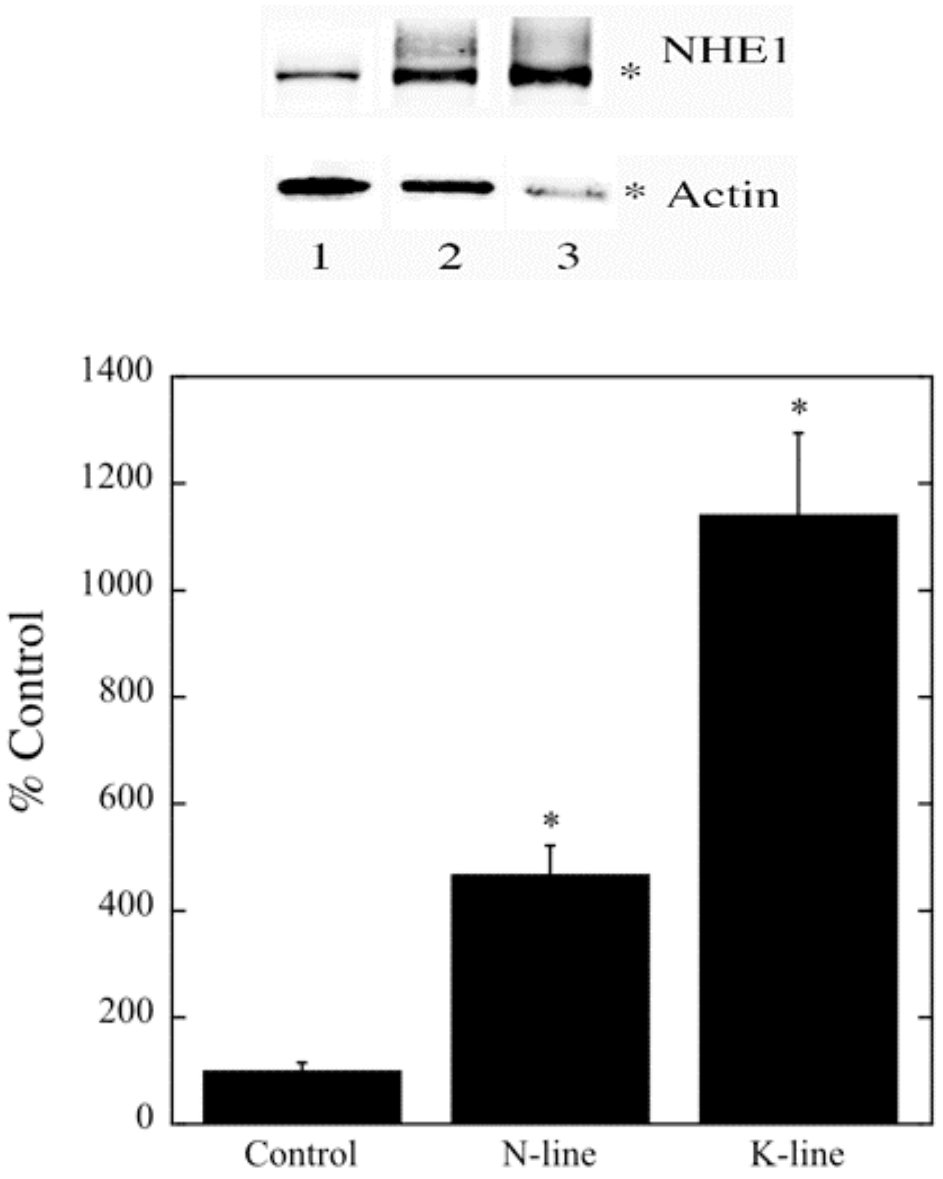

Figure 5.1. Immunoblot analysis of total exogenous and endogenous NHE1 protein expression in hearts from male control, N-line and K-line mice. Upper panel, representative western blot of total NHE1 protein expression detected by anti-NHE1 (90-110 kDa) and anti-actin (40kDa) in hearts from control, N-line (wild type NHE1) or K-line (active NHE1) mice. Lane 1 is a heart lysate from control mice, lane 2 is a heart lysate from N-line mice and lane 3 is a heart lysate from K-line mice. **Bottom panel,** NHE1 protein expression quantified and normalized to actin and expressed as a % of control±%SEM. $^{*}P<0.05$ for controls vs. N-line or K-line or N-line vs. K-line; n=4.

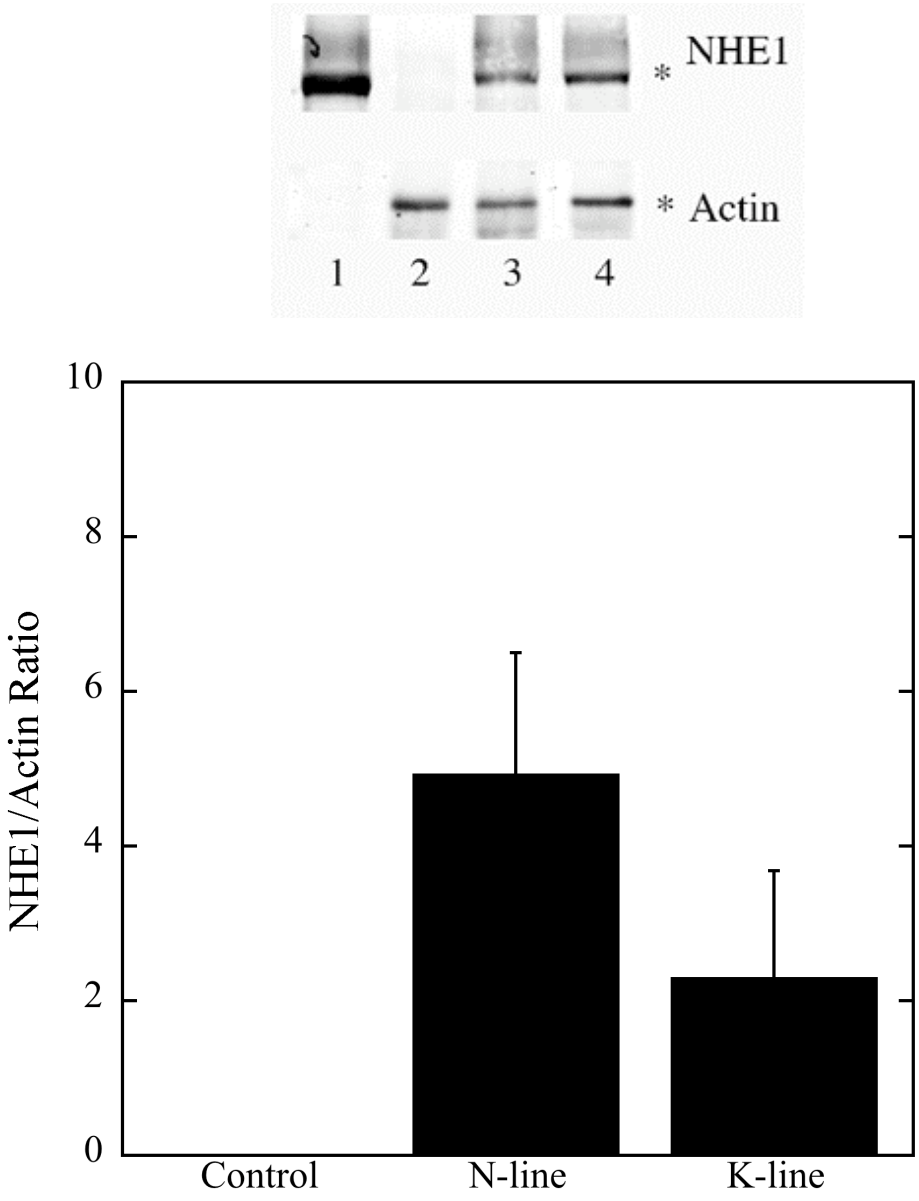

Figure 5.2. Immunoblot analysis of exogenous HA tagged-NHE1 protein expression in hearts from male control, N-line and K-line mice. Upper panel, representative western blot of HA tagged-NHE1 in heart lysates from control (lane 2), N-line (lane 3), and K-line (lane 4) mice. 90-110 kDa NHE1 and 40 kDa actin are indicated by *. The HA tag was detected by rabbit polyclonal anti-HA (Y-11) antibody. Lane 1 is a positive control from AP-1 cells transfected with HA tagged-wild type NHE1 protein. **Bottom panel,** summary of quantification of total exogenous NHE1 protein detected with anti-HA antibody. NHE1 protein levels were quantified and normalized to actin for each group and expressed a ratio of NHE1/actin±SEM. (n=3-4 hearts/group).

After confirming that male NHE1 TG hearts express NHE1, we then compared NHE1 protein expression in female and male NHE1 TG hearts. Male and female NHE1 TG heart lysates were run on the same blot and immunoblotted for NHE1 using a commercial antibody against NHE1. Our initial experiment examined NHE1 protein expression in control mice to ensure that any differences seen between male or female NHE1 protein expression were not due to differences in the animal model. Figure 5.3, upper panel, is a representative western blot of female control heart lysates, represented in lanes 4-6 and male control heart lysates, represented in lanes 1-3. Quantification of a series of experiments showed no significant differences in NHE1 protein expression in heart lysates from female control mice vs. heart lysates from male control mice (Figure 5.3, bottom panel).

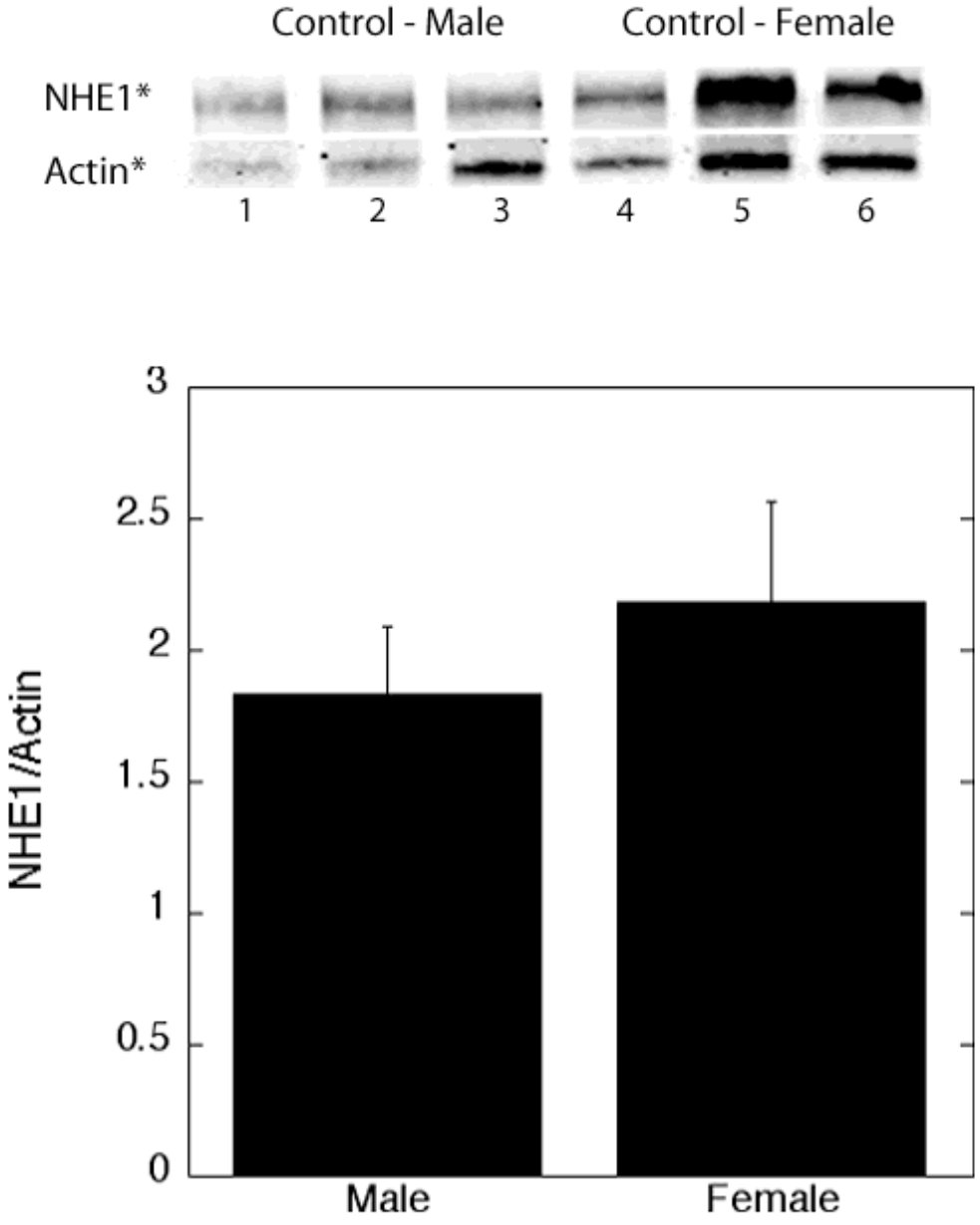

Figure 5.3. Immunoblot analysis of total exogenous and endogenous NHE1 expression in hearts from control male and female mice. Total NHE1 protein expression was detected using mouse monoclonal anti-NHE1 antibody. **Upper panel,** representative western blot of heart lysates from male and female control mice immunoblotted for NHE1 (90-110 kDa) and actin (40 kDa). Lanes 1-3 represent heart lysates from male control mice and lanes 4-6 represent heart lysates from female control mice. **Bottom panel,** NHE1 protein levels were quantified and normalized to actin for each group. Results are expressed as a ratio of NHE/actin±SEM. (n=5-7/group).

In figure 5.4, bottom panel total NHE1 protein expression was quantified in male (lanes 1-3) and female (lanes 4-6) K-line heart lysates. Female K-line heart lysates showed a significantly greater level of NHE1 protein expression vs. male K-line heart lysates ($P<0.05$).

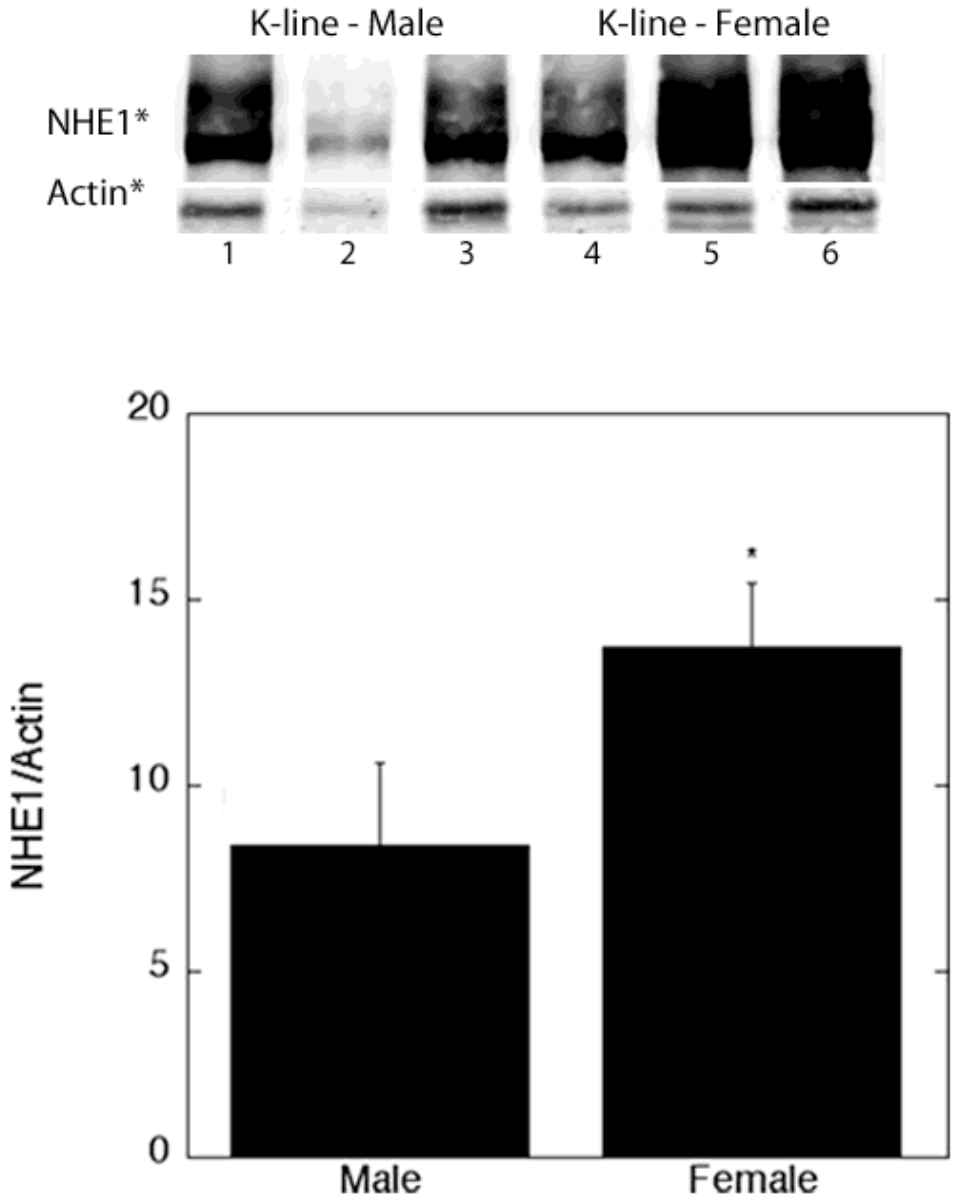

Figure 5.4. Immunoblot analysis of total exogenous and endogenous NHE1 expression in hearts from K-line male and female mice. Total NHE1 protein expression was detected by anti-NHE1. **Upper panel,** representative western blot of K-line male and female heart lysates immunoblotted for NHE1 (90-110 kDa) and actin (40 kDa). Lanes 1-3 represent heart lysates from male K-line mice and lanes 4-6 represent heart lysates from female K-line mice. **Bottom panel,** NHE1 protein levels were quantified and normalized to actin for each group. Results are expressed as a ratio of NHE/actin±SEM. $^{*}P<0.05$ for male K-line vs. female K-line; n=3-4 hearts/group.

5.2.2 Characterization of Cardiac Hypertrophy in Male vs. Female NHE1 Transgenic Mice

To determine whether male NHE1 TG mice express the hypertrophic phenotypes seen in female NHE1 TG mice (as described in Section 3.2.9), various markers of CH were compared including the HW/BW, ANP mRNA expression, CSA and IF. In male control, N-line and K-line mice, the heart weight was normalized by the body weight and the results are shown in Figure 5.5. The HW/BW was significantly increased in male K-line mice (143.0±10.0%, $P<0.05$) compared to both male control (100±3.7%) and N-line (108.4±7.5%) mice. No significant differences were found between male N-line and control mice in the HW/BW. The variations in the HW/BW between groups were due to changes in the heart weight (100±3.9% controls vs. 100.3±3.9% N-line vs. 143.7±10.7% K-line, $P<0.05$), as there were only small and not significant changes in the body weight (100±1.3% controls vs. 92.6±2.6% N-line vs. 100.7±2.2% K-line). Therefore, the male K-line mice showed the same trend in the HW/BW as the female K-line mice (as described in Section 3.2.9), with the HW/BW ratio of K-line mice being significantly greater vs. controls. Unlike the female N-line mice, the male N-line mice did not show any significant increase in the HW/BW vs. controls. When the HW/BW is directly compared between male and female NHE1 transgenic mice using absolute values, female control mice had a significantly smaller HW/BW vs. male controls (0.0068±0.00025 male vs. 0.0050±0.00023 female, mg/g, $P<0.005$) (Figure 5.5). Similarly, female K-line mice had a significantly smaller HW/BW ratio vs. male K-line mice (0.0097±0.00068 male vs. 0.0072±0.00046 female, mg/g, $P<0.05$). No significant difference in the HW/BW was observed between males N-line and females N-line.

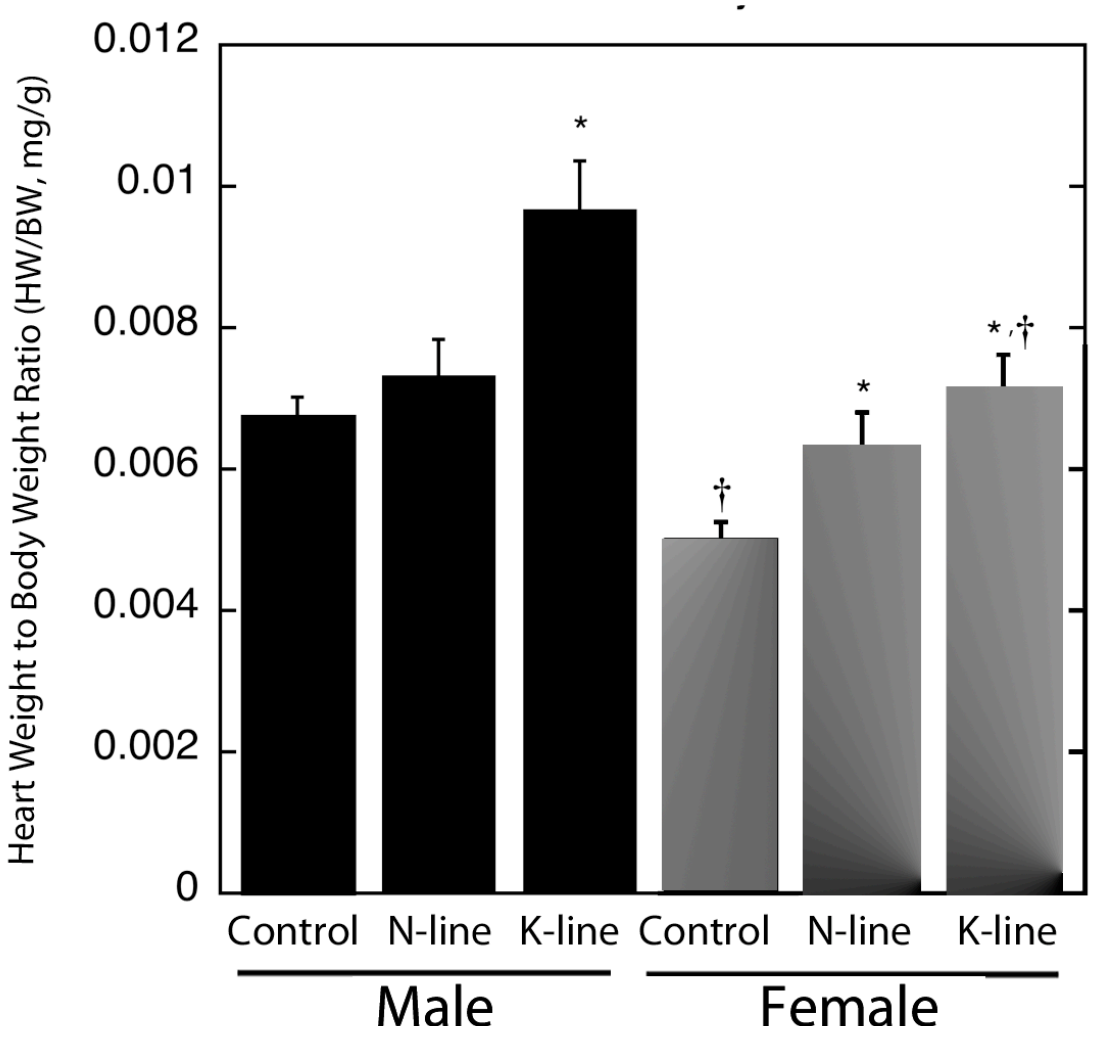

Figure 5.5. HW/BW ratio of male and female control, N-line and K-line mice. Hearts of all groups of mice were excised and compared with body weights. Results are expressed as the HW/BW ratio (mg/g)±SEM. $^{*}P<0.05$ for male K-line vs. N-line or controls, male K-line vs. female K-line, female N-line vs. controls; $^{\dagger}P<0.005$ for male controls vs. female controls, female K-line vs. female controls; n=7-13/ group.

One long term feature of CH involves re-expression of fetal genes, such as ANP[368]. To examine whether this occurred in male N-line and K-line hearts, we measured ANP mRNA expression. ANP mRNA expression showed a trend towards increase in male N-line hearts (0.18±0.08 ANP/18S rRNA) in comparison to that of male control hearts (0.057±0.03 ANP/18S rRNA), but the difference was not significant. A further increase in ANP mRNA expression was observed in male K-line hearts (0.71± 0.4ANP/18S rRNA) relative to male N-line hearts, but again, the difference was not significant (Figure 5.6). Therefore, the male NHE1 TG mice showed a similar trend in ANP mRNA expression as the females (as described in Section 3.2.9), with ANP/18S rRNA ratio of K-line hearts being greater than N-line, which was greater than controls. When the ANP/18S rRNA ratio is directly compared between NHE1 TG males and females using absolute values, no significant differences were found between the male and female groups.

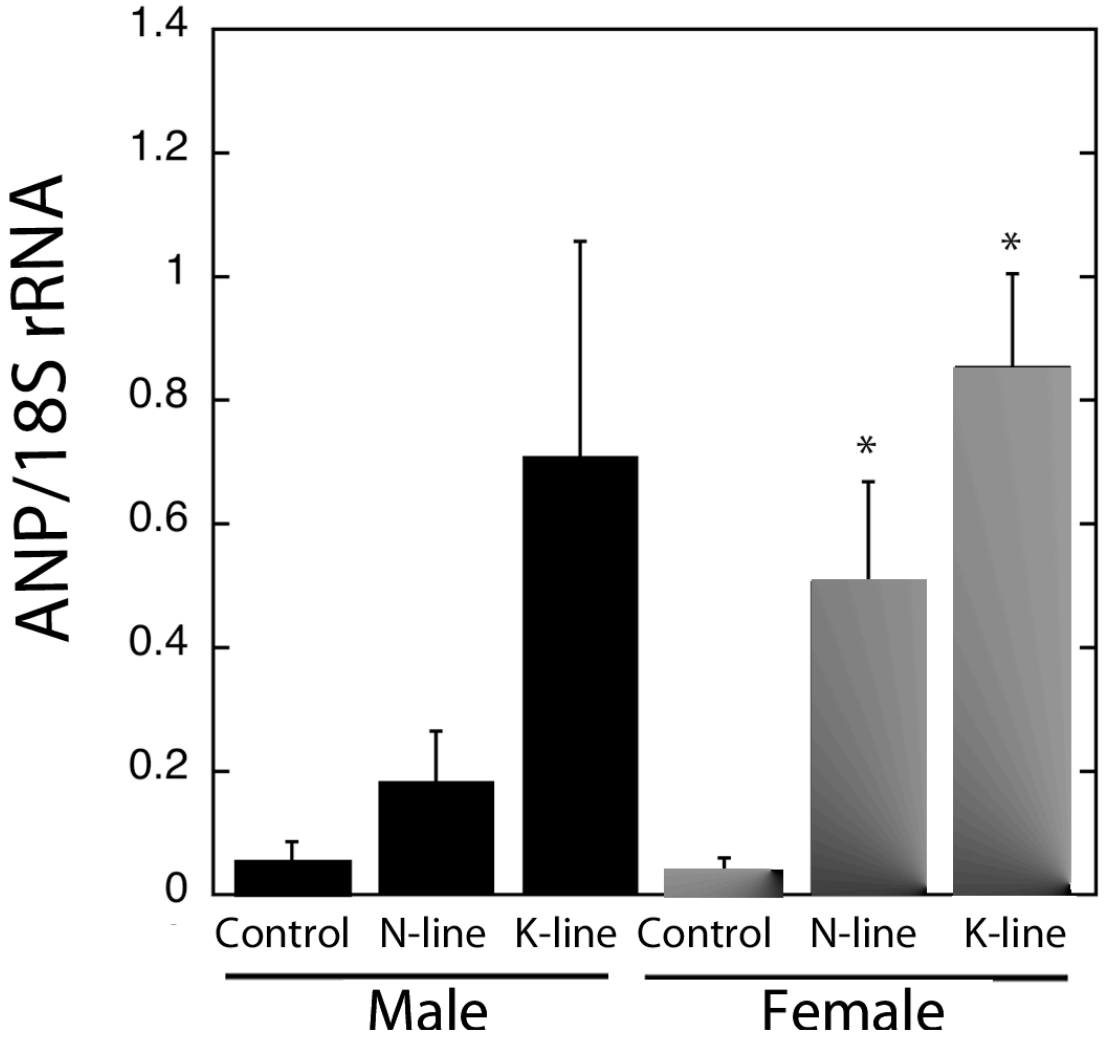

Figure 5.6. ANP mRNA expression of male and female hearts from control, N-line and K-line mice. ANP mRNA expression was determined by real-time PCR for male and female control, N-line and K-line hearts. ANP mRNA expression from male hearts were compared to ANP mRNA expression in female hearts. ANP mRNA expression was normalized to 18S rRNA mRNA expression. Results are presented as the ratio of ANP to 18S rRNA±SEM. $^{*}P<0.05$ for female controls vs. female N-line or K-line hearts; n=3/group.

In addition to causing changes in gene expression, CH is also associated with a number of histological changes. Figure 5.7 examines the CSA from H&E heart cross sections from control, N-line and K-line mice. In male K-line hearts, the CSA (48 649±4076.0 arbitrary units, $P<0.05$) was significantly greater than the CSA of both male N-line (26 010±4339.8 arbitrary units) and male control (24 875±5161.9 arbitrary units) hearts. No significant differences were found in the CSA between male control and male N-line hearts. Therefore, the male NHE1 TG hearts showed a similar trend in CSA as the females (as described in Section 3.2.9), with CSA of K-line hearts being greater than both controls and N-line. When CSA, measured in arbitrary units, is directly compared between male NHE1 TG hearts and female NHE1 TG hearts using absolute values, no significant differences were found.

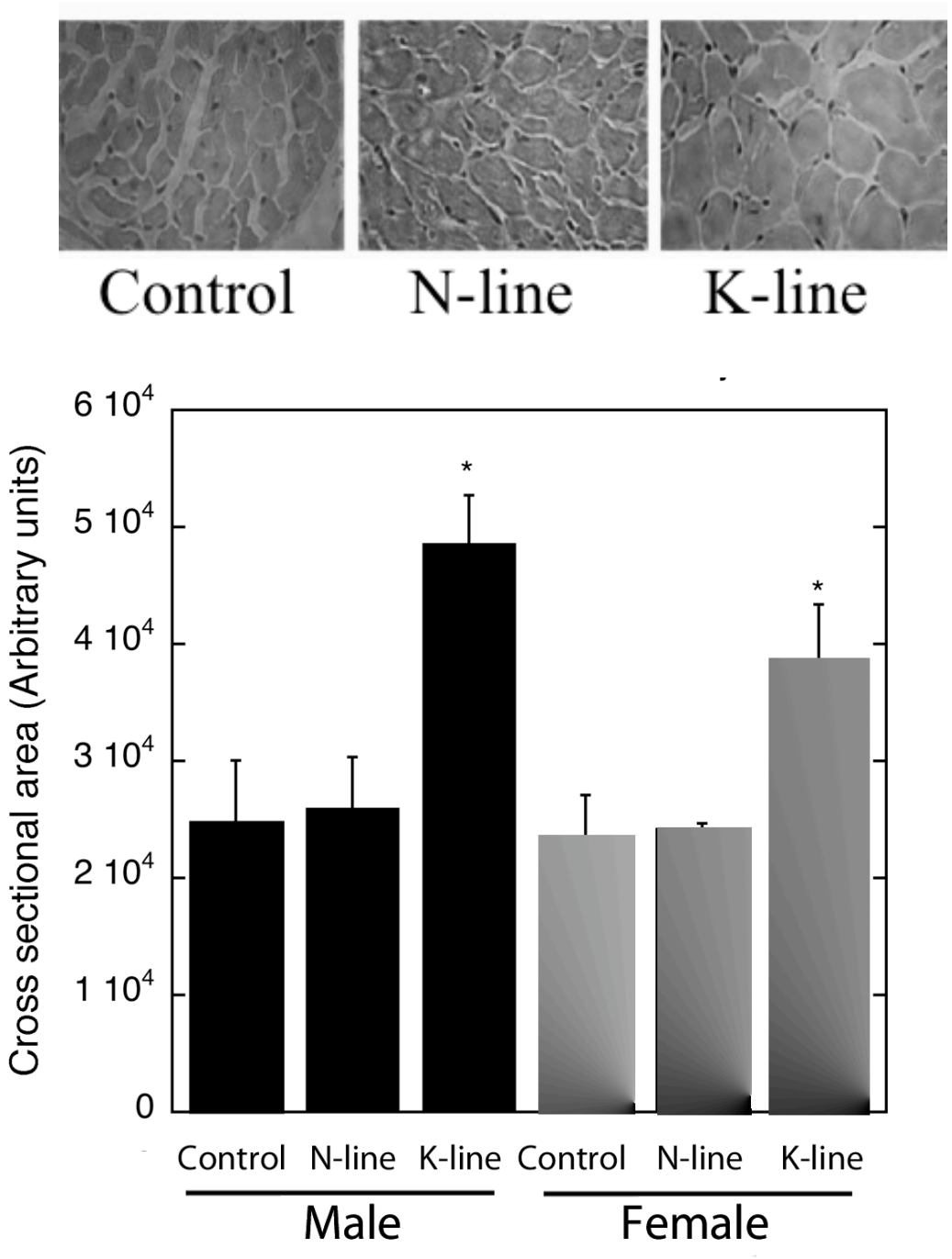

Figure 5.7. Cross sectional area of male and female heart cross sections from control, N-line and K-line mice. Cross sectional area of heart cross sections stained with H&E. **Upper panel,** representative heart cross sections stained with H&E from male control, N-line and K-line hearts. **Bottom panel,** summary of analysis of cross sectional area expressed in arbitrary units±SEM. $^{*}P<0.05$ for male or female K-line vs. control or N-line; n=4-6 mouse hearts/group.

IF was also measured by assessing heart cross sections stained with PSR. Figure 5.8 is a summary of the results. Expression of active NHE1 in male K-line hearts (4.64±0.2%, $P<0.05$) results in significantly greater amounts of IF vs. male control (1.69±0.3%) or male N-line (1.96±0.04%) hearts. The amount of IF was not significantly different in hearts from male control and N-line hearts. Therefore, the male NHE1 TG hearts showed the same trend as the females (as described in Section 3.2.9), with hearts from K-line mice having a greater amount of IF than both hearts from control and N-line mice. When IF levels are directly compared between hearts from male NHE1 TG and female NHE1 TG mice, no significant differences are found.

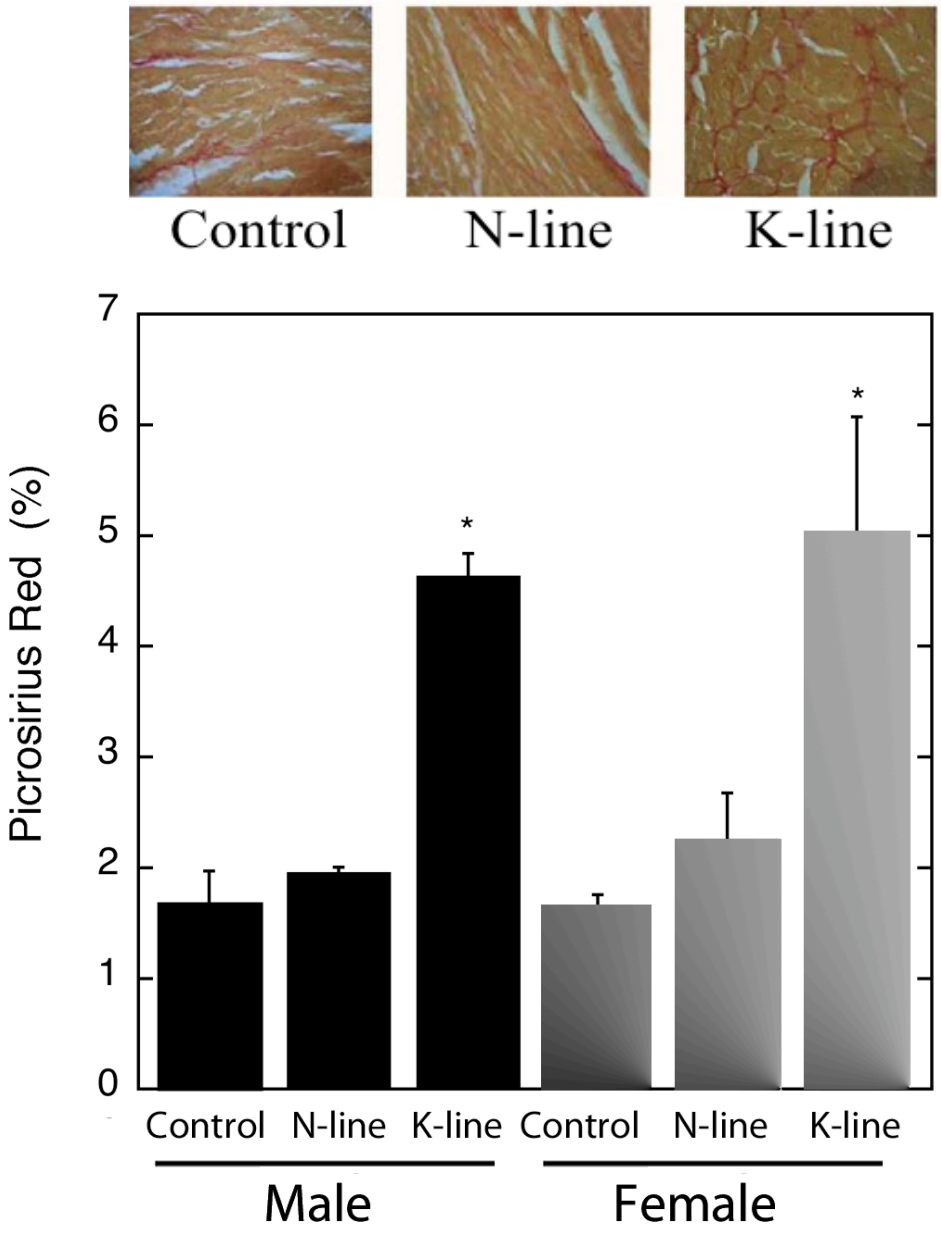

Figure 5.8. Interstitial fibrosis of male and female heart cross sections from control, N-line and K-line mice. Picrosirius red stained heart cross sections were used to assess fibrosis. The maximum fibrosis observed for any section was calculated as the area occupied by red stained connective tissue divided by the areas occupied by connective tissue plus cardiac myocytes x 100. **Upper panel,** representative heart cross sections stained with PSR from male control, N-line and K-line mice. **Bottom panel,** bar graph of quantitative analysis of accumulated IF. Results are expressed as %±SEM. $^{*}P<0.05$ for male or female K-line vs. control or N-line mice; n=4-6 mouse hearts/group.

We also examined cardiac function and morphology in male control, N-line and K-line mice by performing echocardiography (described in Section 2.2.4). *In vivo* echocardiographic assessment of cardiac morphology confirmed our previous indications of NHE1 dependent CH in male NHE1 TG mice. Indicators of CH, LVPW, IVST and LVM, were all significantly greater in K-line mice vs. both control and N-line mice (Table VIII). Cardiac diastolic and systolic function were significantly decreased in K-line mice vs. control and N-line mice. The decrease in systolic function was demonstrated by a decrease in FS and EF. The decrease in diastolic function was demonstrated by an increase in the E/A ratio. This decrease in systolic function in the K-line mice was associated with ventricular dilation, as indicated by the increase in LVID during systole (s) *(P*<0.05 vs. controls or N-line). LVID during diastole was not significantly different in male K-line hearts from male control or N-line hearts, but showed a trend towards increase. The global deterioration in myocardial performance with expression of active NHE1 was further confirmed by the significant increase in the Tei index in male K-line hearts compared with male control and N-line hearts.

Table VIII: Echocardiographic analysis of male control, N-line and K-line mice. IVSTd, diastolic inter-ventricular septal wall thickness; LVPWd, diastolic left ventricular posterior wall thickness; LVM, left ventricular mass; LVIDd and LVIDs, left ventricular internal diameter during diastole and systole; FS, left ventricular % fractional shortening; EF, left ventricular % ejection fraction; Ratio of peak E wave mitral valve velocity to peak A wave mitral valve velocity (MV E/A, ratio). Values are expressed as mean±SEM (n=7-8/group). $^{*}P<0.05$ vs. controls, $^{\dagger}P<0.001$ vs. controls, $^{\S}P<0.05$ for N-line vs. K-line, $^{¥}P<0.001$ for N-line vs. K-line; n=7-8/group.

Parameter	Controls	N-line	K-line
IVSTd, mm	0.79 ± 0.02	0.75 ± 0.01	$0.87 \pm 0.03^{*,\S}$
LVPWd, mm	0.74 ± 0.02	0.74 ± 0.09	$0.86 \pm 0.03^{*,\S}$
LVM , mg	101.6 ± 3.8	95.6 ± 2.4	$142.8 \pm 11.0^{*,¥}$
LVIDd, mm	4.37 ± 0.1	4.28 ± 0.06	4.81 ± 0.2
LVIDs, mm	2.78 ± 0.1	2.85 ± 0.1	$3.75 \pm 0.4^{*,\S}$
FS, %	36.5 ± 1.1	33.5 ± 1.5	$23.1 \pm 3.8^{*,\S}$
EF, %	66.4 ± 1.5	62.3 ± 2.1	$45.2 \pm 6.9^{*,\S}$
MV E/A, ratio	1.98 ± 0.3	1.94 ± 0.2	$3.56 \pm 0.6^{*,\S}$
Tei index	0.49 ± 0.02	0.51 ± 0.02	$0.78 \pm 0.03^{\dagger,¥}$

When echocardiographic parameters were compared between male and female NHE1 TG mice, IVSTd and LVM were significantly less in female control vs. male control male ($P<0.001$) (Table IX). LVM was also significantly reduced in female N-line and K-line vs. male N-line and K-line mice ($P<0.05$). In terms of LVID, it was significantly depressed during both systole and diastole in female control vs. male control mice ($P<0.05$). LVID during diastole was also significantly depressed in female N-line and K-line hearts vs. male N-line and K-line hearts ($P<0.005$, $P<0.05$, respectively).

Table IX: Echocardiographic analysis of control, N-line and K-line mice, males vs. females. IVSTd, diastolic inter-ventricular septal wall thickness; LVPWd, diastolic left ventricular posterior wall thickness; LVM, left ventricular mass; LVIDd and LVIDs, left ventricular internal diameter during diastole and systole; FS, left ventricular % fractional shortening; EF, left ventricular % ejection fraction; Ratio of peak E wave mitral valve velocity to peak A wave mitral valve velocity (MV E/A, ratio). Values are expressed as mean±SEM. $^{*}P<0.05$, $^{\dagger}P<0.001$ and $^{\S}P<0.005$ for males vs. females; n =7-8/group.

	Controls		N-line		K-line	
	Males	**Females**	**Males**	**Females**	**Males**	**Females**
IVSTd, mm	0.79 ± 0.02	0.71 ± 0.01†	0.75 ± 0.01	0.77 ± 0.02	0.87 ± 0.03	0.83 ± 0.03
LVPWd, mm	0.74 ± 0.02	0.74 ± 0.02	0.74 ± 0.09	0.74 ± 0.02	0.86 ± 0.03	0.84 ± 0.02
LVM , mg	102 ± 3.8	81.3 ± 2.1†	95.6 ± 2.4	85.9 ± 3.0*	143 ± 11.0	103 ± 4.6†
LVIDd, mm	4.37 ± 0.1	3.98 ± 0.08*	4.28 ± 0.06	3.98 ± 0.06§	4.81 ± 0.2	4.10 ± 0.08*
LVIDs, mm	2.78 ± 0.1	2.44 ± 0.06*	2.85 ± 0.1	2.69 ± 0.07	3.75 ± 0.4	3.12 ± 0.09
FS, %	36.5 ± 1.1	38.8 ± 0.7	33.5 ± 1.5	32.4 ± 1.1	23.1 ± 3.8	24.0 ± 1.2
EF, %	66.4 ± 1.5	69.8 ± 0.9	62.3 ± 2.1	61.2 ± 1.6	45.2 ± 6.9	48 .1 ± 2.1
MV E/A, ratio	1.98 ± 0.27	1.95 ± 0.1	1.94 ± 0.15	2.65 ± 0.2	3.56 ± 0.60	4 .04 ± 0.6
Tei index	0.49 ± 0.02	0.46 ± 0.02	0.51 ± 0.02	0.5 1 ± 0.02	0.78 ± 0.03	0.70 ± 0.03

5.2.3 Effects of Neuroendocrine Stimulation on Cardiac Hypertrophy in Male NHE1 Transgenic Mice

We also examined the effects of neuroendocrine stimulation on CH. Neuroendocrine stimulation has been shown to both activate NHE1 and induce CH (as described in Section 1.7.3 and Section 1.5.1.1). NHE1 TG mice were stimulated with PE over two weeks using Alzet osmotic mini pumps at a concentration of 50mg/kg/day (as described in Section 2.2.5). This dose of PE has been shown by ourselves (as described in Section 3.2.17) and others[295-297] to induce CH. Stimulation with PE did not significantly increase the HW/BW of male control, N-line and K-line mice (controls*:* 100±6.62% PBS vs. 117.40±9.8% PE; N-line: 100±7.4% PBS vs. 98.98±6% PE; K-line*:* 100±6.02% PBS vs. 109.1±11.85% PE) when compared to the HW/BW of vehicle treated mice within each group (Figure 5.10). This is unlike the female K-line mice, which show a significant increase in the HW/BW when compared to female control mice stimulated with PE ($P<0.05$). When male control, N-line and K-line mice stimulated with PE were compared to female control, N-line and K-line mice, also stimulated with PE, no statistical significance was seen in the HW/BW (controls: 0.0070±0.0006male vs. 0.0056±0.0004female; N-line: 0.0068±0.0004male vs. 0.0062±0.0002female; K-line: 0.0078±0.0009male vs. 0.0095±0.0008female).

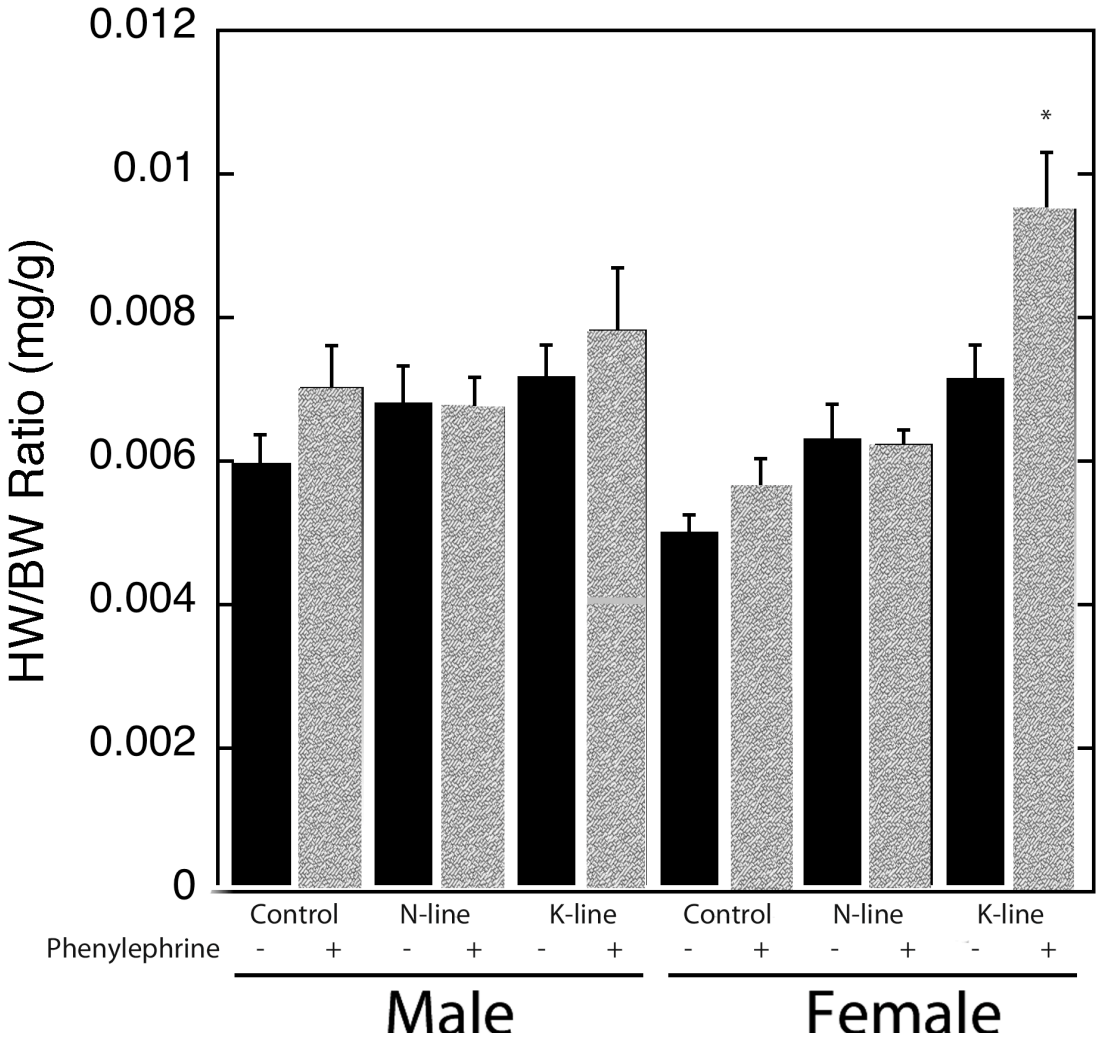

Figure 5.9. HW/BW ratio of male and female control, N-line and K-line mice stimulated with PE or PBS. PE was administered using Alzet osmotic mini pumps at a concentration of 50mg/kg/day over a two week period. Results are expressed as the HW/BW ratio±%SEM. $^{*}P<0.05$ for female K-line stimulated with PE vs. female K-line treated with PBS or control stimulated with PE; n=5-10 hearts/group.

We also examined ANP mRNA expression in male heart lysates from control, N-line and K-line mice following stimulation with PE (Figure 5.11). ANP mRNA expression was normalized to 18S rRNA. No significant differences were found in ANP mRNA expression between PBS treated groups and PE treated groups in male control (100.0±25.8% PBS vs.141.3±8.9% PE) and N-line (100.0±21.9% PBS vs. 84.4±21.4% PE) hearts. ANP mRNA expression in male K-line hearts explanted from K-line mice stimulated with PE (552.0±7.5%, $P<0.01$) was significantly greater vs. male K-line hearts explanted from mice treated with PBS (100±24.5%). ANP mRNA expression was significantly greater in both male and female K-line hearts explanted from mice stimulated with PE vs. hearts explanted from control mice stimulated with PE ($P<0.05$). When ANP mRNA expression in hearts from male control, N-line and K-line mice stimulated with PE was compared to female counterparts also stimulated with PE, no statistical significance was evident (controls: 0.080±0.01 male vs. 0.068±0.02 female; N-line: 0.16±0.06 male vs. 0.65±0.4 female; K-line*:* 3.92±0.6 male vs. 4.18±2.2 female).

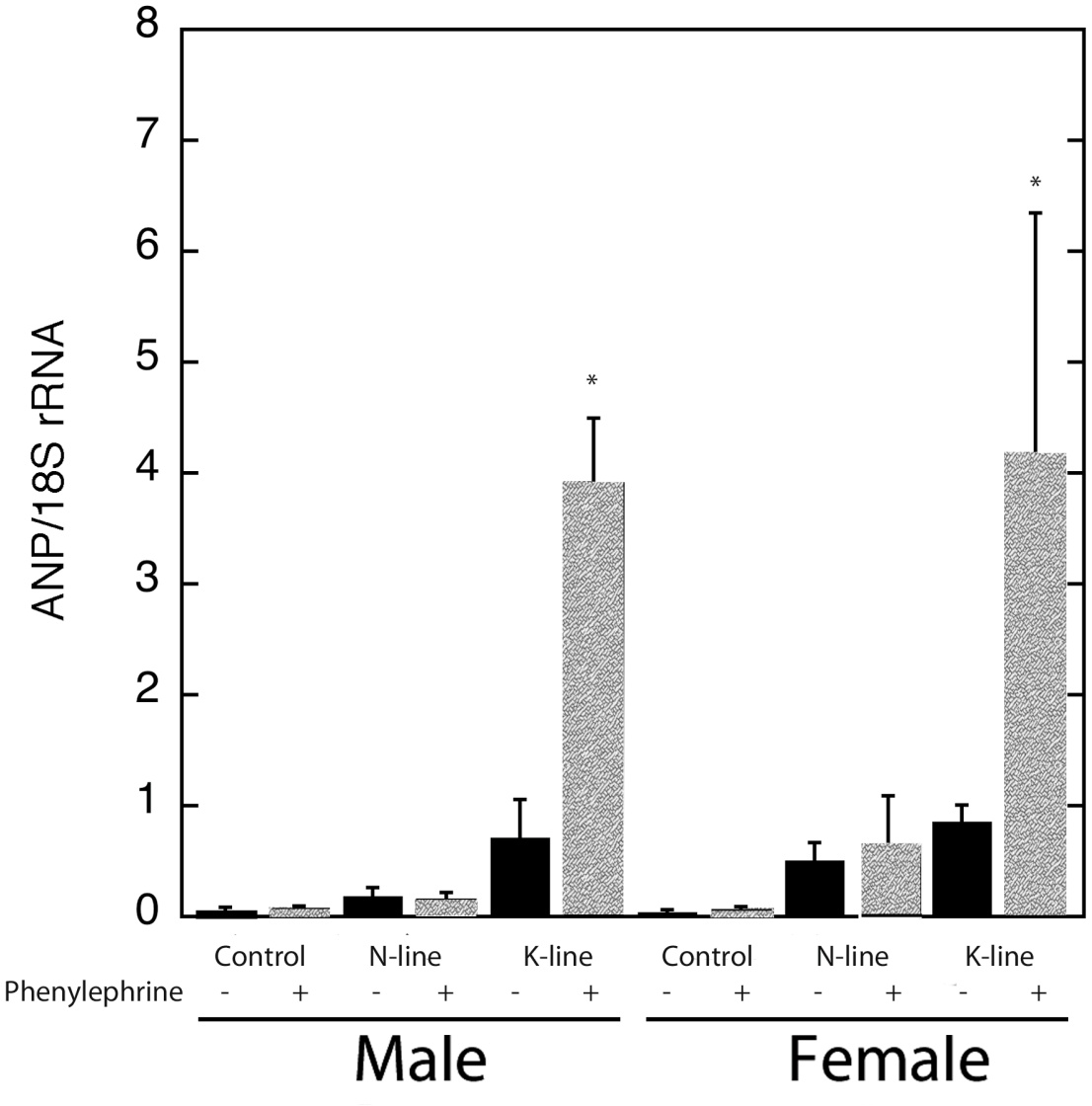

Figure 5.10. ANP mRNA expression of hearts from male and female control, N-line and K-line mice stimulated with PE or PBS. PE was administered using Alzet osmotic mini pumps at a concentration of 50mg/kg/day over a two week period. ANP mRNA expression was determined by real-time PCR for heart lysates from control, N-line (wild type NHE1) and K-line (active NHE1) mice. Results are presented as the ratio of ANP to 18S rRNA and expressed as a % of control (group treated with vehicle PBS)±%SEM. $^{*}P<0.05$ for male and female K-line stimulated with PE vs. K-line treated with PBS and for male and female K-line stimulated with PE vs. control stimulated with PE; n=3 hearts/group.

5.3 Discussion

NHE1 activity has previously been shown to be regulated by sex hormones[365,366]. Regulation of NHE1 by sex hormones has been suggested to result in alterations of the cardiac phenotype. The sex hormone estrogen, at low concentrations produces cardiomyocyte hypertrophy through ERK/NHE1 activation and intracellular alkalinization, whereas antihypertrophic effects were seen with high concentrations of estrogen[365]. These changes induced by sex hormones suggest that the effects of NHE1 inhibitors and phenotypes induced by expression of NHE1 may vary with gender. We have previously shown (as described in Chapter 3) that increased expression of active NHE1 protein potentiates CH. In this study we examined the effects of elevated expression of wild type or constituitively active NHE1 in the myocardium of male mice. The comparative effects of expression of wild type vs. constituitively active NHE1 in the myocardium have not been examined in male mice. The implications of our results are several-fold:

NHE1 induced cardiac hypertrophy is not gender dependent

Expression of NHE1 in TG mice generated a pro-hypertrophic effect in male NHE1 TG mice, but the effects were principally in mice expressing an active form of NHE1 (K-line mice). K-line mice demonstrated increases in all markers of CH including the HW/BW, ANP mRNA expression, IF and CSA. Echocardiography revealed that male K-line mice had a number of morphological defects and global myocardial deterioration. The results with the K-line mice are largely in agreement with a recent study[231] that also expressed active NHE1 in the myocardium. However, in that study, the

gender used was not specified and it is assumed that a mixed population of both males and females were used. In addition, in that study, a large deletion of the NHE1 C-terminus (637-656 base pair region) was used in creating the TG mouse line, as opposed to the specific point mutations in the CaM binding region employed in our study (Figure 1.1) (as described in Section 2.1.2). Cook et al.[324] also compared male and female mice expressing wild type NHE1 subjected to I/R, not CH. They demonstrated that in TG mice expressing wild type NHE1, the effects of I/R on the mouse heart were not gender dependent. In addition to the I/R effects induced by NHE1, they also showed that expression of wild type NHE1 results in spontaneous development of heart failure, premature mortality, increased apoptotic cell death and cardiac remodeling in mice 8-11 months of age. Whether both our female and male mice, either expressing wild type NHE1 or active NHE1 develop such phenotype at that age needs further investigation. Both genders needed to be investigated because differences in the onset and progression of myocardial dysfunction and heart failure have been reported in murine models, with gender being the specific cause (reviewed in[362]). Females usually show a better preservation of function than males. For example, in TG mice expressing an α-MHC mutant[360,369], mice of both genders developed hypertrophy and left ventricular diastolic dysfunction to a similar degree at 3 months of age, and by 9 months the female mice continued to exhibit concentric hypertrophy whereas the male mice began to show signs of left ventricular dilatation, systolic dysfunction and exercise intolerance.

The degree of cardiac hypertrophy does not differ between genders

When the cardiac phenotypes of male and female NHE1 TG mice were

compared, the only significant difference seen was a decrease in the size of female K-line hearts relative to male K-line hearts. This decrease in size was indicated by a decrease in the HW/BW and the echocardiographic parameters, LVM and LVID during diastole. These differences were seen despite the fact that NHE1 expression was elevated in female K-line heart lysates vs. male K-line heart lysates. Similarly, the female control mice had a significantly smaller HW/BW, LVM and LVID during diastole. In addition, the female control mice had a significantly smaller IVSTd and LVID during systole. Whether this decrease in heart size in the female NHE1 TG mice was a result of estrogen could be investigated. These experiments could be carried out by ovariectomizing female NHE1 TG mice and comparing parameters of CH and cardiac function to a sham group. However, since these differences exist in the male vs. female control mice, it could be suggested that differences in the degree of hypertrophy were a result of the animal model not expression of the transgene.

NHE1 expression does not sensitize the myocardium of male NHE1 TG mice to neurohormonal stimulation

Male N-line and K-line mice were not sensitive to neurohormonal PE stimulation, which causes both CH and stimulates NHE1 activity[86,98,330,370]. The HW/BW between hearts treated with PBS vs. hearts stimulated with PE in male control, N-line and K-line hearts were not significantly different. However, we found that hearts from K-line mice stimulated with PE increased ANP mRNA expression. The large elevation of ANP levels by PE in the K-line hearts indicated that there was further progression of the hypertrophic response, but the progression may have not been significant enough to

cause an increase in the HW/BW. The result suggests that the presence of NHE1 in male mice does not sensitize the mice to further hypertrophic stimulation. When male and female hearts from control, N-line and K-line mice stimulated with PE were directly compared, no significant differences were found in the HW/BW and ANP mRNA expression. Since our female K-line hearts were susceptible to PE and were smaller than our male hearts, it could be suggested that male K-line hearts were not susceptible to PE due to the degree of hypertrophy.

Conclusion

Our data agrees with our previous report, which showed that NHE1 expression with elevated activity potentiated CH in female NHE1 TG mice. Increased expression of active NHE1 protein in male mice was also much more detrimental than expression of the wild type protein as was seen with the female NHE1 TG mice. Therefore, the NHE1 induced hypertrophic effect was not gender dependent. The degree of hypertrophy was also not significantly different between male and female NHE1 TG mice. Although, female NHE1 TG mice have smaller hearts and male NHE1 TG mice appear less susceptible than females to neurohormonal stimuli.

.

Chapter 6

Conclusions and Future Directions

6.1 Conclusions

NHE is a ubiquitously expressed plasma membrane glycoprotein, which extrudes one intracellular H^+ in exchange for one extracellular Na^+, and thus regulates pH_i[313]. Ten isoforms of NHE, NHE1-10, have been identified, which share 20-60% amino acid identity (reviewed in[36])[37]. NHE1 is the only cardio-specific plasma membrane isoform. It consists of an N-terminal membrane associated domain involved in ion transport and a C-terminal cytoplasmic regulatory tail (Figure 1.1). NHE1 is active at acidic pH's, but inactive at physiological pH's[68]. NHE1 activity is regulated via various agonists such as ET-1, Ang II, α_1-AR agonists, thrombin, and protein kinases such as the MAPKs, all of which act on the C-terminal tail of NHE1 (reviewed[87]). They change the set point so that the protein is more active at more alkaline pH[68]. NHE1 is also regulated by protein-protein interactions, which act either directly or indirectly on NHE1. The CaM binding site found on the C-terminal tail of NHE1 is an important regulatory site that binds CaM when complexed with Ca^{2+}. In the absence of CaM complexed to Ca^{2+}, the high affinity CaM binding site interacts with another region of NHE1 resulting in autoinhibition of NHE[115,116]. Deletion of the high affinity CaM binding site mimics elevated intracellular Ca^{2+} and results in a constituitively active NHE1 protein[115].

In the myocardium, NHE1 plays a critical role in I/R injury (reviewed in[186]) and is an important mediator of CH (reviewed in[87]). NHE1 protein expression and activity increase in response to various stimuli including acidosis[185,230,331], cardiotoxic metabolites released during I/R (reviewed in[188]) and CH (reviewed in[87]). NHE1 mRNA expression, protein expression or activity have been shown to be elevated in various *in vivo* models of CH[225,226,238,239,240]. Interestingly, in some CH models, NHE1 protein expression and

activity are increased[238,239], while in others NHE1 activity is increased in the absence of any alterations in NHE1 expression[240]. Similarily, during I/R NHE1 activity and mRNA expression were shown to be increased[184,185]. This increase in NHE1 activity/expression during I/R has been proposed to represent a major component of I/R injury (reviewed in[186]). The involvement of NHE1 in CH and I/R injury has been further supported with the use of NHE1 inhibitors, which have been beneficial in the prevention/regression of several models of CH and I/R injury (reviewed in[87,186]). It was unclear whether elevation of the protein level is sufficient for cardiac pathology, or whether activation of the protein is required. Since the unstimulated protein is relatively quiescent at resting physiological pH, it is questionable whether elevation of a non activated protein alone is detrimental to the myocardium. Activation of NHE1 could occur in more pathological situations. Kinases that phosphorylate NHE1 increase in the diseased myocardium[231]. Understanding the fundamental underlying mechanisms in the development of heart failure, particularly during pathological hypertrophy and I/R injury likely holds the key for potentially effective heart failure management.

The objective of my thesis was to understand how increased NHE1 protein and activity affects the myocardium's susceptibility to pathological hypertrophy and I/R injury. To understand the direct role of NHE1 in CH and I/R injury, an *in vivo* and *in vitro* gain-of-function model expressing varying levels and activities of NHE1 were examined. *In vivo*, our N-line mice expressed wild type NHE1 and our K-line mice expressed a constituitively active NHE1. Mutation of the CaM binding site allowed us to create an actived NHE1[115]. For *in vitro* studies, the IRM adenovirus contained wild type NHE1 and the K-IRM adenovirus contained the actived NHE1. A double mutation, L

163 to F and G 174 to S, in the N-terminal of NHE1 increased the resistance to NHE1 inhibition[309]. Having the IRM and K-IRM adenoviruses resistant to inhibition allowed us to study the effects of exogenous NHE1, while inhibiting endogenous NHE1. In order to determine whether further enhancing the activity of NHE1 increases the susceptibility to CH, both our *in vivo* and *in vitro* models were stimulated with PE, a hormonal α_1-AR agonist that is both pro-hypertrophic and a NHE1 stimulator. Our *in vivo* gain-of-function model was also used to understand the role of NHE1 in I/R using the *ex vivo* working heart perfusion model. The *ex vivo* working heart perfusion model includes FAs, the main source of ATP production in normal hearts and during reperfusion[333]. In previous reports the Langendorff perfusion model was used and hearts were perfused with only glucose as a substrate[204,205], which is not representative of the normal physiological substrate used by the myocardium. Lastly, since gender has been suggested to be an independent variable to cardiac phenotype[362,364] and NHE1 activity is regulated by sex hormones[365,366], we examined both male and female NHE1 TG mice expressing varying amounts of NHE1 for CH. The **hypothesis** is that enhanced NHE1 expression in the heart makes the myocardium more susceptible to CH and I/R injury and this is accentuated with further activation of the exchanger.

In NHE1 TG mice, expression of active NHE1 caused significant increases in the HW/BW, apoptosis, CSA, IF and decreased cardiac performance. Wild type NHE1 caused a much milder pathology. The increased expression of wild type NHE1 caused increased HW/BW and ANP mRNA expression. However, no significant changes were observed in the histology of the heart (CSA and IF) in N-line mice. In N-line mice, systolic function (%FS and EF) and diastolic function (MV E/A ratio) were altered, but

not to the degree that would induce global deterioration of the heart. *In vitro*, expression of active NHE1 in NRVMs also promoted CH. Inhibition of endogenous NHE1 with EMD 87580, inhibited expression of CH, thus suggesting that both endogenous and exogenous expression of active NHE1 are required to induce CH *in vitro*. Expression of wild type NHE1 *in vitro* was not sufficient to induce CH. Thus, our *in vivo* and *in vitro* data confirms the direct role of NHE1 in CH and provides further support for the use of NHE1 inhibitors in CH. NHE1 inhibitors have been shown to attenuate CH in various models (reviewed in[87]). We also confirm a previous report[20], which shows that active NHE1 induces CH. Our findings directly distinguish between the effects of increased expression of wild type NHE1 (N-line) vs. expression of active NHE1 (K-line). NHE1 mRNA expression, protein expression or activity have been shown to be elevated in various *in vivo* models of CH[225,226,238,239,240]. However, in some CH models, NHE1 protein expression and activity are increased[238,239], while in others NHE1 activity is increased in the absence of any alterations in NHE1 expression[240]. In our study, we clearly show that enhanced expression of active NHE1 is essential to induce CH.

This NHE1 induced hypertrophic effect in NHE1 TG mice was not associated with any increases in calcineurin or phosphorylation of ERK, p38, JNK or RSK pathways that have been implicated in the development of CH[325,326] and regulation of NHE1[87,326]. A previous report[231], in which active NHE1 was expressed in TG mice demonstrated that p38 and ERK were significantly activated. This discrepancy could be due in part to the differences in regions mutated on the C-terminus of NHE1, which may have caused a more extreme activation of the NHE1 protein. The early and more severe effects of NHE1 expression shown in that study[231] support this suggestion. If activation

of these kinases only occurs with later severe stages of the pathology, the activation of these pathways are likely a later consequence of heart failure. We also did not find any differences in total GSK-3β in hearts from N-line and K-line mice. Catalytically-active GSK-3β has been implicated in anti-hypertrophic signaling[380]. In addition, the activation of GSK-3β has been attributed to the anti-hypertrophic effect of NHE1 inhibition[381]. The lack of GSK-3β expression would be expected since the NHE1 TG mice develop CH.

Numerous studies in humans and experimental animals have demonstrated elevated plasma levels of catecholamines in conditions that are associated with cardiac overload and congestive heart failure. Catecholamines such as PE have also been shown to shift the pH_i/NHE1 activity relationship to the right, thus raising the pH_i threshold for NHE1[93,94]. In order to determine whether further enhancing the activity of NHE1 increases the susceptibility to CH, both our *in vivo* and *in vitro* models were stimulated with PE. Expression of active NHE1 in intact mice increased the sensitivity to PE induced CH, while expression of wild type NHE1 in the intact mice did not increase the susceptibility to PE induced CH. The difference in response to PE could be due to the different gene profile seen with our N-line and K-line mice[384]. Expression of certain genes that maybe upregulated or downregulated with the expression of active NHE1 could account for the increased susceptibility of K-line mice to PE stimulation. In contrast to our *in vivo* data, NRVMs infected with K-IRM (active NHE) adenovirus appeared resistant to further PE stimulation, possibly because they had already reached a maximal level of stimulation. Or this maybe confirming our predication that expression of other genes maybe contributing to the enhanced susceptibility of K-line mice to PE stimulation.

In murine/or rat models, heart failure has been shown to be accelerated in the male animal model[357,358]. Similarly, in humans, the prognosis for women has being significantly better than for men[355,356]. Therefore, we examined both male and female mice for CH. We demonstrated that the NHE1 dependent hypertrophic response was not gender dependent. Both the male and female NHE1 TG mice developed CH. The similar phenotype seen between our male and female NHE1 TG mice is in agreement with Cook et al.[324], who demonstrated that in TG mice expressing wild type NHE1, no differences existed between female and male hearts subjected to I/R. Perhaps the effects of estrogen seen *in vitro*[365] on NHE1 expression and CH does not translate to the *in vivo* model due to a compensatory effect. We suggested that the degree of hypertrophy was also not significantly different between male and female NHE1 TG mice. The significant increase in the HW/BW and echocardiographic parameters maybe be induced by the FVB model, since these changes were observed in both our NHE1 TG mice and control.

While inhibition of NHE1 activity has been shown to be beneficial in several cardiovascular diseases (reviewed in[186]), recent reports have suggested that elevation of NHE1 activity may also have beneficial effects during I/R[204,205], thus protecting the heart from I/R injury. In I/R it was unclear whether elevation of NHE1 was sufficient for cardioprotection, or whether activation of the protein was required. Therefore, we examined the effects of cardiac specific expression of wild type NHE1 (N-line) or activated NHE1 protein (K-line) in hearts subjected to I/R. In our study, intact hearts from control and NHE1 TG mice were perfused under working conditions with FAs and glucose present as substrates, unlike previous reports, which used the Langendorff perfusion model[204,205]. The working heart model was used because it has a higher and

more physiological energy demand compared with the Langendorff perfused hearts[347]. In addition, the KHB perfusate used in our study contained both glucose and FAs, making it more representative of normal human plasma in the setting of ischemia[348]. Palmitate is the preferred energy substrate of the normal perfused heart[332] and is used by the myocardium in reperfusion[301].

Hearts were subjected to 30 minutes of aerobic perfusion, followed by 20 minutes of global no-flow ischemia and 40 minutes of aerobic reperfusion. K-line hearts expressing activated NHE1 recovered to a much greater extent than N-line and control hearts, recovering to almost 75% of their preischemic function. In addition, K-line hearts had elevated FA oxidation, increased glycolysis rates, elevated ATP production rates, and increased cardiac efficiency in the postischemic heart relative to N-line or control hearts. The enhanced ATP production rate is in agreement with our previous report which demonstrated a minor improvement in ATP following I/R in K-line mice[204]. This occurred despite the difference in perfusion models used in both studies. In addition, similar to a previous report[204,205], cardiac specific expression of wild type (N-line) or activated NHE1 (K-line) does not functionally compromise the heart function during aerobic perfusion (preischemia). However, in our study, contrary to previous reports[204,205], only activated NHE1 (K-line) was cardioprotective. Earlier it was found that cardioprotection occurred in both hearts that expressed wild type NHE1 and constituitively active NHE1[204]. Cook et al.[205] also demonstrated that elevated NHE1 expression in TG mice induces a cardioprotective effect in hearts subjected to I/R. The difference between this and previous reports is likely due to the difference in the perfusion conditions. Either inclusion of FAs or the greater workload of the present study

was likely accountable. The activated NHE1 protein maybe more effective at cardioprotection in comparison with increased levels of the non-activated protein as it may provide a more functional protein at a critical pH. This is evident since in our K-line mice we see improved cardioprotection despite elevated proton production. In K-line *ex vivo* working hearts, glycolysis was significantly elevated during both preischemic and postischemic periods, which contributed to higher ATP production rates and proton production. The ability of activated NHE1 to maintain pH_i was shown in our previous report, where NHE1 TG mice were perfused with the Langendorff model[204]. Opie[352] has suggested that enhanced glycolysis is more beneficial to the myocardium when pH_i is maintained appropriately. It maybe that elevated activity of the K-line NHE1 protein coupled with enhanced, but "pH managed" glycolysis, were responsible for at least part of the protective effects that were observed. This is contrary to some reports which show that if glycolysis is increased to a greater extent than glucose oxidation, an increased proton load on the heart can occur, which can contribute to a decrease in cardiac efficiency and a decrease in functional recovery postischemia[339]. In K-line hearts, proton production from uncoupled glycolysis to glucose oxidation was actually increased. Despite this, these hearts showed the best recovery of function postischemia. This data challenges the widely held belief that excessive NHE1 activity contributes to I/R injury, but rather suggests that maintenance of pH is more important in postischemic recovery.

An examination of kinase activation showed that there were no differences between control and NHE1 TG mice in protein expression of AMPK, ERK, p38, RSK or GSK3β levels, pathways activated by myocardial I/R[338,340,341,353]. However, phosphorylated JNK (normalized to total JNK) was significantly decreased in K-line

hearts vs. control and N-line hearts. JNK is activated in response to various cellular stresses including inflammatory cytokines, ischemia, reversible ATP depletion, heat shock, endotoxin, and genotoxic stress[354]. The decrease in phosphorylated JNK protein expression in hearts subjected to I/R provides further evidence that our K-line hearts were not as energetically or functionally stressed as control and N-line hearts. However, ER stress response proteins, calreticulin and PDI, were increased relative to controls. The ER stress response has previously been suggested to contribute to the cardioprotective effects of elevated expression of NHE1[205]. However, no studies examined whether such response occurs in TG mice expressing elevated active NHE1. Induction of multiple ER stress associated genes have been reported to lead to a dramatic reduction in infarct size following I/R injury[346]. We have suggested that the elevated levels of the stress response protein could account for some of their improved cardiac performance during I/R.

Our results demonstrate that elevated levels of NHE1 induce cardioprotection in hearts subjected to I/R despite the increased proton load and alter cardiac energy metabolism. However, in the working heart model with glucose and FAs as substrates, this required an activated NHE1 protein. The data suggests that maintenance of pH is most important to postischemic recovery.

In conclusion, this study examined the direct effect of NHE1 in various cardiac pathologies. I demonstrated for the first time that active NHE1 expression makes the myocardium more susceptible to CH, independent of MAPKs and calcineurin and gender. Expression of wild type NHE1 induces milder hypertrophic responses. Although the active NHE1 induces CH, when subjected to I/R, it protects the heart against I/R injury by increasing FA oxidation, glycolysis rates, thus generating greater ATP

production rates and activating the ER stress response proteins.

6.2 Future Directions

Our present study demonstrated both *in vivo* and *in vitro*, that active NHE1 is directly involved in the development of CH, independent of calcineurin, MAPKs and gender. Also that active NHE1 protects the heart from I/R injury by some how increasing FA oxidation and glycolysis rates. The future studies I have outlined will further examine the role of NHE1 in various cardiac pathologies and contribute to our understanding of how to regulate NHE1 in the myocardium and prevent CH.

6.2.1 NHE1 Loss of Function Model

Although *in vitro* approaches are advantageous when examining a direct effect in the absence of other contributing factors, they do not provide a complete picture of the complex underlying mechanisms contributing to a pathophysiology[199]. Therefore, genetic animal models are widely used for understanding the molecular mechanisms and determinants of heart failure[371]. The findings derived from these studies should also be interpreted carefully, since heart failure is a complex and multifactorial disease often complicated by other underlying complications. In addition, adaptive changes often occur in response to chronic overexpression of a mutated protein. A loss of function model, in which NHE1 is deleted specifically in the heart could be created and characterized for both CH and I/R. This will confirm the role of NHE1 in CH and I/R and ensure that the phenotypes observed in our NHE1 TG mice were not due to an imbalance of the stoichiometry of the expressed protein or compensatory changes[371]. The

ability to selectively eliminate NHE1 from the myocardium, while preserving the remainder of the body in a wild-type state is very important. NHE1 is a ubiquitous protein with many physiological roles (as discussed in Section 1.6), therefore globally deleting NHE1 is detrimental to the functioning of the physiological system. The consequences of the lack of tissue specific gene targeting is clearly demonstrated in the Wang et al.[372] study. In this model, the role of NHE1 was examined in hearts subjected to I/R using hearts from gene-targeted NHE1-null mutant mice. Genetic ablation of NHE1 resulted in cardioprotective effects. However, these results need to be carefully analyzed, since NHE1 gene deletion was not specific and the mice exhibited growth retardation and were subject to slow-wave epilepsy[266,373]. Specific deletion of NHE1 in the heart could be carried out by intercrossing mice expressing the homozygous conditional null mutation in the NHE1 with α-MHC-Cre mice, generating α-MHC-Cre/NHE1-mutant mice[374]. The Cre transgene allows for site-specific gene rearrangement selectively in cardiomyocytes[374].

We believe that the cardiac specific NHE1 loss of function model will be less susceptible to pathological hypertrophy, since expression of NHE1 is required for the induction of CH. However, since NHE1 has a number of physiological roles including cell growth and proliferation (as described in Section 1.6) and N-line mice expressing wild type NHE1 only showed mild hypertrophic expression, we expect that the loss of NHE1 function may be associated with some undue effects. In the NHE1 null mutant mice, the mean body weight and heart weight were both significantly lower than control mice[372]. However, there was no significant difference in the mean heart weight to body weight ratio. It was suggested that the smaller hearts in the knockout were due to growth

retardation. In the working heart model, the absence of NHE1 in hearts subjected to I/R may increase their susceptibility to I/R injury. We have shown that increased levels of NHE1 may be beneficial to hearts subjected to I/R by coping with elevated proton production that occurs with elevated FA oxidation and glycolysis. Therefore, a lack of NHE1 prevents hearts subjected to I/R from coping with elevated proton production. Although these results might contradict the Wang et al. model[372] and data obtained with NHE1 inhibitors (reviewed in[186]), a cardiac specific loss of function model is more representative of the cardiac effects of NHE1 expression and absent from the non specific effects of NHE1 inhibitors. These studies will provide further insight into new potential and different strategies to treat CH and I/R injury.

6.2.2 Characterization of the Aging NHE1 Transgenic Mice

Heart failure is usually a disease of older patients induced by age related alterations in gene expression or signaling pathways[371]. Approximately 38% of individuals aged 40-59 have some form of cardiovascular disease, and this almost doubles to approximately 73% in individuals aged 60-79[375]. Data from the Framingham Heart Study and the Baltimore Longitudinal Study on aging demonstrated that with age, the prevalence of left ventricular hypertrophy increases, diastolic function declines and left ventricular wall thickness increases progressively in both sexes[376]. Cardiac aging in the murine model closely recapitulates the human age-related cardiac changes, the heart becomes hypertrophic and diastolic function declines with age.

Cook et al.[324] previously demonstrated that enhanced expression of wild type NHE1 in mice 8-11 months of age results in spontaneous development of heart failure,

premature mortality, increased apoptotic cell death and cardiac remodeling. The cardiac phenotype induced by expression of wild type NHE1 appears to accumulate and cause more severe pathological changes with age. The importance of age and its relevance to NHE1 during cardiac disease has been emphasized in another report[206]. In this report, NHE1 inhibitors were protective against I/R injury in mature human hearts, but had no benefit on the post-ischemic functional recovery of the aged myocardium.

To further investigate the effects of NHE1 expression in the aged myocardium, both males and female N-line and K-line mice could be examined for parameters of CH at 7, 9 and 11 months. Both genders need to be investigated because gender specific differences in the onset and progression of myocardial dysfunction and heart failure have been reported in murine models (reviewed in[362]). Although NHE1 expression was investigated at various time points (Figure 3.25) and NHE1 protein expression was shown to be maintained, we will expand our time scale and look at NHE1 expression and activity in hearts from NHE1 TG mice 6 months in age and follow up until 12 months of age. This will allow us to ensure that NHE1 expression is maintained. Using the male and female NHE1 TG mice, we could then go on to examine for CH at 7, 9, and 11 months. This may provide further insights into whether NHE1 expression accentuates the hypertrophic response with age, and whether any differences exist in the male and female mice with aging. We expect that with age, NHE1 protein expression will not change, and the influence of age altering genes will accentuate the hypertrophic phenotype in NHE1 TG mice. Although we have not examined age altering genes, we know that our N-line and K-line mice are associated with numerous changes in gene expression. Analysis of gene expression pattern in NHE1 TG mice demonstrated that N-line mice had modest

changes in gene expression (50 up-regulations and 99 down-regulations), whereas K-line hearts had a very strong transcriptional response (640 up-regulations and 677 down-regulations)[384]. The most significant changes in gene expression were involved in CH, cardiac necrosis/cell death and cardiac infarction. Based on the number of changes observed in gene expression, we would expect that our NHE1 TG mice gene profile will change with age and induce age altering genes.

Furthermore, N-line mice expressing wild type NHE1, which have shown mild CH when examined at 10-12 weeks of age (Chapter 3 and 5), are expected to have a more severe hypertrophic response as they age. In our preliminary studies, we examined the survival rate of N-line mice over a nine month period and found that these mice survived throughout the study[275]. However, the survival rate slightly declined following 7 months of age. K-line mice, expressing active NHE1, are predicted not to survive past 11 months of age due to the severity of the phenotype observed at 10-12 weeks of age (Chapter 3 and 5). Our preliminary studies provide further evidence in support of this prediction. Examination of the survival rate of K-line mice over nine months showed that at 8 months of age only 40% of the K-line mice were alive[275]. Furthermore, we have demonstrated that male mice have a greater HW/BW ratio and LVM, IVSTd and LVID, indicators of myocardial remodeling measured by echocardiography vs. female mice (Chapter 5), thus we believe that the male mice will develop a greater degree of hypertrophy with age vs. female NHE1 TG mice. However, this may change when the female NHE1 TG mice reach menopause. Female K-line NHE1 TG mice may also have a lower rate of survival during pregnancy. The K-line female mice appear to be sensitive to the stress induced by pregnancy, causing a relatively high rate of mortality during

gestation that was associated with cardiovascular failure.

We could also investigate the effects of NHE1 expression during I/R in the aged myocardium. The aged myocardium is more susceptible to ischemia and hemodynamic stress than the young myocardium[377]. We believe that even under these conditions, expression of active NHE1 will protect the heart from I/R injury. Since heart failure is usually a disease of older patients and NHE1 has been implicated in various cardiac diseases, understanding its role in the aged myocardium is essential to the development of clinical trials targeting NHE1.

6.2.3 Modulation of Mediators Involved in NHE1 Regulation

Since NHE1 appears to play a double edged sword effect, where on one side it induces CH while on the other side it is protective against I/R injury, it maybe useful to investigate modulation of NHE1 regulators vs. directly targeting NHE1. NHE1 is regulated by a number of factors (as discussed in Section 1.5). RSK is known to phosphorylate and regulate NHE1 activity. It is activated in response to various cardiac pathologies (reviewed[378]). In addition, RSK activity has been reported to be upregulated in the failing human myocardium[379]. The importance of RSK and NHE1 in cardiac pathology are clearly identified in one study, where mice expressing a dominant negative RSK mutant were associated with enhanced myocardial resistance to I/R injury[198]. These dominant negative RSK TG mice exhibit reduced infarct size, decreased cardiomyocyte apoptosis, and partially preserved cardiac function after I/R. In these mice, the activation of RSK and interaction with NHE1 were increased by I/R and inhibited in the dominant negative RSK TG mice. To investigate whether modulation of RSK alters the cardiac

pathology, N-line and K-line mice could be cross bred with TG mice expressing cardiac specific dominant negative RSK. Thus, it would be expected that dominant negative RSK will inhibit NHE1 activity and prevent CH, more so in the K-line mice. Targeting NHE1 activators may be beneficial since in previous clinical trials increased incidence of mortality and cerebrovascular events were reported with direct NHE inhibition (reviewed in[70]). In addition, this maybe a more appropriate solution to a problem with a double edge sword effect.

6.2.5 Summary

NHE1 plays an important role in cardiovascular disease. My present studies provide more information on NHE1's role and regulation in various cardiac pathologies. This includes new insight in the requirement of an activated protein for pathological effects in CH. In addition, we further confirmed that NHE1 has some beneficial effects in I/R, particulary the active form of the protein. Since NHE1 required activation to induce CH, alternative targets such as those that activate NHE1 have been suggested as a means of preventing the detrimental effects see in CH.

Chapter 7

References

1. Garcia-Moreno B. Adaptations of proteins to cellular and subcellular pH. *J Biol*. 2009;8(11):98.

2. Allen DG, Orchard CH. The effects of changes of pH on intracellular calcium transients in mammalian cardiac muscle. *J Physiol*. 1983;335:555-567.

3. Bountra C, Vaughan-Jones RD. Effect of intracellular and extracellular pH on contraction in isolated, mammalian cardiac muscle. *J Physiol*. 1989;418:163-187.

4. Orchard CH, Kentish JC. Effects of changes of pH on the contractile function of cardiac muscle. *Am J Physiol*. 1990;258(6 Pt 1):C967-981.

5. Harrison SM, Frampton JE, McCall E, Boyett MR, Orchard CH. Contraction and intracellular Ca^{2+}, Na^{+}, and H^{+} during acidosis in rat ventricular myocytes. *Am J Physiol*. 1992;262(2 Pt 1):C348-357.

6. Vaughan-Jones RD, Spitzer KW, Swietach P. Intracellular pH regulation in heart. *J Mol Cell Cardiol*. 2009;46(3):318-331.

7. Cordat E, Casey JR. Bicarbonate transport in cell physiology and disease. *Biochem J*. 2009;417(2):423-439.

8. Vaughan-Jones RD. *J. Physiol. (Lond.)*. 1979;295:111.

9. Deitmer JW, Ellis D. Interactions between the regulation of the intracellular pH and sodium activity of sheep cardiac Purkinje fibres. *J Physiol*. 1980;304:471-488.

10. de Hemptinne A, Marrannes R, Vanheel B. Influence of organic acids on intracellular pH. *Am J Physiol*. 1983;245(3):C178-183.

11. Vaughan-Jones RD. Regulation of intracellular pH in cardiac muscle. *Ciba Found Symp*. 1988;139:23-46.

12. Dart C, Vaughan-Jones RD. Na^{+}-HCO_3^{-} symport in the sheep cardiac Purkinje fibre. *J Physiol*. 1992;451:365-385.

13. Hoffmann E, L.O. S. Membrane mechanisms in volume and pH regulation in vertebrate cells. [Review]. *Physiol. Rev*. 1989;69:315-382.

14. Lagadic-Gossmann D, Buckler KJ, Vaughan-Jones RD. Role of bicarbonate in pH recovery from intracellular acidosis in the guinea-pig ventricular myocyte. *J Physiol*. 1992;458:361-384.

15. Xu P, Spitzer KW. Na-independent Cl^--HCO_3^- exchange mediates recovery of pHi from alkalosis in guinea pig ventricular myocytes. *Am J Physiol*. 1994;267(1 Pt 2):H85-91.

16. Sun B, Leem CH, Vaughan-Jones RD. Novel chloride-dependent acid loader in the guinea-pig ventricular myocyte: part of a dual acid-loading mechanism. *J Physiol*. 1996;495 (Pt 1):65-82.

17. Casey JR, Grinstein S, Orlowski J. Sensors and regulators of intracellular pH. *Nat Rev Mol Cell Biol*.11(1):50-61.

18. Niederer SA, Swietach P, Wilson DA, Smith NP, Vaughan-Jones RD. Measuring and modeling chloride-hydroxyl exchange in the Guinea-pig ventricular myocyte. *Biophys J*. 2008;94(6):2385-2403.

19. Poole RC, Halestrap AP, Price SJ, Levi AJ. The kinetics of transport of lactate and pyruvate into isolated cardiac myocytes from guinea pig. Kinetic evidence for the presence of a carrier distinct from that in erythrocytes and hepatocytes. *Biochem J*. 1989;264(2):409-418.

20. Grace AA, Kirschenlohr HL, Metcalfe JC, Smith GA, Weissberg PL, Cragoe EJ, Jr., Vandenberg JI. Regulation of intracellular pH in the perfused heart by external HCO_3^- and Na^+-H^+ exchange. *Am. J. Physiol*. 1993;265(1 Pt 2):H289-H298.

21. Dart C, Vaughan-Jones RD. Na^+-HCO_3^- symport in the sheep cardiac purkinje fibre. *J. Physiol*. 1992;451:365-385.

22. Lagadic-Gossmann D, Buckler KJ, Vaughan-Jones RD. Role of bicarbonate in pH recovery from intracellular acidosis in the guinea-pig ventricular myocyte. *J. Physiol*. 1992;458:361-384.

23. Bers DM, Despa S. Na^+ transport in cardiac myocytes; Implications for excitation-contraction coupling. *IUBMB Life*. 2009;61(3):215-221.

24. Pike MM, Kitakaze M, Marban E. ^{23}Na-NMR measurements of intracellular sodium in intact perfused ferret hearts during ischemia and reperfusion. *Am J Physiol*. 1990;259(6 Pt 2):H1767-1773.

25. Butwell NB, Ramasamy R, Lazar I, Sherry AD, Malloy CR. Effect of lidocaine on contracture, intracellular sodium, and pH in ischemic rat hearts. *Am J Physiol*. 1993;264(6 Pt 2):H1884-1889.

26. Donoso P, Mill JG, O'Neill SC, Eisner DA. Fluorescence measurements of cytoplasmic and mitochondrial sodium concentration in rat ventricular myocytes. *J Physiol*. 1992;448:493-509.

27. Despa S, Islam MA, Weber CR, Pogwizd SM, Bers DM. Intracellular Na^+ concentration is elevated in heart failure but Na/K pump function is unchanged. *Circulation*. 2002;105(21):2543-2548.

28. Pieske B, Houser SR. $[Na^+]_i$ handling in the failing human heart. *Cardiovasc Res*. 2003;57(4):874-886.

29. Pogwizd SM, Sipido KR, Verdonck F, Bers DM. Intracellular Na^+ in animal models of hypertrophy and heart failure: contractile function and arrhythmogenesis. *Cardiovasc Res*. 2003;57(4):887-896.

30. Murphy E, Eisner DA. Regulation of intracellular and mitochondrial sodium in health and disease. *Circ Res*. 2009;104(3):292-303.

31. O'Rourke B, Maack C. The role of Na^+ dysregulation in cardiac disease and how it impacts electrophysiology. *Drug Discov Today Dis Models*. 2007;4(4):207-217.

32. Owen P, Dennis S, Opie LH. Glucose flux rate regulates onset of ischemic contracture in globally underperfused rat hearts. *Circ Res*. 1990;66(2):344-354.

33. Tani M, Neely JR. Na^+ accumulation increases Ca^{2+} overload and impairs function in anoxic rat heart. *J Mol Cell Cardiol*. 1990;22(1):57-72.

34. Sardet C, Franchi A, Pouysségur J. Molecular cloning, primary structure, and expression of the human growth factor-activatable Na^+/H^+ antiporter. *Cell*. 1989;56:271-280.

35. Cingolani HE. Na^+/H^+ exchange hyperactivity and myocardial hypertrophy: are they linked phenomena? *Cardiovasc Res*. 1999;44(3):462-467.

36. Malo ME, Fliegel L. Physiological role and regulation of the Na^+/H^+ exchanger. *Can J Physiol Pharmacol*. 2006;84(11):1081-1095.

37. Lee SH, Kim T, Park ES, Yang S, Jeong D, Choi Y, Rho J. NHE10, an osteoclast-specific member of the Na^+/H^+ exchanger family, regulates osteoclast differentiation and survival [corrected]. *Biochem Biophys Res Commun*. 2008;369(2):320-326.

38. Orlowski J, Grinstein S. Diversity of the mammalian sodium/proton exchanger SLC9 gene family. *Pflugers Arch*. 2004;447(5):549-565.

39. Fliegel L, Sardet C, Pouyssegur J, Barr A. Identification of the protein and cDNA of the cardiac Na^+/H^+ exchanger. *FEBS Lett*. 1991;279(1):25-29.

40. Petrecca K, Atanasiu R, Grinstein S, Orlowski J, Shrier A. Subcellular localization of the Na^+/H^+ exchanger NHE1 in rat myocardium. *Am J Physiol*. 1999;276(2 Pt 2):H709-717.

41. Fliegel L, Dyck JRB, Wang H, Fong C, Haworth RS. Cloning and analysis of the human myocardial Na^+/H^+exchanger. *Mol. Cell. Biochem*. 1993;125:137-143.

42. Orlowski J, Grinstein S. Na^+/H^+ exchangers of mammalian cells. *J. Biol. Chem*. 1997;272:22373-22376.

43. Collins JF, Honda T, Knobel S, Bulus N, Conary J, DuBois R, Ghishan FK. Molecular cloning, sequencing, tissue distribution, and functional expression of a Na^+/H^+ exchanger (NHE2). *Proc. Natl. Acad. Sci. USA*. 1993;90:3938-3942.

44. Wang Z, Orlowski J, Shull GE. Primary structure and functional expression of a novel gastrointestinal isoform of the rat Na^+/H^+ exchanger. *J. Biol. Chem*. 1993;268:11925-11928.

45. Tse CM, Levine SA, Yun CH, Montrose MH, Little PJ, Pouyssegur J, Donowitz M. Cloning and expression of a rabbit cDNA encoding a serum-activated ethylisopropylamiloride-resistant epithelial Na^+/H^+ exchanger isoform (NHE-2). *J Biol Chem*. 1993;268(16):11917-11924.

46. Orlowski J, Kandasamy RA, Shull GE. Molecular cloning of putative members of the Na^+/H^+ exchanger gene family. *J. Biol. Chem*. 1992;267:9331-9339.

47. Hoogerwerf WA, Tsao SC, Devuyst O, Levine SA, Yun CH, Yip JW, Cohen ME, Wilson PD, Lazenby AJ, Tse CM, Donowitz M. NHE2 and NHE3 are human and rabbit intestinal brush-border proteins. *Am J Physiol*. 1996;270(1 Pt 1):G29-41.

48. Tse CM, Brant SR, Walker MS, Pouyssegur J, Donowitz M. Cloning and sequencing of a rabbit cDNA encoding an intestinal and kidney-specific Na^+/H^+ exchanger isoform (NHE3). *J Biol Chem*. 1992;267(13):9340-9346.

49. D'Souza S, Garcia-Cabado A, Yu F, Teter K, Lukacs G, Skorecki K, Moore H-P, Orlowski J, Grinstein S. The epithelial sodium-hydrogen antiporter Na^+/H^+ exchanger 3 accumulates and is functional in recycling endosomes. *J. Biol. Chem*. 1998;273:2035-2043.

50. Baird NR, Orlowski J, Szabo EZ, Zaun HC, Schultheis PJ, Menon AG, Shull GE. Molecular cloning, genomic organization, and functional expression of Na^+/H^+ exchanger isoform 5 (NHE5) from human brain. *J. Biol. Chem*. 1999;274:4377-4382.

51. Klanke CA, Su YR, Callen DF, Wang Z, Meneton P, Baird N, Kandasamy RA, Orlowski J, Otterud BE, Leppert M, Shull GE, Menon AG. Molecular cloning and physical and genetic mapping of a novel human Na^+/H^+ exchanger (NHE5/SLC9A5) to chromosome 16q22.1. *Genomics*. 1995;25:615-622.

52. Szabo EZ, Numata M, Shull GE, Orlowski J. Kinetic and pharmacological properties of human brain Na^+/H^+ exchanger isoform 5 stably expressed in Chinese hamster ovary cells. *J Biol Chem*. 2000;275(9):6302-6307.

53. Nakamura N, Tanaka S, Teko Y, Mitsui K, Kanazawa H. Four Na^+/H^+ exchanger isoforms are distributed to Golgi and post-Golgi compartments and are involved in organelle pH regulation. *J. Biol. Chem*. 2005;280(2):1561-1572.

54. Brett CL, Wei Y, Donowitz M, Rao R. Human Na^+/H^+ exchanger isoform 6 is found in recycling endosomes of cells, not in mitochondria. *Am J Physiol Cell Physiol*. 2002;282(5):C1031-1041.

55. Numata M, Orlowski J. Molecular cloning and characterization of a novel $(Na^+,K^+)/H^+$ exchanger localized to the trans-Golgi network. *J Biol Chem*. 2001;276(20):17387-17394.

56. Wang D, King SM, Quill TA, Doolittle LK, Garbers DL. A new sperm-specific Na^+/H^+ exchanger required for sperm motility and fertility. *Nat Cell Biol*. 2003;5(12):1117-1122.

57. Woo AL, James PF, Lingrel JB. Roles of the Na,K-ATPase alpha4 isoform and the Na^+/H^+ exchanger in sperm motility. *Mol Reprod Dev*. 2002;62(3):348-356.

58. Grinstein S, Woodside M, Waddell TK, Downey GP, Orlowski J, Pouyssegur J, Wong DC, Foskett JK. Focal localization of the NHE1 isoform of the Na^+/H^+ antiport: assessment of effects on intracellular pH. *EMBO J*. 1993;12(13):5209-5218.

59. Biemesderfer D, Dekan G, Aronson PS, Farquhar MG. Assembly of distinctive coated pit and microvillar microdomains in the renal brush border. *Am J Physiol*. 1992;262(1 Pt 2):F55-67.

60. Leem CH, Lagadic-Gossmann D, Vaughan-Jones RD. Characterization of intracellular pH regulation in the guinea-pig ventricular myocyte. *J Physiol*. 1999;517 (Pt 1):159-180.

61. Avkiran M, Haworth RS. Regulatory effects of G protein-coupled receptors on cardiac sarcolemmal Na^+/H^+ exchanger activity: signaling and significance. *Cardiovasc. Res*. 2003;57(4):942-952.

62. Aronson PS. Kinetic properties of the plasma membrane Na^+/H^+ exchanger. *Annu Rev Physiol*. 1985;47:545-560.

63. Paris S, Pouyssegur J. Growth factors activate the Na^+/H^+ antiporter in quiescent fibroblasts by increasing its affinity for intracellular H^+. *J Biol Chem*. 1984;259(17):10989-10994.

64. Wakabayashi S, Pang T, Su X, Shigekawa M. A novel topology model of the human Na^+/H^+ exchanger isoform 1. *J. Biol. Chem*. 2000;275:7942-7949.

65. Wakabayashi S, Hisamitsu T, Pang T, Shigekawa M. Mutations of Arg440 and Gly455/Gly456 oppositely change pH sensing of Na^+/H^+ exchanger 1. *J Biol Chem*. 2003;278(14):11828-11835.

66. Slepkov ER, Rainey JK, Sykes BD, Fliegel L. Structural and functional analysis of the Na^+/H^+ exchanger. *Biochem. J*. 2007;401(3):623-633.

67. Haworth RS, Frohlich O, Fliegel L. Multiple carbohydrate moieties on the Na^+/H^+ exchanger. *Biochem. J*. 1993;289:637-640.

68. Counillon L, Pouysségur J, Reithmeier RAF. The Na^+/H^+ exchanger NHE1 possesses N- and O-linked glycosylation restricted to the first N-terminal extracellular domain. *Biochem*. 1994;33:10463-10469.

69. Benos DJ. Amiloride: a molecular probe of sodium transport in tissues and cells. *Am J Physiol*. 1982;242(3):C131-145.

70. Masereel B, Pochet L, Laeckmann D. An overview of inhibitors of Na^+/H^+ exchanger. *Eur J Med Chem*. 2003;38(6):547-554.

71. Blaauw Y, Beier N, van der Voort P, van Hunnik A, Schotten U, Allessie MA. Inhibitors of the Na^+/H^+ exchanger cannot prevent atrial electrical remodeling in the goat. *J Cardiovasc Electrophysiol*. 2004;15(4):440-446.

72. Scholz W, Albus U, Lang HJ, Linz W, Martorana PA, Englert HC, Scholkens BA. HOE 694, a new Na^+/H^+ exchange inhibitor and its effects in cardiac ischaemia. *Br J Pharmacol*. 1993;109(2):562-568.

73. Scholz W, Albus U, Counillon L, Gogelein H, Lang HJ, Linz W, Weichert A, Scholkens BA. Protective effects of HOE 642, a selective sodium-hydrogen exchange subtype 1 inhibitor, on cardiac ischaemia and reperfusion. *Cardiovasc Res*. 1995;29(2):260-268.

74. Baumgarth M, Beier N, Gericke R. (2-Methyl5(methylsulfonyl)benzoyl)guanidine Na^+/H^+ antiporter inhibitors. *J Med Chem*. 1997;40(13):2017-2034.

75. Gumina RJ, Buerger E, Eickmeier C, Moore J, Daemmgen J, Gross GJ. Inhibition of the Na^+/H^+ exchanger confers greater cardioprotection against 90 minutes of myocardial ischemia than ischemic preconditioning in dogs. *Circulation*. 1999;100(25):2519-2526; discussion 2469-2572.

76. Le Grand B, Marty A, Talmant JM, John GW. HOE 694 affords protection versus veratrine contractures in rat atria by Na^+ channel blockade. *Fundam Clin Pharmacol*. 1996;10(5):467-473.

77. Karmazyn M, Sawyer M, Fliegel L. The Na^+/H^+ exchanger: a target for cardiac therapeutic intervention. *Curr. Drug Targets Cardiovasc. Haematol. Disord*. 2005;5(4):323-335.

78. Mentzer RM, Jr., Lasley RD, Jessel A, Karmazyn M. Intracellular sodium hydrogen exchange inhibition and clinical myocardial protection. *Ann Thorac Surg*. 2003;75(2):S700-708.

79. Jung YS, Kim MY, Kim MJ, Oh KS, Yi KY, Lee S, Yoo SE, Lee BH. Pharmacological profile of KR-33028, a highly selective inhibitor of Na^+/H^+ exchanger. *Eur J Pharmacol*. 2006;535(1-3):220-227.

80. Lee BH, Yi KY, Lee S, Yoo SE. Effects of KR-32570, a new sodium hydrogen exchanger inhibitor, on myocardial infarction and arrhythmias induced by ischemia and reperfusion. *Eur J Pharmacol*. 2005;523(1-3):101-108.

81. Lee BH, Seo HW, Yi KY, Lee S, Yoo SE. Effects of KR-32570, a new Na^+/H^+ exchanger inhibitor, on functional and metabolic impairments produced by global ischemia and reperfusion in the perfused rat heart. *Eur J Pharmacol*. 2005;511(2-3):175-182.

82. Kim J, Jung YS, Han W, Kim MY, Namkung W, Lee BH, Yi KY, Yoo SE, Lee MG, Kim KH. Pharmacodynamic characteristics and cardioprotective effects of new NHE1 inhibitors. *Eur J Pharmacol*. 2007;567(1-2):131-138.

83. Mao D, Xu Y, Hu X, Zhang G, Dong J, Gong G. Synthesis and Na^+/H^+ exchanger-1 inhibitory activity of substituted (quinolinecarbonyl)guanidine derivatives. *Chem Biodivers*. 2009;6(10):1727-1736.

84. Wallert MA, Frohlich O. Na^+/H^+ exchange in isolated myocytes from adult rat heart. *Am. J. Physiol*. 1989;257:C207-C213.

85. Haworth RS, McCann C, Snabaitis AK, Roberts NA, Avkiran M. Stimulation of the plasma membrane Na^+/H^+ exchanger NHE1 by sustained intracellular acidosis. Evidence for a novel mechanism mediated by the ERK pathway. *J. Biol. Chem*. 2003;278(34):31676-31684.

86. Coccaro E, Karki P, Cojocaru C, Fliegel L. Phenylephrine and sustained acidosis activate the neonatal rat cardiomyocyte Na^+/H^+ exchanger through phosphorylation of amino acids Ser770 and Ser771. *Am J Physiol Heart Circ Physiol*. 2009;297(2):H846-858.

87. Karmazyn M, Kilic A, Javadov S. The role of NHE1 in myocardial hypertrophy and remodelling. *J Mol Cell Cardiol*. 2008;44(4):647-653.

88. Wess J. G-protein-coupled receptors:molecular mechanisms involved in receptor activation and selectivity of G-protein recognition. *FASEB J*. 1997;11:346-354.

89. Rockman HA, Koch WJ, Lefkowitz RJ. Seven-transmembrane-spanning receptors and heart function. *Nature*. 2002;415(6868):206-212.

90. Neves SR, Ram PT, Iyengar R. G protein pathways. *Science*. 2002;296(5573):1636-1639.

91. Wollert KC, Drexler H. The renin-angiotensin system and experimental heart failure. *Cardiovasc Res*. 1999;43(4):838-849.

92. Yamazaki T, Komuro I, Kudoh S, Zou Y, Shiojima I, Hiroi Y, Mizuno T, Maemura K, Kurihara H, Aikawa R, Takano H, Yazaki Y. Endothelin-1 is involved in mechanical stress-induced cardiomyocyte hypertrophy. *J Biol Chem*. 1996;271(6):3221-3228.

93. Yokoyama H, Yasutake M, Avkiran M. Alpha1-adrenergic stimulation of sarcolemmal Na^+/H^+ exchanger activity in rat ventricular myocytes: evidence for selective mediation by the alpha1A-adrenoceptor subtype. *Circ Res*. 1998;82(10):1078-1085.

94. Wallert MA, O. F. Alpha1-adrenergic stimulation of Na^+/H^+ exchange in cardiac myocytes. *Am. J. Physiol*. 1992;263:C1096-C1102.

95. Gunasegaram S, Haworth RS, Hearse DJ, Avkiran M. Regulation of sarcolemmal Na^+/H^+ exchanger activity by angiotensin II in adult rat ventricular myocytes: opposing actions via AT(1) versus AT(2) receptors. *Circ Res*. 1999;85(10):919-930.

96. Grace AA, Metcalfe JC, Weissberg PL, Bethell HWL, Vandenberg JI. Angiotension II stimulates sodium-dependent proton extrusion in perfused ferret heart. *Am. J. Physiol*. 1996;270:C1687-C1694.

97. Ito N, Kagaya Y, Weinberg EO, Barry WH, Lorell BH. Endothelin and angiotensin II stimulation of Na^+/H^+ exchange is impaired in cardiac hypertrophy. *J Clin Invest*. 1997;99(1):125-135.

98. Kramer BK, Smith TW, Kelly RA. Endothelin and increased contractility in adult rat ventricular myocytes. Role of intracellular alkalosis induced by activation of the protein kinase C-dependent Na^+/H^+ exchanger. *Circ*. *Res*. 1991;68:269-279.

99. Lagadic-Gossmann D, Vaughan-Jones RD. Coupling of dual acid extrusion inthe guinea-pig isolated ventricular myocyte to alpha1 and Beta-adrenoreceptors. *J*. *Physiol*. 1993;464:49-73.

100. Wu M-L, Tseng Y-Z. The modulatory effects of endothelin-1, carbachol and isoprenaline unpon Na^+/H^+ exchange in dog cardiac purkinje fibres. *J*. *Physiol*. 1993;471:583-597.

101. Guo H, Wasserstrom JA, Rosenthal JE. Effect of catecholamines on intracellular pH in sheep cardiac purkinje fibres. *J*. *Physiol*. 1992;458:289-306.

102. Avkiran M, Yokoyama H. Adenosine A(1) receptor stimulation inhibits alpha(1)-adrenergic activation of the cardiac sarcolemmal Na^+/H^+ exchanger. *Br*. *J*. *Pharmacol*. 2000;131:659-662.

103. Karmazyn M, Liu Q, Gan XT, Brix BJ, Fliegel L. Aldosterone increases NHE1 expression and induces NHE1-dependent hypertrophy in neonatal rat ventricular myocytes. *Hypertension*. 2003;42(6):1171-1176.

104. Mizuno Y, Yoshimura M, Yasue H, Sakamoto T, Ogawa H, Kugiyama K, Harada E, Nakayama M, Nakamura S, Ito T, Shimasaki Y, Saito Y, Nakao K. Aldosterone production is activated in failing ventricle in humans. *Circulation*. 2001;103(1):72-77.

105. Yamamoto N, Yasue H, Mizuno Y, Yoshimura M, Fujii H, Nakayama M, Harada E, Nakamura S, Ito T, Ogawa H. Aldosterone is produced from ventricles in patients with essential hypertension. *Hypertension*. 2002;39(5):958-962.

106. Yasutake M, Haworth RS, King A, Avkiran M. Thrombin activates the sarcolemmal Na^+/H^+ exchanger. *Circ*. *Res*. 1996;79:705-715.

107. Hooley R, Yu C-Y, Symons M, Barber DL. $G_{\alpha 13}$ stimulates Na^+/H^+ exchange through distinct Cdc42-dependent and RhoA-dependent pathways. *J*. *Biol*. *Chem*. 1996;271:6152-6158.

108. Hoque AN, Haist JV, Karmazyn M. Na^+/H^+ exchange inhibition protects against mechanical, ultrastructural, and biochemical impairment induced by low

concentrations of lysophosphatidylcholine in isolated rat hearts. *Circ Res*. 1997;80(1):95-102.

109. Aharonovitz O, Zaun HC, Balla T, York JD, Orlowski J, Grinstein S. Intracellular pH regulation by Na^+/H^+ exchange requires phosphatidylinositol 4,5-bisphosphate. *J. Cell Biol*. 2000;150(1):213-224.

110. Zaun HC, Shrier A, Orlowski J. Calcineurin B homologous protein 3 promotes the biosynthetic maturation, cell surface stability, and optimal transport of the Na^+/H^+ exchanger NHE1 isoform. *J Biol Chem*. 2008;283(18):12456-12467.

111. Pang T, Su X, Wakabayashi S, Shigekawa M. Calcineurin homologous protein as an essential cofactor for Na^+/H^+ exchangers. *J. Biol. Chem*. 2001;276(20):17367-17372.

112. Pang T, Wakabayashi S, Shigekawa M. Expression of calcineurin B homologous protein 2 protects serum deprivation-induced cell death by serum-independent activation of Na^+/H^+ exchanger. *J Biol Chem*. 2002;277(46):43771-43777.

113. Mailander J, Muller-Esterl W, Dedio J. Human homolog of mouse tescalcin associates with Na^+/H^+ exchanger type-1. *FEBS Lett*. 2001;507(3):331-335.

114. Li X, Liu Y, Kay CM, Muller-Esterl W, Fliegel L. The Na^+/H^+ exchanger cytoplasmic tail: Structure, function, and interactions with tescalcin. *Biochemistry*. 2003;42(24):7448-7456.

115. Bertrand B, Wakabayashi S, Ikeda T, Pouyssegur J, Shigekawa M. The Na^+/H^+ exchanger isoform 1 (NHE1) is a novel member of the calmodulin-binding proteins. *J. Biol. Chem*. 1994;269:13703-13709.

116. Wakabayashi S, Ikeda T, Iwamoto T, Pouyssegur J, Shigekawa M. Calmodulin-Binding autoinhibitory domain controls "pH-Sensing" in the Na^+/H^+ exchanger NHE1 through sequence specific interaction. *Biochem*. 1997;36:12854-12861.

117. Li X, Ding J, Liu Y, Brix BJ, Fliegel L. Functional analysis of acidic amino acids in the cytosolic tail of the Na^+/H^+ exchanger. *Biochemistry*. 2004;43(51):16477-16486.

118. Li X, Liu Y, Alvarez BV, Casey JR, Fliegel L. A novel carbonic anhydrase II binding site regulates NHE1 activity. *Biochemistry*. 2006;45(7):2414-2424.

119. Alvarez BV, Johnson DE, Sowah D, Soliman D, Light PE, Xia Y, Karmazyn M, Casey JR. Carbonic anhydrase inhibition prevents and reverts cardiomyocyte hypertrophy. *J Physiol*. 2007;579(Pt 1):127-145.

120. Cassel D, Katz M, Rotman M. Depletion of cellular ATP inhibits Na^+/H^+ antiport in cultured human cells. Modulation of the regulatory effect of intracellular protons on the antiporter activity. *J Biol Chem*. 1986;261(12):5460-5466.

121. Brown SE, Heming TA, Benedict CR, Bidani A. ATP-sensitive Na^+/H^+ antiport in type II alveolar epithelial cells. *Am J Physiol*. 1991;261(6 Pt 1):C954-963.

122. Kapus A, Grinstein S, Wasan S, Kandasamy R, Orlowski J. Functional characterization of three isoforms of the Na^+/H^+ exchanger stably expressed in Chinese hamster ovary cells. ATP dependence, osmotic sensitivity, and role in cell proliferation. *J Biol Chem*. 1994;269(38):23544-23552.

123. Wakabayashi S, Bertrand B, Shigekawa M, Fafournoux P, Pouyssegur J. Growth factor activation and "H^+-sensing" of the Na^+/H^+ exchanger isoform 1 (NHE1). *J. Biol. Chem*. 1994;269:5583-5588.

124. Wakabayashi S, Fafournoux P, Sardet C, Pouyssegur J. The Na^+/H^+ antiporter cytoplasmic domain mediates growth factor signals and controls "H^+-sensing". *Proc. Natl. Acad. Sci. USA*. 1992;89:2424-2428.

125. Fliegel L, Walsh MP, Singh D, Wong C, Barr A. Phosphorylation of the carboxyl-terminal domain of the Na^+/H^+ exchanger by Ca^{2+}/calmodulin-dependent protein kinase II. *Biochem. J*. 1992;282:139-145.

126. Vila-Petroff M, Mundina-Weilenmann C, Lezcano N, Snabaitis AK, Huergo MA, Valverde CA, Avkiran M, Mattiazzi A. Ca^{2+}/calmodulin-dependent protein kinase II contributes to intracellular pH recovery from acidosis via Na^+/H^+ exchanger activation. *J Mol Cell Cardiol*. 2009.

127. Wang Y. Mitogen-activated protein kinases in heart development and diseases. *Circulation*. 2007;116(12):1413-1423.

128. Liu H, Stupak J, Zheng J, Keller BO, Brix BJ, Fliegel L, Li L. Open tubular immobilized metal ion affinity chromatography combined with MALDI MS and MS/MS for identification of protein phosphorylation sites. *Anal Chem*. 2004;76(14):4223-4232.

129. Khaled AR, Moor AN, Li A, Kim K, Ferris DK, Muegge K, Fisher RJ, Fliegel L, Durum SK. Trophic factor withdrawal: p38 mitogen-activated protein kinase activates NHE1, which induces intracellular alkalinization. *Mol. Cell. Biol*. 2001;21(22):7545-7557.

130. Takahashi E, Abe J-I, Gallis B, Aebersold R, Spring DJ, Krebs EG, Berk BC. p^{90}RSK is a serum-stimulated Na^+/H^+ exchanger isoform-1 kinase. Regulatory phosphorylation of serine 703 of Na^+/H^+ exchanger isoform-1. *J. Biol. Chem*. 1999;274:20206-20214.

131. Snabaitis AK, Yokoyama H, Avkiran M. Roles of mitogen-activated protein kinases and protein kinase C in α_{1A}-adrenoreceptor-mediated stimulation of the sarcolemmal Na^+/H^+ exchanger. *Circ. Res*. 2000;86:214-220.

132. Viollet B, Athea Y, Mounier R, Guigas B, Zarrinpashneh E, Horman S, Lantier L, Hebrard S, Devin-Leclerc J, Beauloye C, Foretz M, Andreelli F, Ventura-Clapier R, Bertrand L. AMPK: Lessons from transgenic and knockout animals. *Front Biosci*. 2009;14:19-44.

133. Moopanar TR, Xiao XH, Jiang L, Chen ZP, Kemp BE, Allen DG. AICAR inhibits the Na^+/H^+ exchanger in rat hearts--possible contribution to cardioprotection. *Pflugers Arch*. 2006;453(2):147-156.

134. Snabaitis AK, Cuello F, Avkiran M. Protein kinase B/Akt phosphorylates and inhibits the cardiac Na^+/H^+ exchanger NHE1. *Circ Res*. 2008;103(8):881-890.

135. Ebata S, Muto S, Okada K, Nemoto J, Amemiya M, Saito T, Asano Y. Aldosterone activates Na^+/H^+ exchange in vascular smooth muscle cells by nongenomic and genomic mechanisms. *Kidney Int*. 1999;56(4):1400-1412.

136. Martin-Requero A, Daza FJ, Hermida OG, Butta N, Parrilla R. Role of Ca^{2+} and protein kinase C in the receptor-mediated activation of Na^+/H^+ exchange in isolated liver cells. *Biochem J*. 1997;325 (Pt 3):631-636.

137. Woo SH, Lee CO. Effects of endothelin-1 on Ca^{2+} signaling in guinea-pig ventricular myocytes: role of protein kinase C. *J Mol Cell Cardiol*. 1999;31(3):631-643.

138. Wang QJ, Acs P, Goodnight J, Giese T, Blumberg PM, Mischak H, Mushinski JF. The catalytic domain of protein kinase C-d in reciprocal d and E chimeras mediates phorbol ester-induced macrophage differentiation of mouse promyelocytes. *J. Biol. Chem*. 1997;272:76-82.

139. Barford D, Das AK, Egloff MP. The structure and mechanism of protein phosphatases: insights into catalysis and regulation. *Annu Rev Biophys Biomol Struct*. 1998;27:133-164.

140. MacDougall LK, Jones LR, Cohen P. Identification of the major protein phosphatases in mammalian cardiac muscle which dephosphorylate phospholamban. *Eur J Biochem*. 1991;196(3):725-734.

141. Ennis IL, Garciarena CD, Escudero EM, Perez NG, Dulce RA, Camilion de Hurtado MC, Cingolani HE. Normalization of the calcineurin pathway underlies the regression of hypertensive hypertrophy induced by Na^+/H^+ exchanger-1 (NHE1) inhibition. *Can J Physiol Pharmacol*. 2007;85(3-4):301-310.

142. Misik AJ, Perreault K, Holmes CF, Fliegel L. Protein phosphatase regulation of Na^+/H^+ exchanger isoform I. *Biochemistry*. 2005;44(15):5842-5852.

143. Snabaitis AK, D'Mello R, Dashnyam S, Avkiran M. A novel role for protein phosphatase 2A in receptor-mediated regulation of the cardiac sarcolemmal Na^+/H^+ exchanger NHE1. *J Biol Chem*. 2006;281(29):20252-20262.

144. Meno H, Jarmakani JJ, Philipson KD. Developmental changes of sarcolemmal Na^+/H^+ exchange. *J. Mol. Cell Cardiol*. 1989;21:1179-1185.

145. Haworth RS, Yasutake M, Brooks G, Avkiran M. Cardiac Na^+/H^+ exchanger during post-natal development in the rat: Changes in mRNA expression and sarcolemmal activity. *J. Mol. Cell. Cardiol*. 1997;29:321-332.

146. Takewaki S, Kuro-o M, Hiroi Y, Yamazaki T, Noguchi T, Miyagishi A, Nakahara K, Aikawa M, Manabe I, Yazaki Y, et al. Activation of Na^+/H^+ antiporter (NHE1) gene expression during growth, hypertrophy and proliferation of the rabbit cardiovascular system. *J Mol Cell Cardiol*. 1995;27(1):729-742.

147. Chen F, Jarmakani JM, Van Dop C. Developmental changes in mRNA encoding cardiac Na^+/H^+ exchanger (NHE1) in rabbit. *Biochem. Biophys. Res. Comm*. 1995;212:960-967.

148. Rieder CV, Fliegel L. Developmental regulation of Na^+/H^+ exchanger expression in fetal and neonatal mice. *Am J Physiol Heart Circ Physiol*. 2002;283(1):H273-283.

149. Rieder CV, Fliegel L. Transcriptional regulation of Na^+/H^+ exchanger expression in the intact mouse. *Mol Cell Biochem*. 2003;243(1-2):87-95.

150. Chen L, Gan XT, Haist JV, Feng Q, Lu X, Chakrabarti S, Karmazyn M. Attenuation of compensatory right ventricular hypertrophy and heart failure following monocrotaline-induced pulmonary vascular injury by the Na^+/H^+ exchange inhibitor cariporide. *J Pharmacol Exp Ther*. 2001;298(2):469-476.

151. Jandeleit-Dahm K, Hannan KM, Farrelly CA, Allen TJ, Rumble JR, Gilbert RE, Cooper ME, Little PJ. Diabetes-induced vascular hypertrophy is accompanied by activation of Na^+/H^+ exchange and prevented by Na^+/H^+ exchange inhibition. *Circ Res*. 2000;87(12):1133-1140.

152. Karmazyn M, Liu Q, Gan XT, Brix BJ, Fliegel L. Aldosterone increases NHE1 expression and induces NHE1-dependent hypertrophy in neonatal rat ventricular myocytes. *Hypertension*. 2003;42(6):1171-1176.

153. Haworth RS, Yasutake M, Brooks G, Avkiran M. Cardiac Na^+/H^+ exchanger during postnatal development in the rat: changes in mRNA expression and sarcolemmal activity. *J Mol Cell Cardiol*. 1997;29(1):321-332.

154. Grinstein S, Rotin D, Mason MJ. Na^+/H^+ exchange and growth factor-induced cytosolic pH changes. Role in cellular proliferation. *Biochim. Biophys. Acta*. 1989;988:73-97.

155. Pouyssegur J, Sardet C, Franchi A, L'Allemain G, Paris S. A specific mutation abolishing Na^+/H^+ antiport activity in hamster fibroblasts precludes growth at neutral and acidic pH. *Proc. Natl. Acad. Sci. USA*. 1984;81:4833-4837.

156. Rotin D, Grinstein, S. Impaired cell volume regulation in Na^+/H^+ exchange-deficient mutants. *Am. J. Phyiol*. 1989;257(26):C1158-C1165.

157. Shrode L, Cabado A, Goss G, Grinstein S. Role of the Na^+/H^+ antiporter isoforms in cell volume regulation. *In The Na^+/H^+ Exchanger, Edited by L. Fliegel, R.G. Landes Company*. 1996:101-122.

158. Cox GA, Lutz CM, Yang C-L, Biemesderfer D, Bronson RT, Fu A, Aronson PS, Noebels JL, Frankel WN. Sodium/Hydrogen exchanger gene defect in slow-wave epilepsy mice. *Cell*. 1997;91:139-148.

159. Bell SM, Schreiner CM, Schultheis PJ, Miller ML, Evans RL, Vorhees CV, Shull GE, Scott WJ. Targeted disruption of the murine Nhe1 locus induces ataxia, growth retardation, and seizures. *Am. J. Physiol*. 1999;276:C788-C795.

160. Putney LK, Barber DL. Na-H exchange-dependent increase in intracellular pH times G2/M entry and transition. *J Biol Chem*. 2003;278(45):44645-44649.

161. Alvarez J, Garcia-Sancho J, Mollinedo F, Sanchez A. Intracellular Ca^{2+} potentiates Na^+/H^+ exchange and cell differentiation induced by phorbol ester in U937 cells. *Eur. J. Biochem*. 1989;183:709-714.

162. Hazav P, Shany S, Moran A, Levy R. Involvement of intracellular pH elevation in the effect of 1,25-dihydroxyvitamin D3 on HL60 cells. *Cancer Res*. 1989;49:72-75.

163. Wang H, Singh D, Fliegel L. The Na^+/H^+ antiporter potentiates growth and retinoic- acid induced differentiation of P19 embryonal carcinoma cells. *J. Biol. Chem*. 1997;272:26545-26549.

164. Rao GN, de Roux N, Sardet C, Pouyssegur J, Berk BC. Na^+/H^+ antiporter gene expression during monocytic differentiation of HL60 cells. *J. Biol. Chem*. 1991;266(21):13485-13488.

165. Rao GN, Sardet C, Pouyssegur J, Berk BC. Na^+/H^+ antiporter gene expression increases during retinoic acid-induced granulocytic differentiation of HL60 cells. *J. Cell. Physiol*. 1992;151(2):361-366.

166. Wu KL, Khan S, Lakhe-Reddy S, Wang L, Jarad G, Miller RT, Konieczkowski M, Brown AM, Sedor JR, Schelling JR. Renal tubular epithelial cell apoptosis is associated with caspase cleavage of the Na^+/H^+ exchanger. *Am J Physiol Renal Physiol*. 2003;284(4):F829-839.

167. Rich IN, Worthington-White D, Garden OA, Musk P. Apoptosis of leukemic cells accompanies reduction in intracellular pH after targeted inhibition of the Na^+/H^+ exchanger. *Blood*. 2000;95(4):1427-1434.

168. Wu KL, Khan S, Lakhe-Reddy S, Jarad G, Mukherjee A, Obejero-Paz CA, Konieczkowski M, Sedor JR, Schelling JR. The Na^+/H^+ exchanger recruits ezrin/radixin/moesin proteins to regulate Akt-dependent cell survival. *J Biol Chem*. 2004;279(25):26280-26286.

169. Niggli V, Rossy J. Ezrin/radixin/moesin: versatile controllers of signaling molecules and of the cortical cytoskeleton. *Int J Biochem Cell Biol*. 2008;40(3):344-349.

170. Denker SP, Huang DC, Orlowski J, Furthmayr H, Barber DL. Direct binding of the Na^+/H^+ exchanger to ERM proteins regulates the cortical cytoskeleton and cell shape independently of H^+ translocation. *Mol Cell*. 2000;6(6):1425-1436.

171. Slepkov E, Fliegel L. Structure and function of the Na^+/H^+ exchanger. *Biochem. Cell Biol*. 2002;80:499-508.

172. Denker SP, Huang DC, Orlowski J, Furthmayr H, Barber DL. Direct binding of the Na^+/H^+ exchanger to ERM proteins regulates the cortical cytoskeleton and cell shape independently of H^+ translocation. *Mol Cell*. 2000;6(6):1425-1436.

173. Denker SP, Barber DL. Cell migration requires both ion translocation and cytoskeletal anchoring by the Na^+/H^+ exchanger. *J Cell Biol*. 2002;159(6):1087-1096.

174. Denker SP, Huang DC, Orlowski J, Furthmayr H, Barber DL. Direct binding of NHE1 to ERM proteins regulates the cortical cytoskeleton and cell shape idedpendently of H^+ translocation. *Molecular Cell*. 2000;8:1425-1436.

175. Tominaga T, Ishizaki T, Narumiya S, Barber DL. p160ROCK mediates RhoA activation of Na^+/H^+ exchange. *EMBO J*. 1998;17:4712-4722.

176. Karydis A, Jimenez-Vidal M, Denker SP, Barber DL. Mislocalized scaffolding by NHE1 dominantly inhibits fibronectin production and TGF-beta activation. *Mol Biol Cell*. 2009;20(8):2327-2336.

177. Darmellah A, Rucker-Martin C, Feuvray D. ERM proteins mediate the effects of Na^+/H^+ exchanger (NHE1) activation in cardiac myocytes. *Cardiovasc Res*. 2009;81(2):294-300.

178. Strong K, Mathers C, Leeder S, Beaglehole R. Preventing chronic diseases: how many lives can we save? *Lancet*. 2005;366(9496):1578-1582.

179. Frey N, Katus HA, Olson EN, Hill JA. Hypertrophy of the heart: a new therapeutic target? *Circulation*. 2004;109(13):1580-1589.

180. Levy D, Garrison RJ, Savage DD, Kannel WB, Castelli WP. Prognostic implications of echocardiographically determined left ventricular mass in the Framingham Heart Study. *N Engl J Med*. 1990;322(22):1561-1566.

181. Ballard VL. Stem cells for heart failure in the aging heart. *Heart Fail Rev*.

182. Gwathmey JK, Slawsky MT, Hajjar RJ, Briggs GM, Morgan JP. Role of intracellular calcium handling in force-interval relationships of human ventricular myocardium. *J Clin Invest*. 1990;85(5):1599-1613.

183. Krum H, Abraham WT. Heart failure. *Lancet*. 2009;373(9667):941-955.

184. Gan XT, Chakrabarti S, Karmazyn M. Modulation of Na^+/H^+ exchange isoform 1 mRNA expression in isolated rat hearts. *Am J Physiol*. 1999;277(3 Pt 2):H993-998.

185. Dyck JRB, Maddaford T, Pierce GN, Fliegel L. Induction of expression of the sodium-hydrogen exchanger in rat myocardium. *Cardiovascular Res*. 1995;29:203-208.

186. Avkiran M. Protection of the ischaemic myocardium by Na^+/H^+ exchange inhibitors: potential mechanisms of action. *Basic Res. Cardiol*. 2001;96:306-311.

187. Baczko I, Mraiche F, Light PE, Fliegel L. Diastolic calcium is elevated in metabolic recovery of cardiomyocytes expressing elevated levels of the Na^+/H^+ exchanger. *Can J Physiol Pharmacol*. 2008;86(12):850-859.

188. Karmazyn M, Gan XT, Humphreys RA, Yoshida H, Kusumoto K. The myocardial Na^+/H^+ exchange: structure, regulation, and its role in heart disease. *Circ Res*. 1999;85(9):777-786.

189. Lemasters JJ, Bond JM, Chacon E, Harper IS, Kaplan SH, Ohata H, Trollinger DR, Herman B, Cascio WE. The pH paradox in ischemia-reperfusion injury to cardiac myocytes. *EXS*. 1996;76:99-114.

190. Karmazyn M. Amiloride enhances post ischemic recovery: possible role of Na^+/H^+ exchange. *Am. J. Physiol*. 1988;255:H608-H615.

191. Karmazyn M, Sawyer M, Fliegel L. The Na^+/H^+ exchanger: a target for cardiac therapeutic intervention. *Curr Drug Targets Cardiovasc Haematol Disord*. 2005;5(4):323-335.

192. Wang Y, Meyer JW, Ashraf M, Shull GE. Mice with a null mutation in the Na^+/H^+ exchanger are resistant to cardiac ischemia-reperfusion injury. *Circ Res*. 2003;93(8):776-782.

193. Gumina RJ, Gross GJ. If ischemic preconditioning is the gold standard, has a platinum standard of cardioprotection arrived? Comparison with NHE inhibition. *J Thromb Thrombolysis*. 1999;8(1):39-44.

194. Haist JV, Hirst CN, Karmazyn M. Effective protection by NHE1 inhibition in ischemic and reperfused heart under preconditioning blockade. *Am J Physiol Heart Circ Physiol*. 2003;284(3):H798-803.

195. Avkiran M, Marber MS. Na^+/H^+ exchange inhibitors for cardioprotective therapy: progress, problems and prospects. *J. Am. Coll. Cardiol*. 2002;39(5):747-753.

196. Liu H, Cala PM, Anderson SE. Na^+/H^+ exchange inhibition protects newborn heart from ischemia/reperfusion injury by limiting Na^+-dependent Ca^{2+} overload. *J Cardiovasc Pharmacol*. 2009.

197. Yasutake M, Avkiran M. Exacerbation of reperfusion arrhythmias by alpha 1 adrenergic stimulation: a potential role for receptor mediated activation of sarcolemmal sodium-hydrogen exchange. *Cardiovasc Res*. 1995;29(2):222-230.

198. Maekawa N, Abe J, Shishido T, Itoh S, Ding B, Sharma VK, Sheu SS, Blaxall BC, Berk BC. Inhibiting p^{90} ribosomal S6 kinase prevents Na^+/H^+ exchanger-mediated cardiac ischemia-reperfusion injury. *Circulation*. 2006;113(21):2516-2523.

199. Fliegel L, Karmazyn M. The cardiac Na-H exchanger: a key downstream mediator for the cellular hypertrophic effects of paracrine, autocrine and hormonal factors. *Biochem Cell Biol*. 2004;82(6):626-635.

200. Theroux P, Chaitman BR, Danchin N, Erhardt L, Meinertz T, Schroeder JS, Tognoni G, White HD, Willerson JT, Jessel A. Inhibition of the sodium-hydrogen exchanger with cariporide to prevent myocardial infarction in high-risk ischemic

situations. Main results of the GUARDIAN trial. Guard during ischemia against necrosis (GUARDIAN) Investigators. *Circulation*. 2000;102(25):3032-3038.

201. Zeymer U, Suryapranata H, Monassier JP, Opolski G, Davies J, Rasmanis G, Linssen G, Tebbe U, Schroder R, Tiemann R, Machnig T, Neuhaus KL. The Na^+/H^+ exchange inhibitor eniporide as an adjunct to early reperfusion therapy for acute myocardial infarction. Results of the evaluation of the safety and cardioprotective effects of eniporide in acute myocardial infarction (ESCAMI) trial. *J Am Coll Cardiol*. 2001;38(6):1644-1650.

202. Zeymer U, Suryapranata H, Monassier JP, Opolski G, Davies J, Rasmanis G, Linssen G, Tebbe U, Schroder R, Tiemann R, Machnig T, Neuhaus KL. The Na^+/H^+ exchange inhibitor eniporide as an adjunct to early reperfusion therapy for acute myocardial infarction. Results of the evaluation of the safety and cardioprotective effects of eniporide in acute myocardial infarction (ESCAMI) trial. *J. Am. Coll. Cardiol*. 2001;38(6):1644-1650.

203. Mentzer RM, Jr. Effects of Na^+/H^+ exchange inhibition by cariporide on death and nonfatal myocardial infarction in patients undergoing coronatry artery bypass graft surgery: The Expedition study. *Circulation*. 2003;108:3M:2723 (Abstract).

204. Imahashi K, Mraiche F, Steenbergen C, Murphy E, Fliegel L. Overexpression of the Na^+/H^+ exchanger and ischemia-reperfusion injury in the myocardium. *Am J Physiol Heart Circ Physiol*. 2007;292(5):H2237-H2247.

205. Cook AR, Bardswell SC, Pretheshan S, Dighe K, Kanaganayagam GS, Jabr RI, Merkle S, Marber MS, Engelhardt S, Avkiran M. Paradoxical resistance to myocardial ischemia and age-related cardiomyopathy in NHE1 transgenic mice: a role for ER stress? *J Mol Cell Cardiol*. 2009;46(2):225-233.

206. Simm A, Friedrich I, Scheubel RJ, Gursinsky T, Silber RE, Bartling B. Age dependency of the cariporide-mediated cardio-protection after simulated ischemia in isolated human atrial heart muscles. *Exp Gerontol*. 2008;43(7):691-699.

207. Kuro-o M, Hanaoka K, Hiroi Y, Noguchi T, Fujimori Y, Takewaki S, Hayasaka M, Katoh H, Miyagishi A, Nagai R, et al. Salt-sensitive hypertension in transgenic mice overexpressing Na^+/H^+ exchanger. *Circ Res*. 1995;76(1):148-153.

208. Marano G, Vergari A, Catalano L, Gaudi S, Palazzesi S, Musumeci M, Stati T, Ferrari AU. Na^+/H^+ exchange inhibition attenuates left ventricular remodeling and preserves systolic function in pressure-overloaded hearts. *Br. J. Pharmacol*. 2004;141(3):526-532.

209. Alvarez BV, Ennis IL, Hurtado MCC, Cingolani HE. Effects of antihypertensive therapy on cardiac sodium/hydrogen ion exchanger activity and hypertrophy in spontaneously hypertensive rats. *Can. J. Cardiol*. 2002;18(6):667-672.

210. Krowka MJ. Pulmonary hypertension: diagnostics and therapeutics. *Mayo Clin Proc*. 2000;75(6):625-630.

211. Gaine SP, Rubin LJ. Primary pulmonary hypertension. *Lancet*. 1998;352(9129):719-725.

212. Chen L, Gan XT, Haist JV, Feng Q, Lu X, Chakrabarti S, Karmazyn M. Attenuation of compensatory right ventricular hypertrophy and heart failure following monocrotaline-induced pulmonary vascular injury by the Na^+/H^+ exchange inhibitor cariporide. *J Pharmacol Exp Ther*. 2001;298(2):469-476.

213. Yu L, Quinn DA, Garg HG, Hales CA. Deficiency of the NHE1 gene prevents hypoxia-induced pulmonary hypertension and vascular remodeling. *Am J Respir Crit Care Med*. 2008;177(11):1276-1284.

214. Francis GS. Pathophysiology of chronic heart failure. *Am J Med*. 2001;110 Suppl 7A:37S-46S.

215. Mehra MR, Uber PA, Francis GS. Heart failure therapy at a crossroad: are there limits to the neurohormonal model? *J Am Coll Cardiol*. 2003;41(9):1606-1610.

216. Hill JA, Olson EN. Cardiac plasticity. *N Engl J Med*. 2008;358(13):1370-1380.

217. Pluim BM, Zwinderman AH, van der Laarse A, van der Wall EE. The athlete's heart. A meta-analysis of cardiac structure and function. *Circulation*. 2000;101(3):336-344.

218. Cingolani HE, Camilion de Hurtado MC. Na^+/H^+ exchanger inhibition: a new antihypertrophic tool. *Circ Res*. 2002;90(7):751-753.

219. Dulce RA, Hurtado C, Ennis IL, Garciarena CD, Alvarez MC, Caldiz C, Pierce GN, Portiansky EL, Chiappe de Cingolani GE, Camilion de Hurtado MC. Endothelin-1 induced hypertrophic effect in neonatal rat cardiomyocytes: involvement of Na^+/H^+ and Na^+/Ca^{2+} exchangers. *J Mol Cell Cardiol*. 2006;41(5):807-815.

220. Dorn GW, 2nd, Robbins J, Sugden PH. Phenotyping hypertrophy: eschew obfuscation. *Circ Res*. 2003;92(11):1171-1175.

221. Brower GL, Gardner JD, Forman MF, Murray DB, Voloshenyuk T, Levick SP, Janicki JS. The relationship between myocardial extracellular matrix remodeling and ventricular function. *Eur J Cardiothorac Surg*. 2006;30(4):604-610.

222. Diffee GM, Seversen EA, Stein TD, Johnson JA. Microarray expression analysis of effects of exercise training: increase in atrial MLC-1 in rat ventricles. *Am J Physiol Heart Circ Physiol*. 2003;284(3):H830-837.

223. Dorn GW, 2nd. The fuzzy logic of physiological cardiac hypertrophy. *Hypertension*. 2007;49(5):962-970.

224. Cingolani HE, Ennis IL. Sodium-hydrogen exchanger, cardiac overload, and myocardial hypertrophy. *Circulation*. 2007;115(9):1090-1100.

225. Sandmann S, Yu M, Kaschina E, Blume A, Bouzinova E, Aalkjaer C, Unger T. Differential effects of angiotensin AT1 and AT2 receptors on the expression, translation and function of the Na^+/H^+ exchanger and Na^+-HCO_3^- symporter in the rat heart after myocardial infarction. *J Am Coll Cardiol*. 2001;37(8):2154-2165.

226. Ruetten H, Gehring D, Hiss K, Schindler U, Gerl M, Busch AE, Schaefer S. Effects of combined inhibition of the Na^+/H^+ exchanger and angiotensin-converting enzyme in rats with congestive heart failure after myocardial infarction. *Br J Pharmacol*. 2005;146(5):723-731.

227. Baartscheer A, Schumacher CA, van Borren MM, Belterman CN, Coronel R, Opthof T, Fiolet JW. Chronic inhibition of Na^+/H^+ exchanger attenuates cardiac hypertrophy and prevents cellular remodeling in heart failure. *Cardiovasc Res*. 2005;65(1):83-92.

228. Kusumoto K, Haist JV, Karmazyn M. Na^+/H^+ exchange inhibition reduces hypertrophy and heart failure after myocardial infarction in rats. *Am J Physiol*. 2001;280(2):H738-H745.

229. Chen L, Chen CX, Gan XT, Beier N, Scholz W, Karmazyn M. Inhibition and reversal of myocardial infarction-induced hypertrophy and heart failure by NHE1 inhibition. *Am J Physiol Heart Circ Physiol*. 2004;286(1):H381-387.

230. Yoshida H, Karmazyn M. Na^+/H^+ exchange inhibition attenuates hypertrophy and heart failure in 1-wk postinfarction rat myocardium. *Am J Physiol* 2000;278(1):H300-H304.

231. Nakamura TY, Iwata Y, Arai Y, Komamura K, Wakabayashi S. Activation of Na^+/H^+ exchanger 1 is sufficient to generate Ca^{2+} signals that induce cardiac hypertrophy and heart failure. *Circ Res*. 2008;103(8):891-899.

232. Schluter KD, Schafer M, Balser C, Taimor G, Piper HM. Influence of pH_i and creatine phosphate on alpha-adrenoceptor-mediated cardiac hypertrophy. *J Mol Cell Cardiol*. 1998;30(4):763-771.

233. Ennis IL, Escudero EM, Console GM, Camihort G, Dumm CG, Seidler RW, Camilion de Hurtado MC, Cingolani HE. Regression of isoproterenol-induced cardiac hypertrophy by Na^+/H^+ exchanger inhibition. *Hypertension*. 2003;41(6):1324-1329.

234. Clerk A, Sugden PH. Activation of protein kinase cascades in the heart by hypertrophic G protein coupled receptor agonists. *Am. J. Cardiol*. 1999;83:64H-69H.

235. Moor AN, Fliegel L. Protein kinase mediated regulation of the Na^+/H^+ exchanger in the rat myocardium by MAP-kinase-dependent pathways. *J. Biol. Chem*. 1999;274:22985-22992.

236. Bianchini L, L'Allemain G, Pouyssegur J. The p42/44 mitogen-activated protein kinase cascade determinant in mediating activation of the Na^+/H^+ exchanger (NHE1 isoform) in response to growth factors. *J. Biol. Chem*. 1997;272:271-279.

237. Takewaki S, Kuro-o M, Hiroi Y, Yamazaki T, Noguchi T, Miyagishi A, Nakahara K, Aikawa M, Manabe I, Yazaki Y. Activation of Na^+/H^+ antiporter (NHE1) gene expression during growth, hypertrophy and proliferation of the rabbit cardiovascular system. *J Mol Cell Cardiol*. 1995;27(1):729-742.

238. Chahine M, Bkaily G, Nader M, Al-Khoury J, Jacques D, Beier N, Scholz W. NHE1-dependent intracellular sodium overload in hypertrophic hereditary cardiomyopathy: prevention by NHE1 inhibitor. *J Mol Cell Cardiol*. 2005;38(4):571-582.

239. Engelhardt S, Hein L, Keller U, Klambt K, Lohse MJ. Inhibition of Na^+/H^+ exchange prevents hypertrophy, fibrosis, and heart failure in beta(1)-adrenergic receptor transgenic mice. *Circ Res*. 2002;90(7):814-819.

240. Kilic A, Velic A, De Windt LJ, Fabritz L, Voss M, Mitko D, Zwiener M, Baba HA, van Eickels M, Schlatter E, Kuhn M. Enhanced activity of the myocardial Na^+/H^+ exchanger contributes to cardiac remodeling in atrial natriuretic peptide receptor-deficient mice. *Circulation*. 2005;112(15):2307-2317.

241. Hoehner CM, Williams DE, Sievers ML, Knowler WC, Bennett PH, Nelson RG. Trends in heart disease death rates in diabetic and nondiabetic Pima Indians. *J Diabetes Complications*. 2006;20(1):8-13.

242. Struthers AD, Morris AD. Screening for and treating left-ventricular abnormalities in diabetes mellitus: a new way of reducing cardiac deaths. *Lancet*. 2002;359(9315):1430-1432.

243. Vial G, Dubouchaud H, Couturier K, Lanson M, Leverve X, Demaison L. Na^+/H^+ exchange inhibition with cariporide prevents alterations of coronary endothelial

function in streptozotocin-induced diabetes. *Mol Cell Biochem*. 2008;310(1-2):93-102.

244. Darmellah A, Baetz D, Prunier F, Tamareille S, Rucker-Martin C, Feuvray D. Enhanced activity of the myocardial Na^+/H^+ exchanger contributes to left ventricular hypertrophy in the Goto-Kakizaki rat model of type 2 diabetes: critical role of Akt. *Diabetologia*. 2007;50(6):1335-1344.

245. Chen S, Khan ZA, Karmazyn M, Chakrabarti S. Role of endothelin-1, sodium hydrogen exchanger-1 and mitogen activated protein kinase (MAPK) activation in glucose-induced cardiomyocyte hypertrophy. *Diabetes Metab Res Rev*. 2007;23(5):356-367.

246. Li Z, Bing OH, Long X, Robinson KG, Lakatta EG. Increased cardiomyocyte apoptosis during the transition to heart failure in the spontaneously hypertensive rat. *Am J Physiol*. 1997;272(5 Pt 2):H2313-2319.

247. Olivetti G, Quaini F, Sala R, Lagrasta C, Corradi D, Bonacina E, Gambert SR, Cigola E, Anversa P. Acute myocardial infarction in humans is associated with activation of programmed myocyte cell death in the surviving portion of the heart. *J Mol Cell Cardiol*. 1996;28(9):2005-2016.

248. Narula J, Haider N, Virmani R, DiSalvo TG, Kolodgie FD, Hajjar RJ, Schmidt U, Semigran MJ, Dec GW, Khaw BA. Apoptosis in myocytes in end-stage heart failure. *N Engl J Med*. 1996;335(16):1182-1189.

249. Lee Y, Gustafsson AB. Role of apoptosis in cardiovascular disease. *Apoptosis*. 2009;14(4):536-548.

250. Garciarena CD, Caldiz CI, Portiansky EL, Chiappe de Cingolani GE, Ennis IL. Chronic NHE1 blockade induces an antiapoptotic effect in the hypertrophied heart. *J Appl Physiol*. 2009.

251. Karki P, Fliegel L. Overexpression of the Na^+/H^+ exchanger causes elevated apoptosis in isolated cardiomyocytes after hypoxia/reoxygenation challenge. *Mol Cell Biochem*. 2009.

252. Javadov S, Choi A, Rajapurohitam V, Zeidan A, Basnakian AG, Karmazyn M. NHE1 inhibition-induced cardioprotection against ischaemia/reperfusion is associated with attenuation of the mitochondrial permeability transition. *Cardiovasc Res*. 2007.

253. Yokoyama H, Gunasegaram S, Harding SE, Avkiran M. Sarcolemmal Na^+/H^+ exchanger activity and expression in human ventricular myocardium. *J Am Coll Cardiol*. 2000;36(2):534-540.

254. Knight BP. Atrial fibrillation in patients with congestive heart failure. *Pacing Clin Electrophysiol*. 2003;26(7 Pt 2):1620-1623.

255. hui Y, junzhu C, jianhua Z. Gap junction and Na^+/H^+ exchanger alternations in fibrillating and failing atrium. *Int J Cardiol*. 2008;128(1):147-149.

256. Boer PH. Activation of the gene for atrial natriuretic factor during in vitro cardiac myogenesis by P19 embryonal carcinoma cells. *Exp Cell Res*. 1993;207(2):421-429.

257. Lev S, Kehat I, Gepstein L. Differentiation pathways in human embryonic stem cell-derived cardiomyocytes. *Ann N Y Acad Sci*. 2005;1047:50-65.

258. Wobus AM, Boheler KR. Embryonic stem cells: prospects for developmental biology and cell therapy. *Physiol Rev*. 2005;85(2):635-678.

259. Lei L, Dou L, Yan L, Dou Z, Wang H. [Effect of NHE1 on stem cell differentiation into cardiomyocytes]. *Sheng Wu Gong Cheng Xue Bao*. 2008;24(10):1790-1795.

260. Li X, Karki P, Lei L, Wang H, Fliegel L. Na^+/H^+ exchanger isoform 1 facilitates cardiomyocyte embryonic stem cell differentiation. *Am J Physiol Heart Circ Physiol*. 2009;296(1):H159-170.

261. Shibuya K, Mathers CD, Boschi-Pinto C, Lopez AD, Murray CJ. Global and regional estimates of cancer mortality and incidence by site: II. Results for the global burden of disease 2000. *BMC Cancer*. 2002;2:37.

262. Stock C, Schwab A. Protons make tumor cells move like clockwork. *Pflugers Arch*. 2009;458(5):981-992.

263. Reshkin SJ, Bellizzi A, Caldeira S, Albarani V, Malanchi I, Poignee M, Alunni-Fabbroni M, Casavola V, Tommasino M. Na^+/H^+ exchanger-dependent intracellular alkalinization is an early event in malignant transformation and plays an essential role in the development of subsequent transformation-associated phenotypes. *FASEB J*. 2000;14(14):2185-2197.

264. Harguindey S, Cragoe EJ, Jr. The Na^+/H^+ antiporter in oncology in the light of the spontaneous regression of cancer and cell metabolism. *Med Hypotheses*. 1992;39(3):229-237.

265. Reshkin SJ, Bellizzi A, Cardone RA, Tommasino M, Casavola V, Paradiso A. Paclitaxel induces apoptosis via protein kinase A- and p38 mitogen-activated protein-dependent inhibition of the Na^+/H^+ exchanger (NHE) isoform 1 in human breast cancer cells. *Clin Cancer Res*. 2003;9(6):2366-2373.

266. Bell SM, Schreiner CM, Schultheis PJ, Miller ML, Evans RL, Vorhees CV, Shull GE, Scott WJ. Targeted disruption of the murine Nhe1 locus induces ataxia, growth retardation, and seizures. *Am J Physiol*. 1999;276(4 Pt 1):C788-795.

267. Kuribayashi Y, Itoh N, Kitano M, Ohashi N. Corrigendum to: cerebroprotective properties of SM-20220, a potent Na^+/H^+ exchange inhibitor, in transient cerebral ischemia in rats. *Eur J Pharmacol*. 2000;387(3):349.

268. Ortiz A. Renal cell loss through cell suicide. *Kidney Int*. 2000;58(5):2235-2236.

269. Schelling JR, Abu Jawdeh BG. Regulation of cell survival by Na^+/H^+ exchanger-1. *Am J Physiol Renal Physiol*. 2008;295(3):F625-632.

270. Khan S, Wu KL, Sedor JR, Abu Jawdeh BG, Schelling JR. The Na^+/H^+ exchanger regulates cell survival by activating and targeting ezrin to specific plasma membrane domains. *Cell Mol Biol (Noisy-le-grand)*. 2006;52(8):115-121.

271. Kerrigan CL, Stotland MA. Ischemia reperfusion injury: a review. *Microsurgery*. 1993;14(3):165-175.

272. Juel C, Klarskov C, Nielsen JJ, Krustrup P, Mohr M, Bangsbo J. Effect of high-intensity intermittent training on lactate and H^+ release from human skeletal muscle. *Am J Physiol Endocrinol Metab*. 2004;286(2):E245-251.

273. McAllister SE, Moses MA, Jindal K, Ashrafpour H, Cahoon NJ, Huang N, Neligan PC, Forrest CR, Lipa JE, Pang CY. Na^+/H^+ exchange inhibitor cariporide attenuates skeletal muscle infarction when administered before ischemia or reperfusion. *J Appl Physiol*. 2009;106(1):20-28.

274. Slepkov ER, Rainey JK, Li X, Liu Y, Cheng FJ, Lindhout DA, Sykes BD, Fliegel L. Structural and functional characterization of transmembrane segment IV of the Na^+/H^+ exchanger. *J. Biol. Chem*. 2005;280(18):17863-17872.

275. Coccaro E, Mraiche F, Malo M, Vandertol-Vanier H, Bullis B, Robertson M, Fliegel L. Expression and characterization of the Na^+/H^+ exchanger in the mammalian myocardium. *Mol Cell Biochem*. 2007;302(1-2):145-155.

276. Michalak M, Fliegel L, Wlasichuk K. Isolation and characterization of calcium binding glycoproteins of cardiac sarcolemmal vesicles. *J. Biol. Chem*. 1990;265:5869-5874.

277. Ozkan P, Mutharasan, R. . A rapid method for measuring intracellular pH using BCECF-AM. *Biochem. Biophys. Acta*. 2002;1572:143-148.

278. Chaillet JR, Boron WF. Intracellular calibration of a pH-sensitive dye in isolated, perfused salamander proximal tubules. *J Gen Physiol*. 1985;86(6):765-794.

279. Chaillet JR, Boron WF. Intracellular calibration of a pH-sensitive dye in isolated perfused salamander proximal tubules. *J. Gen. Physiol*. 1985;86:765-794.

280. Yutzey KE, Robbins J. Principles of genetic murine models for cardiac disease. *Circulation*. 2007;115(6):792-799.

281. Hilal-Dandan R, Kanter JR, Brunton LL. Characterization of G-protein signaling in ventricular myocytes from the adult mouse heart: differences from the rat. *J Mol Cell Cardiol*. 2000;32(7):1211-1221.

282. Jiang R, Zatta A, Kin H, Wang N, Reeves JG, Mykytenko J, Deneve J, Zhao ZQ, Guyton RA, Vinten-Johansen J. PAR-2 activation at the time of reperfusion salvages myocardium via an ERK1/2 pathway in in vivo rat hearts. *Am J Physiol Heart Circ Physiol*. 2007;293(5):H2845-2852.

283. Javadov S, Choi A, Rajapurohitam V, Zeidan A, Basnakian AG, Karmazyn M. NHE-1 inhibition-induced cardioprotection against ischaemia/reperfusion is associated with attenuation of the mitochondrial permeability transition. *Cardiovasc Res*. 2008;77(2):416-424.

284. Dawn B, Xuan YT, Marian M, Flaherty MP, Murphree SS, Smith TL, Bolli R, Jones WK. Cardiac-specific abrogation of NF- kappa B activation in mice by transdominant expression of a mutant I kappa B alpha. *J Mol Cell Cardiol*. 2001;33(1):161-173.

285. Chen P, Yuan Y, Wang S, Zhan L, Xu J. Captopril, an Angiotensin-converting enzyme inhibitor, attenuates the severity of acute pancreatitis in rats by reducing expression of matrix metalloproteinase 9. *Tohoku J Exp Med*. 2006;209(2):99-107.

286. Xia Y, Javadov S, Gan TX, Pang T, Cook MA, Karmazyn M. Distinct K_{ATP} channels mediate the antihypertrophic effects of adenosine receptor activation in neonatal rat ventricular myocytes. *J Pharmacol Exp Ther*. 2007;320(1):14-21.

287. Gan XT, Gong XQ, Xue J, Haist JV, Bai D, Karmazyn M. Sodium-hydrogen exchange inhibition attenuates glycoside-induced hypertrophy in rat ventricular myocytes. *Cardiovasc Res*.85(1):79-89.

288. Chen L, Zhang J, Gan TX, Chen-Izu Y, Hasday JD, Karmazyn M, Balke CW, Scharf SM. Left ventricular dysfunction and associated cellular injury in rats exposed to chronic intermittent hypoxia. *J Appl Physiol*. 2008;104(1):218-223.

289. Matsui Y, Jia N, Okamoto H, Kon S, Onozuka H, Akino M, Liu L, Morimoto J, Rittling SR, Denhardt D, Kitabatake A, Uede T. Role of osteopontin in cardiac

fibrosis and remodeling in angiotensin II-induced cardiac hypertrophy. *Hypertension*. 2004;43(6):1195-1201.

290. Henderson NC, Mackinnon AC, Farnworth SL, Poirier F, Russo FP, Iredale JP, Haslett C, Simpson KJ, Sethi T. Galectin-3 regulates myofibroblast activation and hepatic fibrosis. *Proc Natl Acad Sci U S A*. 2006;103(13):5060-5065.

291. Crone SA, Zhao YY, Fan L, Gu Y, Minamisawa S, Liu Y, Peterson KL, Chen J, Kahn R, Condorelli G, Ross J, Jr., Chien KR, Lee KF. ErbB2 is essential in the prevention of dilated cardiomyopathy. *Nat Med*. 2002;8(5):459-465.

292. Goldspink PH, McKinney RD, Kimball VA, Geenen DL, Buttrick PM. Angiotensin II induced cardiac hypertrophy in vivo is inhibited by cyclosporin A in adult rats. *Mol Cell Biochem*. 2001;226(1-2):83-88.

293. Wang Y, Luo J, Chen X, Chen H, Cramer SW, Sun D. Gene inactivation of Na^+/H^+ exchanger isoform 1 attenuates apoptosis and mitochondrial damage following transient focal cerebral ischemia. *Eur J Neurosci*. 2008;28(1):51-61.

294. Dolinsky VW, Chan AY, Robillard Frayne I, Light PE, Des Rosiers C, Dyck JR. Resveratrol prevents the prohypertrophic effects of oxidative stress on LKB1. *Circulation*. 2009;119(12):1643-1652.

295. Nakayama H, Wilkin BJ, Bodi I, Molkentin JD. Calcineurin-dependent cardiomyopathy is activated by TRPC in the adult mouse heart. *FASEB J*. 2006;20(10):1660-1670.

296. Dallabrida SM, Ismail NS, Pravda EA, Parodi EM, Dickie R, Durand EM, Lai J, Cassiola F, Rogers RA, Rupnick MA. Integrin binding angiopoietin-1 monomers reduce cardiac hypertrophy. *FASEB J*. 2008;22(8):3010-3023.

297. Vinge LE, von Lueder TG, Aasum E, Qvigstad E, Gravning JA, How OJ, Edvardsen T, Bjornerheim R, Ahmed MS, Mikkelsen BW, Oie E, Attramadal T, Skomedal T, Smiseth OA, Koch WJ, Larsen TS, Attramadal H. Cardiac-restricted expression of the carboxyl-terminal fragment of GRK3 Uncovers Distinct Functions of GRK3 in regulation of cardiac contractility and growth: GRK3 controls cardiac alpha1-adrenergic receptor responsiveness. *J Biol Chem*. 2008;283(16):10601-10610.

298. Aker S, Snabaitis AK, Konietzka I, Van De Sand A, Bongler K, Avkiran M, Heusch G, Schulz R. Inhibition of the Na^+/H^+ exchanger attenuates the deterioration of ventricular function during pacing-induced heart failure in rabbits. *Cardiovasc Res*. 2004;63(2):273-282.

299. Fujisawa G, Okada K, Muto S, Fujita N, Itabashi N, Kusano E, Ishibashi S. Na^+/H^+ exchange isoform 1 is involved in mineralocorticoid/salt-induced cardiac injury. *Hypertension*. 2003;41(3):493-498.

300. Belke DD, Larsen TS, Gibbs EM, Severson DL. Altered metabolism causes cardiac dysfunction in perfused hearts from diabetic (db/db) mice. *Am J Physiol Endocrinol Metab*. 2000;279(5):E1104-1113.

301. Lopaschuk GD, Belke DD, Gamble J, Itoi T, Schonekess BO. Regulation of fatty acid oxidation in the mammalian heart in health and disease. *Biochim Biophys Acta*. 1994;1213(3):263-276.

302. Liu B, Clanachan AS, Schulz R, Lopaschuk GD. Cardiac efficiency is improved after ischemia by altering both the source and fate of protons. *Circ Res*. 1996;79(5):940-948.

303. Liu Q, Docherty JC, Rendell JC, Clanachan AS, Lopaschuk GD. High levels of fatty acids delay the recovery of intracellular pH and cardiac efficiency in post-ischemic hearts by inhibiting glucose oxidation. *J Am Coll Cardiol*. 2002;39(4):718-725.

304. Folmes CD, Clanachan AS, Lopaschuk GD. Fatty acids attenuate insulin regulation of 5'-AMP-activated protein kinase and insulin cardioprotection after ischemia. *Circ Res*. 2006;99(1):61-68.

305. Moor A, Gan XT, Karmazyn M, Fliegel L. Activation of Na^+/H^+ exchanger-directed protein kinases in the ischemic and ischemic-reperfused rat myocardium. *J Biol Chem*. 2001;27:16113-16122.

306. Kass-Eisler A, Falck-Pedersen E, Alvira M, Rivera J, Buttrick PM, Wittenberg BA, Cipriani L, Leinwand LA. Quantitative determination of adenovirus-mediated gene delivery to rat cardiac myocytes *in vitro* and *in vivo*. *Proc Natl Acad Sci U S A*. 1993;90(24):11498-11502.

307. Zhou YY, Wang SQ, Zhu WZ, Chruscinski A, Kobilka BK, Ziman B, Wang S, Lakatta EG, Cheng H, Xiao RP. Culture and adenoviral infection of adult mouse cardiac myocytes: methods for cellular genetic physiology. *Am J Physiol Heart Circ Physiol*. 2000;279(1):H429-436.

308. He TC, Zhou S, da Costa LT, Yu J, Kinzler KW, Vogelstein B. A simplified system for generating recombinant adenoviruses. *Proc Natl Acad Sci U S A*. 1998;95(5):2509-2514.

309. Grinstein S, Woodside M, Sardet C, Pouyssegur J, Rotin D. Activation of the Na^+/H^+ antiporter during cell volume regulation. Evidence for a phosphorylation-independent mechanism. *J. Biol. Chem*. 1992;267(33):23823-23828.

310. Chan AY, Soltys CL, Young ME, Proud CG, Dyck JR. Activation of AMP-activated protein kinase inhibits protein synthesis associated with hypertrophy in the cardiac myocyte. *J Biol Chem*. 2004;279(31):32771-32779.

311. Stanbouly S, Kirshenbaum LA, Jones DL, Karmazyn M. Sodium hydrogen exchange 1 (NHE1) regulates connexin 43 expression in cardiomyocytes via reverse mode sodium calcium exchange and c-Jun NH2-terminal kinase-dependent pathways. *J Pharmacol Exp Ther*. 2008;327(1):105-113.

312. Zahabi A, Deschepper CF. Long-chain fatty acids modify hypertrophic responses of cultured primary neonatal cardiomyocytes. *J Lipid Res*. 2001;42(8):1325-1330.

313. Fliegel L. The Na^+/H^+ exchanger isoform 1. *Int. J. Biochem. Cell Biol*. 2005;37(1):33-37.

314. Marban E, Koretsune Y. Cell calcium, oncogenes, and hypertrophy. *Hypertension*. 1990;15(6 Pt 1):652-658.

315. Murtazina R, Booth BJ, Bullis BL, Singh DN, Fliegel L. Functional analysis of polar amino-acid residues in membrane associated regions of the mammalian Na^+/H^+ exchanger. *Eur. J. Biochem*. 2001;268(17):4674-4685.

316. Wakabayashi S, Bertrand B, Ikeda T, Pouyssegur J, Shigekawa M. Mutation of calmodulin-binding site renders the Na^+/H^+ exchanger (NHE1) highly H^+-sensitive and Ca^{2+} regulation-defective. *J. Biol. Chem*. 1994;269:13710-13715.

317. Zwadlo C, Borlak J. Disease-associated changes in the expression of ion channels, ion receptors, ion exchangers and Ca^{2+}-handling proteins in heart hypertrophy. *Toxicol Appl Pharmacol*. 2005;207(3):244-256.

318. Lim HW, De Windt LJ, Steinberg L, Taigen T, Witt SA, Kimball TR, Molkentin JD. Calcineurin expression, activation, and function in cardiac pressure-overload hypertrophy. *Circulation*. 2000;101(20):2431-2437.

319. Christophe M, Nicolas S. Mitochondria: a target for neuroprotective interventions in cerebral ischemia-reperfusion. *Curr Pharm Des*. 2006;12(6):739-757.

320. Iaccarino G, Dolber PC, Lefkowitz RJ, Koch WJ. beta-adrenergic receptor kinase-1 levels in catecholamine-induced myocardial hypertrophy: regulation by beta- but not alpha1-adrenergic stimulation. *Hypertension*. 1999;33(1 Pt 2):396-401.

321. Fujita T, Noda H, Ito Y, Isaka M, Sato Y, Ogata E. Increased sympathoadrenomedullary activity and left ventricular hypertrophy in young

patients with borderline hypertension. *J Mol Cell Cardiol*. 1989;21 Suppl 5:31-38.

322. Tarnavski O, McMullen JR, Schinke M, Nie Q, Kong S, Izumo S. Mouse cardiac surgery: comprehensive techniques for the generation of mouse models of human diseases and their application for genomic studies. *Physiol Genomics*. 2004;16(3):349-360.

323. Fliegel L, Karmazyn M. The cardiac Na-H exchanger: a key downstream mediator for the cellular hypertrophic effects of paracrine, autocrine and hormonal factors. *Biochem Cell Biol*. 2004;82(6):626-635.

324. Cook AR, C. BS, Subashini P, Dighe K, Kanaganayagam GS, Jabr RI, Merkle S, Marber MS, Engelhardt S, Avkiran M. Resistance to ischemia/reperfusion-induced myocardial injury and age-related cardiomyopathy in NHE1 transgenic mice displaying ER stress (Abstract). *Int Soc Heart Res. 30th Meeting*. 2008;P100:41.

325. Heineke J, Molkentin JD. Regulation of cardiac hypertrophy by intracellular signalling pathways. *Nat Rev Mol Cell Biol*. 2006;7(8):589-600.

326. Avkiran M, Cook AR, Cuello F. Targeting Na^+/H^+ exchanger regulation for cardiac protection: a RSKy approach? *Curr Opin Pharmacol*. 2008;8(2):133-140.

327. Garciarena CD, Caldiz CI, Portiansky EL, Chiappe de Cingolani GE, Ennis IL. Chronic NHE1 blockade induces an antiapoptotic effect in the hypertrophied heart. *J Appl Physiol*. 2009;106(4):1325-1331.

328. Regula KM, Kirshenbaum LA. Apoptosis of ventricular myocytes: a means to an end. *J Mol Cell Cardiol*. 2005;38(1):3-13.

329. Cande C, Cohen I, Daugas E, Ravagnan L, Larochette N, Zamzami N, Kroemer G. Apoptosis-inducing factor (AIF): a novel caspase-independent death effector released from mitochondria. *Biochimie*. 2002;84(2-3):215-222.

330. Shannon R, Chaudhry M. Effect of alpha1-adrenergic receptors in cardiac pathophysiology. *Am Heart J*. 2006;152(5):842-850.

331. Gan XT, Chakrabarti S, Karmazyn M. Modulation of Na^+/H^+ exchange isoform 1 mRNA expression in isolated rat hearts. *Am J Physiol*. 1999;277:H993-H998.

332. Neely JR, Morgan HE. Relationship between carbohydrate and lipid metabolism and the energy balance of heart muscle. *Annu Rev Physiol*. 1974;36:413-459.

333. Lopaschuk GD, Spafford MA, Davies NJ, Wall SR. Glucose and palmitate oxidation in isolated working rat hearts reperfused after a period of transient global ischemia. *Circ Res*. 1990;66(2):546-553.

334. Lopaschuk GD, Collins-Nakai R, Olley PM, Montague TJ, McNeil G, Gayle M, Penkoske P, Finegan BA. Plasma fatty acid levels in infants and adults after myocardial ischemia. *Am Heart J*. 1994;128(1):61-67.

335. Hardie DG, Hawley SA. AMP-activated protein kinase: the energy charge hypothesis revisited. *Bioessays*. 2001;23(12):1112-1119.

336. Dolinsky VW, Dyck JR. Role of AMP-activated protein kinase in healthy and diseased hearts. *Am J Physiol Heart Circ Physiol*. 2006;291(6):H2557-2569.

337. Russell RR, 3rd, Li J, Coven DL, Pypaert M, Zechner C, Palmeri M, Giordano FJ, Mu J, Birnbaum MJ, Young LH. AMP-activated protein kinase mediates ischemic glucose uptake and prevents postischemic cardiac dysfunction, apoptosis, and injury. *J Clin Invest*. 2004;114(4):495-503.

338. Marsin AS, Bertrand L, Rider MH, Deprez J, Beauloye C, Vincent MF, Van den Berghe G, Carling D, Hue L. Phosphorylation and activation of heart PFK-2 by AMPK has a role in the stimulation of glycolysis during ischaemia. *Curr Biol*. 2000;10(20):1247-1255.

339. Lopaschuk GD, Wambolt RB, Barr RL. An imbalance between glycolysis and glucose oxidation is a possible explanation for the detrimental effects of high levels of fatty acids during aerobic reperfusion of ischemic hearts. *J Pharmacol Exp Ther*. 1993;264(1):135-144.

340. Armstrong SC. Protein kinase activation and myocardial ischemia/reperfusion injury. *Cardiovasc Res*. 2004;61(3):427-436.

341. Juhaszova M, Zorov DB, Yaniv Y, Nuss HB, Wang S, Sollott SJ. Role of glycogen synthase kinase-3beta in cardioprotection. *Circ Res*. 2009;104(11):1240-1252.

342. Rylatt DB, Aitken A, Bilham T, Condon GD, Embi N, Cohen P. Glycogen synthase from rabbit skeletal muscle. Amino acid sequence at the sites phosphorylated by glycogen synthase kinase-3, and extension of the N-terminal sequence containing the site phosphorylated by phosphorylase kinase. *Eur J Biochem*. 1980;107(2):529-537.

343. Tong H, Imahashi K, Steenbergen C, Murphy E. Phosphorylation of glycogen synthase kinase-3beta during preconditioning through a phosphatidylinositol-3-kinase--dependent pathway is cardioprotective. *Circ Res*. 2002;90(4):377-379.

344. Szabadkai G, Rizzuto R. Participation of endoplasmic reticulum and mitochondrial calcium handling in apoptosis: more than just neighborhood? *FEBS Lett*. 2004;567(1):111-115.

345. Xu C, Bailly-Maitre B, Reed JC. Endoplasmic reticulum stress: cell life an{Cook, 2009 #4}d death decisions. *J Clin Invest*. 2005;115(10):2656-2664.

346. Martindale JJ, Fernandez R, Thuerauf D, Whittaker R, Gude N, Sussman MA, Glembotski CC. Endoplasmic reticulum stress gene induction and protection from ischemia/reperfusion injury in the hearts of transgenic mice with a tamoxifen-regulated form of ATF6. *Circ Res*. 2006;98(9):1186-1193.

347. Folmes CD, Wagg CS, Shen M, Clanachan AS, Tian R, Lopaschuk GD. Suppression of 5'-AMP-activated protein kinase activity does not impair recovery of contractile function during reperfusion of ischemic hearts. *Am J Physiol Heart Circ Physiol*. 2009;297(1):H313-321.

348. Tada K, Nagao K, Tanjoh K, Hayashi N. Prognostic value of blood glucose in patients with cardiogenic shock. *Circ J*. 2006;70(8):1064-1069.

349. Ussher JR, Lopaschuk GD. The malonyl CoA axis as a potential target for treating ischaemic heart disease. *Cardiovasc Res*. 2008;79(2):259-268.

350. Wang W, Lopaschuk GD. Metabolic therapy for the treatment of ischemic heart disease: reality and expectations. *Expert Rev Cardiovasc Ther*. 2007;5(6):1123-1134.

351. Cross HR, Radda GK, Clarke K. The role of Na^+/K^+ ATPase activity during low flow ischemia in preventing myocardial injury: a ^{31}P, ^{23}Na and ^{87}Rb NMR spectroscopic study. *Magn Reson Med*. 1995;34(5):673-685.

352. Opie LH. Myocardial ischemia--metabolic pathways and implications of increased glycolysis. *Cardiovasc Drugs Ther*. 1990;4 Suppl 4:777-790.

353. Kudo N, Barr AJ, Barr RL, Desai S, Lopaschuk GD. High rates of fatty acid oxidation during reperfusion of ischemic hearts are associated with a decrease in malonyl-CoA levels due to an increase in 5'-AMP-activated protein kinase inhibition of acetyl-CoA carboxylase. *J Biol Chem*. 1995;270(29):17513-17520.

354. Force T, Pombo CM, Avruch JA, Bonventre JV, Kyriakis JM. Stress-activated protein kinases in cardiovascular disease. *Circ Res*. 1996;78(6):947-953.

355. Adams KF, Jr., Sueta CA, Gheorghiade M, O'Connor CM, Schwartz TA, Koch GG, Uretsky B, Swedberg K, McKenna W, Soler-Soler J, Califf RM. Gender differences in survival in advanced heart failure. Insights from the FIRST study. *Circulation*. 1999;99(14):1816-1821.

356. Simon T, Mary-Krause M, Funck-Brentano C, Jaillon P. Sex differences in the prognosis of congestive heart failure: results from the Cardiac Insufficiency Bisoprolol Study (CIBIS II). *Circulation*. 2001;103(3):375-380.

357. Douglas PS, Katz SE, Weinberg EO, Chen MH, Bishop SP, Lorell BH. Hypertrophic remodeling: gender differences in the early response to left ventricular pressure overload. *J Am Coll Cardiol*. 1998;32(4):1118-1125.

358. Tamura T, Said S, Gerdes AM. Gender-related differences in myocyte remodeling in progression to heart failure. *Hypertension*. 1999;33(2):676-680.

359. Kadokami T, McTiernan CF, Kubota T, Frye CS, Feldman AM. Sex-related survival differences in murine cardiomyopathy are associated with differences in TNF-receptor expression. *J Clin Invest*. 2000;106(4):589-597.

360. Olsson MC, Palmer BM, Leinwand LA, Moore RL. Gender and aging in a transgenic mouse model of hypertrophic cardiomyopathy. *Am J Physiol Heart Circ Physiol*. 2001;280(3):H1136-1144.

361. Oliver PM, Fox JE, Kim R, Rockman HA, Kim HS, Reddick RL, Pandey KN, Milgram SL, Smithies O, Maeda N. Hypertension, cardiac hypertrophy, and sudden death in mice lacking natriuretic peptide receptor A. *Proc Natl Acad Sci U S A*. 1997;94(26):14730-14735.

362. Du XJ. Gender modulates cardiac phenotype development in genetically modified mice. *Cardiovasc Res*. 2004;63(3):510-519.

363. Berridge MJ, Bootman MD, Roderick HL. Calcium signalling: dynamics, homeostasis and remodelling. *Nat Rev Mol Cell Biol*. 2003;4(7):517-529.

364. Xin HB, Senbonmatsu T, Cheng DS, Wang YX, Copello JA, Ji GJ, Collier ML, Deng KY, Jeyakumar LH, Magnuson MA, Inagami T, Kotlikoff MI, Fleischer S. Oestrogen protects FKBP12.6 null mice from cardiac hypertrophy. *Nature*. 2002;416(6878):334-338.

365. Kilic A, Javadov S, Karmazyn M. Estrogen exerts concentration-dependent pro- and anti-hypertrophic effects on adult cultured ventricular myocytes. Role of NHE1 in estrogen-induced hypertrophy. *J Mol Cell Cardiol*. 2009;46(3):360-369.

366. Bupha-Intr T, Wattanapermpool J, Pena JR, Wolska BM, Solaro RJ. Myofilament response to Ca^{2+} and Na^{+}/H^{+} exchanger activity in sex hormone-related protection of cardiac myocytes from deactivation in hypercapnic acidosis. *Am J Physiol Regul Integr Comp Physiol*. 2007;292(2):R837-843.

367. Hillebrand U, Hausberg M, Stock C, Shahin V, Nikova D, Riethmuller C, Kliche K, Ludwig T, Schillers H, Schneider SW, Oberleithner H. 17beta-estradiol increases volume, apical surface and elasticity of human endothelium mediated by Na^+/H^+ exchange. *Cardiovasc Res*. 2006;69(4):916-924.

368. Sugden PH, Clerk A. "Stress-responsive" mitogen-activated protein kinases (c-Jun N-terminal kinases and p38 mitogen-activated protein kinases) in the myocardium. [Review]. *Circ. Res*. 1998;83:345-352.

369. Geisterfer-Lowrance AA, Christe M, Conner DA, Ingwall JS, Schoen FJ, Seidman CE, Seidman JG. A mouse model of familial hypertrophic cardiomyopathy. *Science*. 1996;272(5262):731-734.

370. Schafer M, Schafer C, Michael Piper H, Schluter KD. Hypertrophic responsiveness of cardiomyocytes to alpha- or beta-adrenoceptor stimulation requires sodium-proton-exchanger-1 (NHE1) activation but not cellular alkalization. *Eur J Heart Fail*. 2002;4(3):249-254.

371. Lebeche D, Dalal R, Jang M, del Monte F, Hajjar RJ. Transgenic models of heart failure: elucidation of the molecular mechanisms of heart disease. *Heart Fail Clin*. 2005;1(2):219-236.

372. Wang Y, Meyer JW, Ashraf M, Shull GE. Mice with a null mutation in the NHE1 are resistant to cardiac ischemia-reperfusion injury. *Circ. Res*. 2003;93(8):776-782.

373. Cox GA, Lutz CM, Yang CL, Biemesderfer D, Bronson RT, Fu A, Aronson PS, Noebels JL, Frankel WN. Sodium/hydrogen exchanger gene defect in slow-wave epilepsy mutant mice. *Cell*. 1997;91(1):139-148.

374. Agah R, Frenkel PA, French BA, Michael LH, Overbeek PA, Schneider MD. Gene recombination in postmitotic cells. Targeted expression of Cre recombinase provokes cardiac-restricted, site-specific rearrangement in adult ventricular muscle in vivo. *J Clin Invest*. 1997;100(1):169-179.

375. AHA. Heart Disease and Stroke Statistics. 2009;2009 update
.

376. Dai DF, Rabinovitch PS. Cardiac aging in mice and humans: the role of mitochondrial oxidative stress. *Trends Cardiovasc Med*. 2009;19(7):213-220.

377. Isoyama S, Nitta-Komatsubara Y. Acute and chronic adaptation to hemodynamic overload and ischemia in the aged heart. *Heart Fail Rev*. 2002;7(1):63-69.

378. Avkiran M, Cook AR, Cuello F. Targeting Na^+/H^+ exchanger regulation for cardiac protection: a RSKy approach? *Curr Opin Pharmacol*. 2008;8(2):133-140.

379. Takeishi Y, Huang Q, Abe J, Che W, Lee JD, Kawakatsu H, Hoit BD, Berk BC, Walsh RA. Activation of mitogen-activated protein kinases and p^{90} ribosomal S6 kinase in failing human hearts with dilated cardiomyopathy. *Cardiovasc Res*. 2002;53(1):131-137.

380. Hardt SE, Sadoshima J. Glycogen synthase kinase-3beta: a novel regulator of cardiac hypertrophy and development. *Circ Res*. 2002; 90(10): 1055-63.

381. Javadov S, Rajapurohitam V, Kilic A, Zeidan A, Choi A, Karmazyn M. Anti-hypertrophic effect of NHE1 inhibition involves GSK-3beta-dependent attenuation of mitochondrial dysfunction. *J Mol Cell Cardiol*. 2009; **46**(6): 998-1007.

382. Bristow MR, Hershberger RE, Port JD, Gilbert EM, Sandoval A, Rasmussen R, Cates AE, Feldman AM. Beta-adrenergic pathways in nonfailing and failing human ventricular myocardium. *Circulation*. 1990; 82(2 Suppl): I12-25.

383. Scarabelli TM, Gottlieb RA. Functional and clinical repercussions of myocyte apoptosis in the multifaceted damage by ischemia/reperfusion injury: old and new concepts after 10 years of contributions. *Cell Death Differ*. 2004;11 Suppl 2:S144-152.

384. Xue J, Mraiche F, Zhou D, Karmazyn M, Oka T, Fliegel L, Haddad GG. Elevated Myocardial Na^+/H^+ Exchanger Isoform 1 Activity Elicits Gene Expression that Leads to Cardiac Hypertrophy. *Physiol Genomics*. 2010. *In Press*

Appendix 1

Characterization of NHE1 Transgenic Mice Treated with NHE1 Inhibitors

A.1 Introduction

An increasing number of *in vitro* and *in vivo* studies have supported the concept that inhibition of NHE1 is conducive to attenuation of CH. *In vivo,* the direct reversible effects of NHE1 inhibitors on CH were illustrated in rats subjected to an MI and treated with dietary cariporide (NHE1 inhibitor) one week post MI[1], or in models in which EMD 87580 was administered 4 weeks post MI[2]. The administration of NHE1 inhibitors in both studies completely abrogated the increased length of surviving myocytes and ameliorated contractile dysfunction. In a more severe model of CH, rats were subjected to an MI and observed at 3 months post MI. Treatment with cariporide at 3 months post MI resuted in a 50% reduction in CH[3]. Thus, confirming the direct reversible effects of NHE1 inhibitors on CH, however in a more severe scenario.

In addition to the direct inhibitory effect of NHE1 inhibitors on CH, it has also been shown that NHE1 inhibitors regress the hypertrophic response activated by an increase in mechanical load and upregulation of hormonal, paracrine and autocrine factors[216]. *In vitro*, in NRVMs, NHE1 inhibitors have been shown to inhibit norepinephrine-induced protein synthesis[7]. Stretch-induced stimulation of protein synthesis and alkalinization have also been shown to be blocked by NHE1 inhibitors[5,6].

To determine whether NHE1 inhibitors could prevent CH in K-line mice expressing active NHE1 (as described in Chapter 3, Chapter 5), control or K-line mice were treated with an NHE1 inhibitor and characterized for CH. Using various modes of administration and durations, we were unable to inhibit the cardiac hypertrophic phenotype of the K-line mice.

A.2 Results

A.2.1 Effects of EMD 87580, an NHE1 Inhibitor Administered Using Alzet Osmotic Mini Pumps, on the Cardiac Hypertrophic Phenotype in NHE1 Transgenic Mice

Both male and female control and K-line mice, 10-12 weeks of age, were treated with PBS (vehicle) or EMD 87580. Mice were age and body weight matched. PBS and EMD 87580 were administered using Alzet osmotic mini pumps, which were filled and surgically implanted (as described in Section 2.2.5). We chose to use 10mg/kg/day of EMD 87580 as a preliminary trial based on previous reports[8-10]. Pumps were implanted for 28 days and EMD 87580 was delivered at a rate of 0.25μL/hour. Alzet osmotic mini pumps were chosen as the mode of delivery in effort to reduce stress associated with constant IV injections. To evaluate the effects of treatment with NHE1 inhibitors on CH in K-line mice, various hypertrophic indices including the HW/BW and CSA of heart cross sections stained with H&E, were measured. In male control and K-line mice (Figure A.1), no differences were seen in the HW/BW (Figure A.1, A) and CSA (Figure A.1, B) between PBS and EMD 87580 treated animals. Similar results were seen with female control and K-line mice, no differences were seen in the HW/BW (Figure A.2, A) and CSA (Figure A.2, B) between PBS and EMD 87580 treated animals.

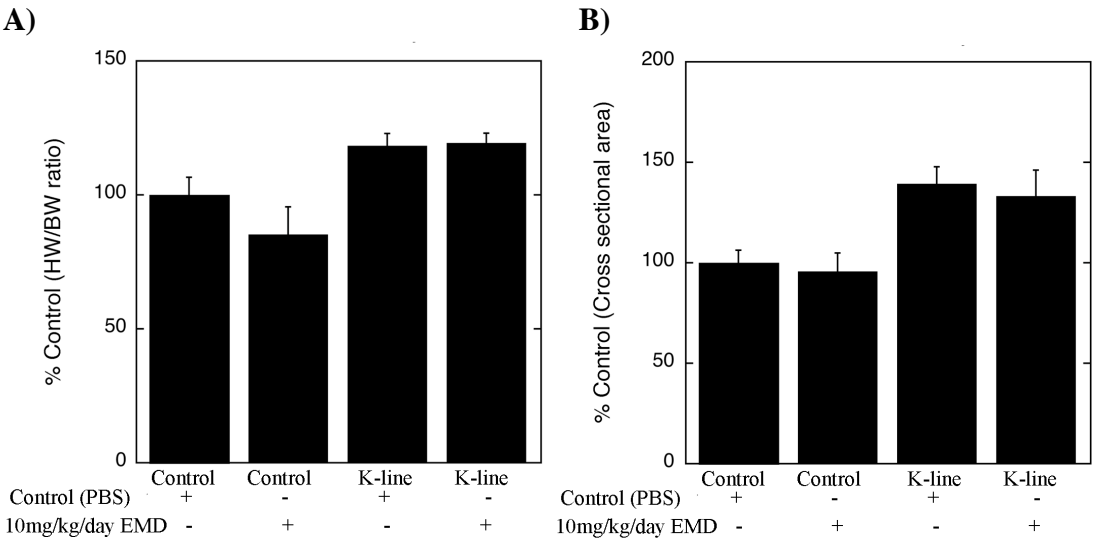

Figure A.1. HW/BW ratio and cross sectional area of male control and K-line mice treated with 10mg/kg/day EMD 87580. 10mg/kg/day EMD or PBS (vehicle) was administered using Alzet osmotic mini pumps, which were surgically implanted as described in Section 2.2.5. EMD or PBS was administered for 28 days at a rate of 0.25μL/hour and hearts were explanted at day 28. **A),** HW/BW ratio, heart weight to body weight ratio. Results are expressed as a % of controls (treated with PBS)±%SEM. PBS treated mice were compared to PE treated mice in each group. (n=4/group). **B),** Cross section area measured from heart cross sections stained with H&E from male control and K-line mice. Results are expressed as a % of controls (treated with PBS)±%SEM. PBS treated mice were compared to PE treated mice in each group. (n=4/group).

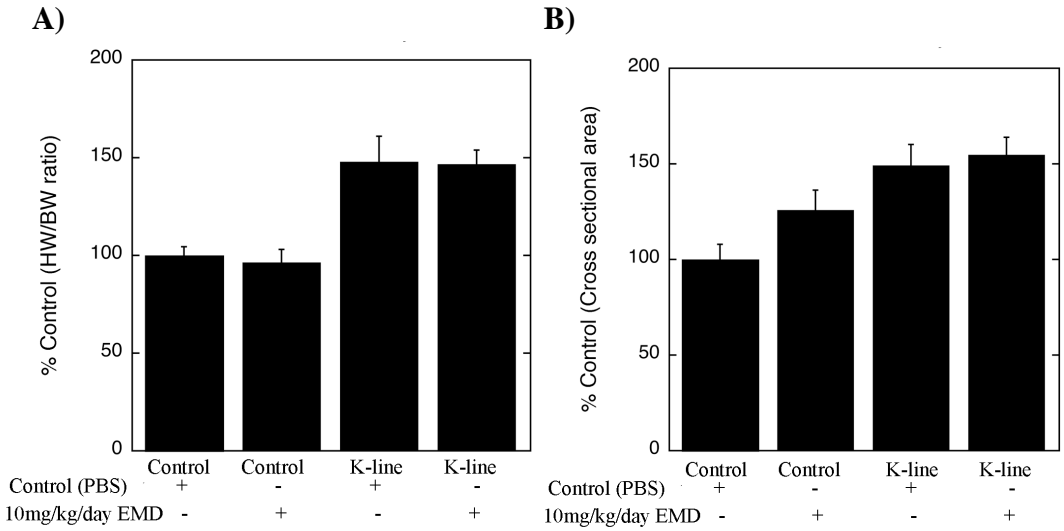

Figure A.2. HW/BW ratio and cross sectional area of female control and K-line mice treated with 10mg/kg/day EMD 87580. 10mg/kg/day EMD or PBS (vehicle) was administered using Alzet osmotic mini pumps, which were surgically implanted as described in Section 2.2.5. EMD or PBS was administered for 28 days at a rate of 0.25μL/hour and hearts were explanted at day 28. **A),** HW/BW ratio, heart weight to body weight ratio. Results are expressed as a % of control (treated with PBS)±%SEM. PBS treated mice were compared to PE treated mice in each group. (n=4/group). **B),** Cross section area measured from heart cross sections stained with H&E. Results are expressed as a % of control (treated with PBS)±%SEM. PBS treated mice were compared to PE treated mice in each group. (n=4/group).

A.2.2 Effects of Administration of 700ppm EMD 87580 Mouse Chow on the Cardiac Hypertrophic Phenotype in NHE1 Transgenic Mice

Female control and K-line mice, 10-12 weeks of age, were fed control or EMD 87580 supplemented mouse chow. The EMD 87580 chow was made using the control chow supplemented with EMD 87580. We chose to use 700ppm of EMD 87580 as a preliminary concentration based on previous reports[11]. This dose was chosen in previous studies in order to achieve a plasma concentration of 600-800 ng/ml, an effective concentration in rats. In our study, mice were age and body weight matched and had free access to control or EMD 87580 chow over a three month period. The effect of treatment with control or EMD 87580 chow on CH was assessed by measuring the HW/BW. No differences were seen in the HW/BW of control and K-line mice when comparing control chow vs. EMD 87580 chow within each group.

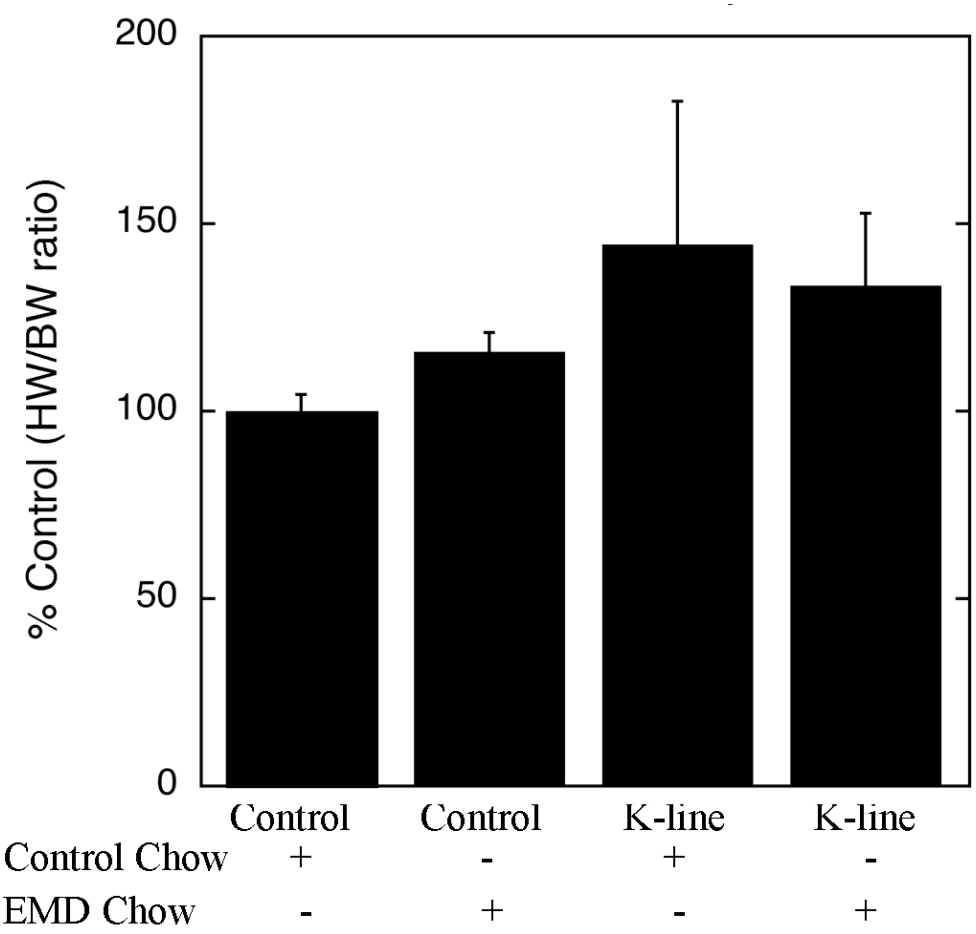

Figure A.3. HW/BW ratio of female control and K-line mice treated with control or EMD 87580 chow. 700ppm EMD or Control chow was administered to control or K-line mice for three months. Hearts were explanted at three months. HW/BW ratio was measured. Results are expressed as a % of controls (treated with PBS)±%SEM. (n=3/group).

A.2.3. Characterization of Control Mice Subjected to PE Stimulation in the Presence of EMD 87580 Chow

The lack of regression of CH with the treatment of NHE1 inhibitors lead us to investigate the effect of NHE1 inhibitors in hearts stimulated with PE, which were previously shown to increase the hypertrophic response of control and K-line hearts, as indicated by the increase in HW/BW (as described in Section 3.2.17). Therefore, male control mice, 10-12 weeks of age, were implanted with Alzet osmotic mini pumps filled with PE (as described in Section 2.2.5). 50mg/kg/day PE was administered over 14 days, and during this time male control mice were fed control or EMD 87580 chow. The EMD 87580 chow was a control chow supplemented with EMD 87580. We chose to use 700ppm of EMD 87580 in this preliminary trial and this was based on previous reports[11]. Animals had free access to control or EMD 87580 chow over a two week period. The effects of treatment with control or EMD 87580 chow on CH were assessed by measuring the HW/BW and cell area of isolated AVMs. No differences were seen in the HW/BW ratio of controls stimulated with PE and feed control or EMD 87580 chow (Figure A.3, A). We also measured cell area (as described in Section 2.2.1.2*)* of AVMs isolated using retrograde perfusion (as described in Section 2.2.1), and no differences were seen between control and EMD 87580 fed animals (Figure A.3, B).

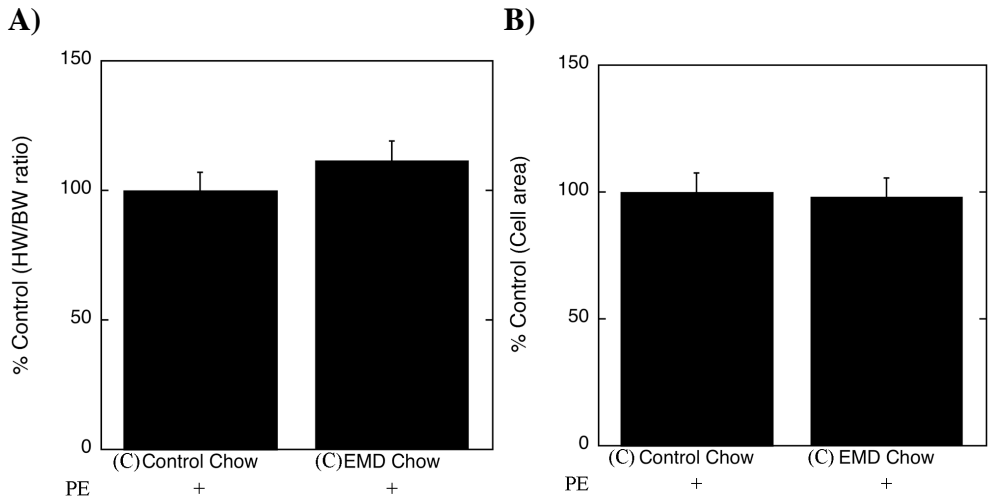

Figure A.4. HW/BW ratio and cell area of adult ventricular cardiomyocytes in male control mice stimulated with PE, while being treated with control or EMD 87580 chow. 700ppm EMD chow or control chow was administered to control mice, which were being stimulated with 50mg/kg/day PE over a period of two weeks. Hearts were explanted on day 14. **A),** HW/BW ratio. Results are expressed as a % of controls (stimulated with PE and fed control chow)±%SEM. (n=4-6/group). **B),** Cell area of isolated AVMs. Results are expressed as a % of controls (stimulated with PE and fed control chow)±%SEM. (n=4-6/group).

A.3 Discussion

NHE1 inhibitors have been used to attenuate CH in response to various stimuli, experimentally induced heart failure or genetic models of heart failure (reviewed in[4]). The beneficial effects of NHE1 inhibitors have been suggested to be due to direct antiremodelling effects. The continuously seen benefits of NHE1 inhibitors in the regression of CH have allowed many authors to conclude that NHE1 inhibitors maybe a potentially effective new therapeutic approach for the treatment of heart failure. In our study, we examined the effects of NHE1 inhibitors on our gain-of-function model, which expressed active NHE1 (K-line mice) and demonstrated phenotypic characteristics of CH (Chapter 3, Chapter 5).

We chose to use EMD 87580 as the NHE1 inhibitor, which was a generous gift from Dr. N. Beier of Merck KGaA (Frankfurt, Germany). Initially, the EMD 87580 was administered using Alzet osmotic mini pumps. We chose twenty eight days, the longest period in which one Alzet osmotic mini pump could be implanted. EMD 87580 was not able to regress the hypertrophic effects in K-line hearts and had no effects on both male and female control hearts. Similar results were seen when EMD 87580 was orally administered for three months. We have determined the phenotypic characteristics of K-line mice are mediated by NHE1, indicated by the lack of activation of MAPKs, RSK and calcineurin pathways, which have been implicated in CH (as described in Section 3.2.15). Therefore, inhibition of NHE1 should regress the CH response, unless other non-specified pathways are contributing to the phenotypic expression of K-line mice.

The lack of inhibitory effect seen by EMD 87580 in NHE1 TG mice expressing elevated NHE1 and CH maybe due to a number of factors including the time and the

inhibitor used, all which have been suggested to be very important to the efficacy of NHE1 inhibition[12]. The role of timing in the efficacy of NHE1 inhibitors is clearly demonstrated in I/R models treated with NHE1 inhibitors. Various NHE1 inhibitors including, HOE 694[13,14], cariporide[15-18] and eniporide[19] have consistently reduced MI size of hearts subjected to I/R in various models (pigs, rabbits, and dogs), when administered prior to the ischemic event. However, administration of NHE1 inhibitors prior to reperfusion reduced the MI size in only a few of these studies[16,17,19]. Therefore, it has been suggested that the most effective time to administer NHE1 inhibitors was before ischemia[12]. Perhaps in our model, the degree of hypertrophy attained in K-line mice at 10-12 weeks is not reversible and NHE1 inhibition needs to be administered at an earlier stage of hypertrophy in order for NHE1 inhibitors to be effective. In a previous report, TG mice expressing NHE1 were treated with NHE inhibitors 20 days post birth and this regressed the hypertrophic phenotype[20], thus confirming that perhaps targeting CH at an earlier stage is required. This idea is further confirmed by another study, which shows that the effects of NHE1 inhibitors are age dependent. Cariporide, an NHE1 inhibitor was protective against I/R only in the mature human hearts, and not in the aged myocardium[21]. Future studies could involve administration of NHE1 at earlier ages.

The specific type of NHE1 inhibitor administered has also been implicated in the effectiveness of its ability to regress cardiac pathologies[12]. EMD 87580 is a useful tool *in vitro* (as described Section 2.4 and 3.2.14), and is known for its selectivity towards NHE1. However, it has been reported that EMD 87580 is less potent than cariporide, having a 50% inhibitory concentration for NHE1 of 113±6 nmol/L compared with 22±2 nmol/L for cariporide[12]. Nakamura et al.[20] used cariporide to treat TG mice expressing

NHE1, which resulted in regression of the cardiac phenotype. In the future, other more potent NHE1 inhibitors could be used. Despite the inability of EMD 87580 to inhibit CH in K-line mice, it is evident in our control mice that using EMD 87580 at the concentrations and modes of delivery used did not result in atrophy or death, thus demonstrating the safety of EMD 87580.

In conclusion, despite the vast amount of literature stating that NHE1 inhibitors regress CH, in our studies, where NHE1 is expressed in TG mice, treatment with EMD 87580 using two modes of delivery, the Alzet osmotic mini pumps and oral dosage, did not regress CH. Further studies, using specific NHE1 inhibitors, at various ages and thus stages of hypertrophy, may regress CH.

A.4 References

1. Yoshida H, Karmazyn M. Na^+/H^+ exchange inhibition attenuates hypertrophy and heart failure in 1-wk postinfarction rat myocardium. *Am J Physiol* 2000;278(1):H300-H304.

2. Chen L, Chen CX, Gan XT, Beier N, Scholz W, Karmazyn M. Inhibition and reversal of myocardial infarction-induced hypertrophy and heart failure by NHE1 inhibition. *Am J Physiol Heart Circ Physiol*. 2004;286(1):H381-387.

3. Kusumoto K, Haist JV, Karmazyn M. Na^+/H^+ exchange inhibition reduces hypertrophy and heart failure after myocardial infarction in rats. *Am J Physiol*. 2001;280(2):H738-H745.

4. Karmazyn M, Kilic A, Javadov S. The role of NHE1 in myocardial hypertrophy and remodelling. *J Mol Cell Cardiol*. 2008;44(4):647-653.

5. Yamazaki T, Komuro I, Kudoh S, Zou Y, Nagai R, Aikawa R, Uozumi H, Yazaki Y. Role of ion channels and exchangers in mechanical stretch-induced cardiomyocyte hypertrophy. *Circ Res*. 1998;82(4):430-437.

6. Cingolani HE, Alvarez BV, Ennis IL, Camilion de Hurtado MC. Stretch-induced alkalinization of feline papillary muscle: an autocrine-paracrine system. *Circ. Res*. 1998;83(8):775-780.

7. Hori M, Nakatsubo N, Kagiya T, Iwai K, Sato H, Iwakura K, Kitabatake A, Kamada T. The role of Na^+/H^+ exchange in norepinephrine-induced protein synthesis in neonatal cultured rat cardiomyocytes. *Jpn Circ J*. 1990;54(5):535-539.

8. Blaauw Y, Beier N, van der Voort P, van Hunnik A, Schotten U, Allessie MA. Inhibitors of the Na^+/H^+ exchanger cannot prevent atrial electrical remodeling in the goat. *J Cardiovasc Electrophysiol*. 2004;15(4):440-446.

9. Aker S, Snabaitis AK, Konietzka I, Van De Sand A, Bongler K, Avkiran M, Heusch G, Schulz R. Inhibition of the Na^+/H^+ exchanger attenuates the deterioration of ventricular function during pacing-induced heart failure in rabbits. *Cardiovasc Res*. 2004;63(2):273-282.

10. Fujisawa G, Okada K, Muto S, Fujita N, Itabashi N, Kusano E, Ishibashi S. Na^+/H^+ exchange isoform 1 is involved in mineralocorticoid/salt-induced cardiac injury. *Hypertension*. 2003;41(3):493-498.

11. Chahine M, Bkaily G, Nader M, Al-Khoury J, Jacques D, Beier N, Scholz W. NHE1-dependent intracellular sodium overload in hypertrophic hereditary

cardiomyopathy: prevention by NHE-1 inhibitor. *J Mol Cell Cardiol*. 2005;38(4):571-582.

12. Corvera JS, Zhao ZQ, Schmarkey LS, Katzmark SL, Budde JM, Morris CD, Ehring T, Guyton RA, Vinten-Johansen J. Optimal dose and mode of delivery of Na^+/H^+ exchange-1 inhibitor are critical for reducing postsurgical ischemia-reperfusion injury. *Ann Thorac Surg*. 2003;76(5):1614-1622.

13. Klein HH, Pich S, Bohle RM, Wollenweber J, Nebendahl K. Myocardial protection by Na^+/H^+ exchange inhibition in ischemic, reperfused porcine hearts. *Circulation*. 1995;92(4):912-917.

14. Rohmann S, Weygandt H, Minck KO. Preischaemic as well as postischaemic application of a Na^+/H^+ exchange inhibitor reduces infarct size in pigs. *Cardiovasc Res*. 1995;30(6):945-951.

15. Garcia-Dorado D, Gonzalez MA, Barrabes JA, Ruiz-Meana M, Solares J, Lidon RM, Blanco J, Puigfel Y, Piper HM, Soler-Soler J. Prevention of ischemic rigor contracture during coronary occlusion by inhibition of Na^+/H^+ exchange. *Cardiovasc Res*. 1997;35(1):80-89.

16. Miura T, Ogawa T, Suzuki K, Goto M, Shimamoto K. Infarct size limitation by a new Na^+/H^+ exchange inhibitor, Hoe 642: difference from preconditioning in the role of protein kinase C. *J Am Coll Cardiol*. 1997;29(3):693-701.

17. Linz W, Albus U, Crause P, Jung W, Weichert A, Scholkens BA, Scholz W. Dose-dependent reduction of myocardial infarct mass in rabbits by the NHE1 inhibitor cariporide (HOE 642). *Clin Exp Hypertens*. 1998;20(7):733-749.

18. Klein HH, Pich S, Bohle RM, Lindert-Heimberg S, Nebendahl K. Na^+/H^+ exchange inhibitor cariporide attenuates cell injury predominantly during ischemia and not at onset of reperfusion in porcine hearts with low residual blood flow. *Circulation*. 2000;102(16):1977-1982.

19. Gumina RJ, Mizumura T, Beier N, Schelling P, Schultz JJ, Gross GJ. A new sodium/hydrogen exchange inhibitor, EMD 85131, limits infarct size in dogs when administered before or after coronary artery occlusion. *J Pharmacol Exp Ther*. 1998;286(1):175-183.

20. Nakamura TY, Iwata Y, Arai Y, Komamura K, Wakabayashi S. Activation of Na^+/H^+ exchanger 1 is sufficient to generate Ca^{2+} signals that induce cardiac hypertrophy and heart failure. *Circ Res*. 2008;103(8):891-899.

21. Simm A, Friedrich I, Scheubel RJ, Gursinsky T, Silber RE, Bartling B. Age dependency of the cariporide-mediated cardio-protection after simulated ischemia in isolated human atrial heart muscles. *Exp Gerontol*. 2008;43(7):691-699.